UNIVERSITAT POLITÈCNICA DE VALÈNCIA

Departamento de Máquinas y Motores Térmicos

DOCTORAL THESIS:

Advancement in understanding the extreme altitude and ambient temperature impact on Diesel engine and aftertreatment performance

---

Presented by: Ms. Bárbara Diesel Costa
Supervised by: Dr. Pedro Piqueras Cabrera

in fulfillment of the requirements for the degree of

Doctor of Philosophy

Valencia, January 2022

Doctoral Thesis

Advancement in understanding the extreme altitude and ambient temperature impact on Diesel engine and aftertreatment performance

Presented by: Ms. Bárbara Diesel Costa
Supervised by: Dr. Pedro Piqueras Cabrera

THESIS EXAMINERS

Dr. Ornella Chiavola
Dr. José Rodríguez Fernández
Dr. Soheil Zeraati Rezaei

DEFENSE COMMITTEE

Chairman: Dr. José Galindo Lucas
Secretary: Dr. Francisco Vera García
Member: Dr. Ornella Chiavola

Valencia, January 2022

Abstract

The increasingly stringent emission standards act as a guide for the development of cleaner vehicles in a context of climate change. The latest European regulations applied to the transportation sector widened the operation range where homologation tests are carried out. The variables of ambient temperature and driving altitude are now extra requirements that must be considered in a way to shorten the gap between those tests and real driving. The understanding of the ambient conditions impact on the engine response becomes fundamental to overcome the drawbacks represented by them, being determinant for the engine response with an extended impact on engine-out emissions.

As a consequence of altitude or ambient temperature variation, the exhaust aftertreatment systems (EATS) boundaries are modified, compromising their operation and impacting on tailpipe emissions. In the specific case of Diesel engines, the two most common EATS are the diesel oxidation catalyst (DOC) and the diesel particulate filter (DPF). In this context, this doctoral thesis proposes different approaches to understand the main factors that extreme ambient conditions impose to the engine and to the DOC and DPF operation. An important part of this work consisted of the set up of an experimental test bench equipped with an altitude simulator and of a one-dimensional (1D) thermo-fluid dynamic modelling tool for a wide-ranging analysis.

Following low temperature steady state conditions experimental outcomes, CO and HC emission contour maps led to the evaluation of how extreme ambient conditions impact on the DOC light-off and pollutant emissions conversion efficiency. The modelling analysis helped to build guidelines that determine the contribution of the flow properties caused by such conditions. Besides, the effect of applying computational exhaust line thermal insulation solutions on the DOC and engine response is additionally addressed. On the other hand, the variable geometry turbine (VGT) actuation on the DPF regeneration process is performed experimentally. The impact that the boost pressure strategy has on the rate of soot depletion during active regeneration as a function of the driving altitude is considered with the guidance of the modelling tools.

The reduction of the regeneration rate in altitude with standard boosting strategies is discussed, leading to the re-evaluation of the VGT actuation for

high altitude practices. Finally, the sensitivity of the VGT position and low pressure exhaust gases recirculation (LP-EGR) rate at a vast array of ambient conditions is experimentally analysed for regular engine operation at partial loads. The results led to the engine calibration redefinition based on EATS inlet temperature increase and the reduction of the specific fuel consumption.

Keywords: Internal combustion engine; altitude; ambient temperature; emissions; aftertreatment systems; operation optimization.

Resumen

El carácter cada vez más estricto de las normativas de emisiones ha provocado el desarrollo de motores de combustión más respetuosos con el medioambiente. La última normativa europea aplicada al sector del transporte ha ampliado el rango de condiciones de operación en el que se realizan las pruebas de homologación. Las variables de temperatura ambiente y altitud de conducción son ahora requisitos adicionales que deben tenerse en cuenta con la intención de reducir la diferencia entre el resultado de esas pruebas y en condiciones de conducción real. La comprensión del impacto de las condiciones ambientales sobre el funcionamiento del motor es algo fundamental para superar los inconvenientes que pueden representar la respuesta del motor y teniendo un gran impacto sobre las emisiones del mismo.

Como consecuencia de la variación de la altitud y de la temperatura ambiente, las condiciones de contorno de los sistemas de postratamiento de los gases de escape (EATS) se modifican, comprometiendo su funcionamiento y repercutiendo en las emisiones liberadas a la atmosfera. En el caso concreto de los motores Diesel, los dos EATS más comunes son el catalizador de oxidación diesel (DOC) y el filtro de partículas diesel (DPF). En este contexto, la presente tesis doctoral propone diferentes enfoques a fin de comprender los principales efectos que las condiciones ambientales extremas provocan en el motor y en el funcionamiento del DOC y del DPF. Una parte importante de este trabajo ha consistido en la puesta en marcha de un banco de pruebas experimental equipado con un simulador de altitud y de una herramienta de modelización termo fluidodinámica unidimensional (1D) para un amplio análisis.

Tras los resultados experimentales en condiciones de estado estacionario a baja temperatura, los mapas de contorno de las emisiones de CO y HC condujeron a la evaluación como las condiciones ambientales extremas repercuten en la temperatura de activación del DOC y en la eficiencia de conversión de las emisiones contaminantes. El análisis computacinal ayudó a elaborar directrices que determinan la contribución de las propiedades del flujo causadas por dichas condiciones. Asimismo, se ha abordado el efecto de la aplicación de soluciones computacionales de aislamiento térmico del escape sobre el DOC y la respuesta del motor. Por otro lado, se ha realizado experimentalmente la actuación de la turbina de geometría variable (VGT) sobre el proceso de regeneración del DPF. El impacto que la estrategia de

presión de sobrealimentación tiene sobre la tasa de consumo de hollín durante la regeneración activa en función de la altitud de conducción se considera con la orientación de las herramientas de modelado.

La discusión de la reducción de la tasa de regeneración en altitud con las estrategias de sobrealimentación estándar ha conducido a la reevaluación de la actuación de la de la turbina de geometría variable (VGT) para condiciones de altitud extrema. Por último, se ha analizado experimentalmente la sensibilidad de la posición del VGT y la tasa de EGR de baja presión (LP-EGR) sobre el comportamiento del motor a cargas parciales en un amplio rango de condiciones ambientales. Los resultados han conducido a la redefinición de la calibración del motor a fin de aumentar la temperatura de entrada del EATS al tiempo que se reduce el consumo específico de combustible.

Palabras clave: Motor de combustión interna; altitud; temperatura ambiente; emisiones; sistemas de postratamiento; optimización del funcionamiento.

Resum

El caràcter cada vegada més estricte de les normatives d'emissions ha provocat el desenvolupament de motors de combustió més respectuosos amb el medi ambient. L'última normativa europea aplicada al sector del transport ha ampliat el rang de condicions d'operació en el qual es realitzen les proves d'homologació. Les variables de temperatura ambient i altitud de conducció són ara requisits addicionals que han de tindre's en compte amb la intenció de reduir la diferència entre el resultat d'aqueixes proves i en condicions de conducció real. La comprensió de l'impacte de les condicions ambientals en el compliment de la normativa pel motor es fonamental per a superar els inconvenients que poden representar per a la resposta del motor amb un ampli impacte en les emissions d'aquest.

A conseqüència de la variació de l'altitud o de la temperatura ambient, els límits dels sistemes de posttractament dels gasos de fuita (EATS) es modifiquen, comprometent el seu funcionament i repercutint en les emissions alliberades a la atmosfera. En el cas concret dels motors Dièsel, els dos EATS més comuns són el catalitzador d'oxidació dièsel (DOC) i el filtre de partícules dièsel (DPF). En aquest context, aquesta tesi doctoral proposa diferents enfocaments per a entendre els principals factors que les condicions ambientals extremes imposen al motor i al funcionament del DOC i del DPF. Una part important d'aquest treball ha consistit en la posada en marxa d'un banc de proves experimental equipat amb un simulador d'altitud i d'una eina de modelització termo fluidodinámica unidimensional (1D) per a una ampla anàlisi.

Després dels resultats experimentals en condicions d'estat estacionari a baixa temperatura, els mapes de contorn de les emissions de CO i HC ha conduí a l'avaluació de com les condicions ambientals extremes repercuteixen en la temperatura d'activació del DOC i en l'eficiència de conversió de les emissions contaminants. L'anàlisi computacinal ha ajudat a elaborar directrius que determinen la contribució de les propietats del flux causades per aquestes condicions. Així mateix, l'efecte de l'aplicació de solucions d'aïllament tèrmic del tubo d'escapament sobre el DOC i la resposta del motor. D'altra banda, s'ha realitzat experimentalment l'actuació de la turbina de geometria variable (VGT) sobre el procés de regeneració del DPF. L'impacte que l'estratègia de pressió de sobrealimentació té sobre la taxa de consum de sutge durant la regeneració activa en funció de l'altitud de conducció es considera amb l'orientació de les eines de modelatge.

La discussió de la reducció de la taxa de regeneració en altitud amb les estratègies de sobrealimentació estàndard ha conduït a la reavaluació de l'actuació de la de la turbina de geometria variable (VGT) per a condicions d'altitud extrema. Finalment, s'ha analitzat experimentalment la sensibilitat de la posició del VGT i la taxa de EGR de baixa pressió (LP-EGR) sobre el comportament del motor a càrregues parcials en un ampli rang de condicions ambientals. Els resultats han conduït a la redefinició del calibratge del motor a fi d'augmentar la temperatura d'entrada del EATS al mateix temps que es redueix el consum específic de combustible.

Paraules clau: Motor de combustió interna; altitud; temperatura ambient; emissions; sistemes de posttractament; optimització del funcionament.

List of publications

The PhD defendant, her supervisor and other I.U.I. CMT-Motores Térmicos (CMT) members are co-authors of the publications mentioned in this Section. Such publications resulted from the research activity performed along the candidate's doctorate, which was supervised by Dr. Pedro Piqueras Cabrera. The defendant performed the relevant experimental activities, results post-processing, analyses and models calibration. Those contents can be found in all publications. The followed methodology was oriented by the defendant's supervisor and discussed with the other co-authors. UPV and CMT laboratories, material and human resources were the foundation of the PhD experimental work. Besides, the computational models licenses were shared by UPV and CMT with the defendant, highlighting the use of the Virtual Engine Model (VEMOD™) software developed by CMT, allowing to perform without any inconvenience the complete modelling work.

The results of the published papers have been compiled, ordered, completed, and further discussed in the present thesis manuscript. The CMT members expertise was shared with the defendant all over the these processes. All segments, analyses, or conclusions from these or any other publication, have been appropriately referred along with the papers.

Nevertheless, for the sake of readiness and to protect the thesis writing style, the publications of this list may not have been specifically cited every time that some of the contents, figures and discussions have been directly imposed from the publications. This disclaimer corrects, compensates, and justifies the fact that the work of the PhD candidate's doctoral thesis are the origin of the innovation component that resulted in the publications mentioned in this section, therefore compiling the thesis.

The PhD candidate is always the last signer of the CMT members in every publication since the protocol among CMT members is signing by seniority order, first the doctors, and last the PhD candidate.

Publications in Journal

[1] J. M. Luján, J. R. Serrano, P. Piqueras, and B. Diesel. "Turbine and exhaust ports thermal insulation impact on the engine efficiency and aftertreatment inlet temperature." *Applied Energy, 240, 409-423* (2019)

[2] J. R. Serrano, P. Piqueras, E. J. Sanchis, and B. Diesel. "A modelling tool for engine and exhaust aftertreatment performance analysis in altitude operation". *Results in Engineering, 4, 100054* (2019)

[3] J. R. Serrano, P. Piqueras, E. J. Sanchis, and B. Diesel. "Analysis of the driving altitude and ambient temperature impact on the conversion efficiency of oxidation catalysts". *Applied Sciences, 11, 1283* (2021)

[4] V. Bermúdez, J. R. Serrano, P. Piqueras, and B. Diesel. "Fuel consumption and aftertreatment thermal management synergy in compression ignition engines at variable altitude and ambient temperature". *Internal Journal of Engine Research, Online First. https://doi.org/10.1177/14680874211035015* (2021)

[5] P. Piqueras, R. Burke, E. J. Sanchis, and B. Diesel. "Fuel efficiency optimisation based on boosting control of the particulate filter active regeneration at high driving altitude". *Under review. Fuel* (2022)

Acknowledgments

In the first place, I wish to thank my supervisor Pedro for his extreme dedication over this entire path, guiding me to accomplish with excellence this scientific work. Secondly, I want to specially thank Enrique, who was there at every moment, shared every single knowledge and was infinitely patient to help me with all issues in modelling and chemistry I had. I also want to thank Maria, my colleague and dearest friend, who shared with me knowledge and good moments, helping me to develop my technical abilities and gave me comfort in all situations over this time. Next, I would like to thank the complete support offered by the CMT staff, counting with the management and secretariat department and the best professors. Thank you Joserra, Paco, Héctor, Pau, Luisme, Jaime, Santi, Roberto, Tiseira, Figo, Bermúdez, Amparo, Habi, Elena...

I want to specially thank Miguel, an excellent engineer, who was the responsible for the experimental installation, and taught me a bunch of things about engines, not to mention the expressions in Valencian and the nice musical taste shared (we still need to go to a Bajoqueta rock concert to listen to "Del l'oli"). Thanks for making the testing days more fun, without you I wouldn't be able to accomplish this work! Additionally, I am immensely grateful to all lab technicians who supported me with testing. A special thanks goes to Vicentón, who shared good humour and helped me with the ECU calibration, also thank you Rafa, Sergi, Fito, Toni, Valentin, Santi, José, Ali and many others...

I would like to warmly thank my office colleagues, who are as well friends, and who in non-pandemic times shared the best moments in the office with nice laughs, music and almuerzos. I will always remember you, my friend, Alex-turbos, who never hesitated in helping me understanding a little bit more about turbochargers, besides of being the best confident. Thank you David, my tennis partner, for all the help with GT-Power and the nice tennis matches. Thank you Roberto, for all the test hours shared in front of the MEDAS, offering me a huge support in understanding its working principles. Thank you my colleagues/friends Vishnu, Sushma, Vitor, Ferran, Johan, Felipe, Lian, Alvin, Fran, Tomas, Santi, ... A special thanks goes to my TFG and TFM students, Mehdi, Ruben, Christian and Ana who helped over this path with nice ideas and hard work, that contributed to build up my thesis.

In addition, I wish to thank all my friends, who have listened to me over this time to talk about thinks that don't make any sense, but who were there to support me and make my days happier, more active and more relaxed. Not to forget the friends I made during my placement in the UoB and my supervisor Richard. You all gave me opportunities to grow, believed in my potential and gave me strength to go through these last troubled months.

Lastly, but above all things, I want to thank with all my heart and return all my love to the ones who are always there, the essentials and indispensables: my family! My big small family who offered me an infinite support and never gave up on me. You are my life and I dedicate this hard work to you! Specially you two, thank you mom and dad, you are the reason I am where I am! Thank you tia Dada for always listening to me talk about the difficulties, thanks to my grannies, aunts, uncles, cousins, and to the brothers and sisters of my heart... And finally, I want to thank the love of my life, Cyril, for everything...

Valencia, January 2022.

"To my family."

Contents

1 Introduction **1**
1.1 Background . . . 2
1.2 Motivation . . . 4
1.3 Objectives . . . 5
1.4 Methodology . . . 6
Bibliography . . . 9

2 Background and state of the art **15**
2.1 Introduction . . . 16
2.2 Main pollutant emissions and their formation in CI engines . . . 17
2.3 ICE response under severe ambient conditions . . . 22
2.4 Impact on EATS boundary conditions . . . 28
2.5 Strategies for EATS operation improvement . . . 34
2.6 Summary . . . 41
Bibliography . . . 42

3 Experimental and computational tools **65**
3.1 Introduction . . . 66
3.2 Experimental facility . . . 67
3.3 Computational tools . . . 77
3.4 Summary and conclusions . . . 97
Bibliography . . . 98

4 Diesel oxidation catalyst operation under extreme ambient conditions **105**
4.1 Introduction . . . 106
4.2 Ambient conditions effect on the DOC performance . . . 107
4.3 Passive strategies for DOC inlet temperature enhancement . . . 126
4.4 Summary and conclusions . . . 157
Bibliography . . . 160

5 DPF active regeneration optimisation in altitude based on air management **165**
5.1 Introduction . . . 166

5.2 Test campaign 167
5.3 Analysis of the experimental and modelling results 169
5.4 VGT position impact on the regeneration rate 180
5.5 Summary and conclusions 186
Bibliography 187

6 Engine and EATS synergy at low partial loads as a function of altitude 189
6.1 Introduction 190
6.2 Test campaign 191
6.3 Engine performance and exhaust temperature 193
6.4 Pollutant emissions 201
6.5 Summary and conclusions 207
Bibliography 209

7 Concluding remarks 211
7.1 Introduction 212
7.2 Main conclusions 213
7.3 Future works 219
Bibliography 223

Global bibliography 225

List of Tables

2.1 *Ambient conditions framework evaluated on RDE tests.* 17

3.1 *Main characteristics of the engine.* 73
3.2 *Main DOC and DPF geometric parameters.* 74
3.3 *Main characteristics of the instrumentation.* 76
3.4 *Main parameters for engine model calibration.* 78

4.1 *Calibration of the DOC reaction rate parameters.* 110
4.2 *Main characteristics of the simulated engine.* 128
4.3 *Simulated engine points.* 128
4.4 *Thermal properties of the materials used in the exhaust ports.* . 134
4.5 *Layer thickness in exhaust ports thermal insulation configuration.* 134
4.6 *Turbine thermal insulation cases.* 140
4.7 *Adiabatic exhaust ports and turbine cases.* 144
4.8 *Feasible cases for exhaust ports and turbine thermal insulation.* 145
4.9 *Selected points from DOC study.* 147

5.1 *DPF pressure drop and soot mass load at the beginning of the regeneration events.* 167
5.2 *Fuel injection profile in regular and regeneration modes at 2000 rpm and pedal 37%.* 169
5.3 *Soot oxidation kinetic parameters in DPF model.* 175

6.1 *Definition of the tested operation conditions.* 192

List of Figures

1.1 *Scheme of the adopted project methodology to investigate extreme ambient conditions effect on the engine and exhaust aftertreatment system response.* 7

2.1 *Common exhaust gas composition percent by volume of Diesel engines [55].* 18
2.2 *The standard Euro 6 automotive aftertreatment system configuration and the main pollutants abated at each step [23].* . . 28
2.3 *Transversal structural illustrations of traditional DPF (left) and schematic three-dimensional (3D) view (right) [163].* 32
2.4 *Four different integrated aftertreatment systems set-ups for a modelling study [194].* 36

3.1 *Picture of the engine placed in the test cell.* 67
3.2 *Picture of the experimental test facility including the altitude simulator on the background.* 68
3.3 *MEDAS connected to the temperature module and to the engine.* 69
3.4 *MEDAS connection with the engine.* 69
3.5 *Layout and conceptual scheme of the altitude simulator featuring the MEDAS coupled to the MTM.* 71
3.6 *Test bench scheme.* 75
3.7 *GT-Power engine model scheme.* 78
3.8 *Measured and modelled results comparison for full load operation from 8 engine speeds ranging from 1000 to 4500 m.* . 79
3.9 *Phases of Diesel combustion [255].* 80
3.10 *Full load measured and modelled results comparison for in-cylinder pressure and rate of heat release at 1500 rpm and 3500 rpm.* 81
3.11 *Prediction of combustion crank angle degree and maximum in-cylinder pressure at full load conditions from 1000 rpm to 4500 rpm.* 82
3.12 *Energy fluxes inside a turbocharger.* 83
3.13 *Scheme of the lumped turbocharger heat transfer model.* 84

3.14 *Prediction of combustion crank angle degree and maximum in-cylinder pressure at full load conditions from 1000 rpm to 4500 rpm.* 85
3.15 *Flow-chart representing the DOC and DPF sub-models processes.* 87
3.16 *Scheme representing the DPF geometry and the sense of the flow [267].* 92

4.1 *Test procedure for every steady-state operating point considered to obtain the CO and HC conversion efficiency contour maps.* . 108
4.2 *Comparison between experimental and modelled HC conversion efficiency evolution along different tested points.* 111
4.3 *CO conversion efficiency as a function of the exhaust mass flow and catalyst inlet temperature.* 112
4.4 *HC conversion efficiency as a function of the exhaust mass flow and catalyst inlet temperature.* 114
4.5 *Adsorption and oxidation contributions to HC conversion efficiency as a function of the exhaust mass flow and catalyst inlet temperature.* 116
4.6 *Dwell time as a function of the exhaust mass flow and catalyst inlet temperature.* 117
4.7 O_2 *partial pressure as a function of the exhaust mass flow and catalyst inlet temperature.* 118
4.8 *Equivalence ratio and LP-EGR rate as a function of the exhaust mass flow and catalyst inlet temperature.* 119
4.9 *Engine-out CO partial pressure as a function of the exhaust mass flow and catalyst inlet temperature.* 121
4.10 *Engine-out HC partial pressure as a function of the exhaust mass flow and catalyst inlet temperature.* 121
4.11 *Inhibition term as a function of the DOC inlet temperature and ambient conditions.* 122
4.12 *Progressive CO and HC light-off curves variation from warm sea-level to cold altitude case considering dwell time and reactants partial pressure separately.* 124
4.13 *Scheme of the engine model in GT-Power.* 129
4.14 *Comparison between experimental data and modelled result for the selected operating points.* 130
4.15 *Temperature and exergy rate variation across the exhaust line in the baseline configuration.* 131
4.16 *Representation of exhaust ports thermal insulation cases.* 133

4.17 *VGT position, VGT inlet pressure and PMEP at low and high load operating points as a function of the exhaust ports thermal insulation configuration.* 135
4.18 *Indicated efficiency and maximum in-cylinder temperature at low and high load operating points as a function of the for exhaust ports thermal insulation configuration.* 136
4.19 *Temperature variation across the exhaust line as a function of the exhaust ports thermal insulation configuration and the engine operation points.* 137
4.20 *Aftertreatment inlet temperature and BSFC variation at low and high load operating points as a function of the exhaust ports thermal insulation configuration.* 138
4.21 *Heat power balance in the turbocharger for the baseline configuration (Case #1).* 140
4.22 *Heat power balance in the turbocharger as a function of the turbine thermal insulation configuration and the operating point.* 141
4.23 *VGT position, inlet turbine pressure and PMEP at low and high load operating points as a function of the turbine thermal insulation configuration.* 142
4.24 *Aftertreatment inlet temperature and BSFC variation at low and high load operating points as a function of the turbine thermal insulation configuration.* 143
4.25 *Aftertreatment inlet temperature and BSFC variation as a function of different adiabatic configurations in the exhaust ports and the turbine.* 145
4.26 *Aftertreatment inlet temperature and BSFC variation at low and high load operating points as a function of different feasible exhaust ports and turbine thermal insulation configurations.* . . 146
4.27 *Comparison between model and experiment for a selected points from the DOC study.* 148
4.28 *DOC inlet temperature at 0 m and 20° C as a function of the engine speed and BMEP.* 150
4.29 *CO conversion efficiency at 0 m and 20° C as a function of the engine speed and BMEP.* 151
4.30 *HC oxidation conversion efficiency at 0 m and 20° C as a function of the engine speed and BMEP.* 153
4.31 *DOC inlet temperature at 2500 m and -7° C as a function of the engine speed and BMEP.* 154

4.32 *CO conversion efficiency at 2500 m and -7°C as a function of the engine speed and BMEP.* 155
4.33 *HC oxidation conversion efficiency at 2500 m and -7°C as a function of the engine speed and BMEP.* 156
4.34 *Summary of impact on VGT outlet temperature and BSFC of (a) adiabatic cases and (b) feasible solutions for exhaust port and turbine thermal insulation.* 159

5.1 *Fuel injection profile and in-cylinder pressure in (a) regular and (b) regeneration modes at 2000 rpm and pedal at 37 %.* 168
5.2 *Actuation on VGT and LP-EGR due to active regeneration strategy and effects on engine performance, air mass flow and boost pressure as a function of altitude and initial DPF pressure drop.* 170
5.3 *Exhaust flow properties at VGT and DPF inlet as a function of the engine operation mode, altitude and initial DPF pressure drop.* 172
5.4 *Experimental and modelled DPF pressure drop and outlet gas temperature as a function of altitude during active regeneration processes with initial DPF pressure drop of 80 and 230 mbar.* . . 174
5.5 *Soot depletion rate and cumulative oxidised soot mass as a function of altitude during active regeneration processes with initial DPF pressure drop of (a) 80 mbar and (b) 230 mbar.* . . . 176
5.6 O_2 *surface coverage as a function of the* O_2 *partial pressure and the substrate temperature.* 177
5.7 *Evolution of* O_2 *surface coverage as a function of altitude during active regeneration processes with initial DPF pressure drop of (a) 80 mbar and (b) 230 mbar.* 178
5.8 *Tailpipe gaseous pollutant emissions and engine-out opacity as a function of the engine operation mode, altitude and initial DPF pressure drop.* 179
5.9 *Engine performance sensitivity to VGT position at 1300 m and 2500 m operating in regeneration mode.* 181
5.10 *Sensitivity to VGT position of VGT and DPF inlet temperatures, fuel post-injection efficiency, DPF inlet* O_2 *partial pressure and DPF dwell time at 1300 m and 2500 m operating in regeneration mode.* 183

5.11 *DPF pressure drop and outlet temperature at VGT optimised opening at altitude compared the altitude and sea-level baseline conditions.* 184
5.12 *Tailpipe gaseous pollutant emissions and engine-out opacity as a function of the engine operation mode, altitude and initial DPF pressure drop.* 185

6.1 *Air mass flow, compressor pressure ratio and VGT position corresponding to 1250 rpm & 3 bar BMEP at 25° C as a function of the altitude.* 194
6.2 *Engine torque and BSFC corresponding to 1250 rpm & 3 bar BMEP at 25° C as a function of the altitude.* 195
6.3 *VGT expansion ratio, inlet temperature and outlet temperature corresponding to 1250 rpm & 3 bar BMEP at 25° C as a function of the altitude, boost pressure and LP-EGR rate.* 196
6.4 *BSFC and VGT outlet temperature at 25° C in ambient temperature as a function of the altitude, boost pressure and LP-EGR rate.* 197
6.5 *BSFC and VGT outlet temperature at 45° C in ambient temperature as a function of the altitude, boost pressure and LP-EGR rate.* 199
6.6 *BSFC and VGT outlet temperature at -10° C in ambient temperature as a function of the altitude, boost pressure and LP-EGR rate.* 200
6.7 *Engine-out* NO_x *emission and opacity as a function of the boost pressure and LP-EGR rate for sea-level at 25° C and 2500 m at -10° C.* 201
6.8 *CA10 and CA50 as a function of the boost pressure and LP-EGR rate for sea-level at 25° C and 2500 m at -10° C.* . . . 202
6.9 *Engine-out CO emission and CO conversion efficiency as a function of the boost pressure and LP-EGR rate for sea-level at 25° C and 2500 m at -10° C: (a) 1250 rpm & 3 bar BMEP, (b) 2000 rpm & 6 bar BMEP and (c) 3000 rpm & 2 bar BMEP.* 204
6.10 *ATS mass flow as a function of the boost pressure and LP-EGR rate for sea-level at 25° C and 2500 m at -10° C: (a) 1250 rpm & 3 bar BMEP, (b) 2000 rpm & 6 bar BMEP and (c) 3000 rpm & 2 bar BMEP.* 206

6.11 *Engine-out HC emission and HC conversion efficiency as a function of the boost pressure and LP-EGR rate for sea-level at 25° C and 2500 m at -10° C: (a) 1250 rpm & 3 bar BMEP, (b) 2000 rpm & 6 bar BMEP and (c) 3000 rpm & 2 bar BMEP.* 208

List of symbols

Latin characters

A	air node
A	catalyst area
C	compressor node
c_p	specific heat capacity
c_w	thermal capacitance
d_c	unit collector diameter
d_p	mean pore diameter
D_s	soot diffusion coefficient
d_s	soot particle diameter
E_{a_r}	activation energy of oxidation reaction r
E_f	filtration efficiency
f_{sp}	fraction of porous wall thickness where the soot is collected
F_w	viscous loss coefficient
f_w	penetrated fraction of porous wall thickness
GAS	gas node
G_{ox}	oxidation inhibition term
H	enthalpy
h	specific enthalpy
H_1	1^{st} internal node between turbine and compressor
H_2	2^{nd} internal node between turbine and compressor
H_3	3^{rd} internal node between turbine and compressor
H_f	enthalpy of formation
i	gas or internal canning surface
IC	compressor inlet
IT	turbine inlet
j	total reactant species
k	permeability
k_m	mass transfer coefficient
k_r	kinetic constant in reaction r
K	Kuwabara's hydrodynamic factor
K_B	Boltzmann constant
K_{S_n}	equilibrium constant of adsorption process of species n

L_{in}	monolith's inlet channel length
L_{mon}	monolith length
L_{out}	monolith's outlet channel length
M	molar weight of chemical species
$\dot{m}$	mass flow
M_C	carbon molecular
m_s	soot mass
$\dot{n}$	gas mole flow
n_n	moles of species n
N_R	interception parameter
OC	compressor outlet
$\mathrm{OC_s}$	isentropic compressor outlet
OT	turbine outlet
$\mathrm{OT_s}$	isentropic turbine outlet
p	gas pressure
p_{amb}	ambient pressure
p_n	partial pressure of species n
Pe	Peclet number
P_f	pre-exponential factor of the oxidation reaction with reactant n
P_{S_n}	pre-exponential factor of adsorption process of reactant n
Q	volumetric flow rate
$\dot{Q}$	heat flow
$\dot{q}_r$	power released by soot oxidation
r	equivalent thermal resistance
R	reaction rate
$\Re$	universal gas constant
Re	Reynolds number
s	specific entropy
S_p	soot specific surface
S_c	sticking coefficient
T	turbine node
T	temperature
t	time
T_w	substrate temperature
u	gas velocity
u_w	filtration velocity
V	monolith volume
v_i	linear fluid velocity

W	water
w	monolith's wall thickness
$\dot{W}$	mechanical power
X	molar fraction
x	axial coordinate
Y	mass fraction
z	radial coordinate

Greek characters

α	monolith's cell size
α_n	completeness index of reactant n
Δ	variation
ε	porosity
η_D	Brownian efficiency
η_{DR}	single unit collector efficiency
η_{int}	diffusion efficiency
η_R	interception efficiency
μ	dynamic viscosity
ν	stoichiometric coefficient of species n
θ	reactant n surface coverage
χ	shape factor
ψ	specific storage capacity
Ψ	maximum moles adsorpted in the active site
ρ	density
σ	cell density
ς	catalyst pressure drop coefficient
τ	dwell time
$\dot{\omega}_n$	depletion rate of every gaseous reactant

Sub- and Superscripts

0	clean conditions
a	adiabatic conditions
ads	adsorption
amb	ambient
ash	ash
atm	atmosphere
B/Amb	referred to flux transferred from node B to the ambient
B/C	referred to flux transferred from node B to the compressor housing
B/Oil	referred to flux transferred from node B to oil circuit
C	compressor
c	collector unit
C/Amb	referred to flux transferred from compressor to the ambient
C/Air	referred to flux transferred from compressor to the air
cat	catalyst
$cell$	cell unit
des	desorption
ef	effective
exh	exhaust
ext	external
$filt$	filtration
Gas/T	referred to flux transferred from gas to turbine housing
gas	exhaust gas
in	inlet
int	internal
$mech$	mechanical losses
mon	monolith
n	species n
pl	particulate layer
Oil	oil node
out	outlet
ox	oxidation
reg	regeneration
$regular$	regular operation mode
S_n	referred to adsorption process of species n
s	referred to soot
sur	surface
T	turbine

T/Amb	referred to flux from turbine to the ambient
T/B	referred to flux from turbine to node B
w	porous wall
wc	washcoat

Acronyms

1D	one-dimensional
3D	three-dimensional
AFR	air-fuel ratio
AOC	ammonia oxidation catalyst
ASC	ammonia slip catalyst
BMEP	brake mean effective pressure
BSFC	brake specific fuel consumption
CA10	crank angle at 10% of burned mass
CA50	crank angle at 50% of burned mass
CDPF	catalyzed diesel particulate filter
CF	conformity factor
CH_4	methane
CI	compression ignition
CO	carbon monoxide
CO_2	carbon dioxide
CO_L	carbon monoxide at low level
CO_H	carbon monoxide at high level
CRT	continuous regenerating trap
CSF	catalyzed soot filter
DI	direct injection
DOC	diesel oxidation catalyst
DPF	diesel particulate filter
EATS	exhaust aftertreatment systems
ECU	engine control unit
EEPS	engine exhaust particle sizer
EGR	exhaust gas recirculation
EUDC	extra urban driving cycle
FBC	fuel borne catalysts
FTP	fedetal test procedure
GPF	gasoline particulate filter
GDI	gasoline direct injection
H_2O	water

HC	hydrocarbons
HCCI	homogeneous charge compression ignition
HP-EGR	high pressure EGR
HSDI	high-speed direct injection
ICE	internal combustion engine
ISA	international standard atmosphere
IVC	intake valve closing
LNT	lean NO_x trap
LHV	lower heating value
LHTESS	latent heat thermal energy storage system
LP-EGR	low pressure EGR
MEDAS	multifunction efficient dynamic altitude simulator
MTM	MEDAS temperature module
NEDC	new european driving cycle
N_2	nitrogen
NH_3	ammonia
NO	nitric oxide
NO_2	nitrogen dioxide
NO_x	nitrogen oxides
O_2	oxygen
OEM	original equipment manufacturer
PCM	phase change materials
Pd	palladium
PID	proportional-integral-derivative controller
PSD	particle size distribution
PF	particulate filter
PM	particulate matter
PM10	particulate matter smaller than 10 μm
PM2.5	particulate matter smaller than 2.5 μm
PN	particle number
PNA	passive NO_x adsorber
PMEP	pumping mean effective pressure
Pt	platinum
RDE	real driving emission
RoHR	rate of heat release
SCF	Stokes-Cunningham factor
SCR	selective catalytic reduction
SCRf	wall-flow particulate filter with selective catalytic reduction function

SOC	start of combustion
SOI	start of the injection
TDC	top dead centre
TES	thermal energy storage
VGT	variable geometry turbine
VVT	variable valve timing
Y_2O_3	yttrium oxide
Y_2O_3	yttrium oxide
YSZ	yttria-stabilized zirconia
ZrO_2	zirconia
WCAC	water charge air cooler
WLTC	worldwide harmonized light vehicle test cycle
WLTP	worldwide harmonized light vehicle test procedure

Chapter 1

Introduction

Contents

1.1 Background **2**
1.2 Motivation **4**
1.3 Objectives **5**
1.4 Methodology **6**
Bibliography **9**

1.1 Background

The reciprocating internal combustion engines (ICEs) have been in constant development over the years. Beginning in the year of 1877, when the four-stroke internal combustion engine started to be released [6], up to nowadays, when the ICEs have reached what was back then unimaginable. About 15 years after Otto's invention, in 1861, the Diesel engine idea came up: the fuel should be injected in a hot environment generated by the gas high compression ratio without requiring spark ignition [7, 8]. This technology represented a more efficient form of combustion, leading to its mass-production for passenger car commercialization, which started around 1936 by Mercedes-Benz [9].

The light-duty engine performance continued to improve, specially by the development of key components like the turbocharger, introduced in 1962 [10], or the common-rail fuel system technique, which was first sold for public use in 1995 [11]. Those were complemented by great advances in combustion and electronic control systems [12], for instance the variable compression ratio powered by electric powertrains [13] and the cam-less valve trains techniques [14]. The advances in the automotive industry have continuously been targeted to engine efficiency. However, in the mid 1900, the rapid increase of motor vehicles in cities due to economic and population growth led to the awareness of fossil fuel reserves depletion and the rise in air pollution [15]. The latter causes serious impacts on public health and on the environment, representing both local and global effects. The global warming stands out as a result of the greenhouse gases effect, being responsible for the increase of the world's temperature from 0.6 to 0.9°C between 1906 and 2005 [16].

Carbon dioxide (CO_2), the main product of the combustion of fossil fuels, represents the largest amount among the greenhouse gases, besides of nitrous oxide, and fluorinated gases [17]. Besides, the combustion in Diesel engines originates further pollutant emissions, namely the nitrogen oxides (NO_x), carbon monoxides (CO), unburned hydrocarbons (HC), soot and particulate matter (PM) [18]. These emissions affect human health, mainly respiratory problems and diseases that vary from coughing and pulmonary function alteration to lung cancer [19], and the environment. Facing this challenge, the automotive sector started employing different technologies aiming to contain the release of these pollutant species to the environment.

Acting directly on the control of the parameters governing the combustion process, such as injection pressure and timing, is a way to minimize the pollutants formation, letting the engine performance as unaltered as possible [20]. Another widely technique used is the addition of recycled exhaust gases, whose technology is known as exhaust gas recirculation. Its main advantage lies on NO_x reduction by decreasing the combustion gas temperature achieved in the cylinder chamber, representing however a significant increase in particulate exhaust emissions [21].

In this regard, exhaust aftertreatment systems came up as complex and sophisticated devices that accounted for physical and chemical processes to promote emissions abatement after the cylinder combustion process is over. A modern automotive aftertreatment configuration counts with a DOC to promote the HC and CO oxidation into water (H_2O) and CO_2, a DPF, responsible for PM filtration, and a final system destined to the NO_x abatement, which is usually a selective catalytic reduction (SCR) system. Another alternative for NO_x reduction is the use of lean NO_x traps (LNTs), that works absorbing the NO_x that is formed under oxygen excess environment in lean mixtures, but with the drawback of being less efficient and more expensive [22]. Not to mention the multiple configurations put in practice nowadays, like the ammonia slip catalyst (ASC) entitled to oxidize the excess of ammonia (NH_3) [23], the HC traps, the passive NO_x adsorbers (PNAs), etc.

As a part of the endeavour of promoting clean and energy-efficient road transportation, governments from different sites of the world continuously implement stringent legislation for type approval vehicle emission [24]. Successive Euro emissions standards since their implementation in 1992 [25] until the current Euro 6 [26] have led to significant reduction of vehicle pollutants. To verify the vehicles compliance with the emissions threshold, they must be submitted and approved on type-approval tests integrated nowadays into the worldwide harmonised light vehicle test procedure (WLTP) [27].

With the view of real-world driving emissions being higher than those measured during the type approval tests, the real riving emission (RDE) tests were put into force. For those tests, which are intended to reduce the gap between laboratory and real driving emissions, the vehicle must be driven under various conditions: up- and down-hill; highways; motorways; urban roads; count with additional payload to the vehicle; and, finally,to drive under different ambient conditions, which include altitude and temperature [26].

For the current Euro 6 standards, the contemplated altitudes vary from sea-level to 1300 meters and the boundary temperatures are in a range from -7 ºC up to 35°C [26]. These requirements lead to the interest for a better understanding of the engine response when subjected to such ambient conditions, making it possible to set up its optimum calibration [28]. Knowing that the environmental characteristics affect not only the engine operation, but also modify the boundary conditions of the EATS, a deep investigation on the impact that ambient conditions have on the processes happening in the EATS, and consequently the tailpipe emissions, is endorsed [29].

1.2 Motivation

Against the background of climate changing and noting the energy policies turning eyes towards sustainable transportation solutions, the vehicles propelled by thermal engines are still the favourite choice amongst the customer [30]. Moreover, ICEs have never been cleaner and capable of emitting less pollutants over a lifetime as nowadays [31]. In this regard, it is vital from the part of this automotive sector to carry on with constant research and innovation.

Compatible with the current legislation, as described in the previous Section, and the European geography [32] and weather conditions, the need for the engine performance evaluation under high altitude combined with a wide temperature range is paramount [33]. The engine performance is very sensitive to the ambient conditions variation, and may result in a negative impact on emissions and fuel consumption [34].

From one side, several studies have so far covered the influence of the high altitude [35] and cold temperature [36] on BSFC [37] and emissions [38] through RDE or laboratory tests [39]. Calibration differences such as EGR settings [40] were important points to notice in order to lead to the optimisation of the overall engine operation. However, it is clear that to concentrate the effort on understanding and improving the engine processes is not enough, since the low ambient temperature additionally modifies the EATS boundary conditions [41]. The lower ambient pressure at higher altitude affects the turbocharger [42] and further engine processes[43], finally impacting on the EATS inlet gas flow conditions from temperature, which emerges as the main parameter governing the aftertreatment response, to pollutants partial pressure or dwell time within the monolithic reactors [44].

In order to assure a high CO and HC emissions conversion efficiency upon flowing through the DOC, a minimum working temperature is required to favour the oxidation processes happening in it [45]. Concerning the DPF, complementary to the soot filtration, the DPF regeneration is imperative for an adequate engine operation to avoid an excessive increase of back pressure, loss of engine power, or even filter clogging. This process also relies on the thermal conditions, which are, in turn, influenced by the DOC, usually placed upstream of the DPF.

The evaluation of these two commonly employed EATS components behaviour under different temperature and altitude conditions gained a great importance. In this context, understanding how the specific engine partials fundamental for the EATS functioning can be affected by ambient conditions, influencing the EATS operation is uncovered topic nowadays. Furthermore, the possibilities to optimize the engine operation along with the EATS under such conditions unleashes a massive potential to be covered in this doctoral thesis.

1.3 Objectives

The aim of this work is to contribute to the evaluation of the impact of extreme ambient conditions, specifically pressure and temperature, on the engine operation, with focus on the aftertreatment systems performance. This is accomplished by going through several partial objectives listed below:

- A comprehensive literature review must be conducted in order to establish the guidelines for this work. This corresponds to the first partial objective. The current placement of the thesis' topic on the global context in terms of effect of ambient pressure and temperature on the engine performance and emissions must be conducted, besides of carrying out a review of the main parameters responsible for the DOC and the DPF operation.
- The second partial objective is to understand the behaviour of the EATS when the engine operates in altitude and at different ambient temperature conditions. The focus will be driven to the DOC response observed in terms of CO and HC conversion efficiency. In the case of the DPF response, the active regeneration process will be studied.

- The third partial objective is the identification of the main agents responsible for the differences in the EATS response when operating in altitude and at different ambient temperature conditions. The engine response in terms of EATS inlet gas properties, as temperature and mass flow, must be conducted.
- The fourth partial objective is the understanding of ambient pressure effect on pollutants partial pressure that encounter the EATS. This concept supports on the previous objective, since the pollutants partial pressure additionally affect the DOC conversion efficiency and the soot depletion rate during the DPF active regeneration.
- The fifth partial objective is focused on the understanding of the sensitivity of the engine and aftertreatment response to the air management strategy under different ambient conditions.
- The sixth and final partial objective is to propose both passive and active strategies oriented to the increase of the EATS thermal level and contribute to the improvement of their operation processes under high altitude and different ambient temperatures. Those strategies must lead to pollutant emissions reduction while looking for benefits on the engine performance.

1.4 Methodology

In order to achieve the stipulated goals, a structured working method was followed. Figure 1.1 summarizes in a flow diagram the main steps carried out during this thesis. The exposed blocks are directly related to each Chapter of this document, which will be commented in the sequence.

Based on the presented scheme, Chapter 1 aims to discuss the first block, corresponding to present the initial issue approached in this work. It does so by exposing the problem and pointing out the objectives and its inherent methodology.

Chapter 2 is dedicated to the correspondent literature review, where essential concepts and past studies are brought into focus. The impact caused by the extreme ambient conditions in the engine performance and in the EATS boundary conditions is described, with reference to the literature.

Besides, the main aspects that dictate the specific studied EATS operation are reviewed. Significant gaps on the EATS operation influence by ambient conditions and engine performance improvement were identified. Additionally this Chapter, results of the EATS operation improvement are considered for the implementation of further techniques.

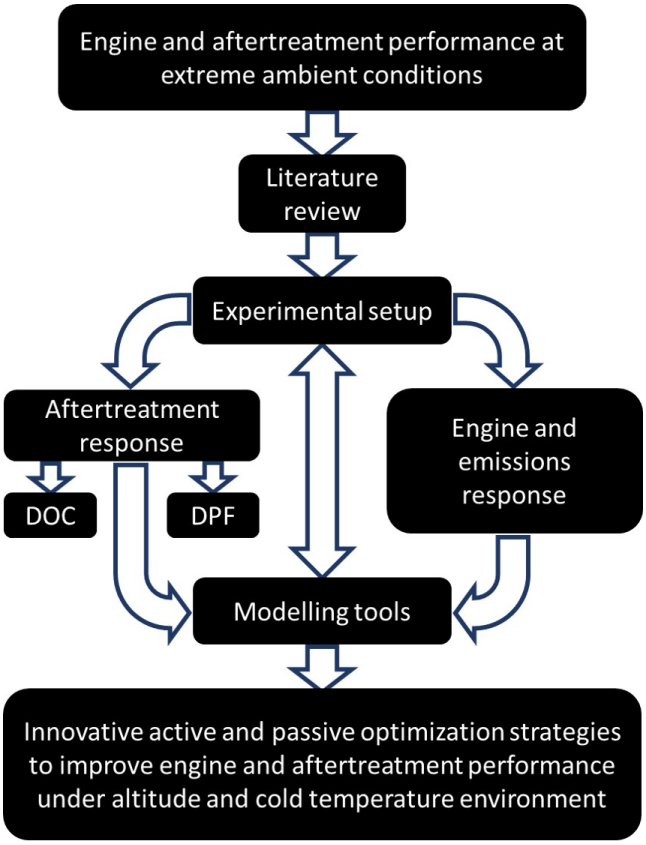

Figure 1.1: Scheme of the adopted project methodology to investigate extreme ambient conditions effect on the engine and exhaust aftertreatment system response.

Both the experimental setup and the employed modelling tools are presented in Chapter 3. A detailed description of the adopted altitude simulator working principles is provided, besides of the full equipment used in the engine test cell, highlighting the engine specifications including aftertreatment system devices that count for a DOC and a selective catalytic

reduction function (SCRf). This last mentioned device is, in fact, one of the aftertreatment systems incorporated in the engine studied in the current doctoral thesis together with the DOC. However, as will be mentioned further, the application is simplified to a DPF do to the absence of the urea injecting unit. The second part of Chapter 3 brings a complete overview of the adopted modelling tools, outlining physical and chemical processes that happen in each particular system.

The body of this doctoral thesis is covered from Chapters 4 to 6. The specific physical and chemical response of the most elemental aftertreatment devices in compression ignition (CI) engines when submitted to extreme ambient conditions operation is analysed in Chapters 4 and 5. Based on experimental results, the impact of altitude and ambient temperature on the CO and HC conversion efficiencies of a DOC catalyst are discussed in Chapter 4. The key factors responsible for the light-off deterioration in extreme ambient conditions are pointed out and evaluated. Besides, different passive solutions for the DOC inlet temperature enhancement as a way to maximize its functionality and the effects on engine performance are covered by means of the modelling tools.

In Chapter 5, the effect of altitude is considered on the DPF active regeneration, evaluating the differences in DPF pressure drop over the regeneration process. The root causes of the soot depletion rate differences are discussed from experimental and modelling results. The conclusions are the guide to conduct successfully the experimental optimisation of the DPF regeneration by means of the air management recalibration during the regeneration event with focus on fuel consumption and emissions balance.

The engine response under different ambient pressures and temperatures at low partial loads, covering the optimal calibration, is finally addressed in Chapter 6. The effect of air management engine calibration in terms of LP-EGR rate and boost pressure is addressed for the optimisation of the engine performance, emissions and aftertreatment boundaries in partial load under several ambient conditions.

Lastly, the main achieved conclusions are brought into line in Chapter 7, opening the way for future works based on the analysis and proposals exposed in this doctoral thesis.

Bibliography

[6] N. Otto. "Improvement in gas-motor engines". Pat. US194047A. 1877 (cit. on p. 2).

[7] R. Diesel. "Internal combustion engine". Pat. US608845A. July 15, 1895 (cit. on p. 2).

[8] F. Sass. *Geschichte des deutschen Verbrennungsmotorenbaus von 1860 bis 1918*. German. Springer, 1962 (cit. on p. 2).

[9] O. von Fersen. *Ein Jahrhundert Automobiltechnik: Personenwagen*. German. Springer, 1986 (cit. on p. 2).

[10] BorgWarner. *Turbo Systems History. Available in: https://www.borgwarner.com/technologies/boosting-technologies. (accessed on 24 November 2021)* (cit. on p. 2).

[11] *Car Throttle. CRDI (common rail direct injection) and its history. Available in: https://www.carthrottle.com/post/y88zde8/. (accessed on 24 November 2021)* (cit. on p. 2).

[12] B. Stewart. *The 15 most important automotive tech milestones of the last 25 years. Available in: https://www.popularmechanics.com/cars/g2778/most-important-automotive-tech-milestones/. (accessed on 24 November 2021)*. Ed. by PopularMechanics. 2016 (cit. on p. 2).

[13] K. Wittek, F. Geiger, and M. G. Justino Vaz. "Characterization of the system behaviour of a variable compression ratio (VCR) connecting rod with eccentrically piston pin suspension and hydraulic moment support". *Energy Conversion and Management, 213, 112814* (2020) (cit. on p. 2).

[14] Z. Dimitrova, M. Tari, P. Lanusse, F. Aioun, and X. Moreau. "Development and control of a camless engine valvetrain". *IFAC-Papers OnLine, 52 (5), 399-404* (2019) (cit. on p. 2).

[15] EPAGOV. *History of reducing air pollution from transportation in the United States. Available in: https://www.epa.gov/transportation-air-pollution-and-climate-change/accomplishments-and-success-air-pollution-transportation. (accessed on 24 November 2021)*. 2021 (cit. on p. 2).

[16] *Earth Observatory NASA. Global warming. Available in: https://earthobservatory.nasa.gov/features/GlobalWarming/page2.php. (accessed on 24 November 2021).* June 3, 2010 (cit. on p. 2).

[17] S. V. Venkataraman, S. Iniyan, and R. Goic. "A review of climate change, mitigation and adaptation". *Renewable and Sustainable Energy Reviews, 16 (1), 878-897* (2012) (cit. on p. 2).

[18] I. A. Reşitoğlu, K. Altinişik, and A. Keskin. "The pollutant emissions from Diesel-engine vehicles and exhaust aftertreatment systems". *Clean Technologies and Environmental Policy, 17, 15-27* (2015) (cit. on pp. 2, 17, 20).

[19] W. K. C. Morgan, R. B. Regerf, and D. M. Tucker. "Health effects of Diesel emissions". *The Annals of Occupational Hygiene, 41 (6), 643-658* (1997) (cit. on p. 2).

[20] J. N. S. Vianna, A. V. Reis, A. B. d. S. Oliveira, A. G. Fraga, and M. T. de Sousa. "Reduction of pollutants emissions on SI engines - accomplishments with efficiency increase". *Journal of the Brazilian Society of Mechanical Sciences and Engineering, 27, 3* (2005) (cit. on p. 3).

[21] N. Ladommatos, S. Abdelhalim, and H. Zhao. "The effects of exhaust gas recirculation on diesel combustion and emissions". *Internal Journal of Engine Research, 1, 107-126* (2000) (cit. on p. 3).

[22] TOTAL. *TOTAL explains how the Lean* NO_x *Trap (LNT) works, the alternative to the selective catalytic reduction (SCR). Available in: https://www.lubricants.total.com/news-press-releases/system. (accessed on 24 November 2021).* 2017 (cit. on p. 3).

[23] M. Soleimani, F. Campean, and D. Neagu. "Reliability challenges for automotice aftertreatment systems: A state-of-the-art perspective". *Procedia Manufacturing 16, 75-82* (2018) (cit. on pp. 3, 28).

[24] K. Kuklinska, L. Wolska, and J. Namiesnik. "Air quality policy in the U.S. and the EU - a review". *Atmospheric Pollution Research 6, 129-137* (2015) (cit. on p. 3).

[25] *Euro 1 emissions legislation. 91/441/EEC Council Directive 91/441/EEC of 26 June 1991 amending Directive 70/220/EEC on the approximation of the laws of the Member States relating to measures to be taken against air pollution by emissions from motor*

vehicles. Available in: eur-lex.europa.eu. (accessed on 24 November 2021). 1991 (cit. on p. 3).

[26] *Commission Regulation (EU) 2017/1154 of 7 June 2017 amending Regulation (EU) 2017/1151 supplementing Regulation (EC) No 715/2007 of the European Parliament and of the Council on type-approval of motor vehicles with respect to emissions from light passenger and commercial vehicles (Euro 5 and Euro 6) and on access to vehicle repair and maintenance information, amending Directive 2007/46/EC of the European Parliament and of the Council, Commission Regulation (EC) No 692/2008 and Commission Regulation (EU) No 1230/2012 and repealing Regulation (EC) No 692/2008 and Directive 2007/46/EC of the European Parliament and of the Council as regards real-driving emissions from light passenger and commercial vehicles (Euro 6) (Text with EEA relevance)*. 2017 (cit. on pp. 3, 4, 220).

[27] *Commission Regulation (EU) 2017/1151 of 1 June 2017 supplementing Regulation (EC) No 715/2007 of the European Parliament and of the Council on type-approval of motor vehicles with respect to emissions from light passenger and commercial vehicles (Euro 5 and Euro 6) and on access to vehicle repair and maintenance information, amending Directive 2007/46/ EC of the European Parliament and of the Council, Commission Regulation (EC) No 692/2008 and Commission Regulation (EU) No 1230/2012 and repealing Commission Regulation (EC) No 692/2008 (Text with EEA relevance)*. 2017 (cit. on pp. 3, 16, 73).

[28] P. Arya, F. Millo, and F. Mallamo. "A fully automated smooth calibration generation methodology for optimization of latest generation of automotive Diesel engines". *Energy 178, 1, 334-343* (2019) (cit. on p. 4).

[29] J. Gómez. "Development of an altitude simulator and analysis of the performance and emissions of turbocharged Diesel engines at different altitudes". PhD thesis. UPV, 2018 (cit. on pp. 4, 72).

[30] *Green Car Congress. Available in: https://www.greencarcongress.com/2020/05/20200513-acea.html. (accessed on 24 November 2021)*. 2020 (cit. on p. 4).

[31] J. R. Serrano, R. Novella, and P. Piqueras. "Why the development of internal combustion engines is still necessary to fight against global climate change from the perspective of transportation". *Applied Sciences, 9 (21), 4597* (2019) (cit. on p. 4).

[32] *UNEP - World Conservation Monitoring Centre. The delineation of European mountain areas. Available in: https://ec.europa.eu/regional_policy/sources/docgener/studies/pdf/montagne/mount4.pdf (accessed on 24 November 2021).* 2000 (cit. on pp. 4, 22).

[33] J. R. Serrano, P. Piqueras, A. Abbad, R. Tabet, S. Bender, and J. Gómez. "Impact on reduction of pollutant emissions from passenger cars when replacing Euro 4 with Euro 6d Diesel engines considering the altitude influence". *Energies, 12, 1278-1302* (2019) (cit. on pp. 4, 16, 26, 39).

[34] S. D'Ambrosio, A. Ferrari, E. Spessa, L. Magroa, and A. Vassallo. "Impact on performance, emissions and thermal behavior of a new integrated exhaust manifold cylinder head Euro 6 Diesel engine". In: *SAE Technical Paper 2013-24-0128.* 2013 (cit. on p. 4).

[35] H. Giraldo and J. I. Huertas. "Real emissions, driving patterns and fuel consumption of in-use diesel buses operating at high altitude". *Transportation Research Part D, 77, 21-36* (2019) (cit. on pp. 4, 26).

[36] J. M. Luján, H. Climent, S. Ruiz, and A. Moratal. "Influence of ambient temperature on Diesel engine raw pollutants and fuel consumption in different driving cycles". *Internal Journal of Engine Research, 20 (8-9), 877-888* (2019) (cit. on pp. 4, 23).

[37] Y. Wang, Y. Ge, J. Wang, X. Wang, H. Yin, L. Hao, and J. Tan. "Impact of altitude on the real driving emission (RDE) results calculated in accordance to moving averaging window (MAW) method". *Fuel, 277, 117929.* (2020) (cit. on pp. 4, 26).

[38] H. Zhou, H. Zhao, Q. Fenf, Z. Yin, J. Li, K. Qin, M. Li, and L. Cao. "Effects of environmental parameters on real-world NO_x emissions and fuel consumption for heavy-duty diesel trucks using an OBD approach". In: *SAE Technical Paper 2018-01-1817.* 2018 (cit. on pp. 4, 27).

[39] A. Ramos, R. García-Contreras, and O. Armas. "Performance, combustion timing and emissions from a light duty vehicle at different altitudes fueled with animal fat biodiesel, GTL and diesel fuels". *Applied Energy, 182, 507-517* (2016) (cit. on pp. 4, 26, 27, 120).

[40] L. Yu et al. "Experimental investigation of the impact of biodiesel on the combustion and emission characteristics of a heavy duty Diesel engine at various altitudes". *Fuel, 115, 220-226* (2014) (cit. on pp. 4, 26, 27).

[41] J. Gao, A. Tian G.and Sorniotti, A. E. Karci, and R. Di Palo. "Review of thermal management of catalytic converters to decrease engine emissions during cold start and warm up". *Applied Thermal Engineering, 147, 177-187* (2019) (cit. on pp. 4, 29).

[42] M. Lapuerta, O. Armas, J. R. Agudelo, and C. A. Sánchez. "Study of the altitude effect on internal combustion engine operation. Part 1: Performance". *Información Tecnológica, 17, 5* (2006) (cit. on p. 4).

[43] L. Shen and Y. Shen. "Combustion process of Diesel engines at regions with different altitude". In: *SAE Technical Paper 950857*. 1995 (cit. on pp. 4, 26).

[44] M. R. Hamedi, O. Doustdar, A. Tsolakis, and J. Hartland. "Thermal energy storage system for efficient diesel exhaust aftertreatment at low temperatures". *Applied Energy, 235, 874-887* (2019) (cit. on pp. 4, 37, 126).

[45] P. Piqueras, A. García, J. Monsalve-Serrano, and M. J. Ruiz. "Performance of a diesel oxidation catalyst under diesel-gasoline reactivity controlled compression ignition combustion conditions". *Energy Conversion and Management, 196, 18-31* (2019) (cit. on pp. 5, 30, 31, 89, 107, 122).

Chapter 2

Background and state of the art

Contents

2.1 Introduction **16**
2.2 Main pollutant emissions and their formation in CI engines **17**
2.2.1 Carbon monoxide 18
2.2.2 Unburned hydrocarbons 19
2.2.3 Nitrogen oxides 20
2.2.4 Particulate matter 21
2.3 ICE response under severe ambient conditions **22**
2.3.1 Impact of temperature in engine performance and emissions 22
2.3.2 Impact of altitude in engine performance and emissions 25
2.4 Impact on EATS boundary conditions **28**
2.4.1 Main flow properties affecting the DOC operation . 29
2.4.2 Main flow properties affecting the DPF operation . 31
2.5 Strategies for EATS operation improvement **34**
2.5.1 Passive strategies 35
2.5.2 Active strategies 38
2.6 Summary **41**
Bibliography **42**

2.1 Introduction

With the solid growth of the internal combustion engines segment of the automotive market over the years, stringent emission standards towards emission reduction along with the ongoing adoption of energy efficient technologies to reduce the impact of the transportation sector on the health and environment [46] are shaping up the industry outlook. In the case of Europe, the regulations have been evolving since the implementation of the Euro 1 in 1992 [47], when the catalytic converter and the electronic fuel injection became mandatory for new registrations, followed by different and constantly tighter restrictions ending up on the actual Euro 6d [27], which came into force in January 2020. Its most relevant impact count with the implementation of gasoline particulate filters (GPFs) for gasoline direct injection (GDI) engines to reduce soot, the SCR system for Diesel engines to reduce NO_x, besides of implementing stricter homologation test procedures where limits for the emissions are stipulated [46].

The regulatory framework is driving the focus to the type-approval procedures. In Europe, chassis dyno tests (worldwide harmonized light vehicles test cycle (WLTC)), are complemented with on-road RDE ones. The RDE tests are executed to supplement laboratory tests, being in the Euro 6d regulations expressly designed to cover extended boundary conditions, *i.e.* temperature and altitude, and to follow the requirements on trip dynamics, which are intended to represent a normal vehicle use routine [48]. Besides, the NO_x emissions must not exceed 2.1 times the allowable emissions under Euro 6d [49] during the on-road tests. A conformity factor (CF) for particle number (PN) of 1.5 (1.0 + 0.5 error margin) was also introduced [50].

The RDE tests must be run under the ambient conditions listed in Table 2.1, where a moderate and an extended frame are considered. Altitudes from 0 to 700 m and ambient temperature ranging from 0°C to 30°C define the moderate range with allowable extension till 1300 m and −7 to 35°C, accounting for the extended frame [51]. The aim is to incorporate common situation encountered in many regions, since many populated cities are 1000 m over sea-level [33], facing a wide ambient temperature window. The European approach is also being applied in other countries with adaptations to the singularities of every region, such as higher temperature range (8 − 45°C) in India or altitude till 2400 m in China for extended ranges [52].

Table 2.1: Ambient conditions framework evaluated on RDE tests.

Frame	**Temperature[°C]**	**Altitude[m]**
Moderate	0∼30	0∼700
Extended	-7∼0 and 30∼35	700∼1300

Taking into account these extended ambient boundary conditions and a possibility of further extension of the current RDE framework [53], it is vital from the part of the original equipment manufacturers (OEMs) to fabricate performant engines compliant with the emissions legislations when operating under those conditions. To do that, it is fundamental the understanding of the effect of different temperatures and low ambient pressure on the engine response in order to be able to build the most convenient strategies to overcome the negative impact that those boundaries can impose. Based on this, many studies are trying to encompass the effect of the extra external conditions of ambient pressure and temperature on the engine response.

In this Chapter, the main literature findings concerning the impact of those two variables on the engine components, performance and emissions and how their response affect the aftertreatment boundary conditions is carried out. In addition, a review of the most significant approaches being applied to overcome the drawbacks imposed by such operations is detailed, considering passive and active strategies. This is particularly extended to the DOC and DPF due to their widespread and most common application in Diesel engines, which are the focus of this work. The Chapter encompasses an overview of the main pollutants emitted by CI engines for a complete understanding and foundation of the main processes responsible for their formation and of the best ways to control them.

2.2 Main pollutant emissions and their formation in CI engines

The ideal diesel fuel combustion process forms, in thermodynamic equilibrium conditions, only CO_2 and H_2O [54]. However, due to the many factors combined in order to make possible the diesel combustion inside the cylinder chamber, further species are formed. The four main pollutant emissions are the CO, HC, NO_x and PM [18].

A common gas composition counting with those four pollutants is shown in Figure 2.1.

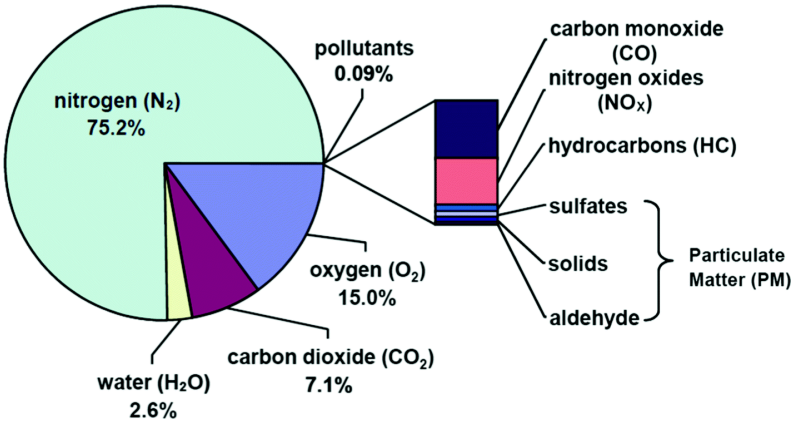

Figure 2.1: Common exhaust gas composition percent by volume of Diesel engines [55].

This section is, thus, destined to provide an overview of those main pollutants formation and main abatement techniques, aiming to help on the comprehension of the effect that ambient conditions imposed on the Diesel engines emissions as will be discussed in the next Sections of this Chapter and in further Chapters of this doctoral thesis.

2.2.1 Carbon monoxide

The carbon monoxide is an intermediate product generated during the fuel molecule combustion. It composes the principal gases causing the smog phenomena [56]. Different conditions of the cylinder chamber can contribute to a not completely CO oxidation into CO_2, so that this pollutant is released to the environment.

One of the main factors promoting its formation consists on the concentration of locally rich zones (where lambda, *i.e.* actual air-fuel ratio over stoichiometric air-fuel ratio, is lower than 1) [57] in the combustion chamber. Those zones are mainly caused by the incomplete air utilization [58], the not sufficient air excess (for example, when lambda is lower than 1.3) [59] or the use of very high EGR rates [60]. Low temperatures environments in

the cylinder chamber, as for example low load operation point with a high lambda [61], can induce a slow combustion and contribute to the incomplete fuel oxidation, causing an increased CO formation [62]. Furthermore, the impact of the injection timing also influences the conditions of the in-cylinder chamber, determining the CO emission. Too early or too late post injections contribute to a higher CO content on the exhaust line [63]. Finally, the CO can also be produced if the injected fuel droplets in a Diesel engine are too large or if insufficient turbulence or swirl is created in the combustion chamber [64].

The main device implemented on the exhaust line of Diesel engines designed to promote the complete CO oxidation through the catalysis is the DOC. Those catalysts convert CO into CO_2 through the action of different precious metals, of which the main ones are the palladium (Pd) and platinum (Pt) [65].

2.2.2 Unburned hydrocarbons

Hydrocarbons consist of thousands of species, such as alkanes, alkenes, and aromatics, being usually stated in terms of equivalent methane (CH_4) content [66]. Similarly to the CO, HCs are combustion products formed during intermediate steps of fuel oxidation, which when not entirely decomposed, are directed to the engine exhaust line [67]. There are two major sources of HC emissions in Diesel engines under normal operating conditions [68]. One is if the concentration of too lean local zones hindering the fuel auto-ignition or the propagation of the premixed flame [69]. The second one corresponds to lean fuel mixtures. One of the reasons for that is the not enough injection pressure from the fuel injector, causing a low velocity from the fuel leaving the nozzle in the combustion process and prejudicing a good fuel mixture [70].

Slow mixing rate of air and fuel lead to over-rich mixture or quenching events, generating general incomplete combustion and pyrolysis products and, therefore, unburned hydrocarbons in the exhaust. Wall quenching is also related to the impingement of sprays onto dry and wet cylinder walls [71]. However, the HC formation is significantly dependent on the temperature and pressure at the end of compression and on the injection timing, if the injection is highly delayed [72].

However, the late post-injections can be eventually desired, being addressed for the special purpose of the DPF regeneration. Through the

intentionally late injection event, the unburned hydrocarbons resulted from the cylinder combustion are directed to be burn in the DOC, increasing the DPF inlet temperature during soot burn off [73].

Finally, sharp engine speed variations, uncontrolled injection, excessive nozzle cavity volumes, and injector needle bouncing can lead to significant quantities of unburned hydrocarbons in the exhaust line [74]. As well as for the CO, the DOC is the main aftertreatment device applied for HC control in compression ignition engines, oxidizing HC into CO_2 and H_2O [75].

2.2.3 Nitrogen oxides

The oxygen and nitrogen (N_2) present in the air or in the fuel can react with each other during the combustion process when temperatures exceed 1900° [76] and form NO_x, comprising nitric oxides (NO) and nitric dioxide (NO_2) [77]. Most of the emitted NO_x is formed early in the combustion process, when the piston is still near the top dead centre (TDC) being the flame temperature the highest [78]. The amount of produced NO_x can be defined as a function of the maximum temperature in the cylinder, oxygen concentrations, and dwell time [18].

Among various types of vehicles, the diesel ones are the most important contributors to NO_x emissions due to the need of higher temperatures for the ignition through compression to occur, being thus responsible for ∼85% of NO_x emissions from the transport sector [79]. Those pollutants represent considerable problems in most major cities and ecosystems worldwide, contributing to the acid rain, the formation of ozone, nutrient enrichment, and smog formation [80]. It can cause biological death on lakes and rivers, besides of affecting the human health, causing inflammation of the airways, emphysema and bronchitis [81].

To deal with this emission, many techniques are applied, controlling its formation directly in the cylinder and by the implementation of specific aftertreatment devices. The most widespread practice adopted on ICEs to suppress NO_x is the use of the EGR technique, helping on reducing the in-cylinder temperature and the air excess [82].

In compression ignition engines, the LNT aftertreatment system actuates adsorbing NO_x molecules and further reducing them by the controlling of

periodic rich injections [83]. The implementation of the SCR also pursues the same objective, usually operating by means of the injection of an urea solution stored in an auxiliary tank. The injected solution undergoes the thermolysis and hydrolysis process to generate NH_3 molecules, which are adsorbed by the catalyst and further react with the NO_x present in the exhaust gas forming nitrogen, water and small amounts of CO_2 [84].

2.2.4 Particulate matter

Finally, the last pollutants presented in this Chapter are PMs [85]. They may be formed during the combustion from the agglomeration of very small carbonic material produced during the combustion process, as unburned fuel, partially burned lubrication oil, and ash content from fuel oil and cylinder lube oil [86].

PM size and shape are key factors to determine the period of time they remain in suspension in the atmosphere before deposition, the probability of being absorbed by plants or inhaled by living beings or the degree of penetration in the pulmonary alveoli [87]. The ones associated to human respiratory risks are usually the PM10, particles with aerodynamic diameter smaller than 10 μm [88], and the PM2.5, which are the ones smaller than 2.5 μm [89].

They can be classified as ash particles composed by carboxylate salts and other inorganic substances [90] or as soot particles derived from a graphite structure [91], representing the most part of PM2.5 found in ICE engines [87]. Soot is mostly formed on low lambda zones and increase progressively with temperature, besides of being favoured by the addition of EGR [92].

The aftertreatment systems designed to eliminate the soot in compression ignition engines are the DPFs [93]. They are constituted of porous wall channels alternatively sealed in each extreme forcing the exhaust gas to pass through the channel walls to reach the tailpipe and retain the solid components by filtration [94]. Therefore, periodic regenerations are needed in order to avoid the excessive back pressure, thus, compromising the engine performance [95].

2.3 ICE response under severe ambient conditions

During car trips in different regions all around the world, the driver can face a variety of ambient conditions counting with different temperatures and altitudes. The international standard atmosphere (ISA) [96] establishes pressure and temperature variations according to the altitude, describing the air pressure as altitude increases.

Regarding the European continent, its geography counts with great variation within relative small areas, counting with several massif regions, from high mountain chains of the Pyrenees and the Alps/Carpathians to hilly uplands at multiple locations [97]. About 60% of its population live in or close to massifs and 20% in mountain municipalities [32], suggesting frequent car trips in those zones.

Extreme temperature and altitude affect the complete engine behaviour, modifying the inlet conditions of each component in a cascade effect. This is finally observed by the engine performance in terms of a potential negative impact on two main outputs: emissions and fuel consumption [98]. The state-of-art of the specific impact of temperature and altitude, separately, on those two variables will be commented in the sequence, providing, thus a solid basis for the concepts addressed in this doctoral thesis.

2.3.1 Impact of temperature in engine performance and emissions

A few studies have gone through the specific effects of the intake air temperature on combustion characteristics, turbocharger operation and their consequences on engine performance and emissions. When the compressor inlet faces higher temperatures, more work is required to produce the same pressure ratio and the compressor outlet temperature is consequently higher [99]. However, the temperature in the cylinders inlet will be a consequence of the development of the air handling units such as intercoolers, exhaust energy recovery systems, which are systems that recover exhaust waste form the engine to power battery or the crankshaft [100], affecting the turbocharger-engine matching [101].

Isolating the combustion process, higher inlet temperatures lead to an increase on the rate of heat release peak, shortening the burn duration and advancing auto-ignition timing [102]. On the other hand, as temperature reduces, combustion instabilities can come up, causing incomplete combustion [103] and eventual misfiring events [104]. Those facts combined with high fuel and oil viscosity and poor fuel evaporation and blow-by problems [105] cause a low combustion efficiency [106].

In this context, the EGR technology is essential for NO_x reduction. While the high-pressure (HP) EGR collaborates for faster warm-up, the LP EGR leads to an unchanged gas flow in the VGT, allowing higher boost pressures to be reached [107]. The combination of high-pressure and low-pressure EGR allows to minimise fuel consumption with reduced NO_x emission [108], besides of being able to handle the lower engine thermal levels in the cylinder inlet [109]. However, extremely cold temperatures can also lead to a decrease on the EGR rate regarding condensation in the LP-EGR path [110].

Low ambient temperatures are critical for fuel consumption during the engine warm-up [111], influencing the cooling system, since lower temperatures imply cooler engine components (cylinder head, liner, piston, etc.), higher oil viscosity and thus higher friction losses and increase of the heat loss [112]. On the other hand, the time spent on cold start decreases significantly with ambient temperature increase [113], representing less damage for engine performance. Luján *et al.* [36] also discussed this result and found a penalty in fuel consumption up to 10% running new European driving cycles (NEDC) and worldwide harmonized light vehicles test cycles at -7°C compared to 20°C ambient temperature. Faria *et al.* [114] evaluated real-life driving data and also found an increase of CO_2 emission at low ambient temperature within the moderate temperature range, being gasoline engines damaged the most. Weilenmann *et al.* [115] even found a linear fuel consumption increase as a function of the temperature decrease when evaluating 23, -7 and -20°C ambient temperature conditions in Euro 3 to Euro 4 engines. Ko *et al.* [116] found a similar trend in cold and warm restarting in a sample of Euro 5 and Euro 6 vehicles, testing NEDC and WLTC cycles. He observed a progressive decrease on CO_2 emission as the ambient temperature increased from -5 to 23°C, including the 14°C temperature.

It is thus evident that when the engine is warmed, ambient temperature has also little impact on particle emissions, being the most important differences observed during warm up processes [117]. Regarding the engine-out CO and

HC emissions during warm up, their reduction is progressively observed as the cylinder intake temperature increases. Zhang *et al.* [118] related this fact to a faster reaction rate encountered at higher intake temperatures, accelerating the production of radicals, which are helpful for the oxidation of CO and HC [119]. Quenching phenomena and misfires are also weakened when reaching higher thermal levels [120], promoting higher burning efficiency and decreasing specially HC emission.

When the engine is cold, the previously described phenomena associated to low combustion efficiency favours the increase on CO and HC emissions [121]. Tian *et al.* [122] also associated the CO and HC increase during the cold start period to the lower air-fuel ratio (AFR) found at low ambient temperature, which, according to them, could be avoided by promoting a higher fuel mass injection. This increase on CO and HC emissions is ascertained in many other works like Weilenmann *et al.* [115] or Lapuerta *et al.* [109], by correlating the CO and HC emissions decrease with increasing coolant temperatures with the LP-EGR strategy applied on NEDC cycles. Emissions were also evaluated in Luján *et al.* [98], who found that HC emissions were in the order of 2.5 to 4 times higher at -7 than 20° during WLTC cycles. The CO emissions were, however, higher only during low load conditions. The lower CO emissions at -7° at medium and high loads of the WLTC were associated to the higher air fuel ratio found at this ambient temperature, being directly related with the EGR activation strategy. Both EGR systems were kept fully closed till 875 s at -7°C in ambient temperature and remained closer at -7°C in all WLTC phases.

As evidenced, the EGR rate reduction at low temperatures is a common practice to avoid formation of condensates in the LP-EGR cooler during warm-up [110] and in the mixing region with fresh air upstream of the compressor [123]. This action causes additionally a damage on NO_x, as observed by Sakunthalai *et al.* [124]. They performed experimentally an engine start and idle run during 3 min at -20, -7 and 20°C evaluating engine performance and the engine-out emissions. Their results match with the previously exposed about the increase on fuel consumption and HC emissions with temperature decrease. Moreover, they observed higher NO_x values over the tested time for the coldest temperature compared to the warmest one. In the same study performed by Luján *et al.* [98] the NO_x emissions were also increased on account of the EGR reduction for a longer time at the WLTC for lower temperature operation. Tian *et al.* [122] also associated the NO_x

emission with the high intake air mass flow for the low ambient scenario, increasing the oxygen availability in the cylinder.

The engine-out particulate number were also found to be higher at lower ambient temperature conditions due to the incomplete combustion of fuel [124], but being also affected according the EGR level [122]. In fact, the lower exhaust line temperature is responsible for the particles diameter to increase by nucleation, coagulation between particulates and condensation of volatile materials [125]. Similar results were found by Olivares *et al.* [126], that compared ambient temperature conditions of -9, 1 and 14° and noted that the strongest effect of ambient temperature is associated with particles of sizes lower than 40 nm.

Many studies demonstrated that tailpipe emissions were at last affected by the ambient temperature in cold starts, being finally conditioned by the aftertreatment systems operation. Faria *et al.* [114] used real-life driving data covering the moderate range for ambient temperature to quantify the tailpipe emissions during cold starts in urban contexts. The results evidenced a clear penalty in emissions during cold start in comparison to hot operation. Ludykar *et al.* [127] evidenced a 5 to 20 times higher tailpipe CO and HC emissions at -20°C compared to 22°C ambient temperature when the vehicle was submitted to an NEDC. Ko *et al.* [116] showed that a low ambient temperature highly affected NO_x and CO emissions, by comparing 5, 14 and 23°C in an Euro 6 Diesel engine, performing NEDC and WLTC cycles. However, in a further study, Ko evidenced an increase of 55% in NO_x when the ambient temperature is increased from 27 to 33°C when realizing consecutive acceleration and deceleration phases in urban areas. The key aspect was that this operation showed more negative effects on the LNT regeneration performance at low ambient temperature. Indeed the aftertreatment systems performance are as well affected by the differences in boundary conditions like in this case, temperature. This question will be, thus, treated separately in detail further on.

2.3.2 Impact of altitude in engine performance and emissions

As the altitude increases the air pressure is lower and accordingly also the air density, impacting on a number of processes that determine a relevant change in the engine response, and a dependence on the calibration of the gas

exchange process. The engine torque range is reduced with altitude increase due to a reduced boosting pressure range related to the ambient pressure reduction [128]. The lower ambient pressure at higher altitude leads the control strategies to push the combustion and boost processes towards several mechanical limits looking for maximum power availability. Therefore, one way to compensate the lower intake air mass flow is to promote the EGR rate reduction [33].

Consequently, the combustion process also suffers an impact [129]. The start of the injection (SOI) is commonly advanced leading to maximum in-cylinder pressure and maximum pressure gradient [43]. However, the start of combustion (SOC) is delayed due to the decreasing intake pressure [40]. The boost requirements also lead to increase the exhaust manifold pressure acting on the turbine expansion. As a consequence, the pumping losses increase as well as the pollutants emissions related to in-cylinder exhaust backflow [128].

Wang *et al.* [130] found a progressive decrease of the brake thermal efficiency with increasing altitude in a heavy duty Diesel engine. This trend matches with the ones found by Giraldo and Huertas [35] in diesel buses operating at high altitude, especially as the vehicle speed increased. In the same way, Szedlmayer and Kweon [131] reported a damage in indicated specific fuel consumption reaching 8% at high altitude and high load, although slight benefits were found at low load. In a similar way, Ramos *et al.* [39] tested a passenger car Diesel engine and observed an increase in fuel consumption during extra-urban driving conditions at $\sim$ 2300 m. In this line, Serrano *et al.* [128] reported a progressive fuel consumption penalty with increasing altitude both in urban and extra-urban driving phases of NEDC, being higher in the extra-urban case. For gasoline engines, the results in the literature are focused on naturally aspirated engines. Zervas [132] reported a decrease in fuel consumption reaching 3.5% in NEDC, 2.6% in fedetal test procedure (FTP) and 6.2% in the highway driving cycle; Wang *et al.* [37] also found a decrease on CO_2 emission as altitude increased for various naturally aspirated gasoline vehicles operating under WLTC mainly because of the intake throttle opening.

Concerning the emissions, Giraldo *et al.* [35] conducted RDE tests in a Diesel engine without any aftertreatment system in Mexico City region, which is located at an altitude higher than 2000 m, and compared the results with similar studies close to sea-level altitudes. A substantially higher CO emissions (more than 290%) than the equivalent track at sea-level conditions

were reported. They attributed this difference to the lower oxygen availability in altitude. Despite the use of turbochargers to minimizes the variations in the boost pressure. These findings agreed with the work of Szedlmayer and Kweon [131], who also reported an increase on engine-out CO emissions in altitude. The oxygen shortage and the in-cylinder temperature conditions also influence the HC radicals disintegration and, therefore, the PMs. release [133].

Giraldo also found that the NO_x emissions were significantly lower in altitude conditions. NO_x emission of vehicles is mainly determined by combustion conditions of the engine. Cylinder combustion temperature and air amount are dominant factors, being the decrease in air mass one responsible agent for the NO_x emission decrease [38]. However, the settings adopted in altitude conditions for the boost strategy and the EGR rate will dictate the gas characteristic in the cylinder. That said, the NO_x emissions are extremely dependent on the EGR ratio settings, that can be kept at low levels while the boost system is below its mechanical limits [40].

In a similar way, medium engine loads demand the turbocharger protection so that the high-pressure EGR rate is decreased to provide compressor surge margin and avoid exceeding the turbine inlet temperature and the turbocharger speed limits [128]. In this case, the NO_x is penalized in altitude operation, together with CO and HC emissions measured downstream the DOC, according to Bermúdez *et al.* [128], who run NEDC cycles at 150 m to 3000 m in a Euro 4 Diesel engine.

By performing WLTP and RDE tests over different altitudes, Ramos *et al.* [39] also noted an increase on NO_x emissions downstream the EATS in altitude associated to the closure of the EGR valve, being in this case this emission ten times higher than the regulation limits for a Euro 4 diesel vehicle. The engine was equipped with a DOC and a DPF, who successfully reduced the HC, CO and PM emissions also in altitude conditions.

Engine-out PM emissions also increased with altitude [134]. The higher in-cylinder temperature accelerates thermal pyrolysis, liberating HC radicals and increasing the particles formation [130]. The engine-out PM in altitude were successfully reduced in the work of McCaffery *et al.* [135] by the addition of a catalyzed GPF to the aftertreatment system of a Tier 3 vehicle. Wang *et al.* [136], however, observed the progressive increase of NO_x emissions as well as CO and particulate matter till almost 3000 m in a China IV Diesel engine, despite being equipped with DOC and DPF systems.

This variety in the results reinforce the analysis of the ambient conditions impact on the EATS functioning through the modification of their boundary conditions according to the engine operation. Therefore, the specific impact of flow properties on the DOC and DPF operation will be next addressed separately.

2.4 Impact on EATS boundary conditions

As previously commented, the effect of the environmental conditions on the engine operation also modifies the boundary conditions of the EATS, thus affecting the tailpipe emissions. According to Soleimani *et al.* [23], a standard Euro 6 Diesel engine aftertreatment set resembles to the standard configuration depicted in Figure 2.2:

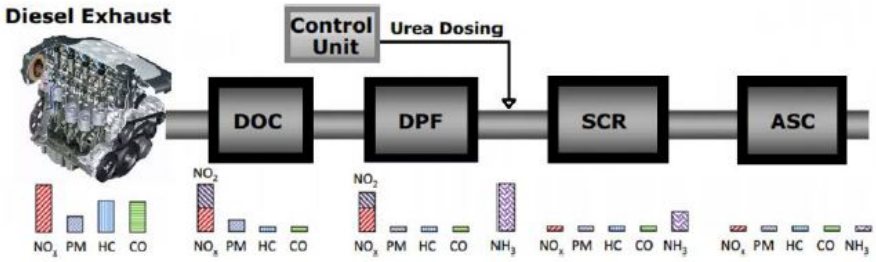

Figure 2.2: The standard Euro 6 automotive aftertreatment system configuration and the main pollutants abated at each step [23].

The DOC is the most adopted aftertreatment system and it is strategically placed first in the exhaust line in a close-coupled location. This configuration enables the HC and CO molecules oxidation, besides the NO_2 formation and temperature enhancement during the DPF active regeneration events, which is the following component on the exhaust line [137]. As previously mentioned, the DOC is responsible for the CO and HC abatement while the DPF executes the particles trapping. Following, the SCR system is placed to deal with NO_x emissions [138] and is usually followed by an ASC to oxidize the ammonia slip from the SCR [139].

However, it is more and more frequent the combination of different EATS, like the SCR with the DPF unit forming the wall-flow particulate filter (PF)

with SCRf function, to improve compactness of the aftertreatment systems, enabling earlier NO_x conversion [140].

2.4.1 Main flow properties affecting the DOC operation

The DOC is a widely applied aftertreatment unit assigned to oxidize CO and HC pollutant emissions [141]. The DOC also oxidises NO into NO_2, that can be employed in the DPF to passively oxidise soot at low temperatures, as well as to promote NO_x reduction in the SCR by the fast mechanism [142]. The DOC consists of a honeycomb monolith across which the exhaust gas flows, being usually manufactured with cordierite [143]. Those structures contain parallel channels coated with a washcoat surface embedded with active catalytic materials such as Pd and Pt [144], as previously mentioned.

The exhaust temperature is the main parameter governing the DOC response [41]. The catalyst principle is to accelerate chemical reactions by lowering their necessary activation energy, promoting the reaction rate to increase. In other words, a lower temperature is consequently needed compared to an uncatalyzed reaction [145]. This particular activation temperature is called the light-off temperature, which is designated as the required temperature to obtain a 50% of each pollutant conversion efficiency [143]. Furthermore, the oxygen adsorption onto the catalyst surface, regardless of the oxidation reaction, can be also promoted by a zeolite layer, which decreases with temperature [146].

Ye *et al.* [143] developed a thin-slice method to undertake a closer inspection of the DOC, finding a wall temperature correlation with the performance of the DOC. Zervas *et al.* [147] performed NEDC cycles finding strongly CO conversion efficiency dependency on exhaust temperature, which is almost linear. In fact, the aggressive part of the NEDC is the one that contributed to the majority of the total emissions conversion efficiency, according to Robinson *et al.* [148], who found that 85% of cumulative conversion contribution is done in the extra urban driving cycle (EUDC) part of the cycle, due to a higher thermal level in the catalyst.

In this context, numerous efforts have been conducted in order to reduce the long warm-up periods [149], looking for faster catalyst light-off. A review of those strategies will be conducted in more details further in this Chapter. However, thermal solutions are not only justified by the increasing periods at low temperature in incoming powertrain systems, but also by the variability of the light-off temperature, which is not the same in all of the operating conditions. EATS boundary conditions, such as pollutants mole fraction or dwell time [45], vary the catalysts light-off response [150]. The dwell time (τ) increase improves the mass transfer of the pollutants towards the catalyst active sites, which implies a higher conversion efficiency, especially at high temperature [151], additionally contributing to a reduction of the light-off temperature [152]. This variable is calculated dividing the monolith length (L_{mon}) by the gas velocity (u), as expressed in Equation (2.1):

$$\tau = \frac{L_{mon}}{u} \tag{2.1}$$

The monolith length is constant whereas the gas velocity changes according to the flow properties. The gas velocity is dependent on the mass flow and inversely dependent on the available transversal area of the catalyst (A) and the exhaust gas density (ρ), as represented in Equation 2.2:

$$u = \frac{\dot{m}}{A \cdot \rho} \tag{2.2}$$

Variations on the exhaust mass flow and gas density than can be ultimately caused by ambient temperature and pressure changes, as previously seen, affect, consequently, the catalyst dwell time [153]. In the high temperature range the surface is nearly covered with oxygen provided that there is an excess. Therefore, the reaction velocity is limited by the rate at which the CO or HC strike the surface [154]. Therefore, an increase in the mass flow rate reduces the dwell time, which decreases the conversion efficiency of the catalysts [155].

The ambient conditions also affect the exhaust pressure, directly related to the third flow property dictating the catalyst performance, which is the pollutants' partial pressure. The resulting exhaust gas composition conditioned by the adapted engine calibration to altitude also has an impact on the pollutants' partial pressure and therefore on their conversion

efficiency [130]. From one side stands the necessity of sufficient oxygen partial pressure to allow the chemisorption in the catalytic surface and its interaction with the reactants [156]. At normal operation conditions [157], Diesel engines usually operate under lean burn combustion, which entails high concentrations and therefore also high partial pressures of oxygen in their exhaust gases.

In parallel, the conversion efficiency can be affected to the change in inhibition that is related to the CO and HC engine-out emission [158]. In a parametric study, Zervas *et al.* [147] also observed a CO and HC light-off temperature increase about 7°C for every 500 ppm of CO added and about 4°C for every 200 ppm of HC added. Ye *et al.* [143] demonstrated the CO inhibition effect on a real engine exhaust observing an excessive drop on the rate of reaction as the CO concentration is increased. Luján *et al.* [98] also observed how the DOC conversion efficiency was affected, specially in the case of the CO, due to CO inhibition [45], that appeared in huge instantaneous emission related to transient load phases at -7°C.

Piqueras *et al.* [159] performed WLTC cycles experimentally and reproduced them in terms of modelling to observe the influence of the cell geometry on the conversion efficiency of a DOC. They observed how the CO conversion efficiency instantly drops along the test cycle due to the vehicle accelerations. This result is the consequence of instantaneous CO raw emission peaks, which increases up to four orders of magnitude the oxidation inhibition term with respect to its mode value along the driving cycle. Russel *et al.* [160] demonstrated experimentally how the adsorption of CO blocks oxygen adsorption to the precious metal surface sites and thus inhibits the reaction. Finally, Voltz *et al.* [161] also observed how the inhibition and the decrease in conversion efficiency is accentuated by the decrease in dwell time.

2.4.2 Main flow properties affecting the DPF operation

As previously commented, wall-flow DPFs are monolithic honeycomb structures with several alternatively plugged axial parallel channels at each end, as seen on Figure 2.3. The gas flow enters the channels and it is forced to pass through the porous walls, as schematically depicted in the right-hand side of Figure 2.3, where soot particles are collected and accumulated until being eventually regenerated [162].

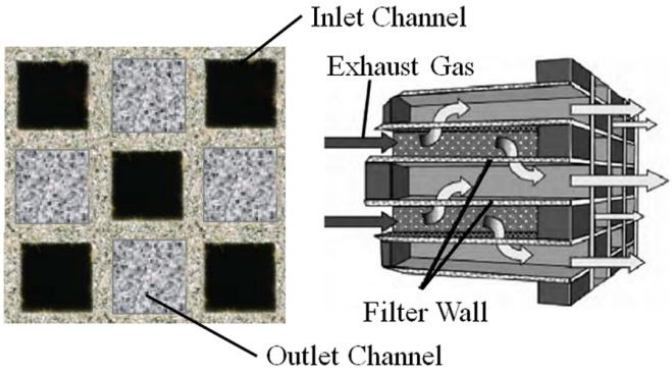

Figure 2.3: Transversal structural illustrations of traditional DPF (left) and schematic three-dimensional (3D) view (right) [163].

During normal engine operation, the wall-flow particulate filters is designed to trap PM in the porous walls [164]. The filtration process comprises two different loading regimes: the deep bed filtration regime, where the soot is first trapped inside a small portion of the porous wall thickness [165], followed by the transition state, where a gradual reduction of the pressure drop increasing rate is noticed, finishing by the cake filtration regime when the porous wall is completely saturated. This last phase is characterized soot accumulation on the porous wall, varying the particulate layer thickness [166]. The main considered mechanisms responsible for the deep bed filtration regime are the Brownian diffusion deposition, consisting of small particles deposition on the collector unit from the random motion of the aerosol particles in the exhaust gas [167], the interception mechanism, from which small particles collide to the collector unit when, by following the stream line, come closer to the obstacle [168], and finally the inertial deposition [169], in which the particle directly comes across the obstacle, being incapable of changing its trajectory due to its high size.

Therefore the soot particle size governs the filtration mechanism responsible for the soot deposition. This is evidenced in Serrano *et al.* [170], that proposed a computational model to evaluate soot filtration, and observed that the filtration efficiency is governed by the mode diameter of the particle size distribution. Additionally, the filtration efficiency is increased at lower gas exhaust flow rates and higher exhaust gas temperature, where the gas density is lower [169]. Those conditions favour the increase of Brownian diffusivity mechanism and inertial contributions in addition to the others already present.

In parallel with the soot filtration, in a normal engine operation, the continuous passive regeneration takes place [171]. For that, the NO_2 emissions react with the soot at temperatures above 250°C [172]. This condition is promoted by the DOC positioned ahead the DPF. Otherwise, the DPF can be catalysed, which is called catalysed DPF (CDPF), being able to accomplish the passive regeneration by using a catalyst coating on the DPF element [173]. As exposed, the level of NO_2 and the DPF inlet temperature, which are conditioned by the engine operation and submitted to the processes happening in the DOC, are determinant to the passive soot oxidation.

Hence, Kandylas *et al.* [171] evaluated the influence of the NO_2/soot ratio on the passive regeneration, together with the effect of temperature. However, the exhaust temperature is completely dependent on the operation point, which will also determine the oxygen availability and the soot emission that will face the DPF inlet [174]. Bai *et al.* [175] also related the increasing on exhaust temperature and NO_2 concentration to the passive regeneration speed up.

In fact, in normal engine operation a stabilization of soot loading and soot oxidation by NO_2 should be evidenced, which is know as the balance point [176]. The balance point is predicted to decrease linearly with dwell time decrease, increasing temperature and ratio of NO_2 to PM ratio in the DPF [177].

Since the balance point is common under passive DPF regeneration, the DPF must be submitted to an active regeneration process, where the soot is oxidized in presence of oxygen (O_2). This reaction is promoted by temperatures ranging from 500 to 600°C in the DPF inlet [178]. This thermal level in the exhaust is only achieved by modifying specific engine settings as the injection strategy, the intake throttle valve opening, the VGT position or the EGR rate during the regeneration time [175], as it will be explained in more detail in the next Section. However, the active regeneration frequency has a potential to be decreased by achieving a proper engine calibration during normal operation mode.

The soot oxidation process is based on a sequence of processes involving first the diffusion of the gaseous reactants from the external to the internal pores, the adsorption of the reactants on the soot surface, producing intermediate products, and their final rearrangement, forming the oxidation products [179]. Macián *et al.* [180] concluded that the internal pore diffusion

efficiency of the gaseous reactants can be determined by the substrate temperature, being negligible below 300°C for NO_2 and 400°C for the O_2 and presenting a linear dependency on temperature up to 650°C for O_2 and 550°C for NO_2. Furthermore, they considered the effects of O_2 adsorption, relating its surface coverage to its concentration and the substrate temperature. The O_2 surface coverage showed a well marked sensitivity to the temperature and a minor dependency on O_2. By analysing the pressure drop and soot depletion rate derivatives, Macián *et al.* concluded that the increase on soot depletion rate is directly governed by the growth of the particulate layer thickness.

The dynamics of the soot oxidation can also be improved not only by increasing the reactant partial pressure, but also, by increasing the dwell time [181]. The exhaust gas velocity additionally impacts on the temperature field distribution in the DPF, increasing the mean DPF temperature [182]. Serrano *et al.* [183] determined the use of a low EGR rate to obtain optimum regeneration conditions, being able to provide higher O_2 partial pressure and dwell time.

2.5 Strategies for EATS operation improvement

The change on flow properties caused by the extreme ambient conditions can imply on a worse response of the aftertreatment systems in terms of pollutant species abatement. It is clear from last Section that temperature arises as one of the main factors conditioning EATS operation. In the case of the DOC, as previously mentioned, optimisation strategies have been focused on the light-off time reduction [149]. Equally, distinct approaches have strived to improve the DPF operation by achieving the required temperature and promoting the chemical kinetics during particulate filter regeneration events [184].

The implemented strategies can be classified in two types. On the one hand, there are the active strategies for the EATS operation improvement. In this case, commonly an external contribution of energy is provided in order to increase the temperature of the exhaust gas [93]. Besides, active strategies require an external action on the system, which is mostly executed through the engine control, to obtain the desired results in terms of temperature or other flow properties in the external system, which is the case of the EATS.

On the other hand, there are the passive strategies. In this case, the solutions aim to favour the normal engine operation without implying an external contribution of energy [185]. For this, the gas flow properties change due to, for example, the presence of other oxidizing agents, due the oxidation reactions activation energy reduction or due to the reduction of thermal losses along the exhaust line.

For both strategy types, the main challenge is to exploit the synergy between engine performance and aftertreatment system efficiency. It means to look for solutions that provide some improvement in fuel consumption. Hence, this last Section is dedicated to present a bibliographic review of the most relevant strategies applied to the aftertreatment systems operation improvement and the evaluate the advantages and drawbacks in terms of engine performance.

2.5.1 Passive strategies

As previously introduced, the passive strategies approach aims to promote the normal aftertreatment operation without an external energy supply nor an explicit external action on the engine calibration. While for the catalysts, the emphasis is put into looking for an earlier light-off, the passive strategies applied on the DPF operation are based on promoting the soot particles oxidation at the typical exhaust gases temperatures found during normal driving operation [186].

The best known solution for passive strategies is to reconsider the aftertreatment's design [187] and/or placement of the components in the exhaust line [188]. Locating the DPF downstream the DOC, called continuous regenerating trap (CRT) technology [189], is a common example of promoting an increase on the DPF NO_2 inlet concentration, favouring the passive regeneration. The DOC is able to perform NO_x redox reactions, converting NO into NO_2 [171]. As previously seen, the NO_2 is capable to oxidize soot at normal operation's gas exhaust temperatures due to its lower activation energy [190].

Going along with the previous strategy, another common approach is the use of a catalytic coating in the particulate filter, forming either systems like the CDPFs or catalysed soot filters (CSFs) [191]. This configuration involves multiple advantages, favouring the NO oxidation into NO_2 in a more compact

structure [192]. Furthermore, the contact between soot and catalyst increases the particles reactivity, speeding up the regeneration process [193].

In this sense, He *et al.* [194] performed a modelling study to evaluate the catalytic conversion response of the integrated aftertreatment system of four different layouts shown in Figure 2.4 based on the standard Euro 6 configuration seen in Figure 2.2. Besides of confirming the ideal positioning of the DOC prior to the particulate filter for an optimum passive regeneration, they observed the effects of different arrangements in terms of tailpipe emissions. For example, by placing the SCR system before the CDPF, the passive regeneration would be much slower, because the conversion of NO_2 into N_2 performed in the SCR decreases the available NO_2 for passive regeneration. From the other hand, the CO emission generated in this process is lower, leading to an overall higher CO conversion efficiency from the system. As is can be noticed, the ammonia oxidation catalyst (AOC) always needs to be placed after the SCR in the EATS line due to its ammonia abatement functionality.

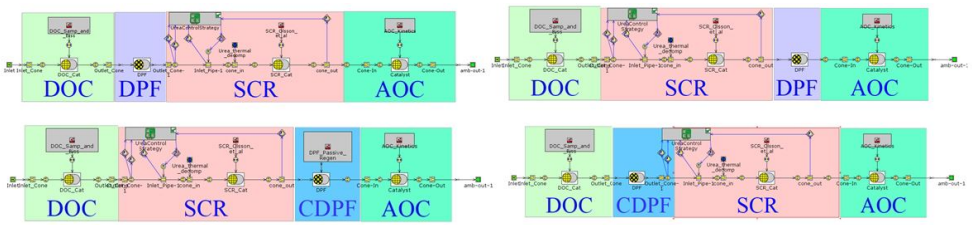

Figure 2.4: Four different integrated aftertreatment systems set-ups for a modelling study [194].

Still regarding the exhaust line's architecture, Luján *et al.* [137] studied under steady-state operation placing the DOC coupled to a DPF before the turbine in order to benefit the pollutants oxidation and the DPF passive regeneration The concept was further explored by Serrano *et al.* [195], discussing the potential and limitations of pre-turbine small-sized catalysts in accelerating the catalyst activation under real driving conditions.

Thermal management strategies have been widely applied in the literature. Pursuing this idea, the exhaust line thermal insulation has been thereupon considered to improve the aftertreatment operation [196]. Xie *et al.* [197] made use of tests and modelling tools to perform an aftertreatment thermal

mapping, identifying the influence of radiation on a DOC + DPF + SCR configuration with in- and outlet aftertreatment thermal insulation. Arnau *et al.* [198] explored computationally the thermal insulation of the exhaust ports and the exhaust manifold in Diesel engines as a way to increase the exhaust temperature during transient operation and reduce the time to reach the DOC light-off. As a result, a 20% and 25% reduction in CO and HC emissions was obtained, respectively, by insulating one of the two components, while both elements insulation provided a decrease of over 40% in those emissions, counting with an 1% in brake specific fuel consumption (BSFC) improvement.

Another option addressed in the literature to deal with the thermal management of the exhaust line, specially focused on reducing cold-start emissions, consists of using thermal energy storage (TES) systems in conjunction with the EATS [199]. Phase change materials (PCM) can be applied in the TES system to absorb the exhaust gas thermal energy, thus, liquefying the PCM and storing it as latent heat [200]. Numerous materials have been studied by different researchers for their potential use as PCMs, including organic and inorganic compounds [201]. Johar *et al.* [202] developed a latent heat thermal energy storage system (LHTESS) that can be integrated to the engine using Erythriol as a phase change material. A higher exhaust temperature could be obtained by saving up to 11.33% of energy but at the expense of 5% in BSFC loss.

Burch *et al.* [203] used an aluminum/silicon PCM for thermal storage in conjunction with a vacuum insulation to enhance the heat retention in a prototype catalytic converter. They concluded that, although the exhaust temperatures were not hot enough to melt the PCM, the vacuum insulation performed well, giving a converter temperature of 146°C after 23 h of cold soak at 27°C and a consequent reduction in CO and HC emissions of 52 and 29 %, respectively. Korin *et al.* [204] tried a catalyst configuration in which 3.8 kg of PCM material were embedded in the monolith looking for a maximum contact area between both. They experimentally performed a short engine start followed by a long period shut-off. During this time, the PCM underwent a partial solidification and released the latent heat maintained the catalyst temperature within the desired range for maximum conversion efficiency, correspondent to more than 90% for NO_x, over 65% for CO and higher than 60% for HC.

Hamedi et al. [44] used a computational model in ANSYS™ to perform NEDC cycles of a Diesel engine equipped with a 2 kg of PCM annular layer

around a metallic substrate oxidation catalyst. The results were compared versus a baseline configuration with a ceramic DOC without PCM. This TES system proved to reduce the cumulative CO and HC emissions by 91.7% and 41.2% respectively. The results also showed the interest for this technology in increasing the conversion efficiency in recurrent cold-start cases, as those in hybrid vehicles [205].

Finally, alternative passive solutions were also considered to improve the DPF passive regeneration, as for example the incorporation of metallic oxides as fuel additives [206], a system called fuel borne catalysts (FBC). That way, the soot formed will carry those substances in their structure. The advantage promoted by those metallic oxides is the formation of nitrates in the soot surface and the oxygen accumulation on the active surface [207], not only favouring soot oxidation by O_2 and NO_2 [208], but also reducing the minimum soot oxidation temperature in passive conditions to values below 260°C [93]. However, the drawbacks presented by this approach are, on the one hand, the need to inject the additive into the cylinder, what implies the installation of a tank and an additional injection system, and, on the other hand, the use of FBC increases the accumulation of ash in the DPF [209].

2.5.2 Active strategies

Unlike the passive strategies, the active ones involve an external supply of energy or an intended external action on the system. Such supplemental energy can be generated either internally or externally to the engine. The internally engine based control measures are relatively straightforward to be implemented [210]. The most common ways to do it is through the fuel injection strategy [211], controlling the intake air dilution by the EGR [86], and the turbine outlet temperature increase with the VGT [212].

The EGR technique has been used to lower NO_x formation and it's one of today's most common emissions control systems [213]. It does so by decreasing the in-cylinder chamber temperature and, consequently, the exhaust gas temperature [86]. This last consequence is adverse for the EATS operation, that requires high exhaust thermal levels for an optimised operation. Therefore, a correct EGR management is fundamental to achieve the best possible trade-off in terms of engine performance, emissions mitigation and EATS conversion efficiency. Additionally, the management between LP-

and HP-EGR must be taken into account. For example, during the engine warm-up, the HP-EGR can be more beneficial than the LP-EGR for the aftertreatment inlet temperature and, consequently, the tailpipe CO and HC emissions [109].

On the other hand, according to Yang *et al.* [214], the VGT is the most flexible technology to provide an optimisation that includes the engine response and the aftertreatment systems inlet temperature [215], specially working at higher altitudes. In order to decrease the loss in engine performance, this technology is an useful way to avoid an excess on pumping losses rise through its opening [33].

Variable valve timing (VVT) strategies, such as the exhaust re-opening or late exhaust valve closing, can be calibrated to manage the thermal level in the exhaust line [216]. However, this measure almost always implicates on a loss in engine performance [217]. Arnau *et al.* [218] achieved, by means of a computational experiment, an increase of 50°C in the aftertreatment inlet temperature at the expense of 5% in BSFC when combined an early exhaust with a late intake valve opening events. This approach has been also considered by Serrano *et al.* [219], who additionally evidenced a 20% reduction in HC and CO pollutant emissions levels.

Considering external energy sources, Horng and Chou [220] investigated the possibility of using heating elements to increase the exhaust temperature during cold-start events upstream and inside the catalytic converter of a motorcycle engine. Khan *et al.* [221] incorporated electrically powered glow plugs to achieve a faster light-off temperature of a catalytic converter installed in a gasoline engine. After 2.5 h soak time, a catalyst pre-heating procedure was conducted, reducing the time to reach the light-off to 2 minutes instead of 13 minutes in the original configuration.

In the same way, Szolak *et al.* [222] developed their own heating system, called CatVap®. It offered a compact design, containing a high power density (45 kW/l). The principle of this device is an electrical heated catalyst (with common industrial coating) in which diesel fuel reacts with the oxygen contained in the exhaust gas and generates heat. This system proved to be functional for both DOC and SCR catalysts, being also effective to control the temperature during continuous DPF regeneration. Facing a variety of different heating systems options, Holmer and Eriksson [223] proposed a model that analyses the process of catalyst heating besides of covering the impact of the

engine operation in terms of load and speed on the catalyst heating efficiency, helping to make the optimal use of this technology.

On the other hand, the engine may sometimes present the need of a punctual engine EATS temperature raise, which is the example of DPF active regeneration events. In these cases, the goal is to achieve a DPF inlet temperature typically over 600°C to promote soot oxidation by O_2 present in the exhaust gases [93]. The most common method to increase the DPF inlet gas temperature is to modify the injection strategy, precisely adding fuel post-injections [224]. This way, an extra amount of hydrocarbons are injected in the cylinder chamber and not burned. Instead, they are carried along the exhaust gas [72] until meeting the DOC. Then, they can be finally oxidized through a strongly exothermic reaction that raises the temperature of the gas leaving this element [225] and potentially increases the DPF inlet temperature.

The characteristics of the post-injection events are key factors to define the amount of hydrocarbons reaching the catalyst [226] and thus the level of temperature in the DPF inlet [227]. Therefore, the post-injection delay with respect to the main injection [228] and the amount of fuel in the post-injections [229] must be carefully considered. For example, in their experiments, Serrano *et al.* [183] obtained the fastest possible regeneration when the post-injection represented a 20% of the fuel mass rate of the main injection. It is, however, important to notice that this practice comes together with the increase on fuel consumption. Besides, the excessive increase in the post-injected fuel may not lead to significant acceleration of the regeneration process since the O_2 availability plays a fundamental role on the soot burning [230].

Therefore, other controlling parameter can be additionally modified during active regeneration strategies, as the EGR valve [230] to favour the oxygen concentration increase on the exhaust line. Ko *et al.* [231] investigated the pros and cons of the EGR partial reduction, affecting soot accumulation in the DPF, leading, however, to higher NO_x emissions. The complete EGR shut-off has been also addressed in the literature, as performed by Liebig *et al.* [232] and Dwyer *et al.* [233].

Aiming to increase the air excess and, thus, favour the DPF regeneration, a good result is obtained by actuating on the intake valve throttle [234]. The point of actuating on the intake throttle valve is to restrict the air in the cylinder and operate, consequently, with higher equivalence ratio [235].

The opening position must be, however, carefully considered. Bai *et al.* [175] obtained in an experimental study an exhaust temperature raise above 140°C together with a reduction on NO_x emissions by opening between 15 an 20% the intake throttle valve. This manoeuvre damages, however, the PM emission. Additionally, further opening of the VGT during the active regeneration can also be beneficial [75], once it can generate a punctual rise on turbine outlet exhaust gas temperature due to the VGT expansion ratio decrease [236].

2.6 Summary

In the second Chapter of this doctoral thesis an initial introduction was conducted relating the current European normative for passenger cars and their required ambient conditions framework applied in the RDE tests with the objective of this thesis. The reinforcement of the need of investigating the ambient conditions effect on the engine performance and aftertreatment operation to be able to optimise their functioning under extreme and normal circumstances was carried out. Those ideas concrete the basis of the concepts that must be considered before moving forward to next Chapters.

Then, still in the first part of the Chapter, the four main pollutants generated in combustion chamber in Diesel engines were addressed, which are the CO, HC, NO_x and particulate matter. The main formation mechanisms have been described. This section also included, for each emission, a brief summary of the main currently adopted technologies to reduce their formation or chemically transform them in less harmful gases, which include the use of aftertreatment systems.

Subsequently, the individual impact of ambient temperature and pressure mainly in the Diesel engine performance, focusing on fuel consumption and emissions, was addressed. While the BSFC is clearly damaged by colder environments, affecting specially cold-start events, and by the altitude, the emissions resulted to be more complex and dependent on the engine calibration and on the handling of the EATS. Referred to this last point, the main factors governing the EATS response can be directly influenced by the different engine behaviour under different ambient temperatures and pressures.

Therefore, an important analysis of how different flow properties imply on the DOC and DPF operation was conducted. On one hand, the DPF

filtration is dependent on the exhaust flow, translated into dwell time, and on soot level in the exhaust gas, whereas the DPF regeneration comes along with the temperature and either the NO_2, in case of passive regeneration, or the O_2, in case of active regeneration, reactants partial pressures. Similarly, the DOC operation is dependent on the oxygen partial pressure, on the dwell time and on the monolith inlet temperature.

Lastly, the main strategies applied to optimise the DOC and the DPF operation were presented. They are divided into passive and active, according to the presence or not of an external energy source for the EATS operation improvement and if a volunteered action upon the engine calibration was executed. Different approaches conduct to an improvement specially on the EATS inlet temperature, including solutions that additionally present positive results in terms of engine fuel consumption.

Bibliography

[18] I. A. Reşitoğlu, K. Altinişik, and A. Keskin. "The pollutant emissions from Diesel-engine vehicles and exhaust aftertreatment systems". *Clean Technologies and Environmental Policy, 17, 15-27* (2015) (cit. on pp. 2, 17, 20).

[23] M. Soleimani, F. Campean, and D. Neagu. "Reliability challenges for automotice aftertreatment systems: A state-of-the-art perspective". *Procedia Manufacturing 16, 75-82* (2018) (cit. on pp. 3, 28).

[27] *Commission Regulation (EU) 2017/1151 of 1 June 2017 supplementing Regulation (EC) No 715/2007 of the European Parliament and of the Council on type-approval of motor vehicles with respect to emissions from light passenger and commercial vehicles (Euro 5 and Euro 6) and on access to vehicle repair and maintenance information, amending Directive 2007/46/ EC of the European Parliament and of the Council, Commission Regulation (EC) No 692/2008 and Commission Regulation (EU) No 1230/2012 and repealing Commission Regulation (EC) No 692/2008 (Text with EEA relevance)*. 2017 (cit. on pp. 3, 16, 73).

[32] *UNEP - World Conservation Monitoring Centre. The delineation of European mountain areas. Available in:*

https://ec.europa.eu/regional_policy/sources/docgener/studies/pdf/montagne/mount4.pdf (accessed on 24 November 2021). 2000 (cit. on pp. 4, 22).

[33] J. R. Serrano, P. Piqueras, A. Abbad, R. Tabet, S. Bender, and J. Gómez. "Impact on reduction of pollutant emissions from passenger cars when replacing Euro 4 with Euro 6d Diesel engines considering the altitude influence". *Energies, 12, 1278-1302* (2019) (cit. on pp. 4, 16, 26, 39).

[35] H. Giraldo and J. I. Huertas. "Real emissions, driving patterns and fuel consumption of in-use diesel buses operating at high altitude". *Transportation Research Part D, 77, 21-36* (2019) (cit. on pp. 4, 26).

[36] J. M. Luján, H. Climent, S. Ruiz, and A. Moratal. "Influence of ambient temperature on Diesel engine raw pollutants and fuel consumption in different driving cycles". *Internal Journal of Engine Research, 20 (8-9), 877-888* (2019) (cit. on pp. 4, 23).

[37] Y. Wang, Y. Ge, J. Wang, X. Wang, H. Yin, L. Hao, and J. Tan. "Impact of altitude on the real driving emission (RDE) results calculated in accordance to moving averaging window (MAW) method". *Fuel, 277, 117929.* (2020) (cit. on pp. 4, 26).

[38] H. Zhou, H. Zhao, Q. Fenf, Z. Yin, J. Li, K. Qin, M. Li, and L. Cao. "Effects of environmental parameters on real-world NO_x emissions and fuel consumption for heavy-duty diesel trucks using an OBD approach". In: *SAE Technical Paper 2018-01-1817.* 2018 (cit. on pp. 4, 27).

[39] A. Ramos, R. García-Contreras, and O. Armas. "Performance, combustion timing and emissions from a light duty vehicle at different altitudes fueled with animal fat biodiesel, GTL and diesel fuels". *Applied Energy, 182, 507-517* (2016) (cit. on pp. 4, 26, 27, 120).

[40] L. Yu et al. "Experimental investigation of the impact of biodiesel on the combustion and emission characteristics of a heavy duty Diesel engine at various altitudes". *Fuel, 115, 220-226* (2014) (cit. on pp. 4, 26, 27).

[41] J. Gao, A. Tian G.and Sorniotti, A. E. Karci, and R. Di Palo. "Review of thermal management of catalytic converters to decrease engine emissions during cold start and warm up". *Applied Thermal Engineering, 147, 177-187* (2019) (cit. on pp. 4, 29).

[43] L. Shen and Y. Shen. "Combustion process of Diesel engines at regions with different altitude". In: *SAE Technical Paper 950857*. 1995 (cit. on pp. 4, 26).

[44] M. R. Hamedi, O. Doustdar, A. Tsolakis, and J. Hartland. "Thermal energy storage system for efficient diesel exhaust aftertreatment at low temperatures". *Applied Energy, 235, 874-887* (2019) (cit. on pp. 4, 37, 126).

[45] P. Piqueras, A. García, J. Monsalve-Serrano, and M. J. Ruiz. "Performance of a diesel oxidation catalyst under diesel-gasoline reactivity controlled compression ignition combustion conditions". *Energy Conversion and Management, 196, 18-31* (2019) (cit. on pp. 5, 30, 31, 89, 107, 122).

[46] A. Joshi. "Review of vehicle engine efficiency and emissions." In: *SAE Technical Paper 2020-01-0352*. 2020 (cit. on pp. 16, 220).

[47] *Council Directive 91/441/EEC of 26 June 1991 amending Directive 70/220/EEC on the approximation of the laws of the Member States relating to measures to be taken against air pollution by emissions from motor vehicles. Available in: eur-lex.europa.eu. (accessed on 24 November 2021)* (cit. on p. 16).

[48] A. Zardini and P. Bonnel. "Real driving emissions regulation: European methodology to fine tune the EU real driving emissions data evaluation method, EUR 30123 EN". *Publications Office of the European Union, Luxembourg, ISBN 978-92-76-17157-7* (2020) (cit. on p. 16).

[49] R. Suarez-Bertoa, M. Pechout, M. Vojtíšek, and C. Astorga. "Regulated and non-regulated emissions from Euro 6 diesel, gasoline and CNG vehicles under real-world driving conditions". *Atmosphere* (2020) (cit. on p. 16).

[50] *Delphi Technologies. Worldwide emissions standards: Passenger cars and light duty vehicles 2019-2020.* Delphi Technologies, 2019 (cit. on p. 16).

[51] *Delphi Technologies. Worldwide emissions standards: Passenger cars and light duty vehicles 2017-2018.* 2017 (cit. on p. 16).

[52] *China's stage 6 emission standard for new light-duty vehicles (final rule).* International Council on Clean Transportation (ICCT), 2012 (cit. on p. 16).

[53] *Flash Cleaner Machine. Available in: https://flashcleanermachine.com/italiano-euro-standard/?doing_wp_cron=1612006181. 2863910198211669921875. (accessed on 24 November 2021)* (cit. on p. 17).

[54] R. Prasad and V. R. Bella. "A review on diesel soot emission, its effect and control". *Bulletin of Chemical Reaction Engineering & Catalysis, 5 (2), 69-86* (2010) (cit. on p. 17).

[55] M. A. H. M. Nawi, M. H. M. Hanid, W. A. Mustafa, and R. I. R. Kasim M. S. Abdullah. "Pollutant emission in Diesel engine". In: *SympoSIMM 2019: Intelligent Manufacturing and Mechatronics, 288-298, Malaysia.* 2019 (cit. on p. 18).

[56] *EPA, Effects of Air Pollutants - Health Effects, Available in: http://www.epa.gov/apti/course422/ap7a.html. (accessed on 24 November 2021)* (cit. on p. 18).

[57] C. W. Wu, R. H. Chen, J. Y. Pu, and T. H. Lin. "The influence of air-fuel ratio on engine performance and pollutant emission of an SI engine using ethanol-gasoline-blended fuels". *Atmospheric Environment, 38, 7093-7100* (2004) (cit. on p. 18).

[58] M. R. Sumanlal, S. Nandakumar, and P. Mohanan. "The effect of air preheating on the performance and emission characteristics of a DI Diesel engine achieving HCCI mode of combustion". *International Journal of Theoretical and Applied Mechanics, 12 (3), 411-421* (2017) (cit. on p. 18).

[59] W. M. Pitts. "The global equivalence ratio concept and the formation mechanisms of carbon monoxide in enclosure fires". *Progress in Energy and Combustion Science, 21, 197-237* (1995) (cit. on p. 18).

[60] T. Alger, T. Chauvet, and Z. Dimitrova. "Synergies between high EGR operation and GDI systems". *SAE International Journal of Engines, 1 (1), 101-114* (2008) (cit. on p. 18).

[61] J. T. Kashdan, P. Anselmi, and B. Walter. "Advanced injection strategies for controlling low-temperature diesel combustion and emissions". *SAE International Journal of Engines, 2 (1), 1835-1856* (2009) (cit. on p. 19).

[62] K. N. Abdalla and E. A. Mustafa. "Effect of exhaust gas recirculation on CO emissions from a turbocharged Diesel engine". *UofKEJ, 4 (2), 43-48* (2014) (cit. on p. 19).

[63] Y. Hardalupas, C. Hong, C. Keramiotis, G. K. Ramaswamy, A. M. K. P. Soulopoulos N. Taylor, D. Touloupis, and M. A. Vourliotakis G. Founti. "Towards identifying flame patterns in multiple, late injection schemes on a single-cylinder optical Diesel engine". *Combustion Science and Technology, 188, 2217-2235* (2016) (cit. on p. 19).

[64] D. Demers and G. Walters. *Guide to exhaust emission control options.* Ed. by B. BAeSAME. 1999 (cit. on p. 19).

[65] R. K. Dadi, K. Daneshvar, D. Luss, V. Balakotaiah, C. M. Kalamaras, and W. Epling. "Comparison of light-off performance of Pt-Pd/γ-Al2O3 dual layer and dual brick diesel oxidation catalysts". *Chemical Engineering Journal, 335, 1004-1017* (2018) (cit. on p. 19).

[66] Y. Hiroyuki, K. Misawa, D. Suzuki, K. Tanaka, J. Matsumoto, M. Fujii, and K. Tanaka. "Detailed analysis of diesel vehicle exhaust emissions: nitrogen oxides, hydrocarbons and particulate size distributions". *Proceedings of the Combustion Institute, 33, 2895-2902* (2011) (cit. on p. 19).

[67] J. Bennett. "Sources of unburned hydrocarbons in a lean burn engine". PhD thesis. United Kingdom, 1992 (cit. on p. 19).

[68] B. Chehroudi. "Diesel engine emissions: Hydrocarbons (HC)". *ResearchGate* (2001) (cit. on p. 19).

[69] X. Miao, G. Zhang, Y. Ju, X. Wang, J. Hong, J. Zheng, X. Qiao, and Z. Huang. "Study on premixed combustion in a Diesel engine with ultra-multihole nozzle". *Journal of Combustion, 471648, 16 pages* (2011) (cit. on p. 19).

[70] M. Zheng, M. C. Mulenga, G. T. Reader, Wang, M. Ting, D. S., and J. Tjong. "Biodiesel engine performance and emissions in low temperature combustion." *Fuel, 87, 714-722* (2008) (cit. on p. 19).

[71] N. S. Ayoub and R. D. Reitz. "Multidimensional modeling of fuel composition effects on combustion and cold-starting in Diesel engines". In: *SAE Technical Paper 952425.* 1995 (cit. on p. 19).

[72] J. O'Connor, M. P. B. Musculus, and L. M. Pickett. "Effect of post injections on mixture preparation and unburned hydrocarbon emissions in a heavy-duty Diesel engine". *Combustion and Flame, 170, 111-123* (2016) (cit. on pp. 19, 40).

[73] K. Yamamoto, K. Takada, J. Kusaka, and Y. Kanno. "Influence of diesel post injection timing on HC emissions and catalytic oxidation performance". In: *SAE Technical Papers 2006-01-3442*. 2006 (cit. on p. 20).

[74] F. Payri, V. R. Bermúdez, B. Tormos, and W. G. Linares. "Hydrocarbon emissions speciation in diesel and biodiesel exhausts." *Atmospheric Environment, 43, 1273-1279* (2009) (cit. on pp. 20, 89, 110).

[75] Q. Xin. *Diesel engine system design, 503-525, Ed. 1.* Elsevier, 2013 (cit. on pp. 20, 41).

[76] K. Akihama, Y. Takatori, K. Inagaki, S. Sasaki, and A. M. Dean. "Mechanism of the smokeless rich diesel combustion by reducing temperature". *SAE Transactions, 110 (3), 648-662* (2001) (cit. on p. 20).

[77] S. E. Hosseini, M. Wahid, and A. Abuelnuor. "High temperature air combustion: Sustainable technology to low NO_x formation". *International Review of Mechanical Engineering, 6 (5), 947-953* (2012) (cit. on p. 20).

[78] T. Lee, J. Park, S. Kwon, J. Lee, and J. Kim. "Variability in operation-based NO_x emission factors with different test routes, and its effects on the real-driving emissions of light diesel vehicles." *Science of the Total Environment, 461-462, 377-385* (2013) (cit. on p. 20).

[79] X. Wang, D. Wasterdahl, H. Jingnan, Y. Wu, H. Yin, X. Pan, and K. M. Zhang. "On-road diesel vehicle emission factors for nitrogen oxides and black carbon in two Chinese cities". *Atmospheric Environment, 46, 45-55* (2012) (cit. on p. 20).

[80] V. Grewe, K. Dahlmann, S. Matthes, and W. Steinbrecht. "Attributing ozone to NO_x emissions: implications for climate mitigation measures". *Atmospheric Environment, 59, 102-107* (2012) (cit. on p. 20).

[81] P. E. Morrow. "Toxicological data on NO_x: An overview". *Journal of Toxicology and Environmental Health, 13, 205-227* (1984) (cit. on p. 20).

[82] P. Bedar and G. N. Kumar. "Exhaust gas recirculation (EGR) - Effective way to reduce NO_x emissions". *Journal of Mechanical Engineering and Biomechanics, 1 (2), 69-73* (2016) (cit. on p. 20).

[83] S. C. Ko, K. C. Oh, C. Seo, and C. B. Lee. "Characteristics on NO_x adsorption and intermediates of LNT catalyst". *International Journal of Automotive Technology, 15 (3), 347-352* (2014) (cit. on p. 21).

[84] F. Gao, X. Tang, H. Yi, S. Zhao, C. Li, J. Li, Y. Shi, and X. Meng. "A review on selective catalytic reduction of NO_x by NH_3 over Mn-based catalysts at low temperatures: Catalysts, mechanisms, kinetics and DFT calculations". *Catalysts, 7, 199* (2017) (cit. on pp. 21, 221).

[85] D. B. Kittelson, W. F. Watts, and J. P. Johnson. "On-road and laboratory evaluation of combustion aerosols - Part1: Summary of Diesel engine results". *Journal of Aerosol Science, 37 (8), 913-930* (2006) (cit. on p. 21).

[86] D. Agarwal and A. K. Agarwal. "Performance and emissions characteristics of Jatrophaoil (preheated and blends) in a direct injection compression ignition engine". *Applied Thermal Engineering, 27 (13), 2314-2323* (2007) (cit. on pp. 21, 38).

[87] J. Weidman and S. Marshall. *Soot Pollution 101. American Progress. Available in: https://americanprogress.org/article/soot-pollution-101/. (accessed on 24 November 2021).* 2012 (cit. on p. 21).

[88] C. A. Pope III and D. W. Dockery. "Acute health effects of PM10 pollution on symptomaticand asymptomatic children". *American Review of Respiratory Disease, 145 (5), 1123-1128* (1992) (cit. on p. 21).

[89] E. Boldo, S. Medina, A. Le Tertre, F. Hurley, H. Mücke, F. Ballester, and I. e. a. Aguilera. "Apheis: Health impact assessment of long-term exposure to PM2.5 in 23 European cities". *European Journal of Epidemiology, 21 (6), 449-458* (2006) (cit. on p. 21).

[90] H. Wiinikka, R. Gebart, C. Boman, D. Boström, and M. Öhman. "Influence of fuel ash composition on high temperature aerosol formation in fixed bed combustion of woody biomass pellets". *Fuel, 86 (1), 181-193* (2007) (cit. on p. 21).

[91] M. M. Maricq. "Chemical characterization of particulate emissions from Diesel engines: a review." *Journal of Aerosol Science, 38, 1079-1118* (2007) (cit. on p. 21).

[92] H. Bockhorn. *Soot Formation in Combustion, Ed. 1.* Springfield, 1994 (cit. on p. 21).

[93] B. Guan, R. Zhan, H. Lin, and Z. Huang. "Review of the state-of-the-art of exhaust particulate filter technology in internal combustion engines". *Journal of Environmental Management, 154 (1), 225-258* (2015) (cit. on pp. 21, 34, 38, 40).

[94] T. Kuki, Y. Miyairi, Y. Kasai, M. Miyazaki, and S. Miwa. "Study on reliability of wall-flow-type diesel particulate filter". In: *SAE Technical Paper 2004-01-0959*. 2004 (cit. on p. 21).

[95] R. Bosch. *Emissions-control technology for Diesel engines.* Robert Bosch GmbH, 2005 (cit. on p. 21).

[96] *ISO, Standard Atmosphere, ISO 2533:1975, International Standard Organization, 2533*. 1975 (cit. on p. 22).

[97] NORDREGIO. "Mountain areas in Europe: Analysis of mountain areas in EU member states, acceding and other European countries - Final report". *European Commission contract, 2002.CE.16.0.AT.136* (2002) (cit. on p. 22).

[98] J. M. Luján, H. Climent, L. M. García-Cuevas, and A. Moratal. "Pollutant emissions and diesel oxidation catalyst performance at low ambient temperatures in transient load conditions". *Applied Thermal Engineering, 129, 1527-1537* (2018) (cit. on pp. 22, 24, 31).

[99] A. Romagnoli, A. Manivannan, S. Rajoo, M. S. Chiong, A. Feneley, A. Pesiridis, and R. F. Martinez-Botas. "A review of heat transfer in turbochargers". *Renewable and Sustainable Energy Reviews, 79, 1442-1460* (2017) (cit. on p. 22).

[100] M. Hamdya, A. A. Akalany, K. Harbya, and N. Kora. "An overview on adsorption cooling systems powered by waste heat from internal combustion engine". *Renewable and Sustainable Energy Reviews, 51, 1223-1234* (2015) (cit. on p. 22).

[101] F. Westin, J. Rosenqvist, and H. E. Angström. "Heat losses from the turbine of a turbocharged SI-engine - Measurements and simulation". In: *SAE Technical Paper 2004-01-0996*. 2004 (cit. on p. 22).

[102] Y. Chang, B. Mendrea, J. Sterniak, and S. V. Bohac. "Effect of ambient temperature and humidity on combustion and emissions of a spark-assisted compression ignition engine". *Journal of Engineering for Gas Turbines and Power, 139 (5), 051501* (2017) (cit. on p. 23).

[103] J. V. Pastor, J. M. García-Oliver, J. M. Pastor, and J. G. Ramírez-Hernández. "Ignition and combustion development for high speed direct injection Diesel engines under low temperature cold start conditions". *Fuel, 90, 1556-1566* (2011) (cit. on p. 23).

[104] Q. Li, P. J. Shayler, M. McGhee, and A. La Rocca. "The initiation and development of combustion under cold idling conditions using a glow plug in Diesel engines". *Internal Journal of Engine Research, 18 (3), 240-255* (2017) (cit. on p. 23).

[105] K. Y. Cheng, P. J. Shayler, and M. Murphy. "The influence of blow-by on indicated work output from a Diesel engine under cold start conditions". *Proceedings of the Institution of Mechanical Engineers, Part D: Journal of Automobile Engineering, 218 (3), 333-340* (2004) (cit. on p. 23).

[106] R. Rahmani, H. Rahnejat, B. Fitzsimons, and D. Dowson. "The effect of cylinder liner operating temperature on frictional loss and engine emissions in piston ring conjunction". *Applied Energy, 191, 568-581* (2017) (cit. on p. 23).

[107] A. Maiboom, X. Tauzia, X. R. Shah, and J.-H. Hétet. "Experimental study of an LP EGR system on an automotive Diesel engine, compared to HP EGR with respect to PM and NO_x emissions and specific fuel consumption". In: *SAE Technical Paper 2009-24-0138*. 2009 (cit. on p. 23).

[108] J. M. Luján, C. Guardiola, B. Pla, and A. Reig. "Switching strategy between HP- and LP EGR systems for reducedfuel consumption and emissions". *Energy, 00, 1-20* (2015) (cit. on p. 23).

[109] M. Lapuerta, A. Ramos, D. Fernández-Rodríguez, and I. González-García. "High-pressure versus low-pressure exhaust gas recirculation in a Euro 6 Diesel engine with lean-NO_x trap: Effectiveness to reduce NO_x emissions". *Internal Journal of Engine Research, 20 (5), 155-163* (2018) (cit. on pp. 23, 24, 39).

[110] J. Galindo, R. Navarro, D. Tarí, and F. Moya. "Development of an experimental test bench and a psychrometric model for assessing condensation on a low-pressure exhaust gas recirculation cooler." *International Journal of Engine Research, 22 (5), 1540-1550* (2020) (cit. on pp. 23, 24).

[111] A. J. Torregrosa, A. Broatch, P. Olmeda, and C. Romero. "Assessment of the influence of different cooling system configurations on engine warm-up, emissions and fuel consumption". *International Journal of Automotive Technology, 9, 447-458* (2008) (cit. on p. 23).

[112] P. Bielaczyc, A. Szczotka, and J. Woodburn. "The effect of a low ambient temperature on the cold-start emissions and fuel consumption of passenger cars". *Proceedings of the Institution of Mechanical Engineers, Part D, 225, 1253-1264* (2011) (cit. on p. 23).

[113] M. Weilenmann, P. Soltic, C. Saxer, A.-M. Forss, and N. Heeb. "Regulated and nonregulated diesel and gasoline cold start emissions at different temperatures". *Atmospheric Environment, 39 (13), 2433-2441* (2005) (cit. on p. 23).

[114] M. V. Faria, R. A. Varella, G. O. Duarte, L. Farias T., and P. C. Baptista. "Engine cold start analysis using naturalistic driving data: City level impacts on local pollutants emissions and energy consumption." *Science of the Total Environment, 630, 544-559* (2018) (cit. on pp. 23, 25).

[115] M. Weilenmann, J.-Y. Favez, and R. Alvarez. "Cold-start emissions of modern passenger cars at different low ambient temperatures and their evolution over vehicle legislation categories". *Atmos Environ, 43, 2419-2429* (2009) (cit. on pp. 23, 24).

[116] J. Ko, D. Jin, W. Jang, C. L. Myung, S. Kwon, and S. Park. "Comparative investigation of NO_x emission characteristics from a Euro 6-compliant diesel passenger car over the NEDC and WLTC at various ambient temperatures". *Applied Energy, 187, 652-662* (2017) (cit. on pp. 23, 25).

[117] T. W. Chan, E. Meloche, J. Kubsh, R. Brezny, D. Rosenblatt, and G. Rideout. "Impact of ambient temperature on gaseous and particle emissions from a direct injection gasoline vehicle and its implications on particle filtration". In: *SAE Technical Paper 2013-01-0527.* 2013 (cit. on p. 23).

[118] C. H. Zhang, J. R. Pan, J. J. Tong, and J. Li. "Effects of intake temperature and excessive air coefficient on combustion characteristics and emissions of HCCI combustion". *Procedia Environmental Sciences, 11, 1119-1127* (2011) (cit. on p. 24).

[119] M. Torres García, F. José Jiménez-Espadafor Aguilar, and T. Sánchez Lencero. "Experimental study of the performances of a modified Diesel engine operating in homogeneous charge compression ignition (HCCI) combustion mode versus the original diesel combustion mode". *Energy, 34 (2), 159-171* (2009) (cit. on p. 24).

[120] W. A. Daniel. "Flame quenching at the walls on an internal combustion engine." *Proceedings of the Combustion Institute, 6, 886-902* (1957) (cit. on p. 24).

[121] A. Roberts, R. Brooks, and P. Shipway. "Internal combustion engine cold-start efficiency: A review of the problem, causes and potential solutions". *Energy Conversion and Management, 82, 327-350* (2014) (cit. on p. 24).

[122] J. Tian, H. Xu, R. A. Sakunthalai, D. Liu, C. Tan, and A. Ghafourian. "Low ambient temperature effects on a modern turbocharged Diesel engine running in a driving cycle". In: *SAE Technical Paper 2014-01-2713*. 2014 (cit. on pp. 24, 25).

[123] J. Galindo, P. Piqueras, R. Navarro, D. Tarí, and C. M. Meano. "Validation and sensitivity analysis of an in-flow water condensation model for 3d-CFD simulations of humid air streams mixing". *International Journal of Thermal Sciences, 136, 410-419* (2019) (cit. on pp. 24, 220).

[124] R. A. Sakunthalai, H. Xu, D. Liu, J. Tian, M. Wyszynski, and J. Piaszyk. "Impact of cold ambient conditions on cold start and idle emissions from Diesel engines". In: *SAE Technical Paper 2014-01-2715*. 2014 (cit. on pp. 24, 25).

[125] Z. Ning, C. S. Cheung, and S. X. Liu. "Experimental investigation of the effect of exhaust gas coolingon diesel particulate". *Journal of Aerosol Science, 35, 333-345* (2004) (cit. on p. 25).

[126] G. Olivares, C. Johansson, J. Ström, and H.-C. Hansson. "The role of ambient temperature for particle number concentrations in a street canyon". *Atmospheric Environment, 41 (10), 2145-2155* (2007) (cit. on p. 25).

[127] D. Ludykar, R. Westerholm, and J. Almén. "Cold start emissions at +22, -7 and -20°C ambient temperatures from a three-way catalyst (TWC) car: Regulated and unregulated exhaust components". *Science of The Total Environment, 235, (1-3), 65-69* (1999) (cit. on p. 25).

[128] V. Bermúdez, J. R. Serrano, P. Piqueras, J. Gómez, and S. Bender. "Analysis of the role of altitude on Diesel engine performance and emissions using an atmosphere simulator". *International Journal of Engine Research, 18, 105-117* (2017) (cit. on pp. 26, 27, 68, 120).

[129] Z. Kan, Z. Hu, D. Lou, P. Tan, Z. Cao, and Z. Yang. "Effects of altitude on combustion and ignition characteristics of speed-up period during cold start in a Diesel engine". *Energy, 150, 164-175* (2018) (cit. on p. 26).

[130] X. Wang, H. Yin, Y. Ge, L. Yu, Z. Xu, C. Yu, X. Shi, and H. Liu. "On-vehicle emission measurement of a light-duty diesel van at various speeds at high altitude". *Atmospheric Environment, 81 (2013) 263-269* (2013) (cit. on pp. 26, 27, 31).

[131] M. Szedlmayer and C. M. Kweon. "Effect of altitude conditions on combustion and performance of a multi-cylinder turbocharged direct injection Diesel engine". In: *SAE Technical Paper 2016-01-0742*. 2016 (cit. on pp. 26, 27).

[132] E. Zervas. "Impact of altitude on fuel consumption of a gasoline passenger car". *Fuel, 90, 2340-2342* (2011) (cit. on p. 26).

[133] C. P. Benjumea, J. Agudelo, and A. Agudelo. "Effect of altitude and palm oil biodiesel fuelling on the performance and combustion characteristics of a HSDI Diesel engine". *Fuel, 88, 725-731* (2009) (cit. on p. 27).

[134] C. A. Chaffin and T. L. Ullman. "Effects of increased altitude on heavy-duty Diesel engine emissions". In: *SAE Technical Paper 940669*. 1994 (cit. on p. 27).

[135] C. McCaffery, H. Zhua, C. Li, T. D. Durbin, K. C. Johnson, H. Jung, R. Brezny, M. Geller, and G. Karavalakis. "On-road gaseous and particulate emissions from GDI vehicles with and without gasoline particulate filters (GPFs) using portable emissions measurement systems (PEMS)". *Science of the Total Environment. 710. 136366* (2020) (cit. on pp. 27, 221).

[136] H. Wang et al. "The real driving emission characteristics of light duty diesel vehicle at various altitudes". *Atmospheric Environment, 191, 126-131* (2018) (cit. on p. 27).

[137] J. M. Luján, J. R. Serrano, P. Piqueras, and O. García-Afonso. "Experimental assessment of a pre-turbo aftertreatment configurations in a single stage turbocharged Diesel engine. Part 2: Transient operation". *Energy, 80, 614-27.* (2015) (cit. on pp. 28, 36, 126).

[138] C. K. Lambert. "Perspective on SCR NO_x control for diesel vehicles". *Reaction Chemistry and Engineering, 4 (6), 969-974* (2019) (cit. on p. 28).

[139] S. Shrestha, M. P. Harold, and K. Kamasamudram. "Experimental and modeling study of selective ammonia oxidation on multi-functional washcoated monolith catalysts". *Chemical Engineering Journal, 278, 24-35* (2015) (cit. on p. 28).

[140] T. C. Watling, M. R. Ravenscroft, and G. Avery. "Development, validation and application of a model for an SCR catalyst coated diesel particulate filter". *Catalysis Today, 188 (1), 32-41* (2012) (cit. on p. 29).

[141] A. P. E. York and A. Tsolakis. "Cleaner vehicle emissions". *Encyclopedia of Materials: Science and Technology, 2, 1-7* (2010) (cit. on p. 29).

[142] M. Fayad, A. Tsolakis, D. Fernández-Rodríuez, J. Herreros, F. Martos, and M. Lapuerta. "Manipulating modern Diesel engine particulate emission characteristics through butanol fuel blending and fuel injection strategies for efficient diesel oxidation catalysts". *Applied Energy, 190, 490-500* (2017) (cit. on p. 29).

[143] S. Ye, Y. H. Yap, S. T. Kolaczkowski, K. Robinson, and D. Lukyanov. "Catalyst 'light-off' experiments on a diesel oxidation catalyst connected to a Diesel engine- Methodology and techniques". *Chemical Engineering Research and Design, 90, 834-845* (2012) (cit. on pp. 29, 31).

[144] J. Cooper and J. Beecham. "A study of platinum group metals in three-way autocatalysts". *Platinum Metals Review, 57 (4), 281-288* (2013) (cit. on p. 29).

[145] P. Tayal. "Light off temperature based approach to determine diesel oxidation catalyst effectiveness level and the corresponding outlet NO and NO_2 characteristics". MA thesis. Purdue University, West Lafayette, United States, 2014 (cit. on p. 29).

[146] D. Kryl, P. Kočí, M. Kubíček, M. Marek, T. Maunula, and M. Härkönen. "Catalytic converters for automobile Diesel engines with adsorption of hydrocarbons on zeolites". *Industrial & Engineering Chemistry Research, 44 (25), 9524-9534* (2005) (cit. on p. 29).

[147] E. Zervas. "Parametric study of the main parameters influencing the catalytic efficiency of a diesel oxidation catalyst: parameters influencing the efficiency of a diesel catalyst". *International Journal of Automotive Technology, 9 (6), 641-647* (2008) (cit. on pp. 29, 31).

[148] K. Robinson, S. Ye, Y. Yap, and S. T. Kolaczkowski. "Application of a methodology to assess the performance of a full-scale diesel oxidation catalyst during cold and hot start NEDC drive cycles". *Chemical Engineering Research and Design, 91 (7), 1292-1306* (2013) (cit. on p. 29).

[149] A. A. Yusuf and F. L. Inambao. "Effect of cold start emissions from gasoline-fueled engines of light-duty vehicles at low and high ambient temperatures: Recent trends". *Case Studies in Thermal Engineering, 14, 100417* (2019) (cit. on pp. 30, 34).

[150] C. Guardiola, B. Pla, P. Bares, and J. Mora. "An on-board method to estimate the light-off temperature of diesel oxidation catalysts". *Intenational Journal of Engine Research, 21 (8), 1480-1492* (2018) (cit. on pp. 30, 107).

[151] S. R. Christensen, B. B. Hansen, K. H. Pedersen, J. R. Thøgersen, and A. D. Jensen. "Selective catalytic reduction of NO_x over V_2O_5-WO_3-TiO_2 SCR catalysts - A study at elevated pressure for maritime pre-turbine SCR configuration". *Emission Control Science and Technology, 5, 263-278* (2019) (cit. on p. 30).

[152] P. Y. Peng, M. P. Harold, and D. Luss. "Sustained concentration and temperature oscillations in a diesel oxidation catalyst". *Chemical Engineering Journal, 5, 263-278* (2019) (cit. on p. 30).

[153] D. Peitz, M. Elsener, and O. Kröcher. "Impact of catalyst geometry on diffusion and selective catalytic reduction kinetics under elevated pressures". *Chemie Ingenieur Technik, 90, 795-802* (2018) (cit. on p. 30).

[154] I. Langmuir. "The mechanism of the catalytic action of platinum in the reaction $2CO + O_2 = CO_2$ and $2H_2 + O_2 = 2H_2O$". *Transactions of the Faraday Society, 17, 607-654* (1922) (cit. on p. 30).

[155] C. Boerensen, D. Roemer, C. Nederlof, E. Smirnov, F. Linzen, F. Goebel, and B. Carberry. "Twin-LNT system for advanced diesel exhaust gas aftertreatment". *SAE International Journal of Fuels and Lubricants, 10, 619-633* (2017) (cit. on p. 30).

[156] F. Payri, F. J. Arnau, P. Piqueras, and M. J. Ruiz. "Lumped approach for flow-through and wall-flow monolithic modelling for real-time automotive applications". In: *SAE Technical Paper 2018-01-0954*. 2018 (cit. on pp. 31, 86, 92, 107).

[157] R. Hasegawa and H. Yanagihara. "HCCI combustion in DI Diesel engine". In: *SAE Technical Paper 2003-01-0745*. 2003 (cit. on p. 31).

[158] S. H. Oh and J. C. Cavendish. "Transients of monolithic catalytic converters. Response to step changes in feedstream temperature as related to controlling automobile emissions". *Industrial & Engineering Chemistry Product Research and Development, 21, 29-37* (1982) (cit. on p. 31).

[159] P. Piqueras, M. J. Ruiz, J. M. Herreros, and A. Tsolakis. "Influence of the cell geometry on the conversion efficiency of oxidation catalysts under real driving conditions". *Energy Conversion and Management, 233,113888* (2021) (cit. on p. 31).

[160] A. Russell and W. S. Epling. "Diesel oxidation catalysts". *Catalysis Reviews - Science and Engineering, 53 (4), 337-423* (2011) (cit. on pp. 31, 106).

[161] S. E. Voltz, C. R. Morgan, D. Liederman, and S. M. Jacob. "Kinetic study of carbon monoxide and propylene oxidation on platinum catalysts". *Industrial & Engineering Chemistry Product Research and Development, 12 (4), 294-301* (1973) (cit. on pp. 31, 90).

[162] O. Chiavola, G. Chiatti, and N. Sirhan. "Impact of particulate size during deep loading on DPF management". *Applied Sciences, 9, 3075* (2019) (cit. on p. 31).

[163] X. Hou, S. Du, Z. Liu, J. Guo, and Z. Li. "A transfer matrix approach for structural-acoustic correspondence analysis of diesel particulate filter". *Advances in Mechanical Engineering, 9 (9), 1-10* (2017) (cit. on p. 32).

[164] A. G. Konstandopoulos, M. Kostoglou, E. Skaperdas, E. Papaioannou, D. Zarvalis, and E. Kladopoulou. "Fundamental studies of diesel particulate filters: transient loading, regeneration, and aging". In: *SAE Technical Paper 2000-01-1016*. 2000 (cit. on p. 32).

[165] S. Choi, K.-C. Oh, and C.-B. Lee. "The effects of filter porosity and flow conditions on soot deposition/oxidation and pressure drop in particulate filters". *Energy, 77 (1), 327-337* (2014) (cit. on p. 32).

[166] A. J. Torregrosa, J. R. Serrano, F. J. Arnau, and P. Piqueras. "A fluid dynamic model for unsteady compressible flow in wall-flow diesel particulate filters". *Energy, 36 (1), 671-684* (2011) (cit. on pp. 32, 66).

[167] K. W. Lee and J. A. Gieseke. "Collection of aerosol particles by packed beds". *Envirnmental Science & Technology ,13 (4), 466-470* (1979) (cit. on pp. 32, 94, 95).

[168] B. van Setten, M. Makkee, and J. A. Moulijn. "Science and technology of catalytic diesel particulate filters". *Catalysis Reviews, 43 (4), 489-564* (2001) (cit. on p. 32).

[169] P. Tandon, A. Heibel, J. Whitmore, N. Kekre, and K. Chithapragada. "Measurement and prediction of filtration efficiency evolution of soot loaded diesel particulate filters". *Chemical Engineering Science, 65, 4751-4760* (2010) (cit. on p. 32).

[170] J. R. Serrano, H. Climent, P. Piqueras, and E. Angiolini. "Filtration modelling in wall-flow particulate filters of low soot penetration thickness". *Energy, 112, 883-898* (2016) (cit. on pp. 32, 93, 94).

[171] I. P. Kandylas and G. C. Koltsakis. "NO_2 - Assisted regeneration of diesel particulate filters: A modeling study". *Industrial & Engineering Chemistry Research, 41, 2115-2123* (2002) (cit. on pp. 33, 35).

[172] S. Quiles-Díaz, J. Giménez-Mañogil, and A. García-García. "Catalytic performance of CuO/Ce 0.8 Zr $0.2O_2$ loaded over SiC-DPF in NO_x-assisted combustion of diesel soot." *RSC Advances, 5 (22)* (2015) (cit. on p. 33).

[173] A. Abdalla, G. Wang, J. Zhang, and S.-J. Shuai. "Simulation of catalyzed diesel particulate filter for active regeneration process using secondary fuel injection". In: *International Powertrains, Fuels & Lubricants Meeting 10.4271/2017-01-2287*. 2017 (cit. on p. 33).

[174] S. Soltani, R. Andersson, and B. Andersson. "The effect of exhaust gas composition on the kinetics of soot oxidation and diesel particulate filter regeneration". *Fuel, 220, 453-463* (2018) (cit. on pp. 33, 166).

[175] S. Bai, G. Chen, Q. Sun, G. Wang, and G.-X. Li. "Influence of active control strategies on exhaust thermal management for diesel particular filter active regeneration". *Applied Thermal Engineering, 119, 297-303* (2017) (cit. on pp. 33, 41).

[176] M. Ahmadinejad, A. Tsolakis, J. M. Becker, C. F. Goersmann, A. D. Newman, and T. C. Watling. "Modelling of soot oxidation by NO_2 in a diesel particulate filter". *SAE International Journal of Fuels and Lubricants, 5, 359-369* (2012) (cit. on p. 33).

[177] T. C. Watling. "Understanding factors affecting the balance point (and rate of balance point approach) of a diesel particulate filter: an analytical expression for the balance point soot loading". *Emission Control Science and Technology, 6, 195-210* (2020) (cit. on p. 33).

[178] S. Bensaid, D. L. Marchisio, and D. Fino. "Numerical simulation of soot filtration and combustion within diesel particulate filters". *Chemical Engineering Science, 65, 357-363* (2010) (cit. on p. 33).

[179] B. R. Stanmore, J. F. Brilhac, and P. Gilot. "The oxidation of soot: A review of experiments, mechanisms and models". *Carbon, 39, 2247-2268* (2001) (cit. on p. 33).

[180] V. Macián, J. R. Serrano, P. Piqueras, and E. J. Sanchis. "Internal pore diffusion and adsorption impact on the soot oxidation in wall-flow particulate filters". *Energy, 179, 407-421* (2019) (cit. on pp. 33, 95, 96, 166, 175).

[181] E. Jiaqiang, M. Liu, Y. Deng, H. Zhu, and J. Gong. "Influence analysis of monolith structure on regeneration temperature in the process of microwave regeneration in the diesel particulate filter". *The Canadian Journal of Chemical Engineering, 94, 168-174* (2016) (cit. on p. 34).

[182] E. Jiaqiang, X. Zhao, L. Qiu, K. Wei, Z. Zhang, Y. Deng, D. Han, and G. Liu. "Experimental investigation on performance and economy characteristics of a Diesel engine with variable nozzle turbocharger and its application in urban bus". *Energy Conversion and Management, 1, 149-161* (2019) (cit. on p. 34).

[183] J. R. Serrano, P. Piqueras, J. de la Morena, and E. J. Sanchis. "Late fuel post-injection influence on the dynamics and efficiency of wall-flow particulate filters regeneration". *Applied Sciences, 2019, 9 (24), 5384* (2019) (cit. on pp. 34, 40, 88, 166, 168, 173).

[184] A. Suresh, A. Yezerets, N. Currier, and J. Clerc. "Diesel particulate filter system . Effect of critical variables on the regeneration strategy development and optimization". In: *SAE Technical Paper 2008-01-0329*. 2008 (cit. on p. 34).

[185] A. Kotrba, T. P. Gardner, L. Bai, and A. Yetkin. "Passive regeneration response characteristics of a DPF system". In: *SAE Technical Paper 2013-04-08*. 2013 (cit. on p. 35).

[186] A. P. E. York, M. Ahmadinejad, T. C. Watling, A. P. Walker, J. P. Cox, J. Gast, P. G. Blakeman, and R. Allansson. "Modeling of the catalyzed continuously regenerating diesel particulate filter (CCR-DPF) system: model development and passive regeneration studies". In: *SAE Technical Paper 2007-01-0043*. 2007 (cit. on p. 35).

[187] K. Ramanathan, D. H. West, and V. Balakotaiah. "Optimal design of catalytic converters for minimizing cold-start emissions". *Catalysis Today, 98, 357-373* (2004) (cit. on p. 35).

[188] A. Gurupatham and Y. He. "Architecture design and analysis of Diesel engine exhaust aftertreatment system and comparative study with close-coupled DOC-DPF system". In: *SAE Technical Paper 2008-01-1756*. 2008 (cit. on p. 35).

[189] L. Tingting. "Analysis on diesel aftertreatment system fault diagnosis for CRT ageing and failure". MA thesis. Beijing Jiaotong University, Beijing, China, 2012 (cit. on p. 35).

[190] A. Strzelec, R. Vander Wal, T. N. Thompson, and T. J. Toops. "NO_2 oxidation reactivity and burning mode of diesel particulates". *Topics in Catalysis, 59 (8), 686-694* (2016) (cit. on p. 35).

[191] A. Srinivasan and K. Price. "Consolidation of DOC and DPF functions into a single component". In: *SAE Technical Paper 2019-01-0583*. 2019 (cit. on p. 35).

[192] A. Punke, G. Grubert, Y. Li, J. Dettling, and T. Neubauer. "Catalyzed soot filters in close coupled position for passenger vehicles". In: *SAE Technical Paper 2006-01-1091*. 2006 (cit. on p. 36).

[193] V. Di Sarli, G. Landi, L. Lisi, A. Saliva, and A. Di Benedetto. "Catalytic diesel particulate filters with highly dispersed ceria: Effect of the soot-catalyst contact on the regeneration performance". *Applied Catalysis B: Environmental, 197, 116-124* (2016) (cit. on p. 36).

[194] N. He, Z. Jiang, and Z. Ning. "Comparison of catalytic conversion characteristics of different integrated aftertreatment systems in Diesel engine". *Journal of Physics: Conference Series, 1578, 012218* (2020) (cit. on p. 36).

[195] J. R. Serrano, P. Piqueras, J. De La Morena, and M. J. Ruiz. "Influence of pre-turbine small-sized oxidation catalyst on engine performance and emissions under driving conditions". *Applied Sciences, 10, 7714* (2020) (cit. on p. 36).

[196] C. Gökçöl and A. Uğurlu. "A review on thermal energy storage systems with phase change materials in vehicles". *Electronic Journal of Vocational Colleges, 2, 1-14* (2012) (cit. on p. 36).

[197] L. Xie, G. Jiang, and F. Qian. "Research on aftertreatment inlet outlet insulation for a non road middle range Diesel engine". *Catalysts, 10, 454* (2020) (cit. on p. 36).

[198] F. J. Arnau, J. Martín, P. Piqueras, and A. Auñón. "Effect of the exhaust thermal insulation on the engine efficiency and the exhaust temperature under transient conditions". *Internal Journal of Engine Research, Online First. https://doi.org/10.1177/1468087420961206* (2020) (cit. on p. 37).

[199] H. Zhang, J. Baeyens, G. Cáceres, J. Degrève, and Y. Lv. "Thermal energy storage: Recent developments and practical aspects". *Progress in Energy and Combustion Science, 53, 1-40* (2016) (cit. on p. 37).

[200] J. Jaguemont, N. Omar, P. Van den Bossche, and J. Mierlo. "Phase-change materials (PCM) for automotive applications: A review". *Applied Thermal Engineering, 132, 308-320* (2018) (cit. on p. 37).

[201] B. Zalba, J. M. Marín, L. F. Cabeza, and H. Mehling. "Review on thermal energy storage with phase change: materials, heat transfer analysis and applications". *Applied Thermal Engineering, 23 (3), 251-283* (2003) (cit. on p. 37).

[202] D. K. Johar, D. Sharma, S. L. Soni, P. K. Gupta, and R. Goyal. "Experimental investigation on latent heat thermal energy storage system for stationary C.I. engine exhaust". *Applied Thermal Engineering, 104, 64-73* (2016) (cit. on p. 37).

[203] S. D. Burch, T. F. Potter, and M. A. Keyser. "Reducing cold-start emissions by catalytic converter thermal management". *SAE Technical Paper 950409* (1995) (cit. on pp. 37, 126).

[204] E. Korin, R. Reshef, D. Tshernichovesky, and E. Sher. "Reducing cold-start emission from internal combustion engines by means of a catalytic converter embedded in a phase-change material". *Proceedings of the Institution of Mechanical Engineers, Part D: Journal of Automobile Engineering, 213 (6)* (1999) (cit. on p. 37).

[205] M. Nicholas, G. Tal, and T. Turrentine. "Advanced plug-in electric vehicle travel and charging behavior". *Advanced Clean Cars Symposium: The Road Ahead, California Environmental Protection Agency, Air Resources Board, Sacramento, CA, USA, 27-28 September* (2016) (cit. on p. 38).

[206] G. Blanchard, C. Colignon, C. Griard, C. Rigaudeau, O. Salvat, and T. Seguelong. "Passenger car series application of a new diesel particulate filter system using a new ceria-based fuel-borne catalyst: from the engine test bench to european vehicle certification". In: *SAE Technical Paper 2002-01-2781.* 2002 (cit. on p. 38).

[207] M. Piumetti, S. Bensaid, N. Russo, and D. Fino. "Nanostructured ceria-based catalystsfor soot combustion: investigations on the surface sensitivity". *Applied Catalysis B: Environmental, 165, 742-751* (2015) (cit. on p. 38).

[208] K. Krishna and M. Makkee. "Pt-Ce-soot generated from fuel-borne catalysts: soot oxidation mechanism". *Topics in Catalysis, 42 (1), 229-236* (2007) (cit. on p. 38).

[209] G. Blanchard, T. Seguelong, J. Michelin, S. Schuerholz, and F. Terres. "Ceria-based fuel-borne catalysts for series diesel particulate filter regeneration". In: *SAE Technical Paper 2003-01-0378.* 2003 (cit. on p. 38).

[210] M. Z. Zheng, G. T. Reader, D. Wang, J. Zuo, R. Kumar, M. C. Mulenga, U. Asad, and M. Ting D. S.-K. andWang. "A thermal response analysis on the transient performance of active diesel aftertreatment". In: *SAE Technical Paper 2005-01-3885*. 2005 (cit. on p. 38).

[211] S. Jindal. "Effect of injection timing on combustion and performance of a direct injection Diesel engine running on Jatropha methyl ester". *International Journal of Energy and Environment, 2 (1), 113-122* (2011) (cit. on p. 38).

[212] M. Zheng, G. T. Reader, and J. G. Hawley. "Diesel engine exhaust gas recirculation - A review on advanced and novel concepts". *Journal of Energy Conversion and Management, 45, 883-900* (2004) (cit. on p. 38).

[213] C. N. Pratheeba and P. Aghalayam. "Effect of exhaust gas recirculation in NO_x control for compression ignition and homogeneous charge compression ignition engines". *Energy Procedia, 66, 25-28* (2015) (cit. on p. 38).

[214] M. Yang, Y. Gu, K. Deng, Z. Yang, and Y. Zhang. "Analysis on altitude adaptability of turbocharging systems for a heavy-duty Diesel engine". *Applied Thermal Engineering, 128, 1196-1207* (2018) (cit. on p. 39).

[215] J. Wang, L. Shen, Y. Bi, and J. Lei. "Modeling and optimization of a light-duty Diesel engine at high altitude with a support vector machine and a genetic algorithm". *Fuel, 285, 119137* (2021) (cit. on p. 39).

[216] T. Lancefield, I. Methley, U. Räse, and T. Kuhn. "The application of variable event valve timing to a modern Diesel engine". In: *SAE Technical Paper 2000-01-1229*. 2000 (cit. on p. 39).

[217] J. R. Serrano, P. Piqueras, R. Navarro, J. Gómez, M. Michel, and B. Thomas. "Modelling analysis of aftertreatment inlet temperature dependence on exhaust valve and ports design parameters". In: *SAE Technical Paper 2016-01-0670*. 2016 (cit. on pp. 39, 74, 222).

[218] F. J. Arnau, J. Martín, B. Pla, and A. Auñón. "Diesel engine optimization and exhaust thermal management by means of variable valve train strategies". *Internal Journal of Engine Research, 22 (4), 1196-1213* (2021) (cit. on pp. 39, 222).

[219] J. R. Serrano, F. J. Arnau, J. Martín, and A. Auñón. "Development of a variable valve actuation control to improve diesel oxidation catalyst efficiency and emissions in a light duty Diesel engine". *Energies, 13, 4561* (2020) (cit. on p. 39).

[220] R. F. Horng and H. M. Chou. "Effect of input energy on the emission of a motorcycle engine with an electrically heated catalyst in cold-start conditions". *Applied Thermal Engineering, 24 (14), 2017-2028* (2004) (cit. on p. 39).

[221] S. R. Khan, M. Zeeshan, and S. Iqbal. "Thermal management of newly developed non-noble metal-based catalytic converter to reduce cold start emissions of small internal combustion engine". *Chemical Engineering Communications, 205 (5), 680-688* (2018) (cit. on p. 39).

[222] R. Szolak, B. Danckert, A. Susdorf, P. Beutel, K. Pautsch, C. Ewert, F. Rümmele, A. Kakadiya, and A. Schaadt. "CatVap®- a new heating measure for exhaust aftertreatment system". In: *Heavy-Duty-, On- und Off-Highway-Motoren, 37-52*. 2019 (cit. on p. 39).

[223] O. Holmer and Eriksson. "Modeling and analytical solutions for optimal heating of aftertreatment systems". *IFAC-PapersOnLine, 53 (5), 523-530* (2019) (cit. on p. 39).

[224] C. Beatrice, S. Di Iorio, C. Guido, and P. Napolitano. "Detailed characterization of particulate emissions of an automotive catalyzed DPF using actual regeneration strategies". *Experimental Thermal and Fluid Science, 39, 45-53* (2012) (cit. on p. 40).

[225] Y. Tanaka, T. Hihara, M. Nagata, N. Azuma, and A. Ueno. "Modeling of diesel oxidation catalyst". *Industrial and Engineering Chemistry Research, 44 (22), 8205-8212* (2005) (cit. on p. 40).

[226] M. Bouchez and J. B. Dementhon. "Strategies for the control of particulate trap regeneration". In: *SAE Technical Paper 2000-01-0472*. 2000 (cit. on p. 40).

[227] J. Parks, S. Huff, M. Kass, and J. Storey. "Characterization of in-cylinder techniques for thermal management of diesel aftertreatment". In: *SAE Technical Paper 2007-01-3997*. 2007 (cit. on p. 40).

[228] M. Jeftić, J. Tjong, G. Reader, M. Wang, and M. Zheng. "Combustion and exhaust gas speciation analysis of diesel and butanol post injection". In: *SAE Technical Paper 2015-01-0803*. 2015 (cit. on p. 40).

[229] J. O'Connor and M. P. B. Musculus. "Post injections for soot reduction in Diesel engines: A review of current understanding". *SAE International Journal of Engines, 6 (1), 400-421* (2013) (cit. on p. 40).

[230] M. Lapuerta, J. J. Hernández, and F. Oliva. "Strategies for active diesel particulate filter regeneration based on late injection and exhaust recirculation with different fuels". *International Journal of Automotive Technology, 15 (2), 209-221* (2012) (cit. on p. 40).

[231] J. Ko, C. Myung, and S. Park. "Impacts of ambient temperature, DPF regeneration, and traffic congestion on NO_x emissions from a Euro 6-compliant diesel vehicle equipped with an LNT under real-world driving conditions". *Atmospheric Environment, 200, 1-14* (2019) (cit. on p. 40).

[232] D. Liebig, R. Clark, J. Muth, and I. Drescher. "Benefits of GTL fuel in vehicles equipped with diesel particulate filters". In: *SAE Technical Paper 2009-01-1934*. 2009 (cit. on p. 40).

[233] H. Dwyer, A. Ayala, S. Zhang, J. Collins, T. Huai, J. Herner, and W. Chau. "Emissions from a diesel car during regeneration of an active diesel particulate filter". *Journal of Aerosol Science, 41 (6), 541-552* (2010) (cit. on p. 40).

[234] A. Mayer, T. Lutz, C. Lämmle, M. Wyser, and F. Legerer. "Engine intake throttling for active regeneration of diesel particle filters". In: *SAE Technical Paper 2003-01-0381*. 2003 (cit. on p. 40).

[235] L. Stenning. "Strategies for achieving pre DPF regeneration temperatures using in cylinder post injection on a common rail Diesel engine with EGR, DOC and intake throttle". In: *SAE Technical Paper Brasil 2010-36-0306*. 2010 (cit. on p. 40).

[236] V. Bermúdez, J. R. Serrano, P. Piqueras, and O. García-Afonso. "Influence of DPF soot loading on engine performance with a pre-turbo aftertreatment exhaust line". In: *SAE Technical Paper 2012-01-0362*. 2012 (cit. on p. 41).

Chapter 3

Experimental and computational tools

Contents

3.1 Introduction **66**
3.2 Experimental facility **67**
3.2.1 MEDAS 68
3.2.2 Engine 73
3.2.3 Instrumentation and integration 74
3.3 Computational tools **77**
3.3.1 Engine model 77
3.3.1.1 Combustion sub-model 80
3.3.1.2 Turbocharger sub-model 82
3.3.2 Aftertreatment sub-model 86
3.3.2.1 DOC sub-model 86
3.3.2.2 DPF sub-model 90
3.4 Summary and conclusions **97**
Bibliography **98**

3.1 Introduction

The current Chapter presents the experimental and modelling tools that were employed during this doctoral thesis. Those tools are of great complexity and importance, constituting the foundations of this work. Besides, those tools will be referenced throughout the three following Chapters.

The first part of the Chapter is dedicated to explain the complete engine test bench. The physical structure were destined to carry on the experiments at sea-level and elevated altitude conditions and ambient temperatures from cold to hot ones. For a complete follow-up, the engine is described in detail considering its aftertreatment, the altitude and ambient temperature simulator and its working principles, besides of the full instrumentation and the measurement systems.

To continue, the computational tools are presented. The modelling part of the thesis constituted the characterization of experimental tests with the available software GT-Power [237] for the engine modelling, and the aftertreatment model, which was implemented into an integral thermo- and fluid dynamic solver for flow-through and wall-flow monoliths integrated into a gas dynamic software called VEMOD™, developed at the Research Institute CMT-Motores Térmicos [166]. The approached computational part has been also applied for the analysis and evaluation of different configurations and strategies, which will be addressed at each correspondent Chapter.

The works, analysis and ideas described in this Chapter were the origins of publication number [2] from the publications list of the author of this doctoral thesis, which is shown at the beginning of the document. For the sake of readiness and to protect the thesis writing style the publication number [2] from author's list of publications have not been specifically cited each time that ideas, figures or discussions contained in it are addressed in this Chapter. This disclaimer corrects, compensates and justifies the fact that the work of the PhD candidate's doctoral thesis are the origin of the innovation component in the publications number [2] listed in the referred Section.

3.2 Experimental facility

This Section aims to describe the facility used to execute the experimental tests. The test bench is located in CMT 8P building, rooms 5 and 6.

The main components of the test set were the engine and the altitude simulator, designated to emulate the desired ambient conditions. Figure 3.1 shows the engine placed in the test cell and the full installation accounting for the altitude simulator MEDAS (multifunctional efficient dynamic altitude simulator) is shown in Figure 3.2. A sequential description of the MEDAS, the engine, as well as the complete system integration and the measurement equipments is conducted next. It is important to mention that there was a team of technicians, who were responsible for the engine and the altitude simulator operation. They accompanied the entire experimental part, providing help and support for any problem.

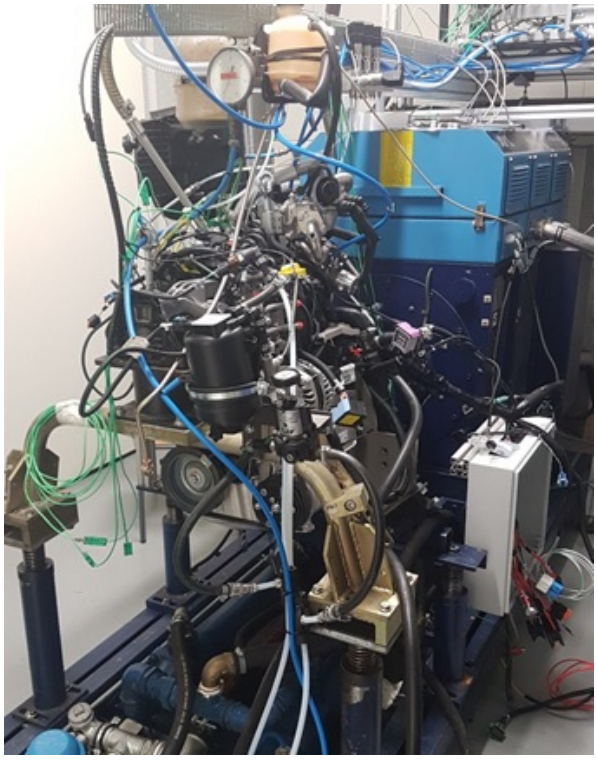

Figure 3.1: Picture of the engine placed in the test cell.

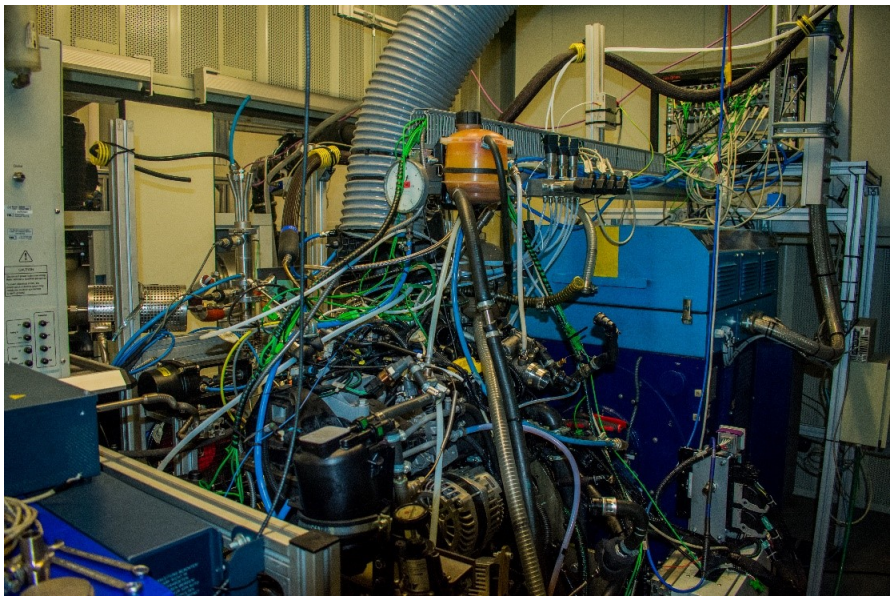

Figure 3.2: Picture of the experimental test facility including the altitude simulator on the background.

3.2.1 MEDAS

The altitude simulator MEDAS is composed by a set of new and innovative systems developed in partnership between the University Politècnica de Valencia's Research Institute CMT-Motores Térmicos and Horiba Europe GmbH. Its operation principle is covered in-depth in [238, 239] and its correspondent design features and performance indicators are presented in the patents [240, 241].

The MEDAS was responsible for ensuring the requested atmospheric boundary conditions during the engine tests, being capable of controlling the psychrometric variables of temperature and pressure. The altitude simulator was composed of a Horiba MEDAS coupled with its temperature module, as it can be seen in Figure 3.3, for an accurate control of ambient pressure, within variable altitude from sea-level to 5000 m, and temperature, which can be controlled between -15 and 45°C [128]. It is, thus, indispensable that the engine intake, exhaust and sump are linked to the altitude simulator. Figure 3.4 shows these connection pipes departing from the MEDAS.

Figure 3.3: MEDAS connected to the temperature module and to the engine.

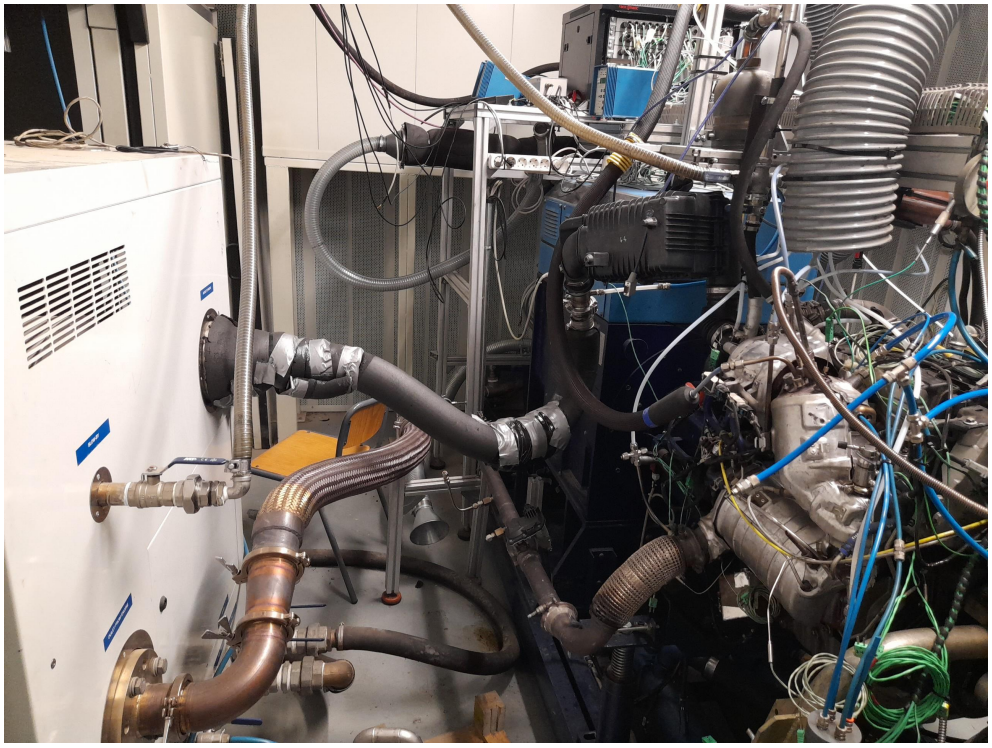

Figure 3.4: MEDAS connection with the engine.

The air path through the altitude simulator is briefly outlined in Figure 3.5. The atmospheric air is first admitted to the MEDAS temperature module (MTM), flowing through a mechanical compressor, increasing the air pressure,

counting with the assistance of the valve A to protect surge from happening in the mechanical compressor. Then, the gas temperature is controlled by the combination of the by-pass valve B and the cooling equipment working in parallel. The valve doses the amount of gas passing by the cooler, which is next directed to an inertial separator, to remove the condensates. After this first stage, the air can be either reheated by an electric heater to achieve the temperature set point or flow through the by pass, being directed to the MTM outlet. Valve C works to set up the target temperature at the end of the MTM line by dosing the flow through the electric heater.

The final tuning is done in the MEDAS module, regulating the pressure and temperature at the engine inlet. Here, the air can follow the shortest path by undergoing an isothermal expansion through valve D. On the other hand, for further cool down, the gas flow can be regulated by the valve E and then expanded in a VGT. A cyclonic separator is placed right after the VGT to remove water droplets or ice from the air before going to the engine intake. A by-pass duct assures the same pressure conditions for intake and exhaust of the engine and makes the MEDAS operation independently from the engine one possible.

The mechanical compressor, preceded by a cooler and a cyclonic separator, which are meant to cool down the engine exhaust gases and protect the mechanical compressor from condensation, controls the mass flow rate through the equipment. This way, the desired engine atmosphere conditions of pressure, temperature and air mass flow are generated in the engine boundaries. The VGT is also mechanically coupled with a turbo-compressor, which moves the flow through the installation. Valve F is a one-way valve, acting in the case that not enough mass flow meets the VGT. This way, the valve allows the reduction of the pressure drop in the installation.

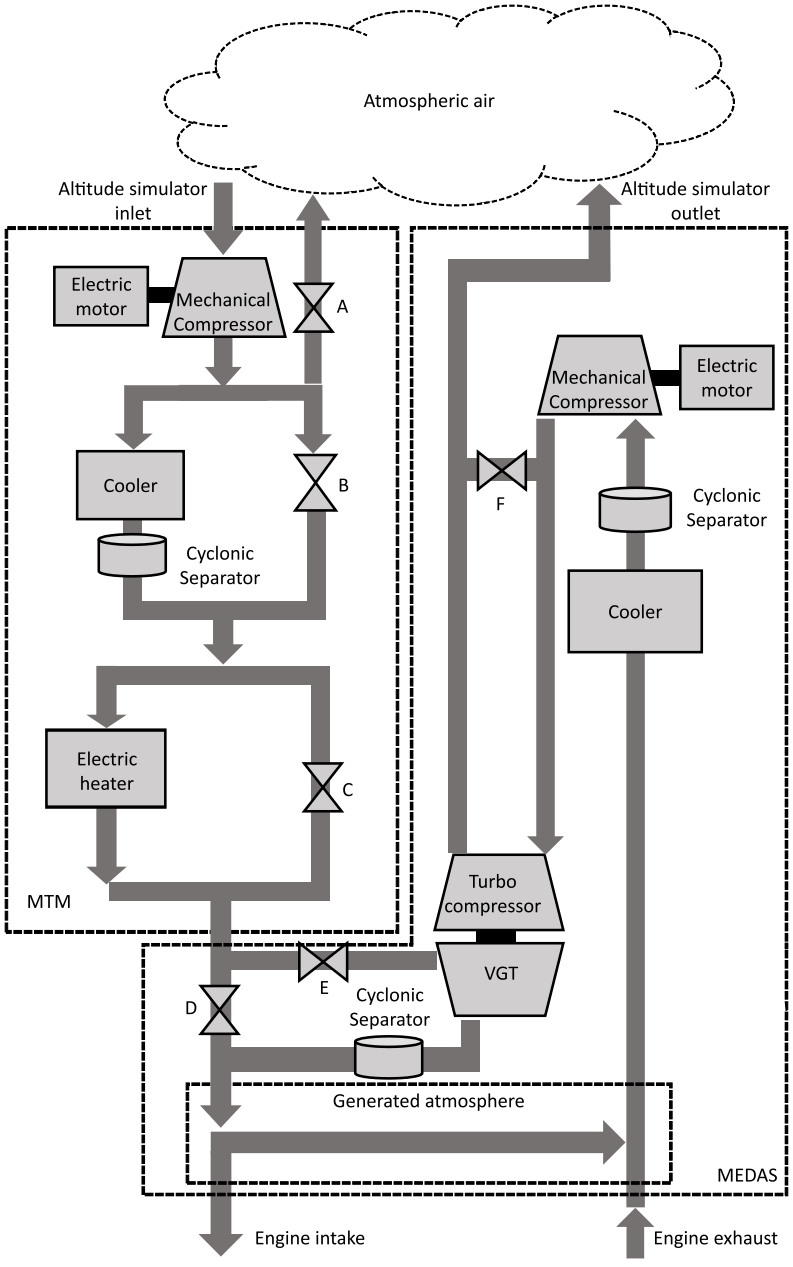

Figure 3.5: Layout and conceptual scheme of the altitude simulator featuring the MEDAS coupled to the MTM.

Complementary, the choice of using MEDAS was a strategical decision, being essentially based on previous research performed in the CMT research institute, which originally developed the MEDAS system. In this regard, it's interesting to point out and compare other common techniques used to reproduce other ambient conditions of pressure and temperature.

The real altitude and temperature environment is the most direct and accurate way to simulate altitude and temperature, showing however the drawbacks of time, efficiency, lack of repetitiveness [242], and higher costs [243]. Climatic and hypobaric chambers can also correctly predict the external environmental conditions, with a much smaller required space [244]. The drawbacks count, however, with high maintenance and overall costs [245, 246], besides presenting human risks in the case of the hypobaric chamber [247].

Similarly to the hypobaric or climatic chamber, the altitude simulator also emulates the desired pressure and temperature conditions, but not interfering in the engine surroundings. Evidently, the heat transfer of the engine [248] and aftertreatment components [249] will suffer an influence from different outside temperatures. Therefore, according to Gómez [29], the use of such machines demands the hardening of some flexible pipes along the engine air path prior to the compressor to avoid the component's collapse because of the higher ambient pressure. Crankshaft seals may also not be enough to withstand vacuum inside crankcase. Those are some of the downsides of using an altitude simulator.

However, the altitude simulators still provide a quite accurate trend in comparison with the real altitude tests [250]. Broatch *et al.* [239] performed a very detailed investigation that revealed similar engine performance and emissions results when testing with the altitude simulator or with the hypobaric chamber, both for 1300 m and 2300 m altitudes. Roberts *et al.* [251] also compared engine dynamometer with on-road tests reproducing with the help of a MEDAS the exact altitude, temperature, and humidity conditions in the engine boundaries. Engine performance partials and cumulative CO_2 were in excellent agreement with the equivalent road tests.

One can conclude that altitude simulators can accurately reproduce road tests for precise engine performance and emissions at different ambient conditions.

3.2.2 Engine

The engine in this work meets the Euro 6d-Temp standards, which contemplates the additional variables of temperature and altitude to be added to the nowadays RDE validations tests. Those two boundary conditions are precisely the ones considered for the investigation in this thesis. To comply with the Euro 6d-Temp regulations is a mandatory condition for new type approvals vehicles since September 2017 and it came into force for all vehicles sold from September 2019 on [27]. Subsequently the Euro 6d regulation started to be progressively introduced. Although the current market offers a wide variety of alternative propulsion systems, the Diesel engines continue to have a relevant market share due to their low CO_2 emissions and compliance with emission standards, in standalone or in hybrid powertrain platforms, as the state-of-art indicates.

Table 3.1 summarizes the main aspects of the studied engine. The fuel injection line was based on common-rail direct injection (DI) technology, whilst the engine air path accounted for a VGT, a water charge air cooler (WCAC) and a HP and a cooled LP-EGR systems. Concerning the EGR lines, only the LP-EGR was actuated in the studies in this doctoral thesis since all studies were performed under steady-state conditions and the engine coolant temperature reached 90°C.

Table 3.1: Main characteristics of the engine.

Engine type	Four-stroke HSDI diesel
Emissions Standards	Euro 6d-Temp
Number of cylinders	4 in line
Displaced volume [cm^3]	1461
Bore [mm] × Stroke [mm]	76 × 80.5
Number of valves	2 per cylinder
Compression Ratio	15.16:1
Rated power @ speed	84 kW @ 3750 rpm
Maximum torque @ speed	253 Nm @ 2500 rpm
Maximum air mass flow @ speed	410 kg/h @ 4500 rpm
Fuel Injection	Common-rail direct injection
Turbocharger	BorgWarner VGT
EGR system	HP- and cooled LP-EGR
ATS system	Closed-coupled DOC+SCRf

An aftertreatment brick composed of a DOC and a SCRF was located downstream of the VGT outlet. The serial underfloor selective catalytic reduction system was omitted. Therefore, this device will be from now on referred to as a DPF in this thesis. The main geometrical parameters of the two employed aftertreatment systems are defined in Table 3.2.

Table 3.2: Main DOC and DPF geometric parameters.

	DOC	DPF
Diameter [mm]	120	170
Channel length [mm]	140	80
Channel cross-section	Square	Square
Cell density [cpsi]	400	400
Cell size [mm]	1.04	0.95
Wall thickness [mm]	0.23	0.32
Catalytic area [m^2]	3.95	
Filtration area [m^2]		2.1
Porosity [-]		0.40
Mean pore diameter [μm]		20.4
Permeability [$\times 10^{13} m^2$]		7.59

Additionally, previous experimental results of a further engine [217] have been used for a specific modelling analysis in Chapter 4. The engine is a high-speed direct injection (HSDI) and it's specific characteristics will be presented in Chapter 4 only, since its use was very punctual, without the need of a global introduction.

3.2.3 Instrumentation and integration

The full experimental set counting with the engine, the altitude simulator, the measurement equipments, the gas and fuel line is represented in Figure 3.6. As previously said, it is important to note from the scheme that the engine intake and tailpipes, and the sump were coupled to the altitude simulator.

Engine speed and torque are controlled by an asynchronous dynamometer, whereas the specific engine operation counting with extra variables is managed by acting on an open engine control unit (ECU), which was available to modify the engine calibration through accessing the ETAS INCA software. In particular, for the tests in altitude, where the atmospheric pressure differs from the test bench room one, a variable referred to environmental pressure

had to be updated via communication with MEDAS. Through an AVL PUMA Open 2 system, temperature and pressure measurements captured by K-type thermocouples and piezo-resistive sensors installed along the gas line are readable in a user-friendly interface. The most significant measured variables together with the sensors features are summarized in Table 3.3.

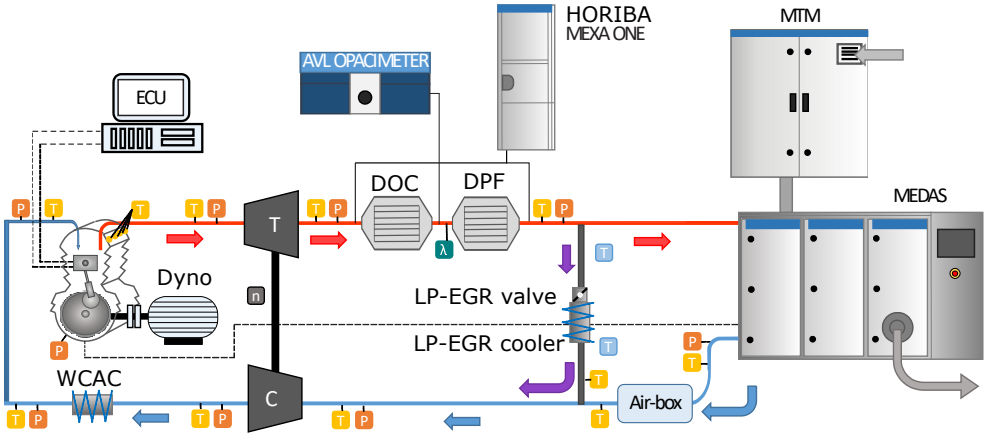

Figure 3.6: Test bench scheme.

The engine and turbocharger performance variables, like torque, engine pedal, engine speed and turbocharger speed, are also displayed in a PUMA monitor for a continuous monitoring during the tests. The engine pedal is regulated through an electrical signal sent straight to the pedal. The air flow is also monitored throughout the INCA software by an on-board flow meter and the fuel mass flow is measured by the gravimetric balance AVL 733S fuel meter. Fuel temperature was further controlled in the AVL 753 equipment, as sketched in the upper left corner of Figure 3.6. Departing from it, the fuel is then directed to the common-rail.

The instantaneous in-cylinder pressure was recorded for each measured point with a help of a glow-plug piezoelectric transducer Kistler 6055B that converts pressure into electrical charge. Then, this electrical charge from the piezoelectric transducer is converted by a charge amplifier Kistler 5011 into a proportional voltage signal. The in-cylinder pressure acquisition was then performed using a Yokogawa DL850V ScopeCorder Series oscillographic recorder with a 16 bits A/D converter module, with a crank angle increment of 0.5°.

The exhaust gas composition was measured using a Horiba Mexa ONE system, whose measurement principles from the main measured parameters are also listed in the Table 3.3. The Horiba Mexa ONE gas analyser is equipped with a line selector that allowed toggling the measure of the gas chemical composition between the aftertreatment inlet and outlet to measure the CO and HC emission conversion efficiencies. Since NO_x abatement was not carried in the EATS, only these respective engine-out emissions were monitored. In addition, the Horiba Mexa ONE also identifies the CO_2 and O_2 concentrations.

Table 3.3: Main characteristics of the instrumentation.

Magnitude	Instrument	Range
Turbocharger speed control	PicoTurn rotational speed sensor	0 to 360 krpm
Speed control	Elin EBG Elektronik dynamometer	0 to 10 krpm
Power control	Elin EBG Elektronik dynamometer	±220 kW
Air mass flow	On-board mass flow meter	0 to 720 kg/h
Fuel mass flow	AVL 733S Fuel meter	0 to 150 kg/h
Temperature	K-type thermocouples	-200 to 1250°C
Mean pressure	Wika and AVL piezo-resistive sensors	0 to 6 bar
In-cylinder pressure	Kistler 6055 BSP	0 to -250 bar
O_2	HORIBA MEXA-ONE NDIR	0 to 25 (% Vol)
CO_2	HORIBA MEXA-ONE NDIR	0 to 20 (% Vol)
CO_L	HORIBA MEXA-ONE NDIR	0 to 5000 (ppm)
CO_H	HORIBA MEXA-ONE NDIR	0 to 12 (% Vol)
HC	HORIBA MEXA-ONE HFID	0 to 5000 (ppm)
NO & NO_x	HORIBA MEXA-ONE CLD	0 to 10000 (ppm)
PM opacity	AVL 439 opacimeter	0 to 100%

In addition, the Horiba Mexa-One also allows the control of LP-EGR rate by means of the analysis of the CO_2 present in the intake gas, referred to as $CO_{2_{in}}$ compared with the concentration in the atmosphere ($CO_{2_{atm}}$) and in the exhaust gas ($CO_{2_{exh}}$), following the Equation (3.1) [252]:

$$EGR(\%) = \frac{CO_{2_{in}} - CO_{2_{atm}}}{CO_{2_{exh}} - CO_{2_{atm}}} \tag{3.1}$$

A lambda sensor was additionally installed between the DOC and the DPF, allowing the access to the DPF inlet O_2 content, required for the topic approached in Chapter 5. Finally, the exhaust gas opacity was registered upstream of the DPF and measured by the equipment AVL 439 opacimeter.

3.3 Computational tools

Together with the experimental part of this thesis, a complete model of the engine and aftertreatment system has been employed, aiming to reproduce, analyse and understand the phenomena governing their response. Besides, it gave the possibility of evaluating the system' response to sensitivity tests and explore other feasible configurations without the need for further testing.

The engine model counted with sub-models to represent the turbocharger functioning, the combustion phenomena and the aftertreatment model, which included the DOC and the DPF sub-models. Each computational model will be explained in detail in the next Subsections.

3.3.1 Engine model

From one side, a 1D fluid dynamic engine model was developed in a GT-Power environment, a tool that is used to assess the engine performance and the response of its components.

This model was applied on the main segments of the gas path, starting from the engine intake and finishing on the engine outlet, as shown in Figure 3.7. The baseline model has been improved by substituting some default sub-models by user functions coming from VEMOD™, which is an open-source gas dynamics software for internal combustion engines and components computation, developed at CMT-Motores Térmicos [253, 254]. In particular, the turbocharger and aftertreatment sub-models have been replaced as next described.

The heat transfer and pressure drop coefficients have been calibrated by means of proportional-integral-derivative controllers (PIDs). The actuation of the intake valve upstream the LP-EGR junction throttles the air charge in the cases where the EGR valve is fully open.

Following the flow path, the WCAC outlet temperature is imposed, in agreement with what has been done during the tests. The boost pressure is regulated by means of a PID acting on the VGT position. The air mass flow is adjusted regulating the cylinder heat-transfer multiplier. Fuel mass flow and the SOI were imposed as boundary conditions.

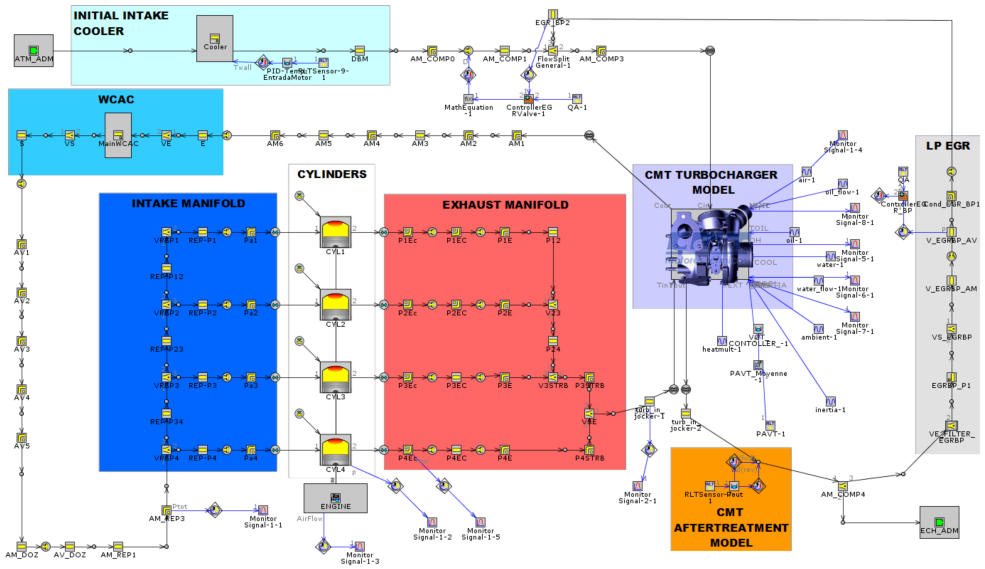

Figure 3.7: GT-Power engine model scheme.

Table 3.4 summarises the main boundaries and governing parameters of the calibration procedure.

Table 3.4: Main parameters for engine model calibration.

Room temperature	Imposed
Ambient temperature	Imposed
Ambient pressure	Imposed
Intake manifold temperature	Imposed
Engine speed	Imposed
Fuel mass flow	Imposed
SOI	Imposed
Exhaust gas composition	Imposed
Boost pressure	PID on VGT position
Air mass flow	Intake ports heat transfer coef.
Turbine inlet temperature	Exhaust ports heat transfer coef.

It is important to note that, in general, MEDAS and MTM define different engine inlet temperature in the experimental setup than the room conditions. In the case of the model, the engine inlet conditions correspond to the ambient ones. It represents miscalculations on the heat transfer and fluid dynamics. For this reason, an extra cooler was placed in the model next to the engine

intake, allowing to impose the room temperature as inlet condition and set the tested engine intake temperature at the cooler outlet. This cooler did not involve any pressure drop.

The model has been setup over a variety of tested points at full load varying the engine speeds from 1000 to 4500 rpm. Figure 3.8 shows the experimental and modelled comparison of the main performance magnitudes, as of torque, BSFC, air mass flow and maximum in-cylinder pressure, showing the good ability of the model to predict the engine performance in full load conditions from low to high engine speed. In overall, all variables have admissible deviations with respect to the experimental data and the model can be considered as predictable.

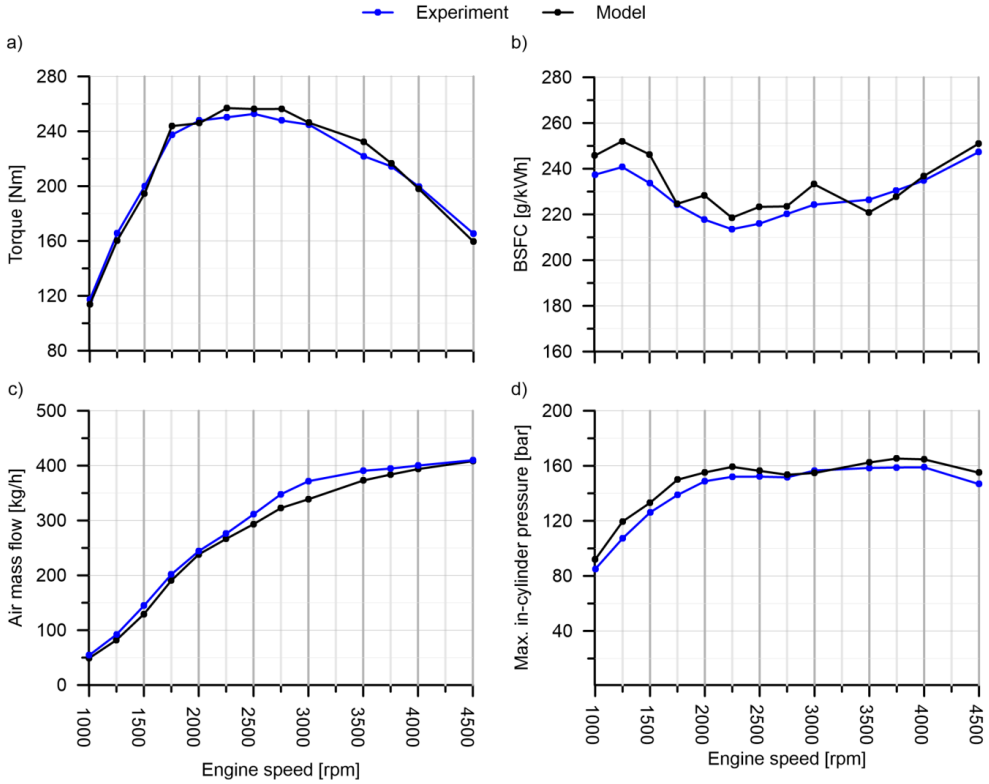

Figure 3.8: Measured and modelled results comparison for full load operation from 8 engine speeds ranging from 1000 to 4500 m.

3.3.1.1 Combustion sub-model

The combustion in Diesel engines is mainly divided into four phases: ignition delay, premixed combustion, mixing controlled combustion and late combustion phase [255]. The rate of heat release shape, as shown in Figure 3.9, depends on the importance of each phase, which is resultant from the injection timing. The well modelling of the combustion rate in the cylinder chamber is imperative to have an accurate representation of the engine operation.

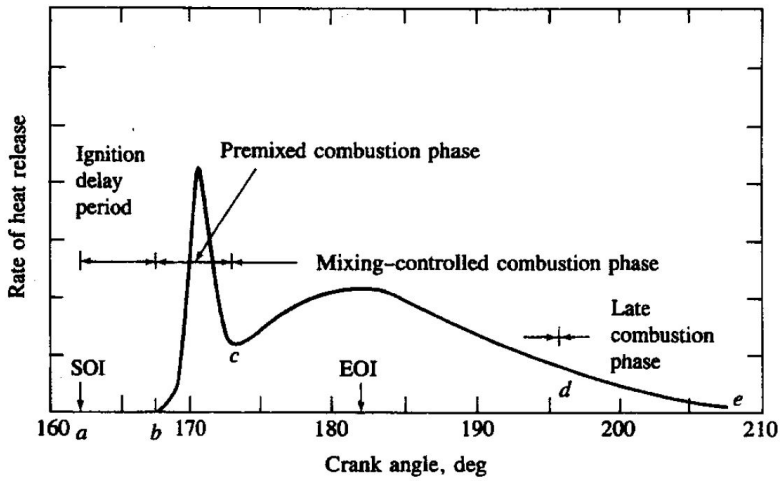

Figure 3.9: Phases of Diesel combustion [255].

The modelling of the instantaneous in-cylinder pressure was performed applying the DI-pulse model [256], a GT-Power feature for combustion prediction in direct-injection Diesel engines with single and multi-pulse injection profiles. The model tracks each injection pulse separately and follows its evaporation, mixing with gas and the burn events. The DI-pulse mode discretizes three thermodynamic zones, each with their own temperature and composition within the cylinder: the unburned zone, which contains the in-cylinder mass at intake valve closing (IVC); the spray unburned zone, which comprises the injected fuel and the entrained gas; and the spray burned zone, which is composed of the combustion products [257]. The model covers the computation of the gas entrainment rate, the ignition delay, the premixed combustion rate and the diffusion combustion rate to predict the in-cylinder pressure trace.

The model correctly represented the combustion process in terms of in-cylinder pressure and rate of heat release (RoHR) at low and high engine speeds, as Figure 3.10 shows for 1500 and 3500 rpm.

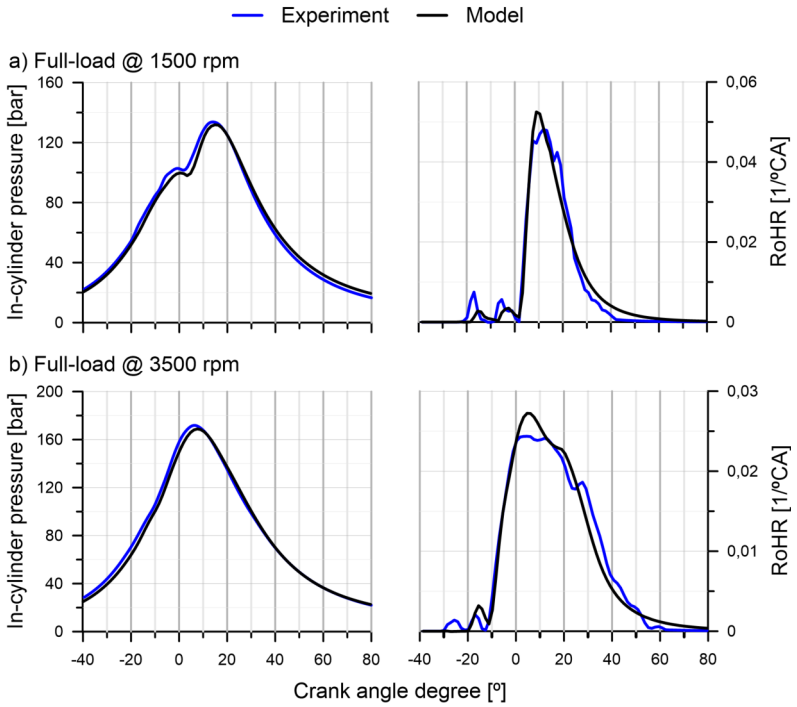

Figure 3.10: Full load measured and modelled results comparison for in-cylinder pressure and rate of heat release at 1500 rpm and 3500 rpm.

The same degree of accuracy is obtained in the remaining engine speeds, whose results are summarised in Figure 3.11 as a function of the combustion completeness and the maximum in-cylinder pressure. As observed, Figure 3.11(a) confirms that the combustion rate is accurate from the start of combustion to the late combustion phase providing a good prediction of the maximum in-cylinder pressure, as represented in Figure 3.11(b).

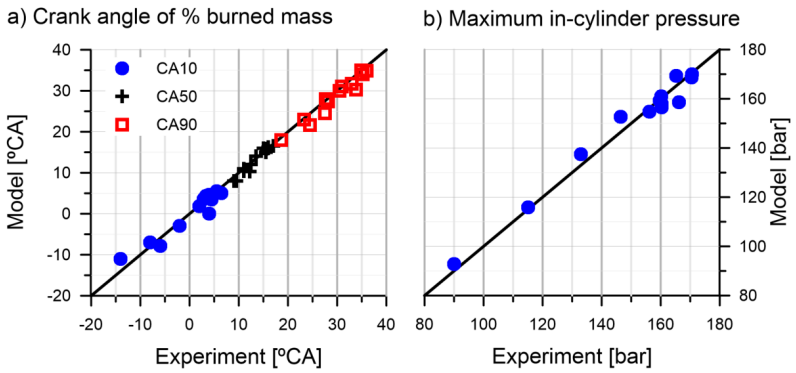

Figure 3.11: Prediction of combustion crank angle degree and maximum in-cylinder pressure at full load conditions from 1000 rpm to 4500 rpm.

3.3.1.2 Turbocharger sub-model

The engine model in GT-Power has been coupled to an advanced turbocharger model in order to properly consider the influence of the heat transfer [258] and mechanical losses [259] in the turbocharger on the prediction of the engine performance and of the exhaust gas properties. The turbine extracts energy from the exhaust gas flow, which is used to drive the compressor accounting for the mechanical losses. The heat balance is closed with the heat losses from the turbine and its transmission from the turbine case across the turbocharger until it reaches the compressor. This heat flux is partly rejected to the lubricating and cooling systems. In the compressor side, the air exchanges heat with the compressor casing [260].

The heat fluxes inside the turbocharger, which are equivalently considered in the model, are depicted in Figure 3.12 [261]. As it can be seen, the heat is led from the exhaust gas flowing in the turbine to the compressor. Part of this heat is directed to the environment, cooling and lubricating fluids, remaining only a fraction of the exhaust gases energy to be converted across the turbine to mechanical work and transferred to the compressor [262].

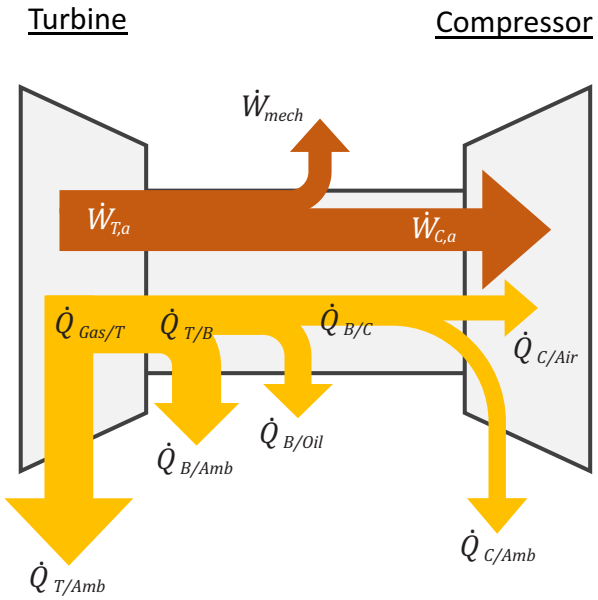

Figure 3.12: Energy fluxes inside a turbocharger.

The turbine extracts wasted kinetic and thermal energy from the exhaust gas flow and produces the power to drive the compressor, causing the later gas enthalpy to rise. Figure 3.13 shows that in addition to work, heat is also transferred between turbine and compressor. The heat losses from the turbine, $\dot{Q}_{GAS/T}$, is transferred from the turbine case (node T) to H_1 and so on until it reaches the compressor (node C). In the node H_2 the heat flux is partly recovered by the lubricating oil and the coolant liquid. Regarding the compressor, it is observed that the air absorbs energy from node C, representing the compressor case.

Finally, the turbocharger power balance is represented by the equation in the lower part of the Figure 3.13, where $\dot{W}_{mech}$ is the mechanical power. $\dot{W}_{C,a}/\dot{m}_C$ represents the specific compression work of the compressor in adiabatic conditions and $\dot{Q}_{C,Air}/\dot{m}_C$ is the specific energy originated in the compression process, from OC to A. This causes the compressor gas enthalpy to rise. OC_s is the point reached on isentropic compression starting from IC. $\dot{Q}_{GAS/T}/\dot{m}_T$ is originated in the expansion process on the turbine, which produces $\dot{W}_{T,a}/\dot{m}_T$, where the turbine gas enthalpy drops. In this case OT_s is the outlet point originated in the isentropic process (ideal process) in the turbine.

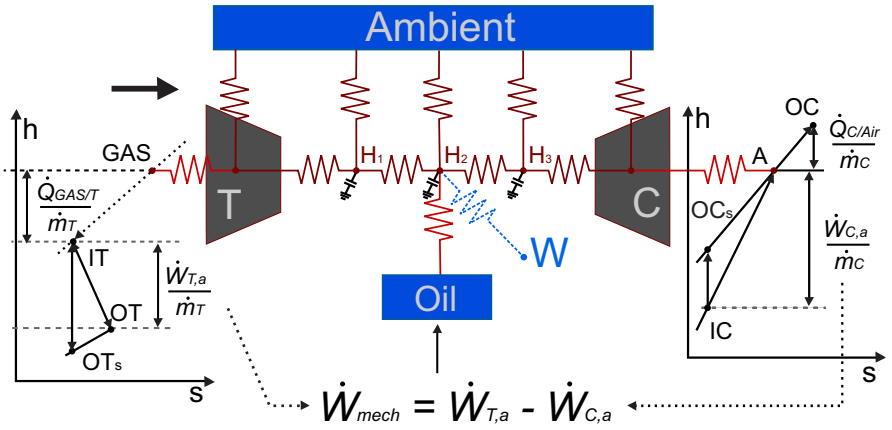

Figure 3.13: Scheme of the lumped turbocharger heat transfer model.

Figure 3.14 represents the comparison between experimental and modelled turbocharger characteristic variables. Plot (a) shows the prediction of the turbocharger speed and its evolution towards values close to its upper limit as the engine speed increases, being the gap accurately predicted by the model. Similarly, plots (c) and (e) focus on working pressures. The good prediction of the combustion process and the computation of the heat fluxes across the turbocharger also leads to a good agreement in gas temperatures both in the compressor and turbine stations, as seen in plots (b), (d) and (f).

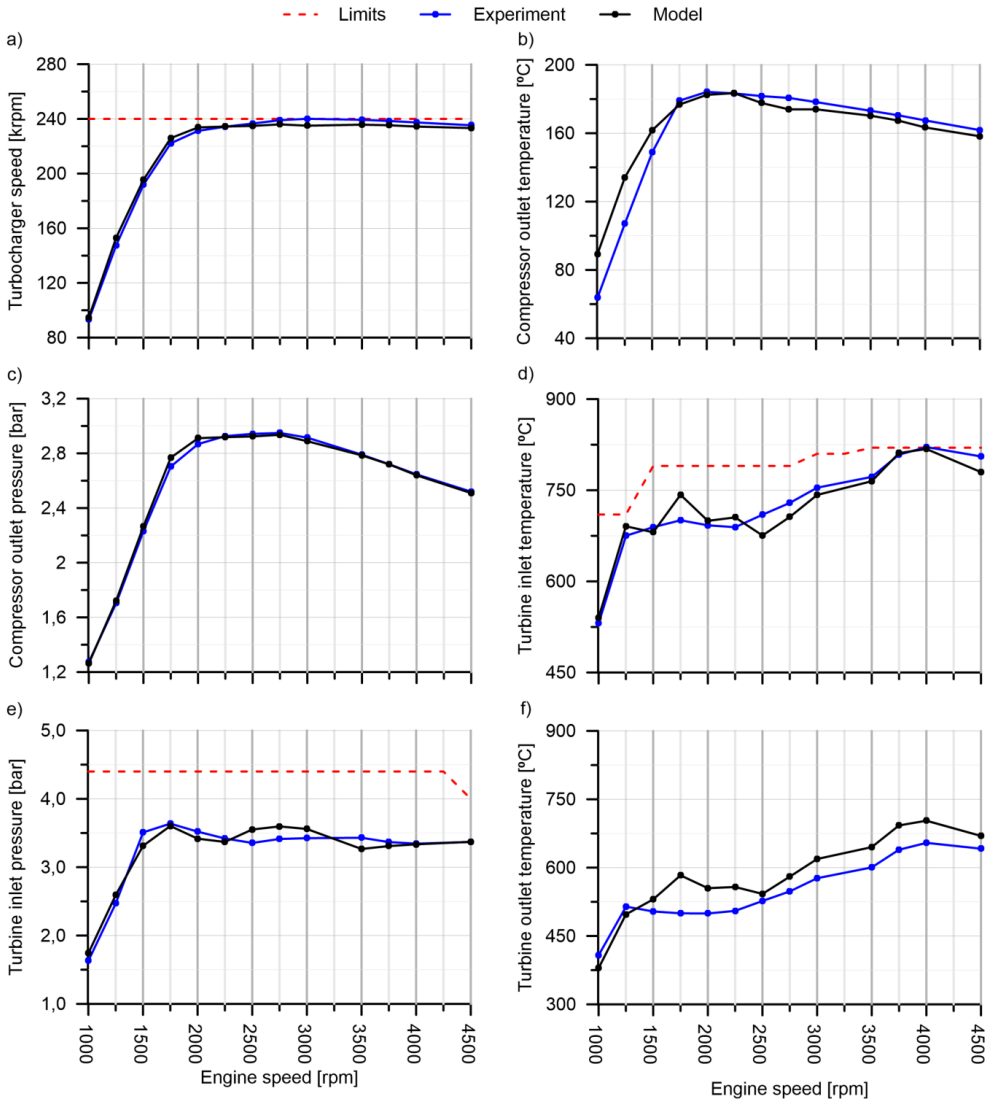

Figure 3.14: Prediction of combustion crank angle degree and maximum in-cylinder pressure at full load conditions from 1000 rpm to 4500 rpm.

3.3.2 Aftertreatment sub-model

Concerning the modelling of the EATS, it is important to highlight that it has been both used in conjunction with the engine model when the intention was to evaluate the global figure and also separately when decided to focus on the aftertretment components performance. When applied together with the engine model, the EATS thermo- and fluid-dynamic inlet properties were predicted by the engine model output. However the gas composition has been always imposed from experimental data.

A lumped approach is used in this work to model the response of the aftertreatment system, which consists of a close-coupled brick composed of a DOC and a DPF in sequence, as sketched in Figure 3.15 [156]. The DPF model was used to represent the processes happening inside the SCRf, once the SCR system was not applied and the device was only performing DPF functions, as mentioned previously.

The model input variables are the aftertreatment inlet pressure and exhaust mass flow when decided for the system's outlet pressure calculation, or pressure drop for the exhaust mass flow calculation. Besides, the values for inlet temperature and pollutant species concentration are requested for determining the outlet temperature and outlet gas composition. For the sake of clarity, the aftertreatment modelling results and each specific calibration procedure will be presented in each respective Chapter.

3.3.2.1 DOC sub-model

The flow-through monolith model proposed by Payri et al. [156] is presented in this Subsection. It comprises the main physical and chemical processes happening in the DOC concerning the CO and HC abatement mechanisms. These are namely the heat transfer, the chemical reactions and the pressure drop inside the monolith, represented by the three small boxes inside the DOC block in Figure 3.15. Firstly, the pressure drop along the flow-through monoliths (Δp_{cat}) is mainly originated due to inertial contributions, being, therefore, dependent on the monolith geometry and the flow inlet properties.

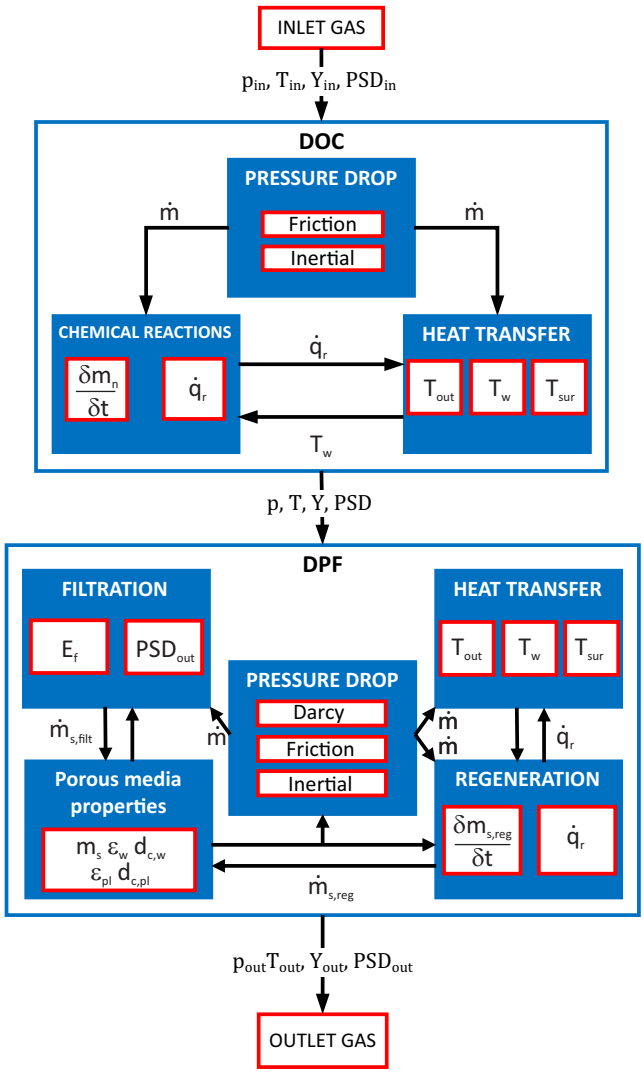

Figure 3.15: Flow-chart representing the DOC and DPF sub-models processes.

Assuming incompressible flow across the catalyst, this value is calculated as a function of the pressure drop coefficient (ς_{cat}), which is specific for each system geometry and calculated as a function of the Reynolds number (Re), the gas density (ρ_{in}) and its velocity (u_{in}), according to Equation (3.2):

$$\Delta p_{cat} = \varsigma_{cat} \rho_{in} u_{in}^2, \tag{3.2}$$

Secondly, the heat transfer model solves the general equations in the axial and tangential directions besides of adding the heat release contribution from the CO and HC abatement chemical reactions ($\dot{q}_r$). Equation (3.3) shows the temperature variation in the wall substrate (ΔT_w) during every time step (Δt). The basis of its calculation is adapted from a 1D modelling approach that follows the equivalent resistances and capacitances scheme proposed by Galindo et al. [249], also evaluating the thermal inertia of every node.

$$\Delta T_w = \frac{\Delta t}{c_w} \left(\sum_i \frac{T_i - T_w}{r_i} + \dot{q}_r \right), \tag{3.3}$$

where Δt represents the time-step, T is the temperature, and r stands for the thermal equivalent resistance between i and the substrate. In these terms, the subscript i represents the gas or internal canning surface. The thermal inertia of the substrate was considered by means of the thermal capacitance (c_w). Finally, the released heat per unit of time onto the washcoat is calculated considering the variation of the reactants mole fractions and surface coverage due to the oxidation and adsorption chemical mechanism, according to:

$$\dot{q}_r = \dot{n}_{gas} \sum_j H_{f,j} \Delta X_j + \Psi_{HC} \frac{\Delta H_{HC,\frac{ads}{des}} \Delta \theta_{HC}}{\Delta t} \tag{3.4}$$

where $\dot{n}_{gas}$ accounts for the total exhaust gas mole flow entering the catalyst, $H_{f,j}$ for the enthalpy of formation of the species j and ΔX_j its mole fraction variation due to the gas phase reactions. The second term is referred to the adsorption/desorption of hydrocarbons, being $\Delta H_{HC,\frac{ads}{des}}$ the heat of adsorption/desorption of HC species in the zeolites and $\Delta \theta_{HC}$ the HC coverage variation.

The chemical model aims to compute the main reactions happening in the monolith, i.e. CO and HC oxidation by the O_2 (Equations (3.5) and (3.6), respectively) and the HC adsorption and desorption on the zeolite washcoat [183] Equation (3.7).

$$CO + \frac{1}{2}O_2 \rightarrow CO_2 \tag{3.5}$$

$$C_nH_m + \left(n + \frac{m}{4}\right) O_2 \rightarrow nCO_2 + \frac{m}{2}H_2O \tag{3.6}$$

$$C_nH_m + Zeolite \rightleftarrows C_nH_m \cdot Zeolite \tag{3.7}$$

Decane was the fuel compound considered for the chemical reactions for being one of the most commonly HC molecules found in engine-out emissions for diesel applications [74]. The equations dictating the reaction mechanism are derived from the one-dimensional chemical species transport in [45], considering the reactants partial pressure (p_n) instead of mole fraction to make explicit the impact of the gas pressure on the reaction rate. This is considered appropriate for general aftertreatment applications [263], but specially when dealing with comparisons between quite different exhaust gas pressures, which are particularly found in different altitude environments. The chemical transport equations allow evaluating the CO and HC conversion efficiencies by the monolith, following the assumption of a quasi-steady flow, flat velocity and negligible concentration gradients in the washcoat [263]. Equation (3.8) represents the bulk gas transport, which involves the convective transport of the species n along the monolith channels and its diffusion towards the washcoat interface,

$$u_{in}\frac{\partial p_n}{\partial x} = -S_{p,gas}k_{m,n}\left(p_n - p_{n,wc}\right) \tag{3.8}$$

$S_{p,gas}$ represents the geometric surface area related to the catalyst surface to the gas volume ratio, while $k_{m,n}$ is the bulk mass transfer coefficient [264]. Equation (3.9) refers to the chemical transport equation in the washcoat of the pollutants species n, being $S_{p,wc}$ the washcoat specific surface, which is related to the volume to catalytic surface ratio,

$$\sum_i \nu_n R_i + S_{p,wc}k_{m,n}\left(p_n - p_{n,wc}\right) = 0 \tag{3.9}$$

R is the reaction rate, also defined as function of the reactants partial pressures in Equations (3.10 and 3.11), instead of their molar fractions:

$$R_{ox,n} = \frac{k_{ox,n}}{G_{ox}} p_{O_2} p_{n,wc}, \quad \text{where n} = \text{CO}, \text{HC} \tag{3.10}$$

$$R_{ads,HC} = k_{ads,HC}(1 - \theta_{HC})\psi_{HC} p_{HC,wc} \tag{3.11}$$

$$R_{des,HC} = k_{des,HC}\theta_{HC}\psi_{HC} \tag{3.12}$$

In Equations (3.10) to (3.12), the kinetic constant (k) is defined according to the Arrhenius expression (3.13) as a function of the substrate temperature,

$$k_r = P_f e^{-\frac{E a_r}{\Re T_w}} \tag{3.13}$$

θ and ψ represent, respectively, the HC surface coverage and the specific storage capacity. Finally, G_{ox} is the inhibition term for the CO and HC oxidation reactions, which accounts for the competition between CO, HC and NO species during the oxidation process that prevent them from the depletion. This term is calculated as proposed by Voltz *et al.* [161]:

$$G_{ox} = T_w(1 + K_1 p_{CO,wc} + K_2 p_{HC,wc})^2(1 + K_3 p_{CO,wc}^2 p_{HC,wc}^2)(1 + K_4 p_{NO,wc}^{0.7}) \tag{3.14}$$

3.3.2.2 DPF sub-model

The DOC outlet gas properties determine the boundaries for the DPF modelling. The DPF sub-model takes into account the main physical and chemical processes governing the DPF, i.e. pressure drop, heat transfer, soot filtration, regeneration and the change in meso-and micro-geometry of the inlet channels and the porous medium due to particulate matter accumulation. As for the catalyst, the inertial pressure drop in the DPF is calculated by Equation (3.15), with the difference that in wall-flow monoliths, the

importance of the inertial contributions is even higher due to their reduced open area [265].

$$\Delta p_{inertial} = \varsigma_{DPF_t} \rho_{in} u_{in}^2 \tag{3.15}$$

This equation also includes its respective DPF total pressure drop coefficient (ς_{DPF_t}). In addition to inertial pressure drop, the DPF counts with the friction pressure drop, due to the flow friction in the channels, and additional contributions from the flow being forced to pass across the porous wall and the particulate layer, in case of soot or ash accumulation, which is referred to Darcy contribution. Therefore, assuming incompressible flow, the DPF pressure drop can be expressed as Equation (3.16):

$$\Delta p_{DPF} = \Delta p_{inertial} + \Delta p_{friction} + \Delta p_{Darcy} \tag{3.16}$$

Equations (3.17) and (3.18) show the friction and Darcy contributions to the pressure drop calculation, respectively:

$$\Delta p_{friction} = \frac{1}{3} F_w \mu \left[\frac{u_{in} L_{in}}{\alpha - 2(w_{pl} + w_{ash})^2} + \frac{u_{out} L_{out}}{\alpha^2} \right] \tag{3.17}$$

$$\Delta p_{Darcy} = \frac{\mu Q L_{ef}}{2 V_{ef} \sigma L_{in}} \left(\frac{w_w}{k_{w,ef} \alpha} + \frac{1}{2k_{pl}} ln \left(\frac{\alpha - 2w_{ash}}{\alpha - 2(w_{pl} + w_{ash})} \right) + \frac{1}{2k_{ash}} ln \left(\frac{\alpha}{\alpha - 2w_{ash}} \right) \right) \tag{3.18}$$

where, F_w is viscous loss coefficient, set to 28.454 based in [266], μ is the gas dynamic viscosity and Q is the volumetric flow rate, which is directly related to the filtration velocity. The monolith geometric parameters considered by the model are the effective volume (V_{ef}) and the cell density (σ). The geometry values of the length and size are illustrated in 3.16, with en extra consideration of L_{ef} as the effective length, which is calculated by discounting the ash and soot plug formed at the rear end of the inlet channel from the monolith intake length (L_{in}).

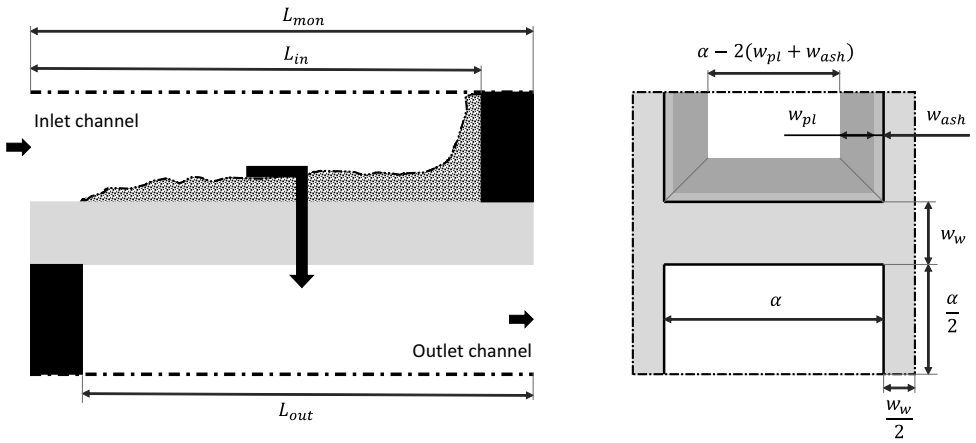

Figure 3.16: Scheme representing the DPF geometry and the sense of the flow [267].

Finally, k_w is the porous wall permeability. In clean porous wall conditions, this variable assumes the denotation k_{w0}, that, is computed following Equation (3.19), where f(ε_w) is a function of the Kuwabara's hydrodynamic factor (K) [268] and the Stokes-Cunningham factor (SCF) is a function of the gas mean free path and the mean pore diameter [156]. The permeability relates the pressure drop with the microscopic parameters [269], being dependent on the pore structure, that determines the slip-flow effect through the Stokes-Cunningham factor [270]:

$$k_{w_0} = f(\varepsilon_{w_0}) d_{c,w_0}^2 SCF_{w_0} \tag{3.19}$$

The porous structure is considered to be a set of spherical unit cells bearing the porosity (ε_w) of the medium [271]. In the porous substrate, the soot is deposited during the filtration around the unit collector with a determined diameter ($d_{c,w}$), which in clean conditions is represented by Equation (3.20). For the clean porous wall, the cell unit is defined as the sphere with the collector unit inside. Its diameter ($d_{cell,w}$) is calculated by the Equation (3.21):

$$d_{c,w_0} = \frac{3}{2}\left(\frac{1-\varepsilon_{w_0}}{\varepsilon_{w_0}} d_{p,w_0}\right) \tag{3.20}$$

$$d_{cell,w} = \sqrt[3]{\frac{d_{c,w_0}^3}{1-\varepsilon_{w_0}}} \tag{3.21}$$

Those properties vary along the soot loading within the unit cell, and can be analogously calculated as a function of the soot load, being the the variation of porosity and unit collector diameter also computed. The partial soot penetration is addressed based on a two layer porous wall concept [170, 272, 273, 274]. Therefore, the effective permeability is related to the permeability over the soot loading and in clean conditions according to:

$$\Delta p = \frac{\mu u_w w_w}{k_{w,ef}} = \frac{\mu u_w w_w f_{sp}}{k_w} + \frac{\mu u_w w_w (1-f_{sp})}{k_{w_0}} \tag{3.22}$$

being finally given by:

$$k_{w_{ef}} = \frac{k_w k_{w_0}}{f_{sp} k_{w_0} + (1-f_{sp}) k_w} \tag{3.23}$$

where f_{sp} is the fraction of porous wall thickness where the soot is collected. The growth of the unit collector diameter is thus expressed as:

$$d_{c,w} = 2\left(\frac{d_{c,w_0}^3}{8} + \frac{3 m_{s,cell}}{4\pi\chi\rho_{s,w}}\right)^{\frac{1}{3}} \tag{3.24}$$

It is seen that this variable is as a function of the porous diameter in clean conditions (d_{c,w_0}), of the soot mass in the unit cell ($m_{s,cell}$), of the soot packing density ($\rho_{s,w}$) and of a parameter called shape factor (χ), which is related to the effective hydrodynamic diameter of the unit collector, and ranges from 0 to 1. It also increases over the soot loading as a function of the soot mass in the loaded porous wall fraction. Since the diameter of the unit collector is variable with the soot load, the porosity and the mean pore diameter can be separately calculated as described by the Equations (3.25) and (3.26) respectively:

$$\varepsilon_w = 1 - \frac{d_{c,w}}{d_{cell,w}} \tag{3.25}$$

$$d_{p,w} = \frac{2}{3}\left(\frac{\varepsilon_w}{1-\varepsilon_w}\right) \tag{3.26}$$

The porous media properties are responsible not only for the pressure drop, but also for the filtration efficiency, computed by the filtration process block in the DPF sub-model. This part of the model predicts the amount of soot collected per unit cell. Besides, the filtration sub-model calculates the filtration efficiency as a function of the particle size, allowing to shape the particle size distribution (PSD). The considered filtration mechanisms in the model are the Brownian and interception collection around a single sphere, being the inertial contribution neglected [170].

The Brownian diffusion mechanism is the governing mechanism for small size particles at low flow velocities, increasing its contribution as the filtration velocity decreases, as introduced in Chapter 2. The filtration efficiency for a single unit collector due to Brownian diffusion is obtained according to Equation (3.27):

$$\eta_D = 3.5\left(\frac{\varepsilon_w}{K}\right)^{\frac{1}{3}} Pe_w^{-\frac{2}{3}} \tag{3.27}$$

This efficiency is dependent on the Peclet number (Pe), defined as the rate at which particles diffuse to the sphere surface to that at which particles approach towards the sphere surface within its cross-sectional area ratio [167]. It is calculated according to Equation (3.28), being a function of the filtration velocity (u_w), the microgeometry of the loaded porous medium $\frac{d_{c,w}}{\varepsilon_w}$ and the particle diffusivity, represented by the particle diffusion coefficient (D_s). This last parameter is directly affected by the gas temperature and is calculated by the Equation (3.29):

$$Pe_w = \frac{u_w d_{c,w}}{\varepsilon_w D_s} \tag{3.28}$$

$$D_s = \frac{TK_B SCF_w}{3\pi\mu d_s} \tag{3.29}$$

Complementary to the Brownian diffusion, the interception mechanism grows importance insofar as the particle size increases. The particles flow

with the streamline until being adhered on a unit collector on its external surface. The interception efficiency of a single sphere is quantified according to Lee and Gieseke [167] as:

$$\eta_R = 1.5 \frac{N_R^2}{1 + N_R^{\frac{3-2\varepsilon_w}{3\varepsilon_w}}} \frac{\varepsilon_w}{K} \tag{3.30}$$

It depends on ε_w and the interception parameter N_R, defined as the particle size to unit collector diameter ratio. Then, the combined filtration efficiency of an isolated single collector is obtained applying the independence rule [275] to consider the mutual effect of both mechanisms:

$$\eta_{DR} = \eta_D + \eta_R - \eta_D \eta_R \tag{3.31}$$

Known the collection efficiency of a single collector unit, the overall filtration efficiency of a packed of spherical particles composing the porous wall by integrating within the control volume is obtained by Equation 3.32 [276]:

$$E_f = 1 - e^{-\frac{3\eta_{DR}(1-\varepsilon_w) w_w f_w S_c}{2\varepsilon_w d_{c,w}}} \tag{3.32}$$

Aside the filtration process, the regeneration is also one of the main physical and chemical processes governing the DPF response computed in the DPF model. The model considers the soot oxidation by means of its reactivity with O_2 and NO_2 according to the respective following chemical reactions:

$$C + \alpha_{O_2} O_2 \rightarrow 2(\alpha_{O_2} - 0.5) CO_2 + 2(1 - \alpha_{O_2}) CO \tag{3.33}$$

$$C + \alpha_{NO_2} NO_2 \rightarrow \alpha_{NO_2} NO + (2 - \alpha_{NO_2}) CO + (\alpha_{NO_2} - 1) CO_2 \tag{3.34}$$

Assuming a quasi-steady process [277], the reaction rate of the reactant n can be calculated in terms of the molar fraction (X_n), accounting for the solid-to-gas main steps. Hence, the depletion rate of every gaseous reactant is obtained from the solution of the 1D transport equation of chemical species across the porous medium layer as [180]:

$$\dot{\omega}_n = u_w \frac{\partial p_n}{\partial z} = -\left(S_{p,ext} + \eta_{int_n} S_{p,int}\right) \alpha_n k_n \frac{K_{S_n} p_n}{1 + K_{S_n} p_n} \tag{3.35}$$

where α_n represents the index of oxidation completeness for the reactant n according to Jeguirim *et al.* [278]. The reaction rate is proportional to the kinetic constant of the soot oxidation k_n, calculated from the Arrhenius equation (3.13) as a function of substrate temperature. The Equation (3.35) also reinforces the reaction rate dependency on the specific surface (S_p) and the internal pore diffusion efficiency of the reactant n (η_{int_n}) related to the soot particles properties [279]. The last term $\frac{K_{S_n} p_n}{1+S_n p_n}$ comes from the general Langmuir isotherm expression [280],

$$\theta = \frac{K_{S_n} p_n}{1 + S_n p_n} \tag{3.36}$$

where θ is called surface coverage, i.e., the fraction of surface positions in the soot particle that are occupied by the reactant species. It represents the reaction dependency on the reactant partial pressure (p_n) and on the equilibrium constant (K_{S_n}) for the adsorption and desorption processes of the oxidizing agent on the surface. It is conditioned by the substrate temperature (T_w) and, thus, calculated explicitly in Equation (3.37):

$$K_{S_n} = P_{S_n} e^{-\frac{\Delta H_{S_n}}{\Re T_w}} \tag{3.37}$$

The value for adsorption enthalpy (ΔH_{S_n}) is defined by the deduction of desorption activation energy ($E_{a_{des_n}}$) from the adsorption activation energy ($E_{a_{ads_n}}$). P_{S_n} is the pre-exponential factor [180]. Knowing the depletion rate $\left(\frac{\partial n}{\partial t}\right)$ of each reactant (O_2 and NO_2) at every layer from its molar fraction variation, the amount of oxidised soot mass can be determined according to Equation (3.38), which takes into account both chemical reactions:

$$\frac{\partial m_{s,reg}}{\partial t} = M_C \left(-\frac{1}{\alpha_{NO_2}} \frac{\partial n_{NO_2}}{\partial t} - \frac{1}{\alpha_{O_2}} \frac{\partial n_{O_2}}{\partial t} \right) \tag{3.38}$$

In Equation (3.38), M_C is the carbon molecular weight and α is the stoichiometric coefficient of the gaseous reactants. Finally, equation (3.39)

represents the soot mass variation rate within the monolith, conditioned by the dynamics of the filtrated versus regenerated soot mass:

$$\frac{\partial m_s}{\partial t} = \frac{\partial m_{s,filt}}{\partial t} - \frac{\partial m_{s,reg}}{\partial t} \tag{3.39}$$

Finally, following the same principle as in the DOC, the heat power released ($\dot{q}_{reg}$) during the regeneration process in every layer of the porous media is determined from the stoichiometric coefficients and the enthalpy of formation of the involved species:

$$\dot{q}_{reg} = \sum_n \dot{q}_{reg,n} = \sum_n \sum_k \frac{\nu_{k,n}}{\alpha_n} H_{f,k} \frac{\partial n_n}{\partial t} \tag{3.40}$$

3.4 Summary and conclusions

This Chapter was dedicated to present the experimental and modelling tools employed in this thesis. They are the foundation of the research conducted during this doctoral thesis since their application supports the concepts addressed in the three following Chapters, where the DOC, the DPF and the engine performance under altitude and temperature conditions will be discussed. All experimental tests have been performed in the same Euro 6d-Temp engine.

From the one side, the experimental set counted with a complete facility for tests destined to reproduce different altitudes and temperatures. This is possible thanks to the use of an altitude simulator coupled to the engine intake and tailpipe, besides of the engine sump, emulating the correspondent temperature and pressure to the gas flowing across the engine. Additionally, a description of the engine and the instrumentation was conducted.

From the other side, the modelling software is a key tool for the powertrain performance evaluation and precise estimation when dealing with different ambient conditions operations, saving time and costs. In this perspective, modelling becomes a very valuable option for these studies. The full modelling of the main engine components is thus contemplated in this Chapter. The engine model accounted, as main feature, for an externally

user-defined turbocharger and aftertreatment sub-models and a GT-Power featured combustion sub-model. The engine model calibration procedure was presented and the results showed a good agreement with the experimental ones. This outcome allows the use of this tool for the complete research conducted in this thesis to support the understanding of the engine behaviour, besides of expanding its application towards the study of different engine configurations without the need of physical testing.

Finally, the full aftertreatment model description was also provided, with focus on the main phenomena happening inside the DOC and the SCRf. The operation of the SCRf was reproduced by making use of a DPF model, since the SCR system was inoperative. The model counted with a close-coupled brick system composed of a DOC and DPF, with the potential to predict the outlet flow properties. Particular focus is put on pressure drop, heat transfer and chemical mechanisms in the catalyst as well as in soot filtration and regeneration in the wall-flow monolith. Besides of assisting the tests analysis and understanding, the computational model also allowed the reproduction of studies with different inlet gas properties, building a complex analysis of the phenomena happening at different ambient temperature and pressure conditions. Noting that the aftertreatment calibration procedure and the modelling results will be introduced in each respective Section due to their great relevance in the scope of this doctoral thesis.

Bibliography

[2] J. R. Serrano, P. Piqueras, E. J. Sanchis, and B. Diesel. "A modelling tool for engine and exhaust aftertreatment performance analysis in altitude operation". *Results in Engineering, 4, 100054* (2019) (cit. on pp. xii, 66).

[27] *Commission Regulation (EU) 2017/1151 of 1 June 2017 supplementing Regulation (EC) No 715/2007 of the European Parliament and of the Council on type-approval of motor vehicles with respect to emissions from light passenger and commercial vehicles (Euro 5 and Euro 6) and on access to vehicle repair and maintenance information, amending Directive 2007/46/ EC of the European Parliament and of the Council, Commission Regulation (EC) No 692/2008 and Commission Regulation (EU) No 1230/2012 and repealing Commission Regulation*

(EC) No 692/2008 (Text with EEA relevance). 2017 (cit. on pp. 3, 16, 73).

[29] J. Gómez. "Development of an altitude simulator and analysis of the performance and emissions of turbocharged Diesel engines at different altitudes". PhD thesis. UPV, 2018 (cit. on pp. 4, 72).

[45] P. Piqueras, A. García, J. Monsalve-Serrano, and M. J. Ruiz. "Performance of a diesel oxidation catalyst under diesel-gasoline reactivity controlled compression ignition combustion conditions". *Energy Conversion and Management, 196, 18-31* (2019) (cit. on pp. 5, 30, 31, 89, 107, 122).

[74] F. Payri, V. R. Bermúdez, B. Tormos, and W. G. Linares. "Hydrocarbon emissions speciation in diesel and biodiesel exhausts." *Atmospheric Environment, 43, 1273-1279* (2009) (cit. on pp. 20, 89, 110).

[128] V. Bermúdez, J. R. Serrano, P. Piqueras, J. Gómez, and S. Bender. "Analysis of the role of altitude on Diesel engine performance and emissions using an atmosphere simulator". *International Journal of Engine Research, 18, 105-117* (2017) (cit. on pp. 26, 27, 68, 120).

[156] F. Payri, F. J. Arnau, P. Piqueras, and M. J. Ruiz. "Lumped approach for flow-through and wall-flow monolithic modelling for real-time automotive applications". In: *SAE Technical Paper 2018-01-0954*. 2018 (cit. on pp. 31, 86, 92, 107).

[161] S. E. Voltz, C. R. Morgan, D. Liederman, and S. M. Jacob. "Kinetic study of carbon monoxide and propylene oxidation on platinum catalysts". *Industrial & Engineering Chemistry Product Research and Development, 12 (4), 294-301* (1973) (cit. on pp. 31, 90).

[166] A. J. Torregrosa, J. R. Serrano, F. J. Arnau, and P. Piqueras. "A fluid dynamic model for unsteady compressible flow in wall-flow diesel particulate filters". *Energy, 36 (1), 671-684* (2011) (cit. on pp. 32, 66).

[167] K. W. Lee and J. A. Gieseke. "Collection of aerosol particles by packed beds". *Envirnmental Science & Technology ,13 (4), 466-470* (1979) (cit. on pp. 32, 94, 95).

[170] J. R. Serrano, H. Climent, P. Piqueras, and E. Angiolini. "Filtration modelling in wall-flow particulate filters of low soot penetration thickness". *Energy, 112, 883-898* (2016) (cit. on pp. 32, 93, 94).

[180] V. Macián, J. R. Serrano, P. Piqueras, and E. J. Sanchis. "Internal pore diffusion and adsorption impact on the soot oxidation in wall-flow particulate filters". *Energy, 179, 407-421* (2019) (cit. on pp. 33, 95, 96, 166, 175).

[183] J. R. Serrano, P. Piqueras, J. de la Morena, and E. J. Sanchis. "Late fuel post-injection influence on the dynamics and efficiency of wall-flow particulate filters regeneration". *Applied Sciences, 2019, 9 (24), 5384* (2019) (cit. on pp. 34, 40, 88, 166, 168, 173).

[217] J. R. Serrano, P. Piqueras, R. Navarro, J. Gómez, M. Michel, and B. Thomas. "Modelling analysis of aftertreatment inlet temperature dependence on exhaust valve and ports design parameters". In: *SAE Technical Paper 2016-01-0670*. 2016 (cit. on pp. 39, 74, 222).

[237] GAMMA Technologies, Available in: www.gtisoft.com. (accessed on 25 November 2021) (cit. on p. 66).

[238] J. Galindo, J. R. Serrano, P. Piqueras, and J. Gómez. "Description and performance analysis of a flow test rig to simulate altitude pressure variation for internal combustion engines testing". *SAE International Journal of Engines, 4 (7), 1686-1696* (2014) (cit. on p. 68).

[239] A. Broatch, V. Bermúdez, J. R. Serrano, R. Tabet, J. Gómez, and S. Bender. "Analysis of passenger car turbocharged Diesel engines performance when tested at altitude and of the altitude simulator device used". In: *Proceedings of the ASME 2018 Internal Combustion Engine Division Fall Technical Conference*. San Diego, CA, USA, 2018 (cit. on pp. 68, 72).

[240] J. M. Desantes, J. Galindo, F. Payri, P. Piqueras, and J. R. Serrano. *Device for atmosphere conditioning for testing combustion engines, and associated method and use*. Patent WO 2015/110683 A1. 2015 (cit. on p. 68).

[241] J. M. Desantes, J. Galindo, F. Payri, P. Piqueras, and J. R. Serrano. *Device for conditioning the atmosphere in test of alternative internal combustion engines, method and use of said device*. Patent WO 2016/116642 A1. 2016 (cit. on p. 68).

[242] V. Betageri and R. Mahesh. "Effects of the real driving conditions on the NO_x emission of a medium duty diesel commercial vehicle". In: *SAE Technical Paper 2017-26-0124*. 2017 (cit. on p. 72).

[243] A. Ashtari, E. Bibeau, and S. Shahidinejad. "Using large driving record samples and a stochastic approach for real-world driving cycle construction: Winnipeg driving cycle". *Transportation Science, 48, 170-183* (2014) (cit. on p. 72).

[244] AVL. *Intake air conditioning. Available in: https://www.avl.com/adas_simulation/-/asset_publisher/TzaHJXCoGgln/content/intake-air-conditioning. (accessed on 17 January 2022).* 2021 (cit. on p. 72).

[245] R. García-Contreras, A. Gómez, P. Fernández-Yáñez, and O. Armas. "Estimation of thermal loads in a climatic chamber for vehicle testing". *Transportation Research Part D: Transport and Environment, 65, 761-771* (2018) (cit. on p. 72).

[246] D. G. Gardner, V. A. Zaccardi, P. A. Jalbert, and M. Denise Bryant. "Reducing the cost of aircraft engine emission measurements". *Proceedings of the International Instruments Symposium, 49, 57-66* (2003) (cit. on p. 72).

[247] G. Osculati et al. "Effects of hypobaric hypoxia exposure at high altitude on left ventricular twist in healthy subjects: Data from HIGHCARE study on Mount Everest". *European Heart Journal: Cardiovascular Imaging,17, 635-643* (2016) (cit. on p. 72).

[248] J. M. Desantes, A. J. Torregrosa, and P. Broatch A. Olmeda. "Experiments on the influence of intake conditions on local instantaneous heat flux in reciprocating internal combustion engines". *Energy, 36, 60-69* (2010) (cit. on p. 72).

[249] J. Galindo, J. R. Serrano, P. Piqueras, and O. García Afonso. "Heat transfer modelling in honeycomb wall-flow diesel particulate filters". *Energy, 43, 201-213* (2012) (cit. on pp. 72, 88).

[250] D. M. Human, T. L. Ullman, and T. M. Baines. "Simulation of high altitude effects on heavy-duty diesel emissions". In: *SAE Technical Paper 1990-04-01, 900883.* 1990 (cit. on p. 72).

[251] P. Roberts, A. Mason, A. Headley, L. Bates, S. Whelan, and K. Tabata. "RDE plus - A road to rig development methodology for whole vehicle RDE compliance: Road to engine perspective". In: *SAE Technical Papers 2021-01-1223.* 2021 (cit. on p. 72).

[252] D. Serio, A. Oliveira, and J. R. Sodré. "Effects of EGR rate on performance and emissions of a diesel power generator fueled by B7". *Journal of the Brazilian Society of Mechanical Sciences and Engineering, 39 (1-3)* (2017) (cit. on p. 76).

[253] OpenWAM webpage, CMT-Motores Tèrmicos, Universitat Politècnica de València, www.openwam.org. (Cit. on p. 77).

[254] J. Galindo, J. R. Serrano, F. J. Arnau, and P. Piqueras. "Description of a semi-independent time discretization methodology for a one-dimensional gas dynamics model". *Journal of Engineering for Gas Turbines and Power, 131 (3), 034504* (2009) (cit. on p. 77).

[255] J. B. Heywood. *Internal combustion engine fundamentals. pp. 506.* New York: McGraw-Hill, 1988 (cit. on p. 80).

[256] Gtisoft.com, (2015). Available in: *http://www.gtisoft.com/applications/a_Engine_Performance.php* (accessed on 20 Jun 2018) (cit. on p. 80).

[257] V. Venkateshmohan and M. Kumar. "Predictive diesel combustion using DI-Pulse in GT-Power". MA thesis. Chalmers University of Technology, 2015 (cit. on p. 80).

[258] J. R. Serrano, P. Olmeda, F. J. Arnau, A. Dombrovsky, and L. Smith. "Analysis and methodology to characterize heat transfer phenomena in automotive turbochargers". *Journal of Engineering for Gas Turbines and Power, 137 (2), 021901* (2015) (cit. on p. 82).

[259] J. R. Serrano, P. Olmeda, F. J. Arnau, and A. Dombrovsky. "Turbocharger heat transfer and mechanical losses influence in predicting engines performance by using one-dimensional simulation codes". *Energy, 86, 204-218* (2015) (cit. on p. 82).

[260] J. R. Serrano, P. Olmeda, A. Páez, and F. Vidal. "An Experimental Procedure to Determine Heat Transfer Properties of Turbochargers". *Measurement Science and Technology, 21 (3), 035109* (2010) (cit. on p. 82).

[261] R. D. Burke, P. Olmeda, F. J. Arnau, and M. Rayes-Belmonte. "Modelling of turbocharger heat transfer under stationary and transient conditions". In: *11th International Conference on Turbochargers and Turbocharging. London.* 2014 (cit. on p. 82).

[262] N. Baines, K. D. Wygant, and A. Dris. "The analysis of heat transfer in automotive turbochargers". *Journal of Engineering for Gas Turbines and Power, 132, 042301* (2010) (cit. on p. 82).

[263] M. Tu, R. Ratnakar, and V. Balakotaiah. "Reduced order models with local property dependent transfer coefficients for real time simulations of monolith reactors." *Chemical Engineering Journal, 383, 123074* (2020) (cit. on p. 89).

[264] R. D. Hawthorn. "Afterburner catalysts effects of heat and mass transfer between gas and catalyst surface." *American Institute of Chemical Engineers-Institution of Chemical Engineers, 70, 428-438* (1974) (cit. on p. 89).

[265] M. Masoudi. "Hydrodynamics of diesel particulate filters". In: *SAE Technical Paper 2002-01-1016*. 2002 (cit. on p. 91).

[266] A. G. Konstandopoulos and J. H. Johnson. "Wall-flow diesel particulate filters -Their pressure drop and collection efficiency". In: *SAE Technical Paper 890405*. 1989 (cit. on p. 91).

[267] E. J. Sanchis. "Modelado de la oxidación del hollín en filtros de partículas Diésel". PhD thesis. Universitat Politècnica de València, p. 36, 2019 (cit. on p. 92).

[268] A. G. Konstandopoulos. "Flow resistance descriptors for diesel particulate filters: Definitions, measurements and testing". In: *SAE Technical Paper 2003-01-0846*. 2003 (cit. on p. 92).

[269] A. Suresh, A. Khan, and J. H. Johnson. "An experimental and modeling study of cordierite traps - pressure drop and permeability of clean and particulate loaded traps". In: *SAE Technical Paper 2000-01-0476*. 2000 (cit. on p. 92).

[270] E. A. Kladopoulou, S. L. Yang, J. H. Johnson, G. G. Parker, and A. G. Konstandopoulos. "A study describing the performance of diesel particulate filters during loading and regeneration - A lumped parameter model for control applications". In: *SAE Technical Paper 2003-01-0842*. 2003 (cit. on p. 92).

[271] F. Payri, A. Broach, J. R. Serrano, and P. Piqueras. "Experimental-theoretical methodology for determination of inertial pressure drop distribution and pore structure properties in wall-flow diesel particulate filters". *Energy, 36, 6731-6744* (2011) (cit. on p. 92).

[272] J. R. Serrano, F. J. Arnau, P. Piqueras, and O. García Afonso. "Packed bed of spherical particles approach for pressure drop prediction in wall-flow (diesel particulate filters) DPF sunder soot loading conditions". *Energy, 58, 644-654* (2013) (cit. on p. 93).

[273] R. A. Yapaulo, E. Wirojsakunchai, T. Orita, D. E. Foster, M. Akard, L. R. Walker, and M. J. Lance. "Impact of filtration velocities and particulate matter characteristics on Diesel particulate filter wall loading". *International Journal of Engine Research, 10 (5), 287-304* (2009) (cit. on p. 93).

[274] C. Kamp, A. Sappok, and V. Wong. "Soot and ash deposition characteristics at the catalyst-substrate interface and intra-layer interactions in aged Diesel particulate filters illustrated using focused ion beam (FIB) milling". In: *SAE Technical Paper 2012-01-0836*. 2012 (cit. on p. 93).

[275] W. Feller. *An introduction to probability theory and its applications, Vol. 1, Ed. 3*. Wiley, 1968 (cit. on p. 95).

[276] B. Logan, D. G. Jewett, R. G. Arnold, E. J. Bouwer, and C. O'Melia. "Clarification of clean-bed filtration models". *Journal of Environmental Engineering, 121, 869-873* (1995) (cit. on p. 95).

[277] C. K. Dardiotis, O. A. Haralampous, and G. C. Koltsakis. "Catalytic oxidation in wall-flow reactors with zoned coating". *Chemical Engineering Science, 63 (4), 1142-1153* (2008) (cit. on p. 95).

[278] M. Jeguirim, V. Tschamber, J. F. Brilhac, and P. Ehrburger. "Oxidation mechanism of carbon black by NO_2: effect of water vapour". *Fuel, 84 (14), 1949-1956* (2005) (cit. on p. 96).

[279] M. M. Maricq and N. Xu. "The effective density and fractal dimension of soot particles from premixed flames and motor vehicle exhaust". *Journal of Aerosol Science, 35 (10), 1251-1274* (2004) (cit. on p. 96).

[280] A. Messerer, R. Niessner, and U. Pöschl. "Comprehensive kinetic characterization of the oxidation and gasification of model and real diesel soot by nitrogen oxides and oxygen under engine exhaust conditions: Measurement, Langmuir-Hinshelwood, and Arrhenius parameters". *Carbon, 44, 307-324* (2006) (cit. on pp. 96, 175).

Chapter 4

Diesel oxidation catalyst operation under extreme ambient conditions

Contents

4.1 Introduction **106**
4.2 Ambient conditions effect on the DOC performance **107**
4.2.1 Study definition 107
4.2.2 Model validation 109
4.2.3 CO and HC conversion efficiency variation 112
4.2.4 Flow properties influence on the conversion efficiency 117
4.2.5 Light-off curves sensitivity analysis 123
4.3 Passive strategies for DOC inlet temperature enhancement **126**
4.3.1 Study definition 127
4.3.2 Thermal insulation of the exhaust ports 133
4.3.3 Turbine thermal insulation 139
4.3.4 Combination of exhaust ports and turbine thermal insulation 144
4.3.5 DOC efficiency enhancement potential 147
4.4 Summary and conclusions **157**
Bibliography **160**

4.1 Introduction

Oriented by the discussion proposed on Chapter 2, the effect of the environmental conditions on the engine operation is also reflected on the EATS. The DOC is typically the first component following the turbine on the exhaust line [160], being effective on the control of CO and HC emissions.

Knowing that, this Chapter aims to evaluate the impact of high altitude and low ambient temperature on the CO and HC conversion efficiencies of a DOC in a Euro 6d-Temp Diesel engine passenger car. It does so by pointing out the role of the dwell time and the reactant species' partial pressure, which are affected due to the ambient pressure, and consequently engine operation, variation.

This can be achieved by making use of the altitude simulator coupled to engine in- and outlet to perform experimentally comparable tests under steady-state conditions at a designated baseline working condition of 20°C and 0 m, and at the extreme ambient condition of 2500 m and −7°C. Departing from the experimental findings, the DOC model has been calibrated to represent the tested results and add a contribution on the evaluation and understanding of the CO and HC conversion efficiencies deterioration.

The second part of the Chapter is dedicated to computationally study possible passive solutions for the DOC inlet temperature increase, favouring the optimisation of the CO and HC abatement at low engine loads. Particularly, the thermal insulation of the exhaust ports and the turbine were explored using the GT-Power engine model presented in Chapter 3 to provide the engine response as an input for the DOC model.

By doing this, in addition to evaluate the potential in terms of temperature gain and engine performance, it can be conclusively demonstrated the emissions conversion efficiency increment capability.

The works, analysis and ideas described in this Chapter were the origins of publications number [1, 3] from the publications list of the author of this doctoral thesis, which is shown at the beginning of the document. For the sake of readiness and to protect the thesis writing style the publications number [1, 3] from author's list of publications have not been specifically cited each time that ideas, figures or discussions contained in them are addressed in this Chapter. This disclaimer corrects, compensates and justifies the fact that the work of

the PhD candidate's doctoral thesis are the origin of the innovation component in the publications number [1, 3] listed in the referred section.

4.2 Ambient conditions effect on the DOC performance

This first section is dedicated to study the parameters influencing the variability of the light-off temperature according to the ambient condition. The pollutants light-off curve is sensitive to changes on EATS boundary conditions [150], such as oxygen and pollutants partial pressure and dwell-time [45]. With that in mind, an experimental and modelling study was conducted to cover the response of those parameters at different ambient conditions and analyse how they affect the DOC response.

First, a description of the tests carried out in the test facility presented in Chapter 3 is conducted. The experimental results are the basis of the first developed study, which aims to compare the DOC performance in terms of CO and HC conversion efficiency under two different ambient conditions. The test results were compared against the modelled ones obtained from the flow-through monolith model [156], also presented in Chapter 3. The calibration procedure is also described in detail, showing the setup of the main chemical parameters.

Accordingly, both obtained data compose the necessary tools for the evaluation of the chemical and physical processes influencing the CO and HC conversion efficiency when moving the engine from warm sea level to cold altitude ambient conditions. Besides, by making use of the model it was possible to evaluate the differences between comparable light-off curves for each ambient condition and the impact of each boundary variable of dwell time, O_2 partial pressure and the CO and HC partial pressures on the deterioration of the light-off curve in extreme ambient conditions.

4.2.1 Study definition

The experimental tests consisted on measuring a set of selected low temperature and low exhaust mass flow points, where the light-off region

was covered, under state conditions for at sea-level and 20°C and at 2500 m, i.e., 0.747 bar in ambient pressure, and −7°C. The first boundary condition will be referred as warm sea-level case and used as the baseline for comparison with the results at extreme ambient conditions tests, referred as cold altitude case.

CO and HC conversion efficiencies comparable contour maps could be outlined as a function of the DOC gas inlet temperature and exhaust gas mass flow. To obtain those results, every test was carried out keeping the engine under constant torque and speed [281], thus ensuring that the DOC boundary conditions were stable once thermal stabilization was reached. It is important to remark that only LP-EGR was used in this study, so that its variation with ambient conditions affects the DOC performance because of the effect on dwell time.

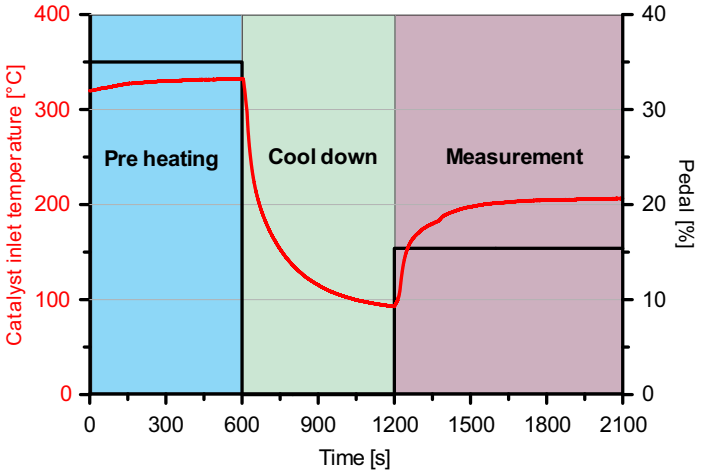

Figure 4.1: Test procedure for every steady-state operating point considered to obtain the CO and HC conversion efficiency contour maps.

Every measured point consisted of a combination of engine speed and catalyst inlet temperature, covering the engine speeds of 1000 rpm, 1250 rpm, and 1500 rpm in warm sea-level, moving the speed range to higher values in cold altitude to cover similar exhaust mass flow in both cases. The gas temperature at the inlet of the catalyst was also controlled within the same range (100 to 300°C) for both atmospheres by acting on the engine pedal. For each point, the measurement procedure, which is sketched in Figure 4.1, was

applied following the variations of engine pedal and DOC inlet temperature designed for each point. The example represents the operating conditions of 1500 rpm and 200°C in DOC inlet temperature for sea-level operation.

In the first step of the test an engine pedal of 35 % was imposed, providing a DOC inlet temperature above 300°C. It consisted on an initial preheating stage, where the high temperature produces the desorption of all accumulated HC in the DOC due to previous tests [282]. This operating condition was maintained for 10 minutes. This step was followed by a cooling phase, which lasted another 10 minutes. In this stage, the DOC inlet temperature was lead to levels lower than 100°C, so that all tests started at the same DOC state. The final step was designated to the measurement. Here, for every point, the designed combination of catalyst inlet temperature and engine speed was searched, aiming to complete the determined region for the contour maps. The measurements were taken continuously during 15 minutes, ensuring the exhaust thermal stabilization.

During the thermal transient observed in the the measurement phase, the synergy between the oxidation and adsorption mechanisms responsible for HC abatement was observed. Whereas the adsorption is responsible for the high HC conversion efficiency at low temperature, its contribution is ceased at higher catalyst inlet temperatures, when more HC is desorbed, and the oxidation takes place. This evaluation is only accurate by carrying on continuous measurements. As complement of the experimental activity, the DOC modelling, which consisted of simulating every steady-state operating point along the entire test duration, was carried out, thus, quantifying the evolution of each contribution to the HC abatement along the test.

4.2.2 Model validation

That said, Table 4.1 summarizes the calibrated kinetic constants and inhibition terms of the oxidation reactions. The calibration of the kinetic constants considered the influence of the thermal transient on the oxidation and adsorption/desorption equilibrium, along with the impact of the gradual HC accumulation on the adsorption/desorption reaction rate. However, the contour maps show the conversion efficiency only at the end of the test, and by means of the modelling procedure, it is possible to distinguish the HC oxidation and adsorption conversion efficiencies at every ambient condition.

It is also important to remark, as already commented in Chapter 3 that the component used for the HCs modelling was the decane due to its high representativeness in the diesel application field, according to Payri *et al.* [74]. For the sake of practicality and due to the good results obtained only using the decane, it was decided to not use low and high reactivity species in the calibration.

Table 4.1: Calibration of the DOC reaction rate parameters.

	Kinetic constant			Inhibition terms	
	$\mathbf{P_f}$ [−]	$\mathbf{E_a}$ [J/mol]		$\mathbf{P_f}$ [−]	$\mathbf{E_a}$ [J/mol]
HC adsorption	0.67	0	K_1	455	−7990
HC desorption	1×10^9	110000	K_2	1×10^3	-3×10^3
HC oxidation	1×10^{16}	85000	K_3	2.98	−96534
CO oxidation	9×10^{15}	80000	K_4	4.79×10^5	31036

Figure 4.2 shows the modelling of a selection of four different operating points compared to the experimental HC conversion efficiency along the measurement phase. These points cover sea-level and cold altitude and low (100°C) and high (250°C) catalyst inlet temperature, to be able to identify different levels of HC adsorption.

Figure 4.2(a) and (b) represent operation points were the adsorption was strongly influencing the HC conversion efficiency, knowing that their catalyst inlet temperature is 100°C, which was the minimum temperature of the study. While the first point conditions were of 1000 rpm and 10 Nm (39 kg/h and 100°C) for ambient conditions corresponding to warm sea-level, the second one performed 1250 rpm and 3 Nm (42 kg/h and 100°C) tested in cold altitude. Those conditions of low temperature and low engine load can be found during transient periods in RDE cycles [283] or in certain urban driving conditions [284].

Again, as it can be seen, the modelling covered the whole tested time, aiming to obtain a final figure of the conversion efficiency at the end of the test. That said, it is possible to identify the good predictability offered by the model from initial conditions, with empty HC surface coverage, to the end of the test, once thermal stability was reached in the engine exhaust. The progressive reduction over time of the HC conversion efficiency was correctly caught by the model, accounting for the gradual increase of the HC surface coverage, which favoured the HC desorption and decreased, therefore, the adsorption contribution to the conversion efficiency.

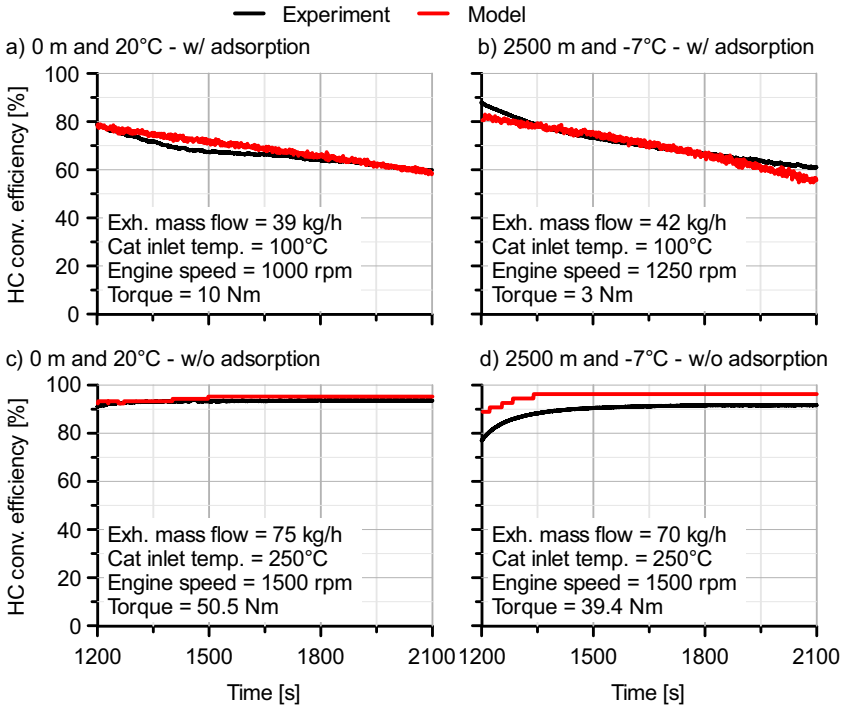

Figure 4.2: Comparison between experimental and modelled HC conversion efficiency evolution along different tested points.

In parallel, the model also captured the conversion efficiency over time for the points where the adsorption was less present, since the catalyst inlet temperature was higher. It can be observed in Figure 4.2(c), showing the HC conversion efficiency test at 1500 rpm and 50.5 Nm (75 kg/h and 250°C) for warm sea-level conditions, and in Figure 4.2(d), which corresponds to 1500 rpm and 39.4 Nm (70 kg/h and 250°C) conditions at cold altitude.

The exempt of the HC adsorption in those points can be also observed by the conversion efficiency values evolution over time, that, unlike what was shown for the low temperature tests, became constant after the thermal stabilization cut-off period. This is because the HC oxidation, which is the one that governs the chemical reaction in these tests, is independent of the state of the zeolite loading, but is only dependent on the temperature.

4.2.3 CO and HC conversion efficiency variation

Once the model results were presented for different points along the measurement time, the modelled and experimental results concerning CO and HC conversion efficiencies once the thermal stabilization was reached are described in this sub-section. The discussion covers the warm sea-level to cold altitude conditions differences and also between CO and HC conversion efficiencies. It will lead to the investigation of the causes responsible for these variations, addressed thereafter in Sub-section 4.2.4.

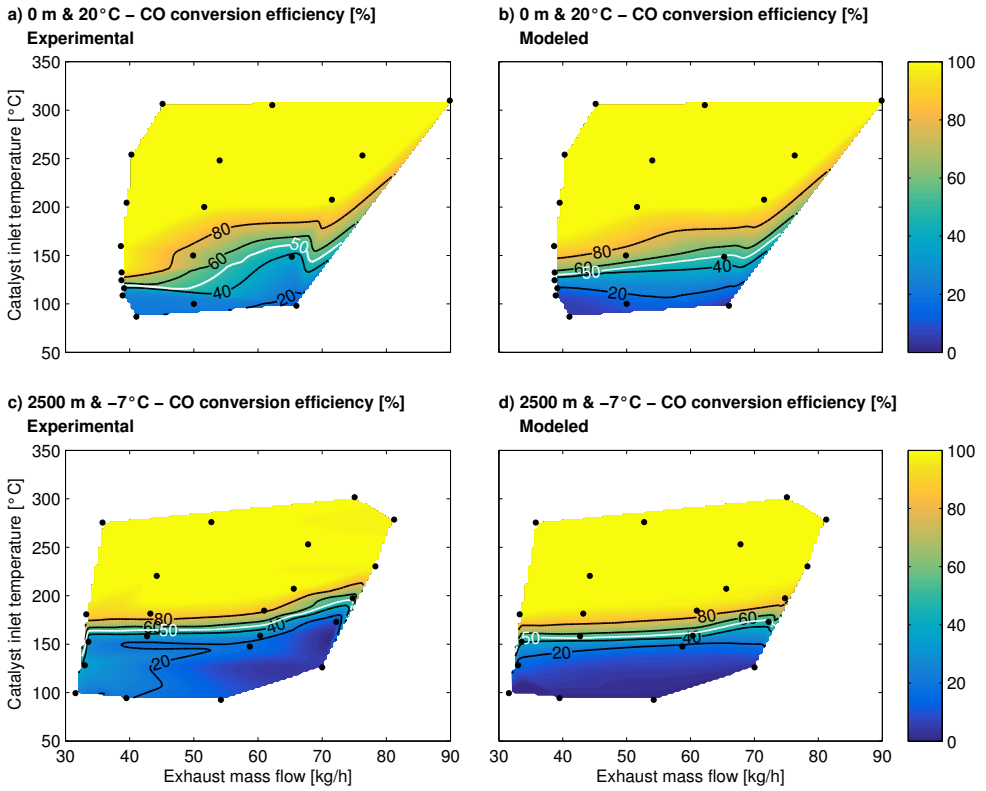

Figure 4.3: CO conversion efficiency as a function of the exhaust mass flow and catalyst inlet temperature.

Figure 4.3 shows the CO conversion efficiency contour maps for the two tested ambient conditions as a function of the exhaust gas mass flow and

DOC inlet temperature. While the upper row represents the experimental (Figure 4.3(a)) and modelled (Figure 4.3(b)) CO conversion efficiency at sea-level and 20°C, respectively, Figure 4.3(c) and (d) cover the same results for 2500 m and −7°C ambient conditions. The black dots on the contours represent each measured point at steady-state.

The comparison between Figure 4.3(a) and (b) reveals that the model was able to capture the trends in CO conversion efficiency in warm sea-level. By analysing Figure 4.3(a), the CO conversion efficiency increases as the DOC inlet temperature increases for the entire exhaust mass flow range, showing higher sensitivity as the exhaust mass flow is higher. The the CO light-off shows a marked dependence on the exhaust mass flow, increasing from ∼ 120°C at 40 kg/h to ∼ 150°C at 68 kg/h, evidenced both in the experimental and also modelled results.

From this exhaust mass flow on, the light-off temperature shows an even higher sensitivity to the mass flow. The model also accurately predicts the region where the full CO conversion efficiency is reached. Again, the maximum conversion efficiency was reached earlier for minimum mass flow, increasing slowly from ∼ 160°C in DOC inlet temperature at 40 kg/h to ∼ 210°C at 71 kg/h. In summary, in this temperature range, a further increase of the exhaust mass flow at constant temperature also led to a faster deterioration of the CO conversion efficiency.

By looking at the cold altitude (Figure 4.3(c) and (d)), it can be seen that the model also predicts this ambient condition with high accuracy. By comparing those results with those correspondent to warm sea-level, is evidenced a modification on the CO conversion efficiency trend. For this extreme ambient condition, the CO light-off temperature was delayed until ∼ 165 °C at 40 kg/h and remained almost constant until 60 kg/h. This represents an increase on the light-off temperature ranging between 45 and 15°C with respect to the warm sea-level. Higher temperatures were also necessary to reach the complete CO abatement, which varied linearly from ∼ 190 °C to ∼ 230 °C between 40 kg/h and 78 kg/h. The deterioration of the CO conversion efficiency in cold altitude is thus evidenced, being extensible to the entire exhaust mass flow range, although it was more penalized at low exhaust mass flows.

Equivalently, Figure 4.4 shows the experimental and modelled contour maps of the HC conversion efficiency at each ambient condition in the same

manner. An overview of the results confirms that the model was also accurate regarding HC abatement prediction, with high sensitivity to the exhaust mass flow and DOC inlet temperature for both ambient conditions.

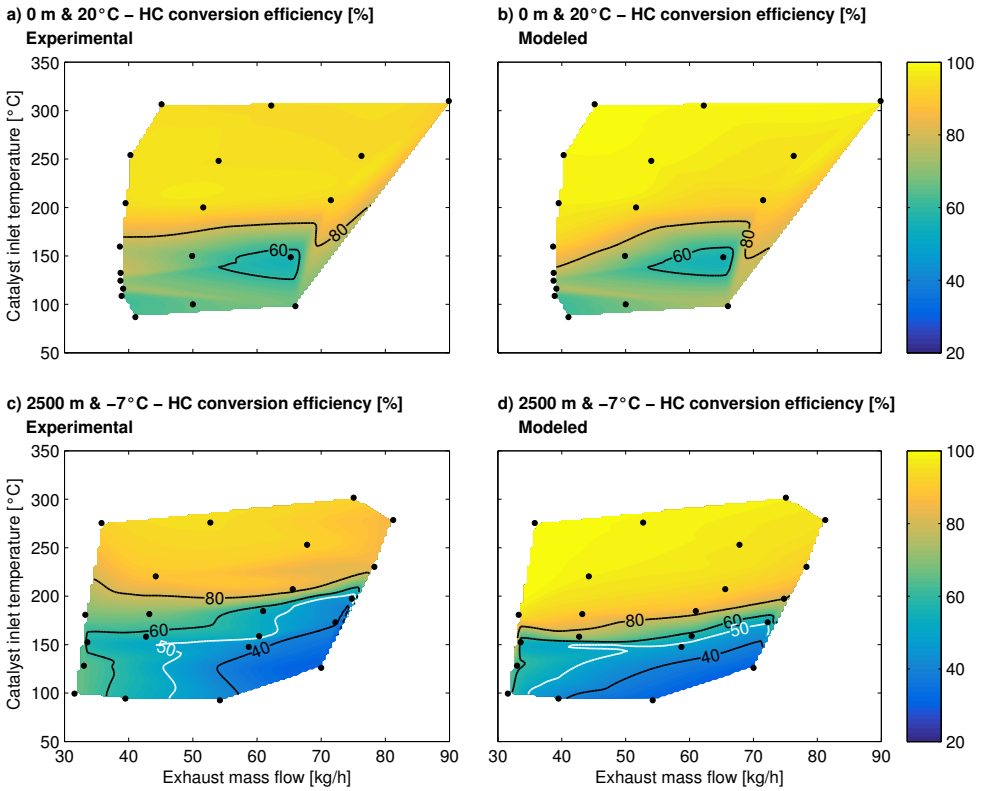

Figure 4.4: HC conversion efficiency as a function of the exhaust mass flow and catalyst inlet temperature.

By operating under cold altitude conditions the HC conversion efficiency is also moved down at the same considered range than at warm sea-level, although with different trends to the CO case due to the HC adsorption on the zeolites, leading to higher conversion efficiencies at low temperature than those found for CO. In warm sea-level, the HC conversion efficiency was over 60% and reached 80% at $\sim$ 170 °C. This temperature was kept almost constant until 70 kg/h, from which a decrease on the HC conversion efficiency started, as also found in the CO case. The model provided similar

trend results, although with a slightly higher conversion efficiency variation up to 55 kg/h of exhaust mass flow. Above 170 °C in DOC inlet temperature, the HC conversion efficiency increased very slowly and it was only greater than 90% for temperatures above ∼ 250 °C.

It is observed that, unlikely the CO, the HC full depletion was not reached in the tested DOC inlet temperature window, which was most probably due to the existence of very low reactivity HC species [285]. This result was similar for both ambient conditions. As previously introduced, higher DOC inlet temperature was required to reach the same conversion efficiency in cold altitude. As example, 200 °C were required to reach 80% of HC conversion efficiency in cold altitude, i.e., 30 °C higher than for the warm sea-level conditions. In fact, the HC conversion efficiency in cold altitude drops fast below this temperature, showing a clear dependence on the exhaust mass flow at lower catalyst inlet temperatures. Whilst the HC conversion efficiency remained around 60% between 100–150 °C at a low exhaust mass flow, it sharply decreased as the mass flow increased, reaching 30% at 70 kg/h and 125 °C.

The phenomena leading to the decrease on the conversion efficiency are common for CO and HC, as later discussed in Section 4.2.4. However, as previously stated, the CO and HC conversion efficiency patterns were different because of the HC adsorption. This was more easily observed by computing the HC conversion efficiencies due to adsorption and oxidation phenomena separately. Figure 4.5 represents these contributions as a function of the exhaust mass flow and the DOC inlet temperature, as the previous HC conversion efficiency graphs. Plots (a) and (b) in Figure 4.5 are related to the HC oxidation conversion efficiency in warm sea-level and cold altitude, respectively, and plots (c) and (d) in Figure 4.5 show the adsorption contribution. As observed, the trends in Figures 4.5(a) and (b), referring to the HC oxidation, were exactly the same as those obtained for CO conversion efficiency (comparison with Figure 4.3) at each tested atmosphere.

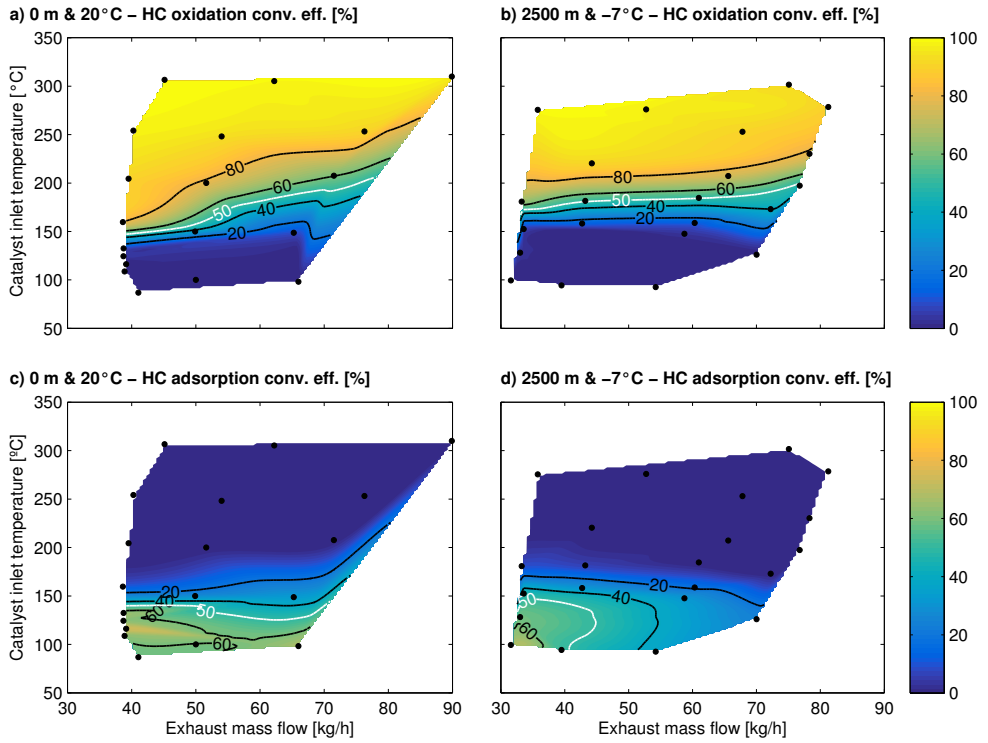

Figure 4.5: Adsorption and oxidation contributions to HC conversion efficiency as a function of the exhaust mass flow and catalyst inlet temperature.

In the case of HC, the oxidation and adsorption contributions to the total HC conversion efficiency are distinguished. The CO and HC oxidation conversion efficiency increase with the DOC inlet temperature, while the HC adsorption conversion efficiency shows decreasing values. It happens because the same expressions govern the oxidation reaction rate for CO and HC, being the quantitative differences original from the lower HC reactivity and the CO/HC partial pressures to a lesser extent, as forward discussed. Therefore, the adsorption was indeed the main source of discrepancy between CO and HC conversion efficiencies.

Noting that the results correspond to the conditions after 15 min of operation (the adsorption is a time-governed process), the HC adsorption conversion efficiency in warm sea-level was $\sim 60\%$ until $\sim$125 °C, regardless of the mass flow and it dropped quickly as the DOC inlet temperature increased,

reaching ∼20% at ∼ 150 °C. Equivalently, the adsorption conversion efficiency drops by increasing the DOC inlet temperature. In cold altitude, these orders of magnitude were only obtained at very low mass flow (Figure 4.5(d)). In these conditions, the HC adsorption conversion efficiency was highly penalized as the mass flow increased, in contrast to the warm sea-level (Figure 4.5(c)). The adsorption-desorption equilibrium is determined by the HC partial pressure and the HC surface coverage evolution over time, according to Equations (3.11) and (3.12) from Chapter 3. Section 4.2.4 discusses their impact on the resulting adsorption HC conversion efficiency.

4.2.4 Flow properties influence on the conversion efficiency

The DOC inlet temperature and exhaust mass flow are engine parameters that are intimately related to the air and thermal management. In addition, the results presented in Section 4.2.3 have shown that those parameters represent a relevant impact on the pollutants abatement. However, since the tested ranges are the same for warm sea-level and cold high altitude cases, the underlying causes explaining the change in conversion efficiency must be found in additional parameters as commented in Chapter 2, namely dwell time and reactants partial pressure.

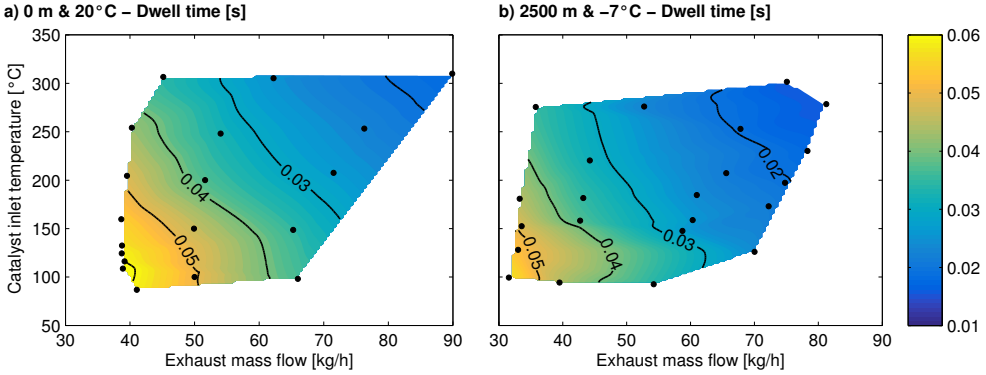

Figure 4.6: Dwell time as a function of the exhaust mass flow and catalyst inlet temperature.

Figure 4.6 represents the dwell time, depicted in the same manner as the conversion efficiency figures, as a function of the exhaust mass flow and DOC inlet temperature for the tested ambient conditions. This variable is calculated dividing the monolith length by the flow velocity, as expressed in Equation (2.1), from Chapter 2. The flow velocity, in turn, increases as the gas density decreases. Therefore, the dwell time is evidently lower when working in altitude conditions for the same exhaust mass flow and DOC inlet temperature, as expected from the lower exhaust pressure after the VGT expansion in altitude operation. In this particular study, the altitude dwell time was decreased by a $\sim 25\%$ in all covered range with respect to sea-level, agreeing with the ambient pressure reduction from sea-level ($\sim$ 1 *bar*) to 2500 m ($\sim$ 0.75 *bar*). Consequently, this parameter is negatively affecting the conversion efficiency in the cold altitude case in an homogeneous way throughout the tested range.

Opposite to dwell time, the reactants partial pressures can be differently affected as a function of the exhaust mass flow and DOC inlet temperature because of their relationship with the engine operating point. Partial pressure provides dual sensitivity because of the exhaust pressure at the VGT outlet, which is mostly given by the altitude, and the mole fraction, which is determined by the engine management as a function of altitude and ambient temperature.

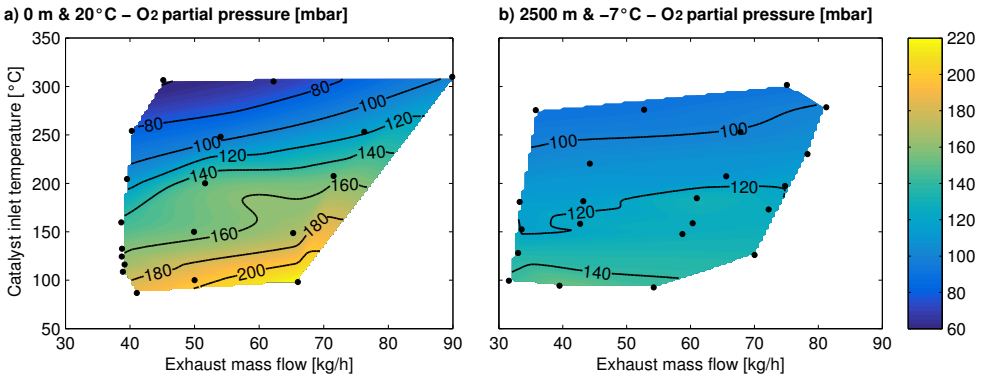

Figure 4.7: O_2 *partial pressure as a function of the exhaust mass flow and catalyst inlet temperature.*

Figure 4.7 plots the O_2 partial pressure. Differently from the dwell time, the O_2 partial pressure was variable with catalyst inlet temperature and with exhaust mass flow. On one hand, at very low temperature, the O_2 partial pressure was lower in cold altitude than in the warm sea-level. This was expected from the lower ambient pressure in altitude conditions. As a consequence, it contributed to lower CO and HC reactivity in the oxidation light-off and warm-up regions during altitude operation. This result is in agreement with the trends in conversion efficiency that are described in Section 4.2.3. On the other hand, the O_2 partial pressure resulted in being lower at sea-level above 250°C for low exhaust mass flows than in the altitude counterpart. These trends evidence that additional engine variables are conditioning the DOC performance.

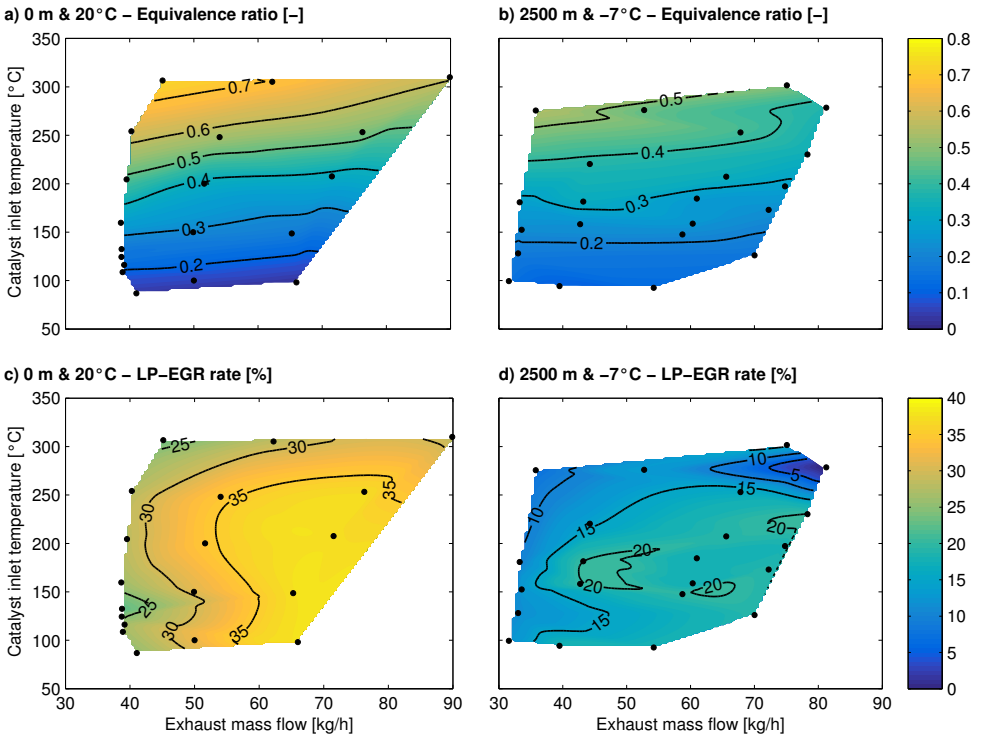

Figure 4.8: Equivalence ratio and LP-EGR rate as a function of the exhaust mass flow and catalyst inlet temperature.

Figure 4.8 represents the values for equivalence ratio and LP-EGR rate in the tested conditions. According to plots (a) and (b) shown in Figure 4.8, the equivalence ratio was higher for warm sea-level in the entire tested range, but especially at high DOC inlet temperature. Comparatively, it contributed to offsetting the expected differences in O_2 partial pressure due to altitude operation. The increasing O_2 partial pressure with exhaust mass flow at constant DOC inlet temperature corresponding to warm sea-level (Figure 4.7) was also dictated by the inverse trend in equivalence ratio. As a remark, the operation in cold altitude required higher engine speed and fuel mass flow, besides higher boost pressure (closer VGT, and higher turbine inlet pressure and temperature), for the same exhaust mass flow and DOC inlet temperature.

In addition, the differences in the equivalence ratio were also influenced by the huge variation in LP-EGR rate between the sea-level and altitude cases. The engine control closed the LP-EGR valve, which, besides the increase of the boost pressure, offset the air mass flow reduction with respect to sea-level driving [128] and contributed to setting an adequate equivalence ratio [39]. Figures 4.8(c) and (d) show that the variables of LP-EGR present equivalent trends in warm sea-level and in cold altitude. The LP-EGR rate increases with the exhaust mass flow (engine speed), but the increasing rate is lower as the mass flow increases. It also contributes to explaining the lower equivalence ratio and higher O_2 partial pressure at high exhaust mass flow.

Regarding the CO conversion efficiency, Figure 4.9 represents the engine-out CO partial pressure for the two tested ambient conditions. A change in the sensitivity of the CO partial pressure with exhaust mass flow and catalyst inlet temperature is observed between the warm sea-level and cold altitude cases. While in the warm sea-level condition, the CO partial pressure was highly dependent on the temperature at low exhaust mass flow, the CO emission became increasing as the exhaust mass flow did. By contrast, the CO partial pressure was mostly dependent on the DOC inlet temperature in cold altitude operation. It is very interesting to note that, despite the lower ambient pressure, the highest CO partial pressure was found in these conditions at a low DOC inlet temperature.

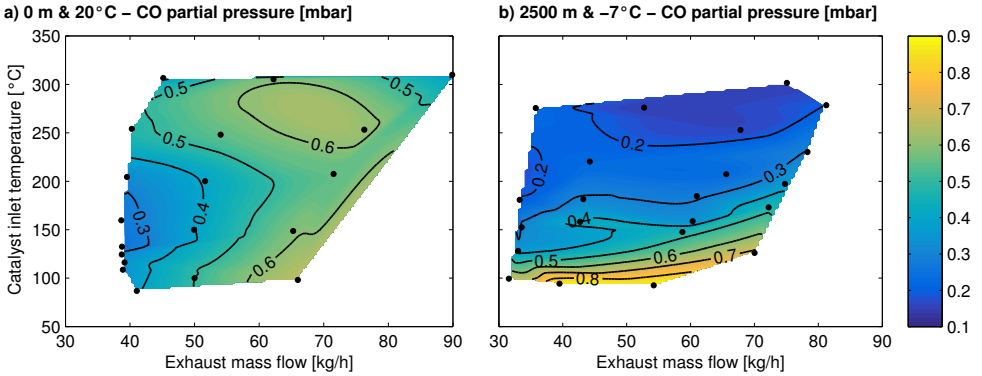

Figure 4.9: Engine-out CO partial pressure as a function of the exhaust mass flow and catalyst inlet temperature.

The engine-out HC partial pressure, represented in Figure 4.10, show very similar trends to those found for the CO. Likewise, the maximum HC partial pressure took place at low DOC inlet temperature in the case of altitude operation. The fact that the CO and HC partial pressures were higher in a cold altitude than the warm sea-level counterparts evidenced higher engine-out emission (mole fraction). This trend covers the entire engine-out HC field but only the medium-low DOC inlet temperature range for CO.

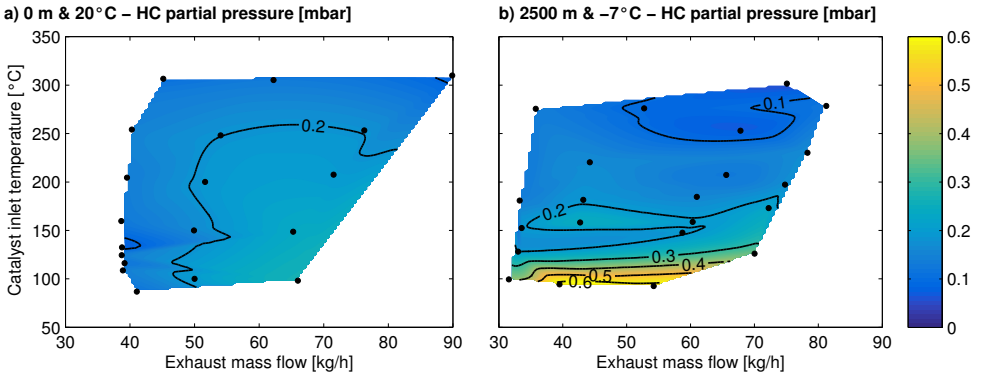

Figure 4.10: Engine-out HC partial pressure as a function of the exhaust mass flow and catalyst inlet temperature.

In the case of HC, it is also remarkable that the high engine-out HC emission at low temperature determined the adsorption efficiency along time. Higher HC emission at altitude conditions meant higher HC adsorption conversion efficiency at the beginning of the test. However, the faster increase of the HC surface coverage as time went by made the desorption rate increase. This is the reason why the HC adsorption conversion efficiency was lower in cold altitude than in warm sea-level at the end of the tests (Figures 4.5(c) and (d)), especially as the exhaust mass flow increased, since it caused greater HC surface coverage.

Regarding a first-order reaction kinetic term, high CO/HC partial pressures at low temperature in altitude operation should contribute to offset the decrease in conversion efficiency caused by the lower dwell time and O_2 partial pressure. However, a high partial pressure of pollutant species also produces a penalty in inhibition [45].

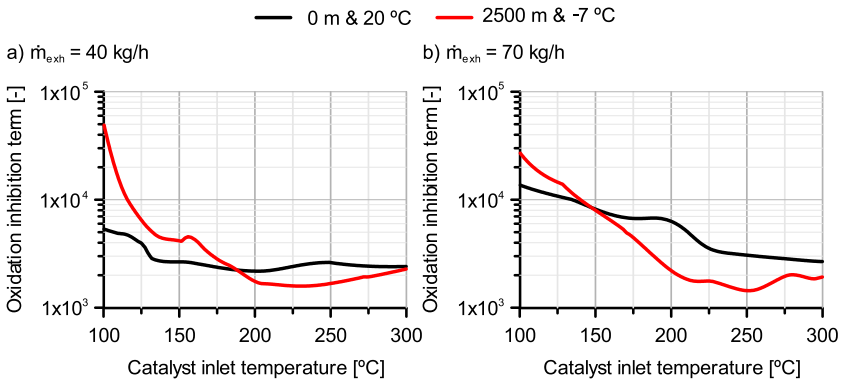

Figure 4.11: Inhibition term as a function of the DOC inlet temperature and ambient conditions.

Figure 4.11 depicts the oxidation inhibition term for two tested exhaust mass flows, a lower and a higher one, as a function of the DOC inlet temperature and ambient condition. The high CO and HC partial pressures at low temperature caused high inhibition in the cold altitude conditions. In both of the tested cases, the inhibition decreased as the temperature was increased because of the reduction in CO and HC partial pressures. The reduction of the engine-out emission combined with the lower ambient pressure gave,

as a result, even lower inhibition than at sea-level. Therefore, the trends in partial pressures at low temperature (lower O_2, and higher CO and HC partial pressures in altitude) explain the decrease of the CO and HC conversion efficiency at high altitude, along with the dwell time decrease. Complementary, the DOC performance at high temperature was only damaged by the dwell time, with its penalty being reduced by the lower inhibition and the null influence of O_2. Hence, CO and HC conversion efficiencies resulted in being very similarly above $\sim 170°C$, regardless of the ambient condition.

4.2.5 Light-off curves sensitivity analysis

Light-off curves of CO and HC were computed in order to evaluate the impact of the dwell time and the reactants partial pressure on the conversion efficiency separately. A set of light-off simulations were carried out for two exhaust mass flows (40 and 70 kg/h), imposing a DOC inlet temperature ramp of 1°C/min from 100 °C to 300 °C. This small temperature ramp makes the efficiencies shown in the light-off curve equivalent to those that would be obtained when the catalyst operates under steady-state conditions at every temperature. The gas composition was taken from the contour maps for every reactant.

Figure 4.12 represents the CO and HC light-off curves. In the case of HC, the adsorption mechanism was cancelled, since it depends not only on temperature, but also on the time through the instantaneous surface coverage. Therefore, only the HC oxidation light-off curve was computed.

Figures 4.12(a) and (b) represent the CO and HC light-off curves, respectively, corresponding to 40 kg/h, whilst plots (c) and (d) correspond to 70 kg/h. Four modeled series are compared in every plot to analyse, step-by-step, the change in conversion efficiency from warm sea-level to cold altitude conditions:

- The black series corresponds to the baseline warm sea-level case, i.e., experimental dwell time and gas composition at 0 m and 20°C.
- As a first step, the dark gray series represents the results of a simulation where the warm sea-level setup was modified, imposing the dwell time that corresponds to cold altitude.

- Next, the light gray series was obtained from warm sea-level case, but imposing both the dwell time and O_2 partial pressure of the cold altitude case.
- Finally, the red series corresponds to the baseline cold altitude, i.e., dwell time, O_2 partial pressure, and pollutants partial pressure (kinetic term and inhibition) impact with respect to warm sea-level results.

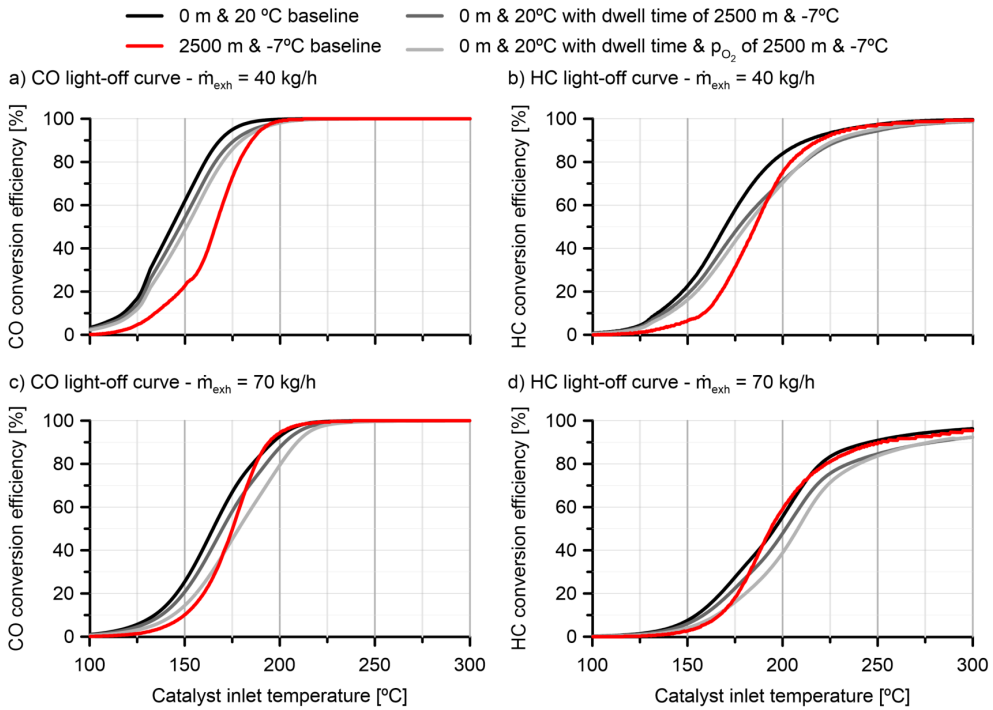

Figure 4.12: Progressive CO and HC light-off curves variation from warm sea-level to cold altitude case considering dwell time and reactants partial pressure separately.

As a common trend in every plot of Figure 4.12, the decrease of dwell time in altitude conditions produced a shift of the light-off curves towards higher temperatures ($\sim 5.5°C$, on average). The decrease of the O_2 partial pressure also shifted the curves towards higher temperature in the light-off region. In this case, the penalty depended on the engine operating conditions, due to the variation of the O_2 partial pressure difference between warm sea-level and cold altitude as a function of the exhaust mass flow. The light-off temperature

was further delayed $\sim$ 4.5°C at 40 kg/h increasing the penalty until $\sim$ 7°C at 70 kg/h. Nevertheless, the higher O_2 partial pressure at high temperature in cold altitude cancelled its negative impact and slightly increased the HC conversion efficiency above $\sim$ 225°C, as observed in Figure 4.12(b).

Despite the deterioration of the light-off temperature due to dwell time and O_2 contributions in cold altitude, the red series evidenced that the most relevant parameters are the pollutants partial pressures due to the inhibition effect. At low exhaust mass flow (40 kg/h) and low DOC inlet temperature, the CO and HC light-off curves were moved towards very high temperature, given rise to a substantial delay of the light-off temperature. It was more marked in the CO case (Figure 4.12(a)) due to its baseline low light-off temperature, which corresponds to an operating region where the CO and HC partial pressures were much more higher in the cold altitude than warm sea-level conditions. By contrast, the CO and HC partial pressures at a high temperature were lower in cold altitude than in warm sea-level. Consequently, the HC conversion efficiency improved with respect to the warm sea-level case above 200°C, offsetting both the dwell time and O_2 partial pressure penalties. This result was not observed for CO in the 40 kg/h case due to the fact that its conversion efficiency was almost 100% at this temperature range.

As the mass flow increased (70 kg/h), the CO and HC partial pressures in cold altitude were only higher than in warm sea-level for a very low temperature, but rapidly decreased below the baseline condition. As a result, the light-off curves underwent a very fast increase of their slope in the cold altitude case (Figures 4.12(c) and (d)). The resulting CO light-off temperature was not further damaged and partially compensated the dwell time and O_2 partial pressure effects. Above this temperature, the benefits of the lower pollutants partial pressure became more evident and the light-off curves of the two tested ambient cases were even coincident from 185°C on. The HC light-off benefited more from these boundary conditions, taking place earlier in cold altitude than in warm sea-level. In any case, both of the light-off curves converged from 50% in conversion efficiency.

4.3 Passive strategies for DOC inlet temperature enhancement

As evidenced in the Section 4.2, low temperature DOC operation is harmful for CO and HC emissions, independently from altitude. This problematic fomented the interest for early aftertreatment light-off solutions during warm-up periods through the application of passive strategies. To achieve that, several strategies have been proposed in the literature, as discussed in Chapter 2. A solution involving the aftertreatment placement upwards the turbine was proposed by Luján *et al* [137], for example, leading to a remarkable increase in the aftertreatment inlet temperature due to the absence of the expansion and cool down processes that happen in the turbine.

The use of TES and PCM technologies also proved themself promising regarding the studies of Hamedi [44] and Burch *et al.* [203] addressed in Chapter 2. However, the interest of a practical applicability on the current context with a more straightforward implementation was inspired by the initiative of the exhaust line thermal insulation. The idea emerged back in the 70s by the pioneering work done by Kamo and Bryzik [286, 287], that used thermally insulating materials such as silicon nitride to insulate the combustion chamber.

Other materials as the YSZ (yttria-stabilized zirconia) have been also proved to reduce the thermal loss up to 50°C when applied to exhaust manifolds [288]. This magnitude can represent an important difference to increase the emissions conversion efficiency. Also different strategies of thermal insulation have been successfully demonstrated in the literature allowing to contain the exhaust thermal loss, as, for example, the use of a heat shield proposed by Rajadurai *et al.* [289].

This Section is dedicated to computationally evaluate different exhaust line thermal insulation strategies. By the use of the software GT-Power, the suggested configurations can be pondered, aiming to point out the most promising strategies to elevate the aftertreatment inlet temperature. Besides, the engine response in terms of BSFC is also taken into account, looking for the optimal trade-off between BSFC and catalyst inlet temperature.

It is important to remark that the sequence of contents composing this doctoral thesis is not the same as the chronological one. Thus, for an optimal use of the time, at the same time as the experimental installation was being prepared, it was decided to analyse how the thermal insulation can contribute to increase the catalyst inlet temperature on an already setup engine model of a comparable HSDI Diesel engine, as mentioned in Chapter 3, than the one experimentally characterised.

To close the Chapter, the best feasible thermal insulation strategies are applied on the GT-Power engine model presented in Chapter 3, corresponding to the tested engine used along this doctoral thesis to asses the DOC response to new boundaries produced by the thermal insulation. With those data in hands, new inputs are entered in the DOC model to obtain the CO and HC conversion efficiency maps as a function of each insulation method for different ambient conditions.

4.3.1 Study definition

To perform the simulations, the 1D commercial fluid dynamic engine modelling software GT-Power was employed in the same manner as it was described in Section 3.3.1, replacing the standard turbocharger model by an external heat transfer and friction losses turbocharger model to correctly predict the turbine outlet temperature. Regarding this part of the model, more details are found in Section 3.3.1.2. The basic characteristics of the simulated engine are detailed in Table 4.2.

In order to cover a wide range in the engine operation map, six engine operating points have been simulated departing from the experimental data, as shown in Table 4.3. The operating points #A, #B and #C are related to low load conditions whereas #D, #E and #F represent high load, in a way that different trends and quite a few variations can be addressed.

Table 4.2: Main characteristics of the simulated engine.

Type	Turbocharged HSDI Diesel
Regulation	Euro 4
Displacement	1997 cm^3
Bore	85 mm
Stroke	88 mm
Number of cylinders	4 in line
Number of intake valves	2 per cylinder
Number of exhaust valves	2 per cylinder
Turbocharger model	VGT
Compression ratio	15.5:1
Maximum power @ speed	120 kW @ 3750 rpm
Maximum torque @ speed	340 Nm @ 2000 rpm
EGR type	Cooled, high pressure with intake throttle

Table 4.3: Simulated engine points.

Point ID	Speed [rpm]	Load[%]
#A	1500	10
#B	1500	25
#C	2000	25
#D	1250	75
#E	2000	75
#F	3500	100

The GT-Power engine model scheme is presented in Figure 4.13, where the intake manifold, cylinders, exhaust manifold and turbocharger model are indicated by the blue lines. The exhaust system is highlighted and divided into 3 sections as in the experimental engine. The 1^{st} and 2^{nd} sections represent the exhaust ports. The two individual channels in the 1^{st} section merge roughly halfway through the ports, forming one larger cylindrical channel in the 2^{nd} section. The mixture is finally discharged in the exhaust manifold, represented by the 3^{rd} section. The turbine inlet and outlet positions are designated by the numbers 4 and 5, respectively.

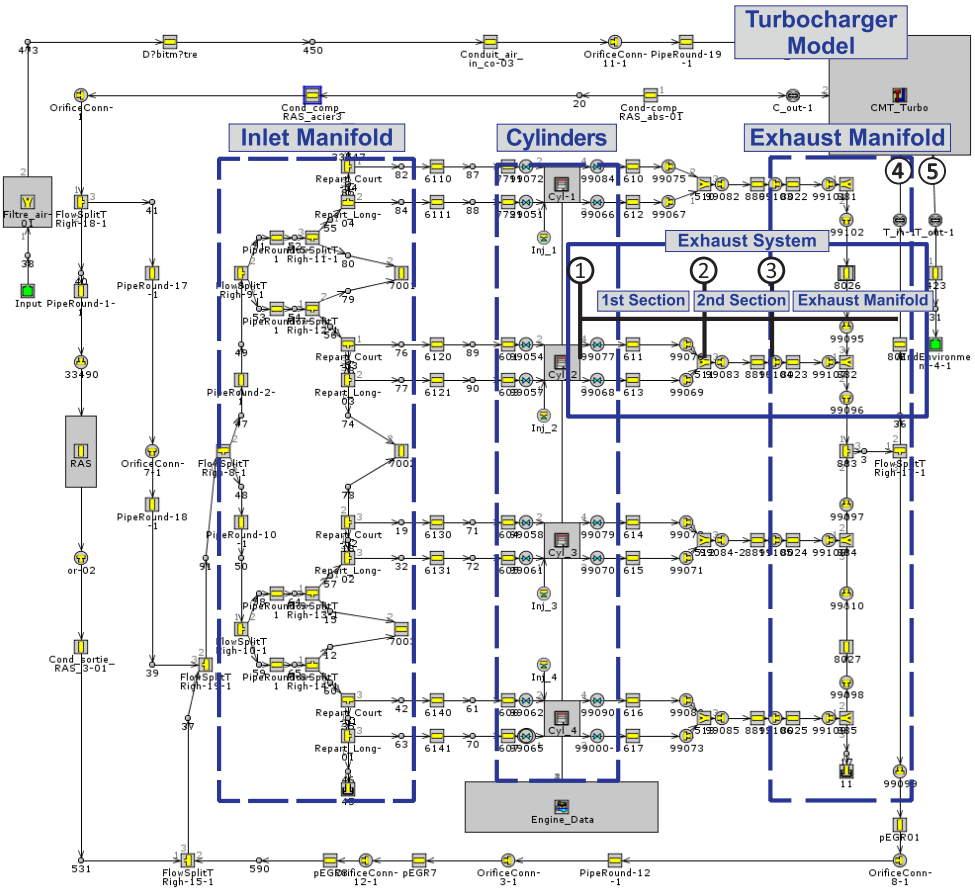

Figure 4.13: Scheme of the engine model in GT-Power.

Figure 4.14 evidences the reliability of the model over the six chosen points through the main engine variables of BSFC, fuel injected mass, VGT outlet temperature, air mass flow, VGT inlet temperature and turbocharger speed. For all experimental conditions the same fitting coefficients have been set, reason why some operating points show bigger errors than others. Otherwise, the parameters present a good balanced agreement between measured data and modelled results.

In all parametric studies, torque and intake manifold pressure were kept constant using PID controllers. Unlike in the Euro 6d-Temp engine, where injected fuel quantity was imposed, this variable is now regulated to control

the torque. It is depicted in Figure 4.14(f). However, the intake manifold pressure has been governed in the same manner by the VGT opening and the air mass flow was regulated by the combination of the high pressure EGR and the intake throttle valves.

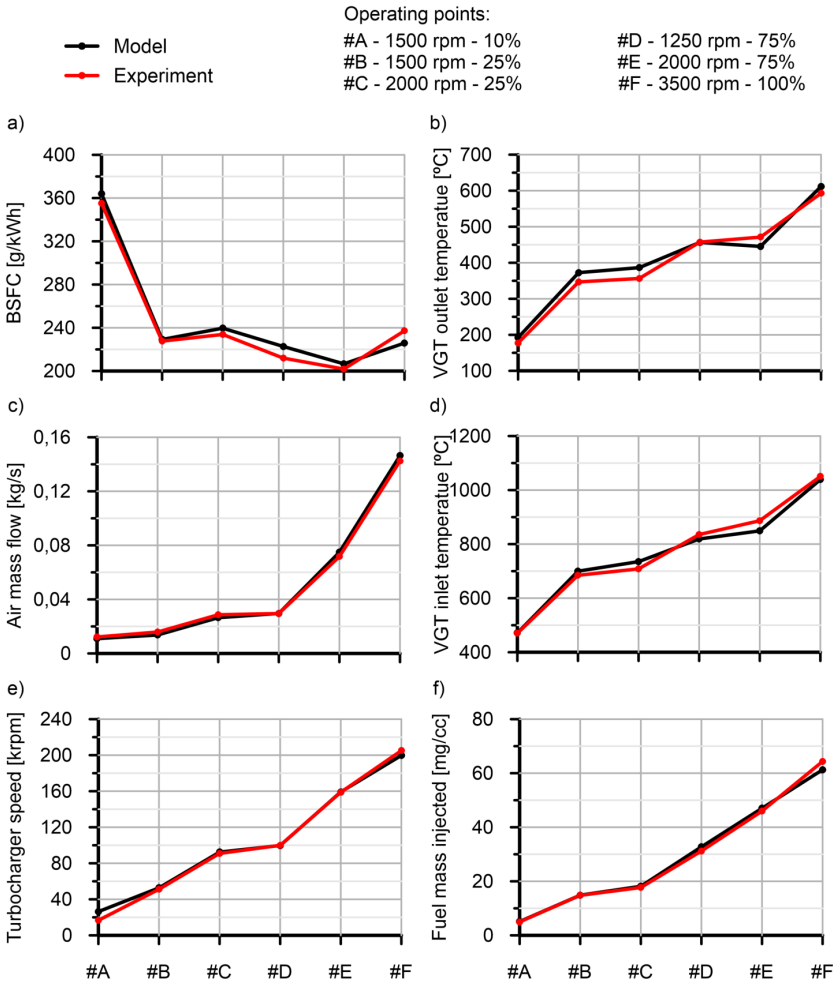

Figure 4.14: Comparison between experimental data and modelled result for the selected operating points.

The temperature and the exergy rate evolution through the exhaust line for the six chosen operation points are displayed in Figure 4.15 in order to investigate the main source of the energy loss.

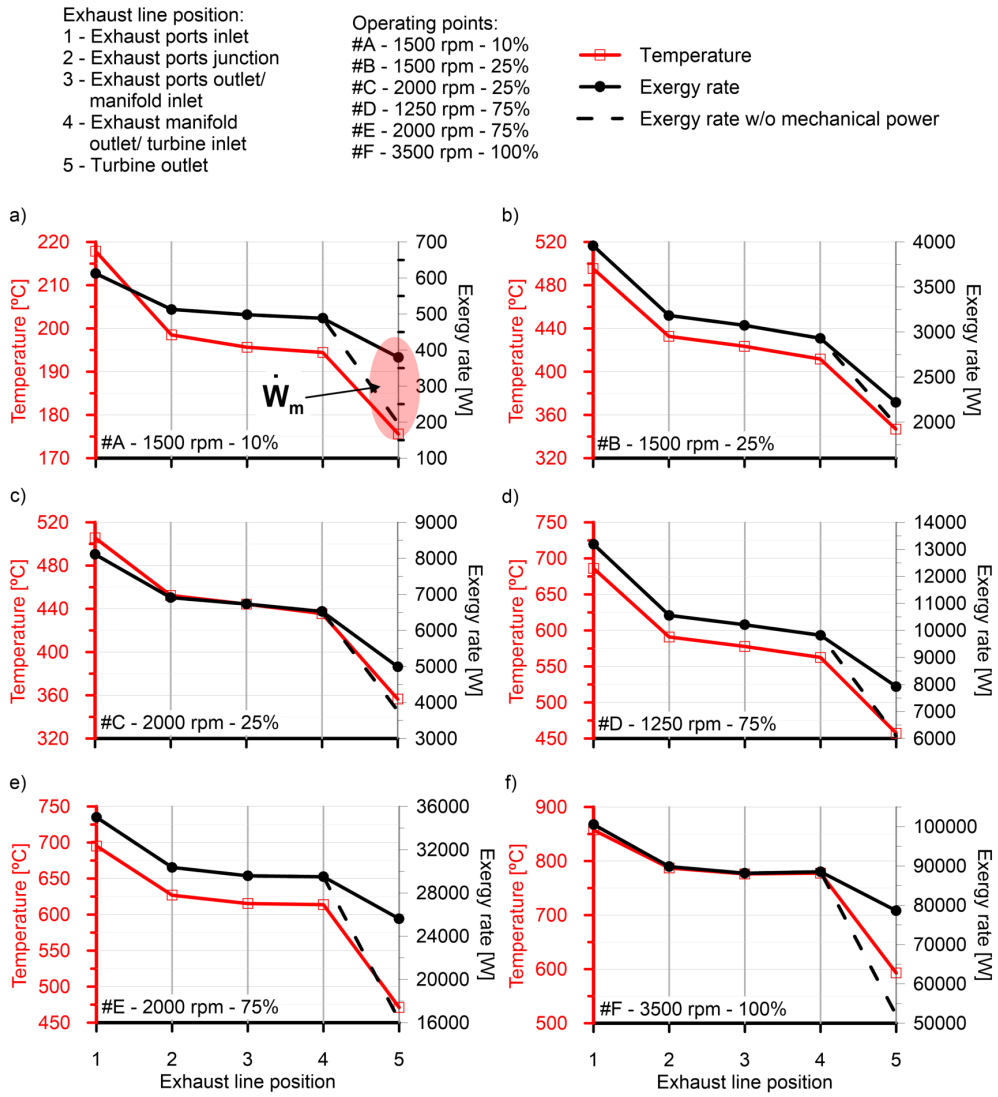

Figure 4.15: Temperature and exergy rate variation across the exhaust line in the baseline configuration.

The exhaust line position in the x-axis of each chart in Figure 4.15 are correspondent to the position labels of the exhaust system showed in Figure 4.13. Looking at both variables evolution, it is observed an accentuated drop in the 1st section of the exhaust manifold, then a smoother loss of temperature and exergy rate from point #2 to point #4 and finally an abrupt drop again in the turbine, between point #4 and #5. The exergy rate can be calculated according to Equation (4.1):

$$ExergyRate_i = (h_i + \frac{{v_i}^2}{2} - T_{amb}\Delta s_i) \cdot \dot{m} \tag{4.1}$$

A huge difference from exergy rate between the dotted and the full line can be seen in the last section of the curves. This difference corresponds to the exergy rate from mechanical power, which is only considered at the turbine outlet. This result means that not only the isentropic expansion of the gas in the turbine reduces the temperature but there is also a relevant exergy rate destruction.

This behaviour triggers an interest in reducing the temperature loss in these two locations: between stations #1 and #2, where the individual channels of the exhaust ports are located, and from #4 to #5 where the actively cooled (by oil and water) turbine is located. Conventional exhaust ports lose significant heat because they transport hot gas at the highest temperature from the cylinder to the exhaust manifold being water-cooled and the high temperature drop in the turbine is caused by the expansion of the exhaust gas to produce mechanical energy and by wall heat transfer to the ambient and to the cooling and lubrication systems of the turbocharger bearing housing.

For this reason, the parametric studies have been focused on two separate strategies, which are exhaust ports and turbine thermal insulation, to obtain less temperature drop and, consequently, a higher VGT outlet temperature. At the same time it is sought to cause as little prejudice in BSFC as possible, or even to achieve some improvements on it and others engine parameters.

4.3.2 Thermal insulation of the exhaust ports

The temperature sensitivity in the 1^{st} section of the exhaust manifold underlines an interest for an optimum design of the exhaust ports integrating both fluid mechanics and heat transfer criteria. Therefore, the first studied strategy consists of insulating the exhaust ports, reducing heat exchange with the surroundings and temperature loss in this section of the exhaust system. This insulation corresponds to the 1^{st} section in Figure 4.13, comprehending the exhaust port positions #1 to #2 in Figure 4.15.

Four different insulation types were performed to accomplish this objective, which are sketched in Figure 4.16. Case #1 represents the baseline design. Case #2 evaluates the effect of an air chamber in the inner part of the exhaust pipes, whilst Case #3 includes a ceramic coating between the air chamber and the exhaust pipe. Finally, for comparison proposals, Case #4 corresponds to an adiabatic configuration.

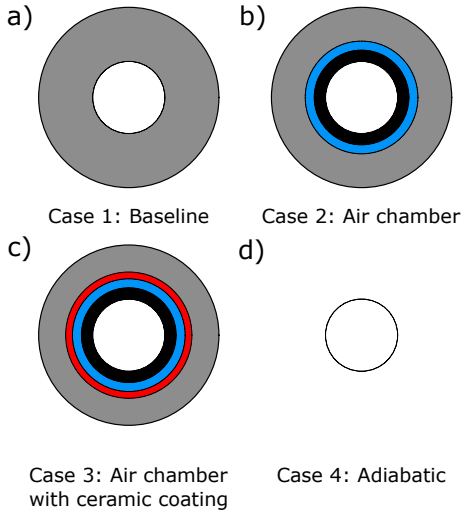

Figure 4.16: Representation of exhaust ports thermal insulation cases.

Table 4.4 shows the material properties applied in the four different configurations, which includes density, thermal conductivity, specific heat and surface emissivity. Aluminium is the material applied in the original exhaust ports. Stainless steel is set in the inner part of the port, when an air chamber and YSZ, a ceramic in which zirconium dioxide (ZrO_2) is reinforced with

yttrium oxide (Y_2O_3) [290] to obtain a stable structure at room temperature are added in the configuration. Additionally, the thickness of each layer is listed for every case in Table 4.5.

Table 4.4: Thermal properties of the materials used in the exhaust ports.

Material [-]	Color [-]	Density [kg/m^3]	Thermal Conductivity [W/mK]	Specific heat [J/kgK]	Surface Emissivity[-]
Stainless steel	Black	7900	25.4	611	0.85
Air	Blue	1.1614	0.0667	1141	-
YSZ	Red	4950 [291]	1.2 [291]	490 [291]	0.729 [292]
Aluminium	Grey	2700	204	240	0.8

Table 4.5: Layer thickness in exhaust ports thermal insulation configuration.

	Thickness [mm]			
Case	Stainless steel	Air	YSZ	Aluminium
#1 (baseline)	0	0	0	15
#2	3	2	0	10
#3	3	2	1	9
#4		Adiabatic		

Exhaust ports insulation results in a higher VGT inlet temperature because of the heat loss reduction. This increase on VGT inlet temperature makes the VGT to open, as it can be observed in Figure 4.17(a) and (b), for low and high load operating points respectively. Consequently the pressure before the turbine decreases, as shown in plots (c) and (d) in Figure 4.17. A decrease in VGT inlet pressure also represents a benefit for pumping losses, as demonstrated in the graphics 4.17(e) and (f). The effective efficiency is increased not only by the reduction of the pumping losses, but also because of an increment of the indicated efficiency.

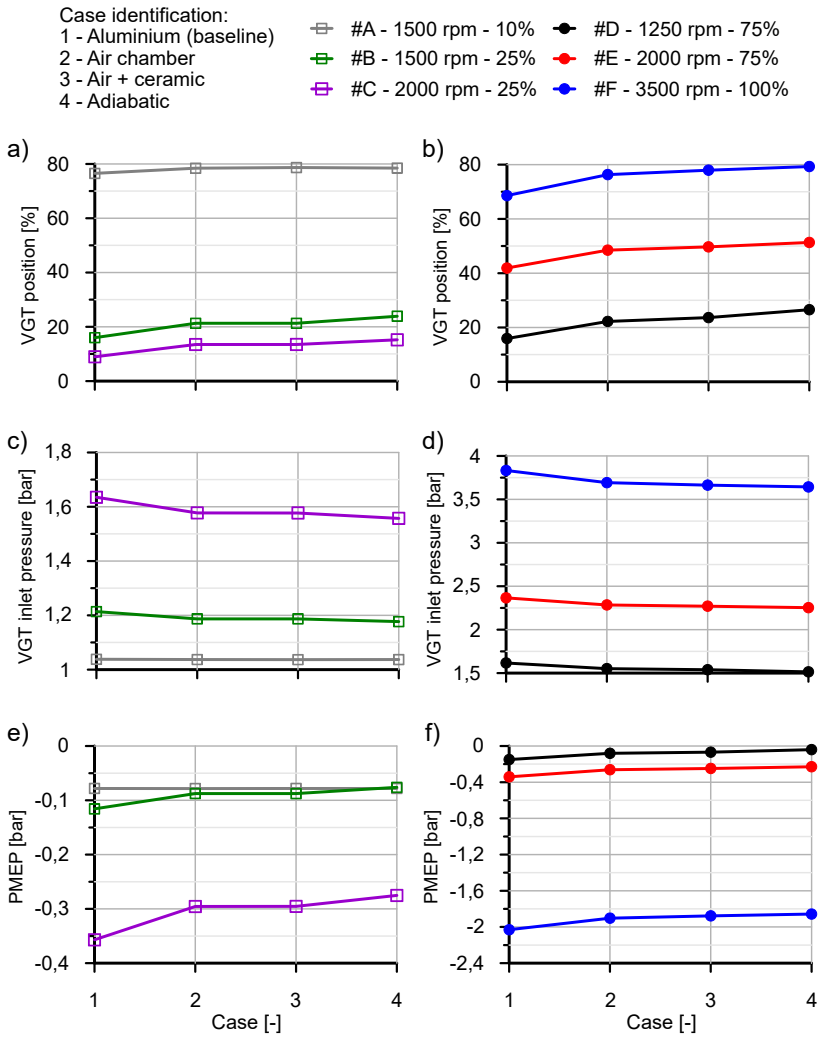

Figure 4.17: VGT position, VGT inlet pressure and PMEP at low and high load operating points as a function of the exhaust ports thermal insulation configuration.

The reason for this increment is due to the maximum in cylinder temperature decrease, as illustrated in Figure 4.18, and, therefore, the one in heat losses inside the cylinder.

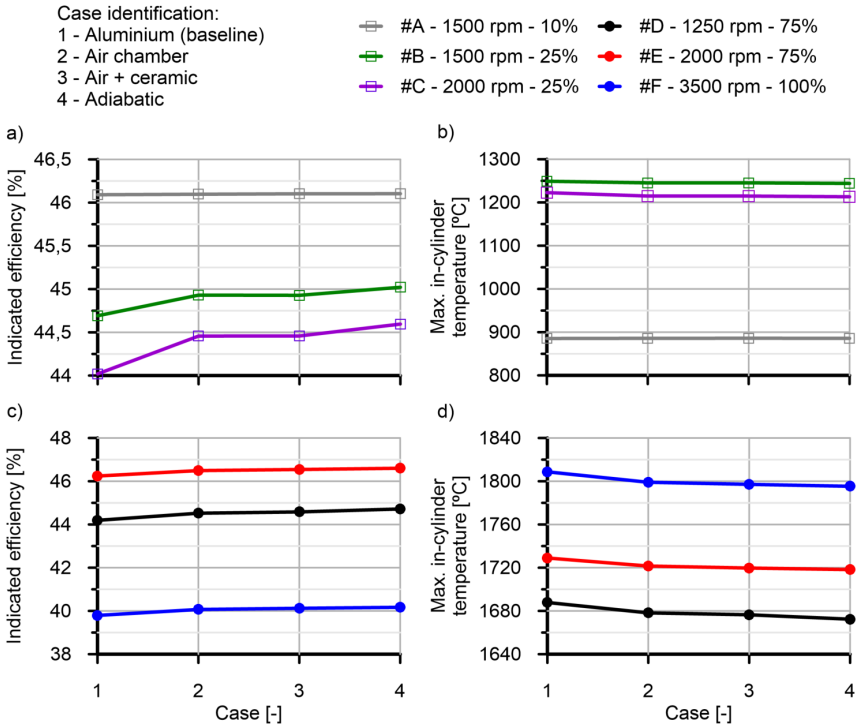

Figure 4.18: Indicated efficiency and maximum in-cylinder temperature at low and high load operating points as a function of the for exhaust ports thermal insulation configuration.

Figure 4.19 displays the temperature variation over the exhausts ports for the six simulated engine operation points at each described parametric study. As indicated, the less loss of temperature between positions 1 and 2 is reflected along all the exhaust line, showing a higher temperature, until exhaust position 5, determining the VGT outlet temperature. Also, as expected, the adiabatic curve shows the highest temperatures for all operation points and the extra ceramic coating added in addition to the air chamber, *i.e.* Case #3, represents little or almost no improvement in comparison with Case #2, which has only an air chamber in the inner part.

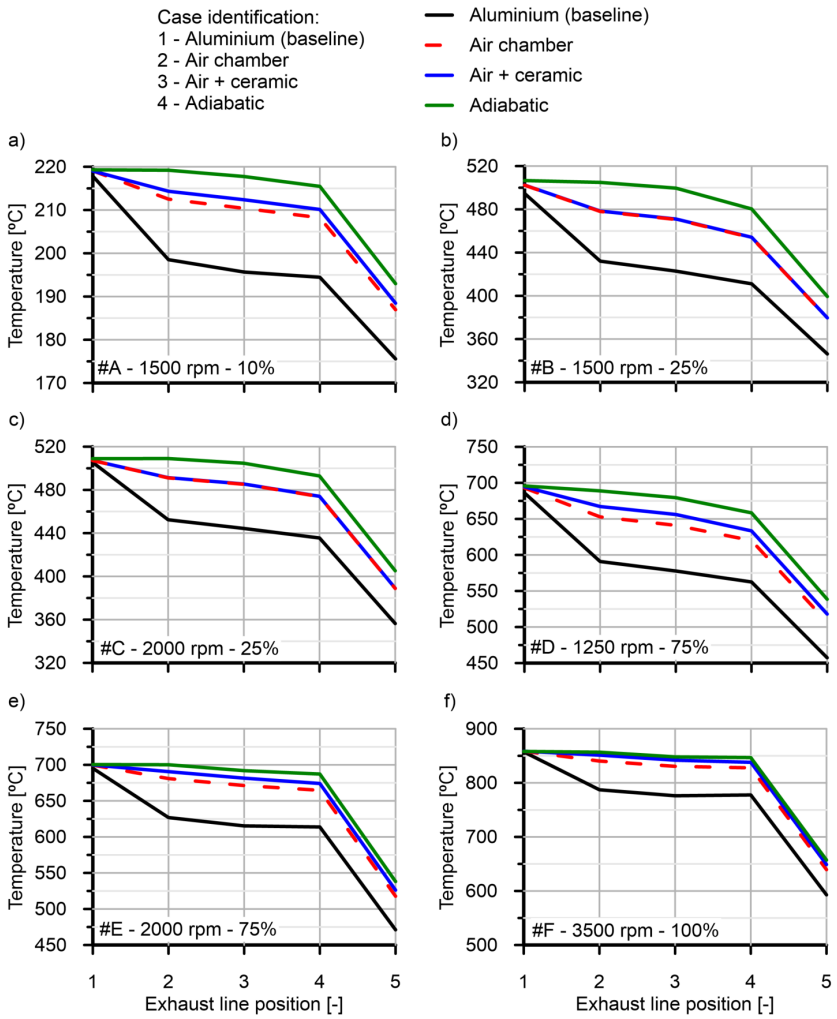

Figure 4.19: Temperature variation across the exhaust line as a function of the exhaust ports thermal insulation configuration and the engine operation points.

Finally, Figure 4.20 summarizes the VGT outlet temperature and BSFC variation in comparison to the baseline for the 4 studied parametric cases, given that Equations (4.2) and (4.3) express how these values are obtained in reference to the baseline, remarking that T_{VGTout} corresponds to the temperature upstream of the catalyst.

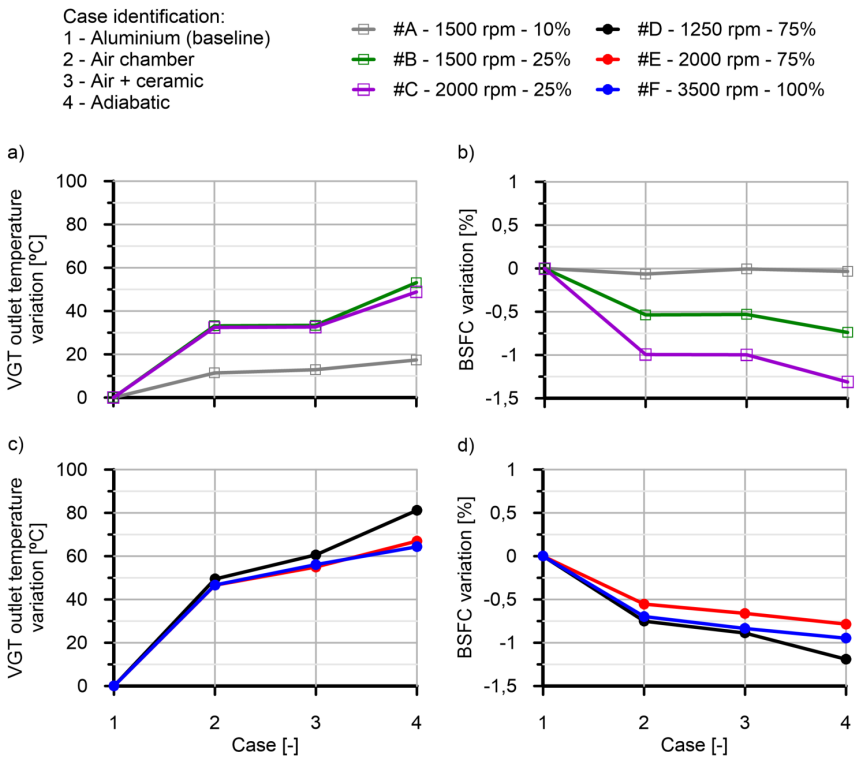

Figure 4.20: Aftertreatment inlet temperature and BSFC variation at low and high load operating points as a function of the exhaust ports thermal insulation configuration.

$$\Delta T_{VGTout} = T_{VGTout_{Case\#i}} - T_{VGTout_{baseline}} \tag{4.2}$$

$$\Delta BSFC[\%] = \frac{BSFC_{Case\#i} - BSFC_{baseline}}{BSFC_{baseline}} \times 100 \tag{4.3}$$

As shown in Figure 4.20(a) and (c) and already above mentioned, the exhaust ports thermal insulation produces an increment on the VGT outlet temperature for all cases. The Case #4, which represents the adiabatic situation, is the one where the highest VGT outlet temperature is obtained,

since there is no heat exchange with the wall. However, the Cases #2 and #3, which are the realistic configurations, also present a relevant increment in VGT outlet temperature, in the range of 10 to 30°C increase in low loads up to 50 to 60°C for high loads.

This effect is due to a much lower thermal conductivity and higher specific heat of the materials present on the two cases containing insulation than purely aluminium, which is the only material used in the exhaust port for the baseline configuration. It is possible to see that adding 1 mm of YSZ ceramic coating does not produce a significant improvement on insulation to the system when compared to the air chamber in the inner part of the exhaust pipes, since its material properties are not as excellent as air for insulation, being its effect cancelled out.

Besides benefits in aftertreatment inlet temperature, fuel economy improvements are also reached, as shown in Figure 4.20(b) and (d), especially at high load, due to pumping losses reduction and indicated efficiency improvement, as seen in Figures 4.17 and 4.18. Figure 4.20 depicts that for very low load, there is almost no improvement on BSFC because the gain in VGT outlet temperature is less representative. This in agreement with VGT inlet pressure and pumping mean effective pressure (PMEP), which present a small variation in comparison to the baseline case. As load and engine speed increase, BSFC is reduced up to approximately -1.25% since PMEP and VGT inlet pressure improvements are more significant for these cases.

4.3.3 Turbine thermal insulation

The temperature sensitivity between #4 and #5 exhaust port positions in Figures 4.13 and 4.15 also emphasises the interest for a turbine heat exchange optimisation, minimizing the heat loss by means of insulating the turbine. Regarding this strategy, five cases have been applied to achieve an increase on VGT outlet temperature, as described in Table 4.6. Case #1 represents the baseline design, Case #5 performs a reduction of 50% in the contact area between the turbine and the housing place, in case #6 water cooling is suppressed and the turbine is equipped with a thermal shield, in case #7 the turbine contains an internal ceramic coating (1 mm of YSZ material) and case #8 represents an adiabatic turbine.

Table 4.6: Turbine thermal insulation cases.

Case #1	-	Baseline
Case #5	-	Contact area between turbine and housing place 50% reduced
Case #6	-	Turbine without water cooling and with thermal shield
Case #7	-	Turbine with internal ceramic coating in the volute (1 mm YSZ)
Case #8	-	Adiabatic turbine

Figure 4.21 compares the turbocharger heat transfer balance in the baseline turbocharger (turbine) configuration for the studied operating points. This is an indicator of the heat power exchanged between two or more environments. For each operating point, two columns are depicted. The one on the left side represents the heat transferred from the gas flow to the walls of the turbocharger while the right on stands for the heat transferred from the walls to the fluid flow.

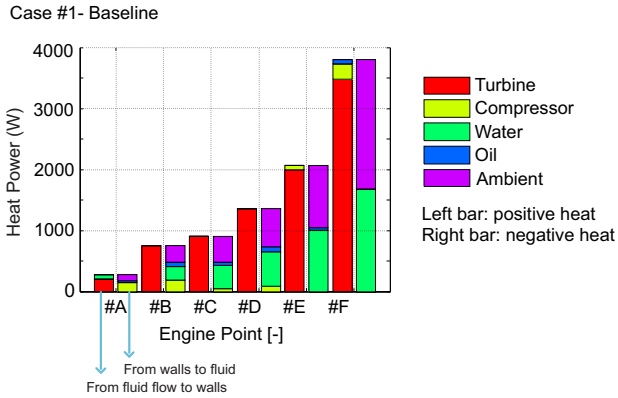

Figure 4.21: Heat power balance in the turbocharger for the baseline configuration (Case #1).

Almost only the gas flowing across the turbine heats up the walls in low load operating points. In these cases, the walls transfer heat to fresh air in the compressor, to the water cooling flow, to the oil flow and finally to the ambient. At high load, high pressure and temperature are originated, making not only the turbine but also the compressor to transfer heat to the walls, what also makes the wall temperature to increase. Finally, the oil flow also heats up

the turbocharger walls at high load since it reaches higher temperature due to higher friction losses power.

The heat transfer balance for the additional four configurations listed in Table 4.6 are illustrated in the Figure 4.22. In the adiabatic case (Case #8), shown in plot (a), the turbine component heat transfer disappears, so that heat only exchanges between the other mentioned fluids. For the half area case (Case #5), plot (b) evidences that although the contact area between the turbine and the housing place is decreased by half and the heat transfer is directly proportional to the surface area, the heat exchange is still very similar to the baseline case. If one compares Figure 4.21 with Figure 4.22(b), it is possible to clearly see (especially in the operating point #F) how the heat flux to the ambient is proportionally increased, in spite of the heat flux to the water cooling in the bearing housing has been reduced.

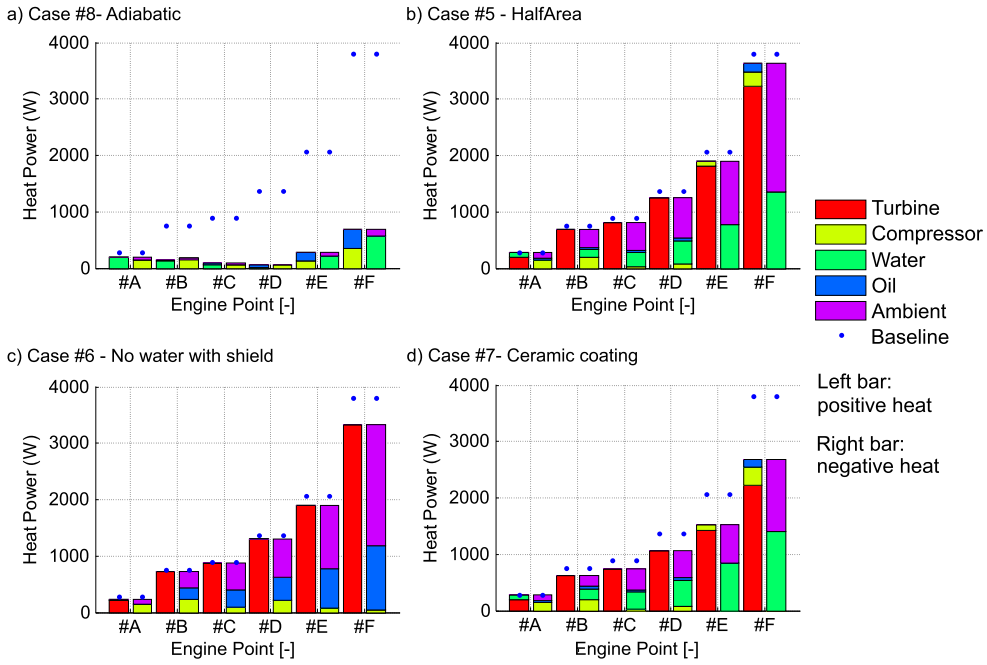

Figure 4.22: Heat power balance in the turbocharger as a function of the turbine thermal insulation configuration and the operating point.

Plot (c) in Figure 4.22 shows the configuration removing water cooling but insulating the turbine with a thermal shield (Case #8). The heat transfer

to the coolant fluid is now zero since it is absent. Besides, the lubricant oil portion has substantially increased compared to all previous cases, once the heat transferred to water cooling fluid in the other cases is this time mainly transmitted to the oil flow.

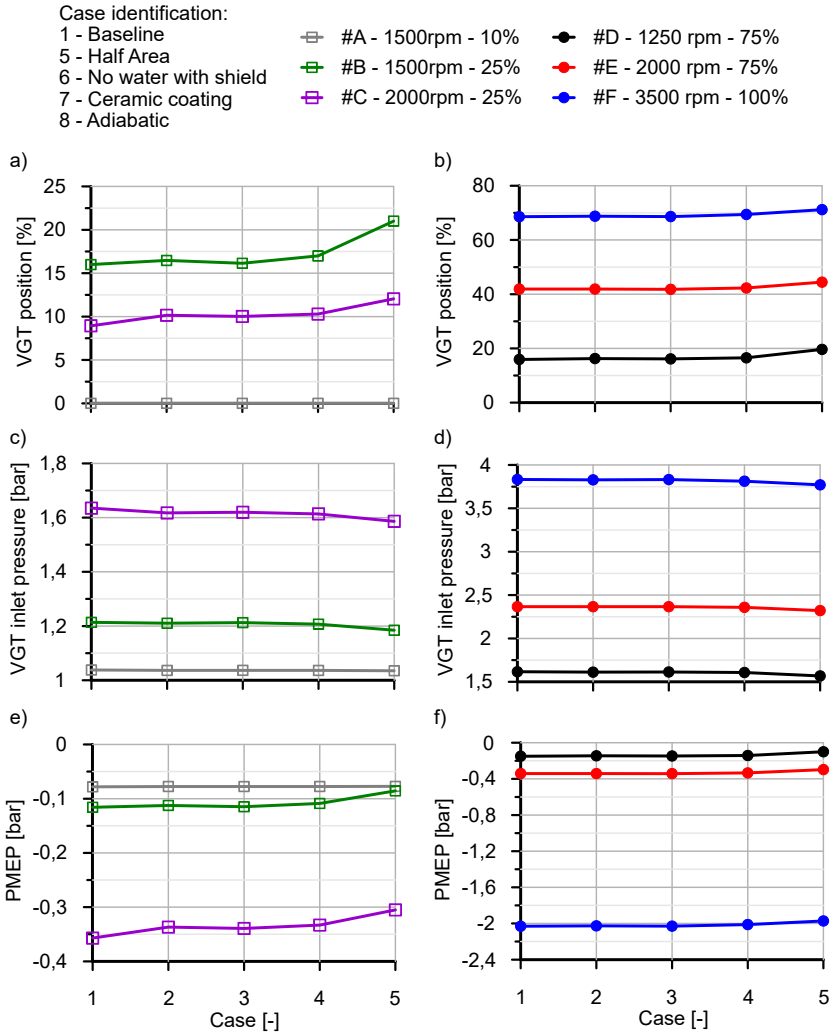

Figure 4.23: VGT position, inlet turbine pressure and PMEP at low and high load operating points as a function of the turbine thermal insulation configuration.

In addition, due to the thermal shield included in this configuration, the heat losses from the turbine are lower than in the baseline case. Finally, the ceramic coating case (Case #7) provides a significant reduction in the heat losses coming from the turbine. In fact, they are lower than in a the case containing thermal shield insulation, as can be seen in Figure 4.22(d), specially evident at high load operation points. It happens because, as defined in Table 4.6, the ceramic coating reduces the heat flow already through the turbine volute wall.

As illustrated in Figure 4.23(a) and (b), the heat loss reduction makes the VGT to open, mainly for the Case #8, since, according to the Figure 4.22(a), the adiabatic case presents less heat losses from the turbine and there are passive changes downstream of the turbine inlet. Thus, VGT inlet pressure, which is represented in plots (c) and (d) for low and high loads, and pumping losses are reduced (Figures 4.23(e) and (f)).

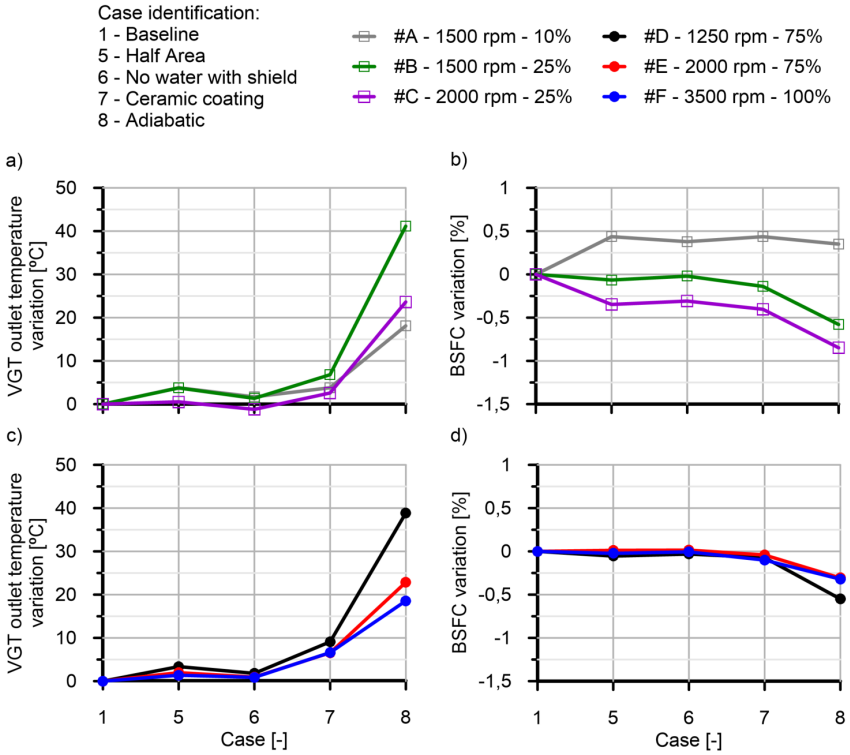

Figure 4.24: Aftertreatment inlet temperature and BSFC variation at low and high load operating points as a function of the turbine thermal insulation configuration.

For a final comparison, Figure 4.24 displays the VGT outlet temperature and BSFC variation with respect to the baseline case. X-axis represents each of the 5 parametric studies described in Table 4.6. It is noticed, according to the comments in the previous paragraph, that the adiabatic case provides the highest temperature gain for VGT outlet temperature, varying from 20 to 40°C. In therms of realistic configurations, Case #7 (ceramic coating) shows the highest improvement, with 10°C increase from baseline case. Also BSFC shows a slight improvement, mainly for the adiabatic study, with the only exception of the very low load operation point #A.

4.3.4 Combination of exhaust ports and turbine thermal insulation

After exposing two different strategies to achieve VGT outlet temperature improvement, a possible further step to adopt is to employ both of them at the same time, expecting to obtain a synergistic result. That said, a third study was undertook evaluating two configurations: the first one is a combination of both adiabatic cases to observe the maximum value of VGT outlet temperature that could be achieved using these strategies; and the second considers merging two cases that present feasible technological solutions. Table 4.7 shows the four compared cases for the first part of this third study.

Table 4.7: Adiabatic exhaust ports and turbine cases.

Case #1	-	Baseline
Case #8	-	Adiabatic turbine
Case #4	-	Adiabatic exhaust ports
Case #9	-	Combining Case #8 and Case #4

Figure 4.25 represents VGT outlet temperature and BSFC variation for all four cases. As expected, Figure 4.25(a) and (c) show further improvement on temperature when both strategies are applied at the same time. For all running points, a pronounced increase almost lineal is observed, making it possible to reach up to 130°C of temperature variation. Fuel consumption has also presented a noticeable improvement when both strategies are employed. Figures 4.25(b) and (d) illustrate BSFC values for all parametric studies and evidence that for this last study, BSFC is reduced up to 2%.

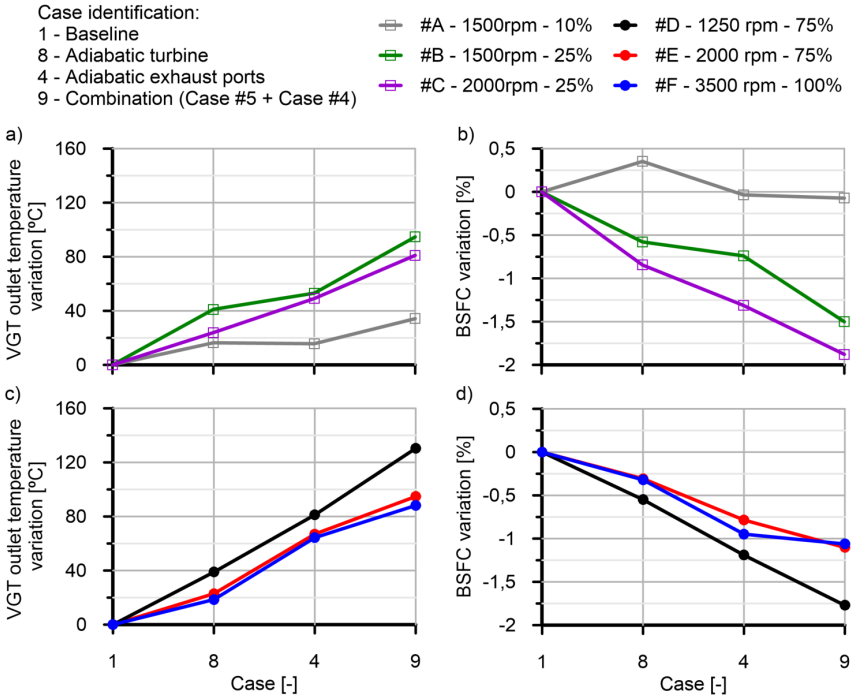

Figure 4.25: Aftertreatment inlet temperature and BSFC variation as a function of different adiabatic configurations in the exhaust ports and the turbine.

Apart of the theoretical optimal case, a realistic strategy has been considered, where turbine with ceramic coating in the volute is employed at the same time as the exhaust ports are insulated with an air chamber. This way, the results will be compared between the studies listed in Table 4.8.

Table 4.8: Feasible cases for exhaust ports and turbine thermal insulation.

Case #1	-	Baseline
Case #7	-	Turbine with ceramic coating in the volute (1mm YSZ)
Case #2	-	Exhaust ports with an air chamber
Case #10	-	Combining Case #2 and Case #7

The results of this comparison are illustrated in Figure 4.26, where positive results are found for the fourth parametric studies. With respect to VGT outlet temperature, it can be observed in plots (a) and (c) that the VGT

outlet temperature reaches up to 50°C for low loads and 80°C for high loads, respectively. The combination is also favourable for BSFC, with the only exception of point #A, which has already presented fuel penalty in comparison to the baseline for the turbine insulation case. For the rest, fuel consumption is significantly improved, around 1%.

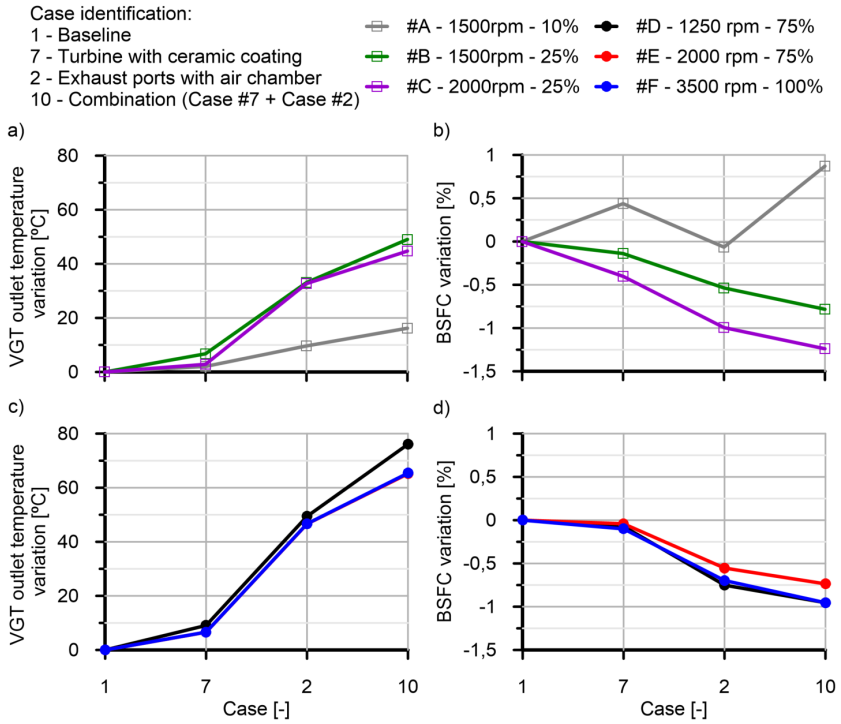

Figure 4.26: Aftertreatment inlet temperature and BSFC variation at low and high load operating points as a function of different feasible exhaust ports and turbine thermal insulation configurations.

Analysing the results in more detail, it can be confirmed a synergistic effect, since combining both solutions produces an effect greater than the sum of their individual effects. For example, analysing operating point #D, the sum of results for the VGT outlet temperature variation in turbine with ceramic coating (10°C) and exhaust ports with air chamber (50°C) is 60°C, but the actual temperature variation for the combination of both solutions is 75°C. The same phenomena happens for almost all cases considering the BSFC variation.

Therefore, it is noticed that only turbine insulation produces a not so expressive effect, but, in the other hand, for the combined case, with a prior exhaust ports insulation, VGT inlet temperature is higher and VGT inlet pressure is lower, maintaining the same global enthalpy. For operating point #B, the value for VGT inlet pressure is 1.21 bar in the baseline case, 1.20 bar for Case #7, 1.18 bar for Case #2 and 1.17 bar for the Case #10. This response evidences how additional benefits in VGT outlet temperature increase allows the VGT to open even more.

For the same operating point #B, the VGT position is 16% in the baseline case, increasing to 16.9% for the insulated turbine, to 21.2% when the exhaust ports are insulated and up to 23.8% when combining both solutions in Case #10. Being the VGT more opened the pumping losses will be even more reduced and the gas expansion over the turbine will be also lower, causing a smaller drop in temperature from VGT inlet to outlet temperature. Therefore, the outlet temperature reaches a higher value compared to the baseline than adding separately the individual variations for Cases #2 and #7.

4.3.5 DOC efficiency enhancement potential

Based on these findings, the same strategy has been applied to the Euro 6d-Temp engine GT-Power model presented in Section 3.3.1, considering the same operating points discussed in Section 4.2. The idea was to be able to apply the optimum insulation Cases #2 and #7, with the result, evaluate the DOC conversion efficiency response through the EATS model.

Table 4.9: Selected points from DOC study.

Point ID	Altitude [m]	DOC inlet temp. [°C]	Speed [rpm]	Load[%]
#G	0	200	1500	19
#H	0	150	1500	8
#I	0	100	2000	0.5
#J	2500	180	1250	16
#K	2500	150	1500	6
#L	2500	175	1750	5

It is important to recall that the model calibration in GT-Power led to accurate results for the full load operation, according to Figure 3.8 in Chapter 3. In addition, Figure 4.27 shows the comparison between measured

and modelled variables for a selection of the measured points in Section 4.2, named #G to #L. The represented variables include a torque representation instead of fuel injected quantity, once this last variable is imposed in the model configuration for the Euro 6d-Temp engine.

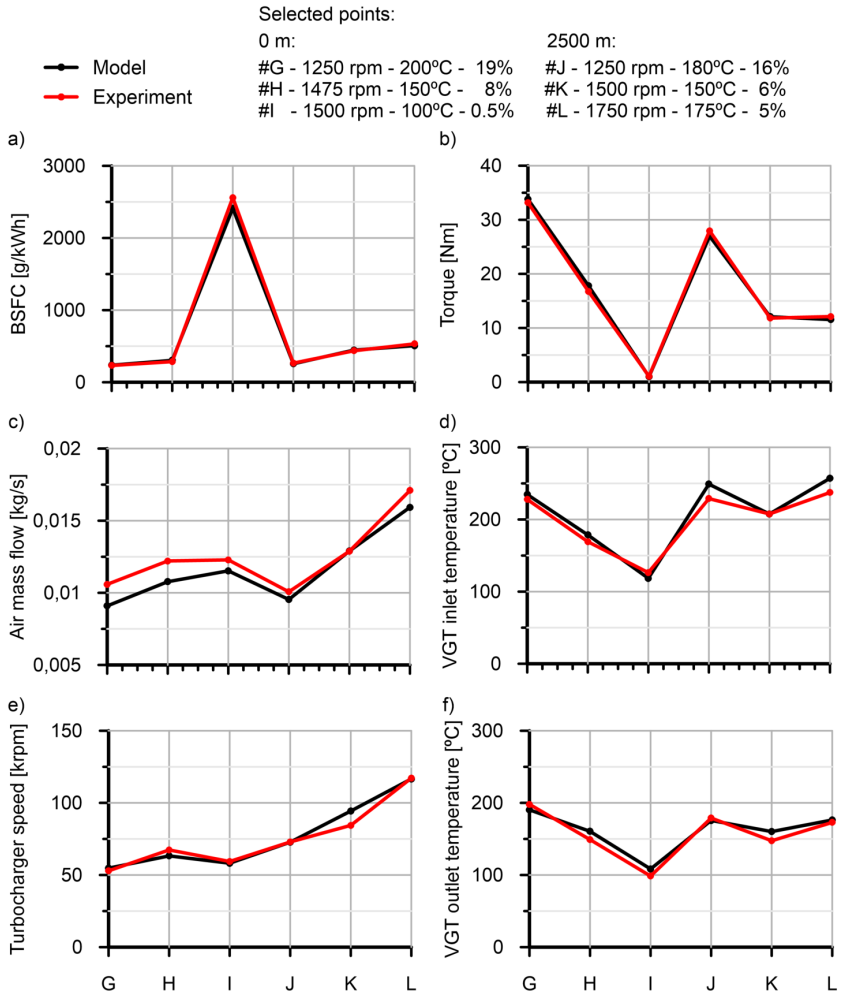

Figure 4.27: Comparison between model and experiment for a selected points from the DOC study.

The selected points compose a variety of engine speeds and loads addressed in this Chapter, besides of considering both studied driving altitudes, as shown

in Table 4.9. Figure 4.27 reveals the additional validity of the engine model for low load operation conditions and also for different altitude operations, providing minimal errors and fully representative trends in all relevant engine parameters.

By applying the three listed insulation cases from Table 4.8 in the Euro 6d-Temp engine model, new boundary conditions were set to the DOC model, providing the conversion efficiency response for each insulation case. It was chosen to represent the outputs against brake mean effective pressure (BMEP) in the y-axis and engine speed in the x-axis. That is because by representing the results against catalyst inlet temperature, what would be seen is just a shifting of the points towards higher catalyst inlet temperatures, keeping the same map structure.

By fixing the x- and y-axis, the effect caused by the thermal insulation can be more easily identified, as seen in the DOC inlet temperature results in Figure 4.28. However, as stated in the previous section, BMEP is also affected by the exhaust thermal insulation strategies. In any case, its variation is very low in comparison to VGT outlet temperature, an BMEP is still useful to obtain comparable conversion efficiency maps.

Figure 4.28 shows the GT-Power model DOC inlet temperature of Case #1 (baseline) compared to the exhaust thermal insulation Cases #2, #7 and #10 as a function of BMEP and engine speed at 0 m and 20°C. It is observed how in every case compared to the baseline, the temperature is moved towards higher values.

The tendency presented by the temperature variation, as a consequence of the exhaust line insulation, is very similar to the one observed in the previous Section, where some improvement in the EATS inlet temperature is observed in Cases #2 and #7 for low loads and an even more pronounced temperature enhancement is achieved applying the insulation Case #10. Additionally, as the BMEP increases, the temperature variation in higher. This value achieves the magnitude of almost 50°C for the points with BMEP superior to 4 bar in Case #10, as seen in Figure 4.28(d). However, this increment is much smaller at the bottom of all plots, where the low loads are located, being insignificant for BMEPs lower than 1 bar.

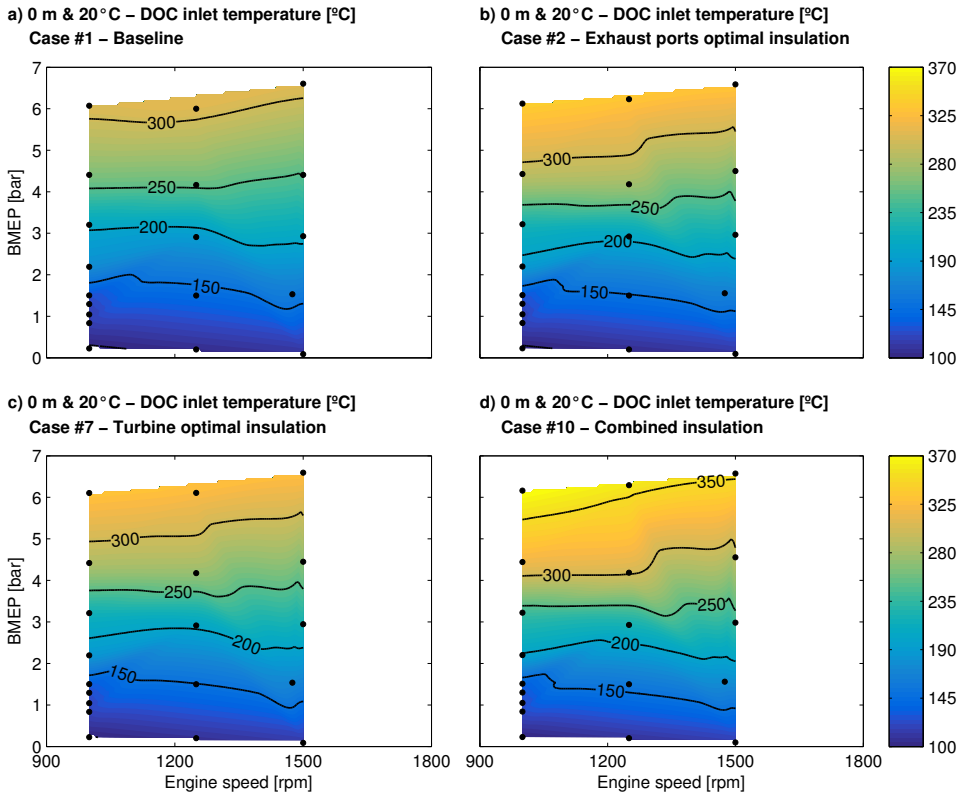

Figure 4.28: DOC inlet temperature at 0 m and 20° C as a function of the engine speed and BMEP.

The CO and HC conversion efficiencies resulting from EATS model calculation with the DOC inlet temperatures inputs from the four strategies application at 0 m and 20°C are represented in Figure 4.29 and Figure 4.30, respectively.

The comparison between Figure 4.29(a) and (c) reveals an increase of the CO conversion efficiency due to the VGT outlet temperature enhancement provoked by the turbine insulation, *i.e.* Case #7. The variation is, however, more pronounced at higher engine speeds. The conversion efficiency sensitivity to the catalyst inlet temperature was higher as the exhaust mass flow increased. Therefore, applying same levels of temperature change for both exhaust mass flows generates a more evident response at higher engine speeds.

The conversion efficiency of the point located at BMEP $\sim$ 1.6 bar and 1475 rpm engine speed increases from $\sim$ 60% to $\sim$ 75%, gaining 15% of more conversion efficiency, while the point presenting BMEP $\sim$ 1.5 bar and 1000 rpm engine speed barely moves from under the 40% conversion efficiency line.

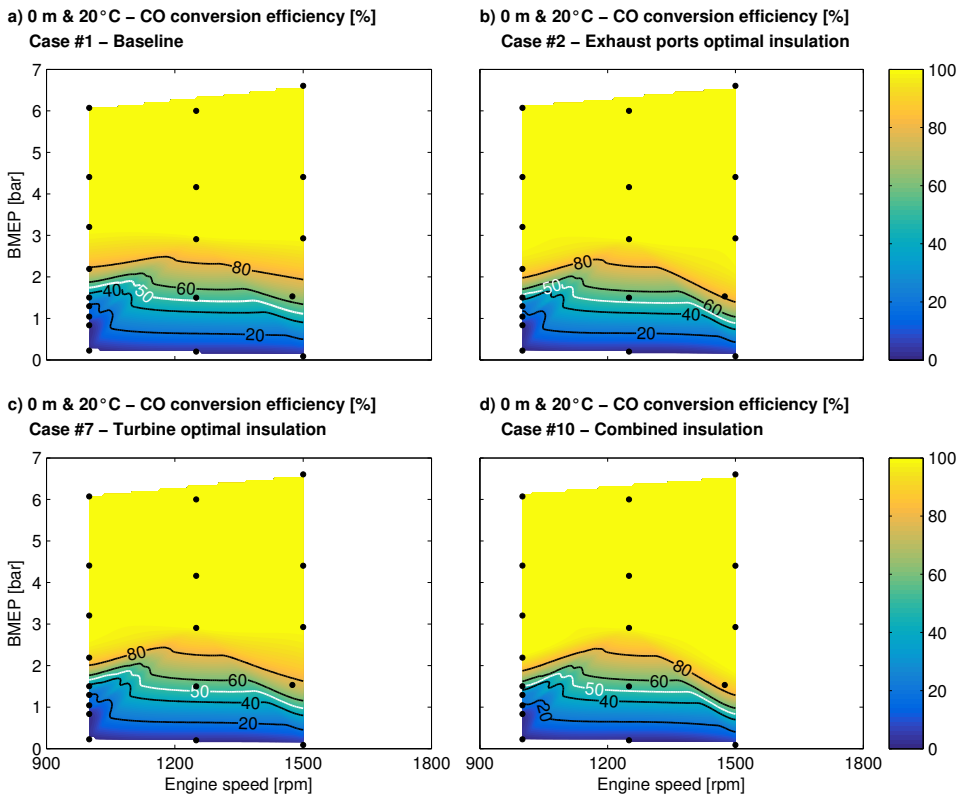

Figure 4.29: CO conversion efficiency at 0 m and 20° C as a function of the engine speed and BMEP.

For Case #2 (insulation of the exhaust ports with an air chamber) the improvement is slightly better, causing a further increment of 10% for the point with BMEP $\sim$ 1.6 bar and 1475 rpm, going from $\sim$ 60% to $\sim$ 85% conversion efficiency, and making the point containing BMEP $\sim$ 1.5 bar and 1000 rpm to gain around 5% in conversion efficiency. The combination of both strategies, Case #10, in Figure 4.29(d), leads to an even more positive result. It is noticed how the 80% conversion efficiency line is displaced downwards in

BMEP, meaning that the full conversion efficiency is reached for even lower load points. Although the low engine speed and low BMEP points are still penalized in terms of emission abatement, it is seen how the point with BMEP $\sim$ 1.6 bar and 1475 rpm reaches almost 100% of CO conversion efficiency and the point with BMEP $\sim$ 1.5 bar and 1000 rpm shows a CO conversion of higher than $\sim$ 50%.

Subsequently, the HC conversion efficiency maps are shown for the same four configurations. Again, it was chosen to depict only the HC oxidation conversion efficiency, since the adsorption mechanism depends not only on temperature, but also on the time through the instantaneous surface coverage. Due to the fact that the HC partial pressure remains the same as the baseline for all cases and that the HC oxidation is governed by the same chemical equations as the CO, the effects observed are very similar to the ones discussed for the CO. Therefore, Figure 4.30 displays how the HC conversion efficiency in warm sea-level conditions varies depending on the insulation case, showing, similarly, a greater sensibility on temperature at higher engine speeds.

The point presenting $\sim$ 2.2 bar of BMEP and engine speed of 1000 rpm suffers an HC conversion efficiency change from $\sim$ 35% for the baseline case (Figure 4.30(a)) to $\sim$ 50% when applying the turbine optimal insulation (Figure 4.30(c)) and/or by insulating the exhaust ports (Figure 4.30(b)), reaching up to $\sim$ 65% for the combined insulation strategy (Figure 4.30(d)). On the other hand, for the point with BMEP of $\sim$ 1.6 bar and engine speed of 1475 rpm, the HC conversion efficiency is increased from $\sim$ 28% at the baseline case (Figure 4.30(a)) to $\sim$ 35% when applying the turbine optimal insulation (Figure 4.30(c)), to $\sim$ 45% by insulating the exhaust ports (Figure 4.30(b)) and finally to $\sim$ 55% by using both insulation strategies (Figure 4.30(d)). It represents a maximum variation of 20% in HC conversion efficiency at low engine speed versus 27% at higher ones.

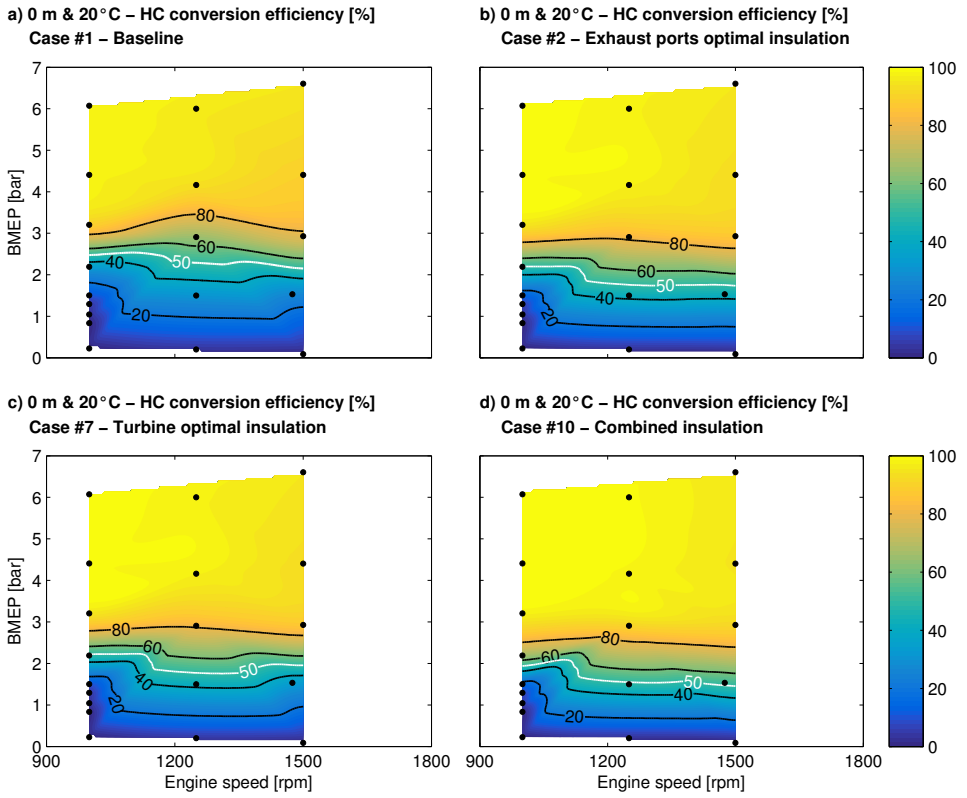

Figure 4.30: HC oxidation conversion efficiency at 0 m and 20° C as a function of the engine speed and BMEP.

The DOC inlet temperatures due to the exhaust insulation strategies for cold altitude are depicted in Figure 4.31. Here, the temperature variation is higher than the comparable range at 0 m and 20° and even more pronounced at low BMEPs, reaching up to 60°. This difference can be explained by the lower gas density that comes together with the lower pressure in the exhaust gas in altitude operation. This way, the thermal insulation avoids even more the heat loss from the exhaust line.

Consequently, by looking at Figure 4.32, it is seen that a significant improvement of the CO conversion efficiency due to the exhaust thermal insulation is also given at BMEPs around and even lower than 1 bar. Additionally, it can be seen that the conversion efficiency is more equally

improved over all points range. As evidenced in Figure 4.3(c) and (d), the CO conversion efficiency is less sensitive in cold altitude to exhaust mass flow as in sea-level conditions.

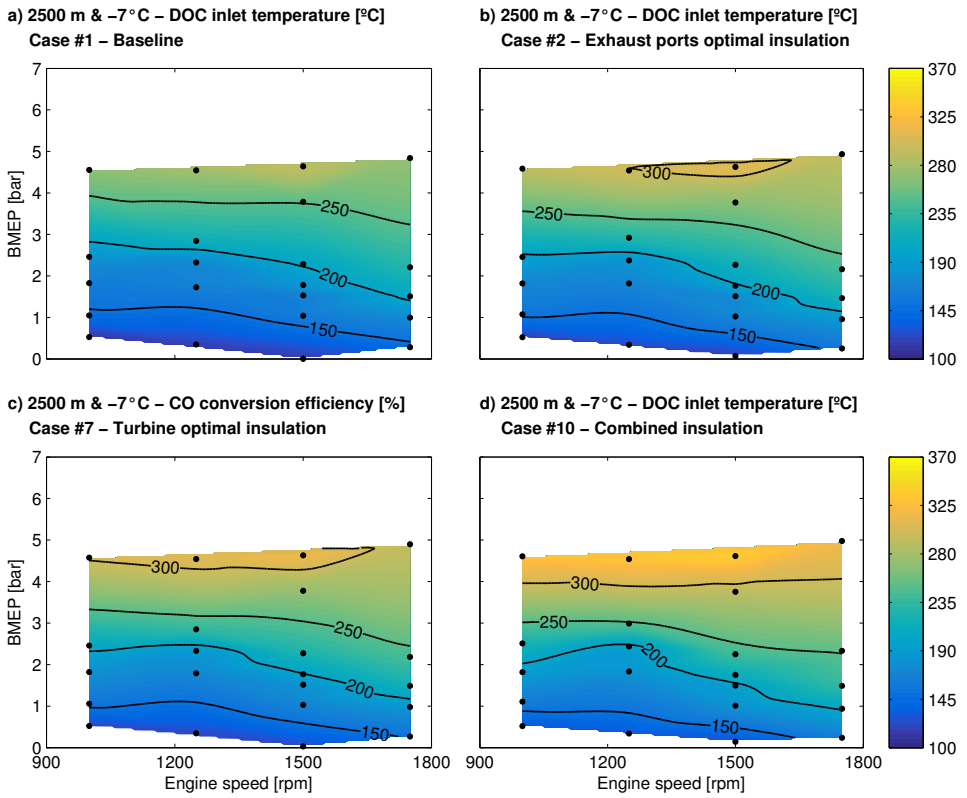

Figure 4.31: DOC inlet temperature at 2500 m and -7° C as a function of the engine speed and BMEP.

Therefore, the point with BMEP $\sim$ 1 bar and 1000 rpm, for example, moves from $\sim$ 30% conversion efficiency in the baseline (Figures 4.32(a)) to around 60% for the exhaust ports and turbine insulation cases (Figures 4.32(b) and (c)) and finally $\sim$ 80% for the combined strategies case (Figures 4.32(d)). In return, point containing BMEP $\sim$ 1 bar and 1750 rpm goes from 50% conversion efficiency in the baseline (Figures 4.32(a)) to $\sim$ 70% for the exhaust ports and turbine insulation cases (Figures 4.32(b) and (c)) and $\sim$ 90% for

the Case #10, with both insulations (Figures 4.32(d)). It represents the same percentage increment in CO conversion efficiency for both engine speeds.

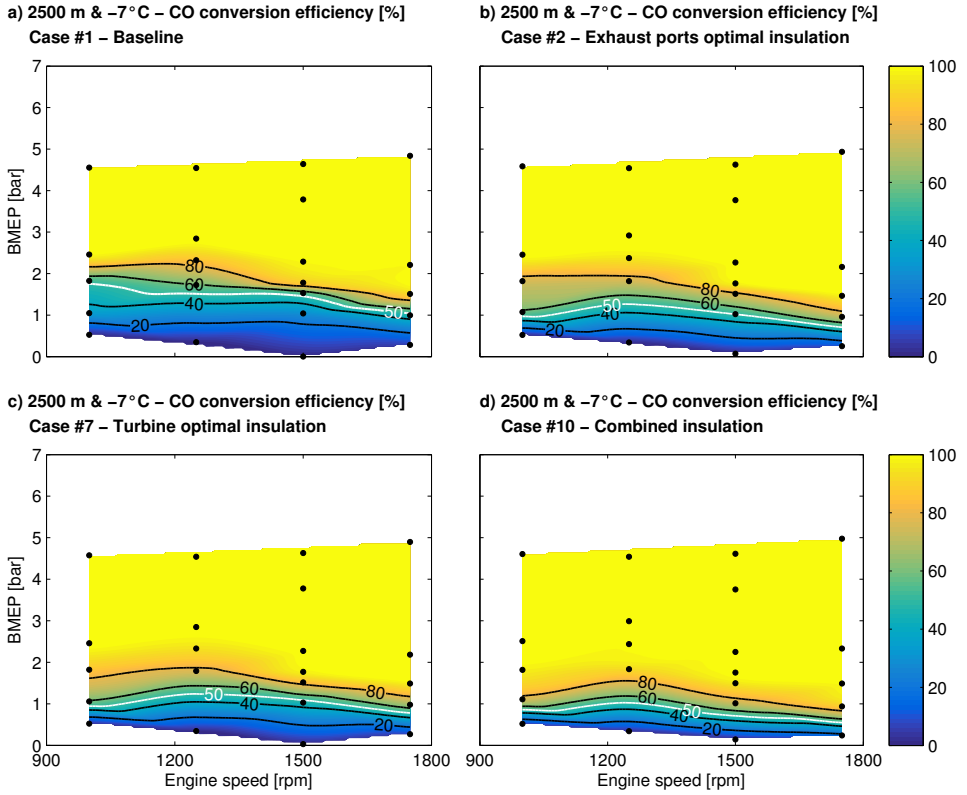

Figure 4.32: CO conversion efficiency at 2500 m and -7° C as a function of the engine speed and BMEP.

If one compares Figure 4.29 with Figure 4.32, the CO conversion efficiency improvement by applying the insulation cases is more accentuated for 2500 m and -7°C than for 0 m and 20°C over the middle of the light-off range. The light-off curve representing the 50% abatement almost stays at the same positions for warm sea-level, while at cold altitude it gradually moves downwards from plots (a) to (d), laying at levels of almost 1 bar less. However, the full conversion suffers a considerable improvement at 0 m and 20°C specially at higher engine speeds, representing at the combined insulation Case #10 (Figure 4.29(d)) all points higher than $\sim$ 2.8 bar against the baseline Case

#1 (Figure 4.29(a)), where the complete CO abatement is only observed at higher BMEPs than $\sim$ 6 bar.

Regarding the response at cold altitude for the HC (Figure 4.33), again an analogous behaviour to the CO is identified, showing less sensibility for the HC oxidation conversion efficiency improvement to engine speed. For example, both points, one with BMEP $\sim$ 1.8 bar and 1250 rpm engine speed and the other showing BMEP $\sim$ 1 bar and 1750 rpm, suffer an increase of 30% in conversion efficiency from the baseline to the combined case, increasing from 20 to 50%. Moreover, for the combined configuration, the HC full abatement can be evidenced in higher portion of the contour map compared to the baseline, which only shows this magnitude on the upper left corner.

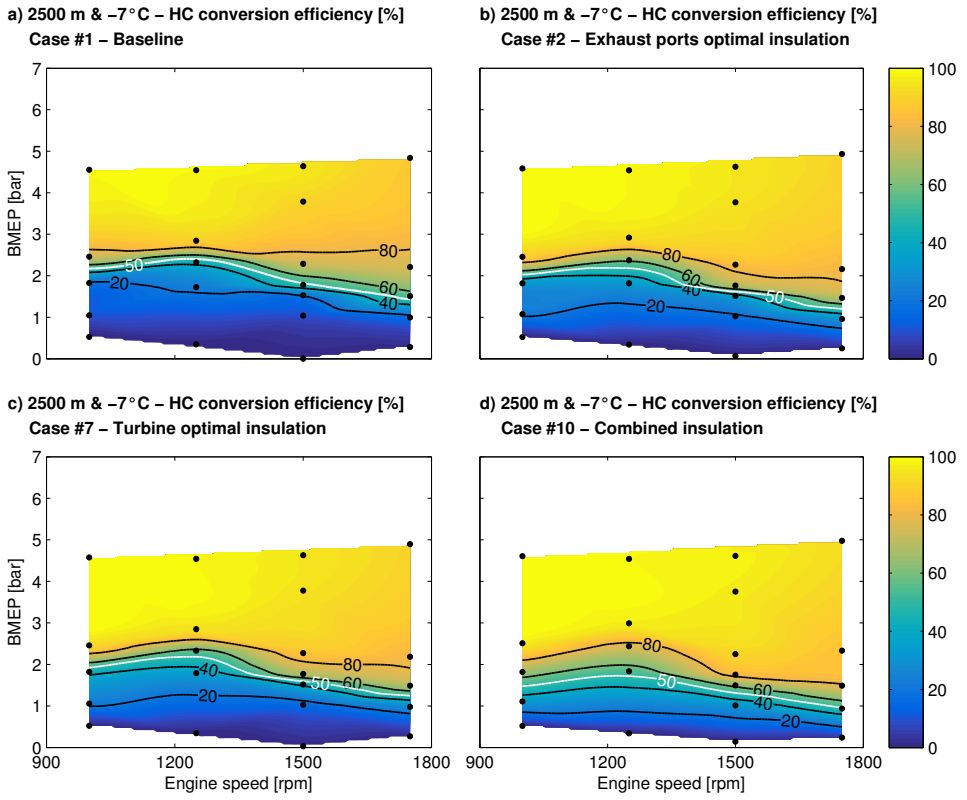

Figure 4.33: HC oxidation conversion efficiency at 2500 m and -7° C as a function of the engine speed and BMEP.

It is finally concluded that both pollutants and in both ambient conditions reveal three main tendencies: a decrease on the zone presenting 20% of oxidation conversion efficiency; a shifting on the transition from low to high abatement contour curves (shift on the light-off) towards lower BMEP; and an increase on the full abatement zone.

4.4 Summary and conclusions

This Chapter brought a discussion about the diesel oxidation catalyst performance in terms of CO and HC conversion variation over the ambient conditions, finishing by presenting a modelling application of passive strategies to improve its performance. The evaluation of the catalyst performance was carried out in a Euro 6d-Temp Diesel engine that operated under steady-state conditions within a common range of exhaust mass flow and catalyst inlet temperature at the ambient conditions of warm sea-level (0 m and 20°C) and extreme operation in cold altitude (2500 m and −7°C).

A deterioration at low temperature for both CO and HC conversion efficiencies in cold altitude condition was observed, evidenced by the increase of the light-off temperature, although with different trends for CO and HC. Regarding the CO, a marked decrease on the conversion efficiency was specially noted at low exhaust mass flow, where the light-off was delayed approximately 45°C. As the exhaust mass flow increased, the penalty progressively decreased, but it was still present. The damage in HC was more accentuated in cold altitude condition, were very low conversion efficiency regions were found, specially at high mass flow, compared to a minimum of 50% for warm sea-level. The HC light-off was not reached until 150°C from 50 kg/h onwards in exhaust mass flow for cold altitude operation.

The cause of the differences between CO and HC conversion efficiency laid mainly on the adsorption process. The HC partial pressure at low temperature in cold altitude was higher than the one in warm sea-level, despite the lower ambient pressure, highly influenced the adsorption to desorption reaction rate. The higher HC partial pressure increase the adsorption at the beginning of the test. However, once the engine reached the steady-state conditions, the high HC surface coverage penalized the HC conversion efficiency in the low temperature region.

The oxidation conversion efficiency also presented differences between altitudes, which contributed to the global conversion efficiency increase in cold altitude operation for both HC and CO. The oxidation light-off temperature variation was strongly influenced by the the dwell time and O_2 partial pressure. While the dwell time is unavoidable, the O_2 partial pressure also depends on the equivalence ratio. This last parameter only damaged altitude operation at very low temperature, adding its negative contribution to the light-off temperature increase. Moreover, the huge increase on pollutant engine-out emission in altitude operation at low temperature affected the pollutants partial pressure. Consequently, a high increase on the CO and HC oxidation inhibition was produced in this range of working conditions, thus highlighting the importance of an optimal engine control and EATS matching.

The second part of the Chapter presented a study willing to improve the aftertreatment performance over the two previously studied ambient conditions. To do so, a proposal of the exhaust ports and the turbine thermal insulation was applied in a turbocharged Diesel engine, leading to the aftertreatment inlet temperature enhancement. The results have been obtained computing a gas dynamic engine model in GT-Power coupled to an advanced heat transfer and mechanical losses model the turbocharger previously calibrated against experimental data.

Figure 4.34 summarizes the optimal strategies as a function of the impact on VGT outlet temperature and BSFC for each studied operating point at this section. Figure 4.34(a) illustrates the response of adiabatic turbine, the adiabatic exhaust ports and the case with both strategies combined. This information helps to identify the maximum possible values that could be obtained applying this configuration. On the other hand, Figure 4.34(b) shows the results for feasible solutions concerning exhaust ports and turbine thermal insulation. In both figures, the top left quadrant stands for the ideal case, where VGT outlet temperature increase and BSFC reduction are obtained. This region is where most of the results are concentrated. The top right quadrant denotes the cases that present temperature improvement, though BSFC penalty.

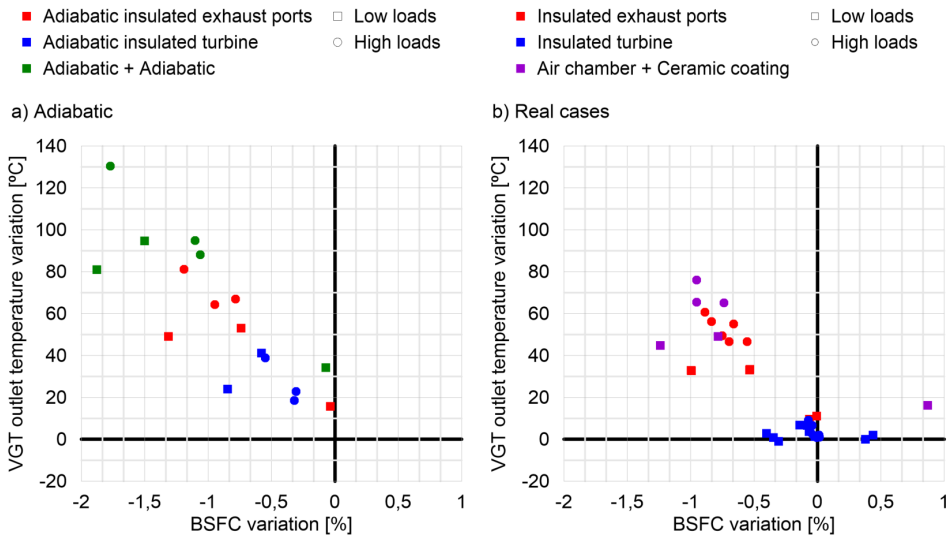

Figure 4.34: Summary of impact on VGT outlet temperature and BSFC of (a) adiabatic cases and (b) feasible solutions for exhaust port and turbine thermal insulation.

It is clear that all the results for adiabatic conditions report only positive results, less fuel consumption and close to double the VGT outlet temperature increase than the best realistic solutions. However, plot (b) in Figure 4.34 shows the vast majority of results on the top left of the graphic and none of them represents a decrease of the VGT outlet temperature, meaning that all cases have significant influence in both variables. The points for the cases where turbine is insulated still present some results with negligible influence on the VGT outlet temperature and also some cases presenting BSFC penalty, that are mainly obtained at very low load conditions. Exhaust ports insulation demonstrates to be a good strategy, showing positive results for VGT outlet temperature and BSFC, in addition to being better than the ones with the insulated turbine. Besides, the combination of both strategies produces remarkable VGT outlet temperature increase and BSFC reduction, showing a synergistic effect, which means that the VGT outlet temperature also presents an increment potential based on turbine inlet temperature.

Increasing VGT outlet temperature represents a positive impact on the warm-up process, reducing the time for light-off in the different exhaust aftertreatment devices. With that in mind, the optimal real cases strategies

(Figure 4.34 (b)) have been applied in the Euro 6d-Temp Diesel engine for both studied ambient conditions to evaluate the DOC response in terms of CO and HC oxidation conversion efficiency. For both species, it was evidenced an increase on the conversion efficiency gradually from the baseline to the turbine and exhaust ports insulation, and finally leading to a synergistic improvement when applied the combination of the insulation techniques.

At 0 m and 20°C, the catalyst performance is mostly improved at higher engine speeds gaining up to 40% in CO and 27% in HC absolute conversion efficiency for the combined insulation. At 2500 m and −7°C both insulations together also proved to be capable of increasing up to 40% for the CO and 30% for the HC conversion efficiency, although with a more equal distribution as a function of the studied engine speed range. Finally, the still considerable difference between the adiabatic and the feasible results in Figure 4.34 leaves the way open for further optimisation of thermal insulation solutions or combination between two or more methods, specially looking for a previous increase in exhaust manifold temperature. That way, an even further improvement in terms of performance, not only of a diesel oxidation catalyst, but also of any aftertreatment device could be obtained.

Bibliography

[1] J. M. Luján, J. R. Serrano, P. Piqueras, and B. Diesel. "Turbine and exhaust ports thermal insulation impact on the engine efficiency and aftertreatment inlet temperature." *Applied Energy, 240, 409-423* (2019) (cit. on pp. xii, 106, 107).

[3] J. R. Serrano, P. Piqueras, E. J. Sanchis, and B. Diesel. "Analysis of the driving altitude and ambient temperature impact on the conversion efficiency of oxidation catalysts". *Applied Sciences, 11, 1283* (2021) (cit. on pp. xii, 106, 107, 205, 206).

[39] A. Ramos, R. García-Contreras, and O. Armas. "Performance, combustion timing and emissions from a light duty vehicle at different altitudes fueled with animal fat biodiesel, GTL and diesel fuels". *Applied Energy, 182, 507-517* (2016) (cit. on pp. 4, 26, 27, 120).

[44] M. R. Hamedi, O. Doustdar, A. Tsolakis, and J. Hartland. "Thermal energy storage system for efficient diesel exhaust aftertreatment at low

temperatures". *Applied Energy, 235, 874-887* (2019) (cit. on pp. 4, 37, 126).

[45] P. Piqueras, A. García, J. Monsalve-Serrano, and M. J. Ruiz. "Performance of a diesel oxidation catalyst under diesel-gasoline reactivity controlled compression ignition combustion conditions". *Energy Conversion and Management, 196, 18-31* (2019) (cit. on pp. 5, 30, 31, 89, 107, 122).

[74] F. Payri, V. R. Bermúdez, B. Tormos, and W. G. Linares. "Hydrocarbon emissions speciation in diesel and biodiesel exhausts." *Atmospheric Environment, 43, 1273-1279* (2009) (cit. on pp. 20, 89, 110).

[128] V. Bermúdez, J. R. Serrano, P. Piqueras, J. Gómez, and S. Bender. "Analysis of the role of altitude on Diesel engine performance and emissions using an atmosphere simulator". *International Journal of Engine Research, 18, 105-117* (2017) (cit. on pp. 26, 27, 68, 120).

[137] J. M. Luján, J. R. Serrano, P. Piqueras, and O. García-Afonso. "Experimental assessment of a pre-turbo aftertreatment configurations in a single stage turbocharged Diesel engine. Part 2: Transient operation". *Energy, 80, 614-27.* (2015) (cit. on pp. 28, 36, 126).

[150] C. Guardiola, B. Pla, P. Bares, and J. Mora. "An on-board method to estimate the light-off temperature of diesel oxidation catalysts". *Intenational Journal of Engine Research, 21 (8), 1480-1492* (2018) (cit. on pp. 30, 107).

[156] F. Payri, F. J. Arnau, P. Piqueras, and M. J. Ruiz. "Lumped approach for flow-through and wall-flow monolithic modelling for real-time automotive applications". In: *SAE Technical Paper 2018-01-0954*. 2018 (cit. on pp. 31, 86, 92, 107).

[160] A. Russell and W. S. Epling. "Diesel oxidation catalysts". *Catalysis Reviews - Science and Engineering, 53 (4), 337-423* (2011) (cit. on pp. 31, 106).

[203] S. D. Burch, T. F. Potter, and M. A. Keyser. "Reducing cold-start emissions by catalytic converter thermal management". *SAE Technical Paper 950409* (1995) (cit. on pp. 37, 126).

[281] D. C. Quiros, S. Hu, S. Hu, E. S. Lee, S. Sardar, X. Wang, J. S. Olfert, H. S. Jung, Y. Zhu, and T. Huai. "Particle effective density and mass during steady-state operation of GDI, PFI, and diesel passenger cars." *Journal of Aerosol Science, 83, 39-54* (2015) (cit. on p. 108).

[282] C. Guardiola, B. Pla, P. Piqueras, J. Mora, and D. Lefebvre. "Model-based passive and active diagnostics strategies for diesel oxidation catalysts." *Applied Thermal Engineering, 110, 962-971* (2017) (cit. on p. 109).

[283] C. M. Allen, M. C. Joshi, D. B. Gosala, G. M. Shaver, L. Farrell, and J. McCarthy. "Experimental assessment of Diesel engine cylinder deactivation performance during low-load transient operations". *Internal Journal of Engine Research, 22 (2), 606-615* (2019) (cit. on p. 110).

[284] R. Suarez-Bertoa, V. Valverde, M. Clairotte, J. Pavlovic, B. Giechaskiel, V. Franco, Z. Kregar, and C. Astorga. "On-road emissions of passenger cars beyond the boundary conditions of the real-driving emissions test". *Environmental Resesearch, 176, 108572* (2019) (cit. on p. 110).

[285] I. Lefort and A. Herreros J. M. Tsolakis. "Reduction of low temperature engine pollutants by understanding the exhaust species interactions in a diesel oxidation catalyst." *Environment Science and Technology, 48, 2361-2367* (2014) (cit. on p. 115).

[286] R. Kamo and W. Bryzik. "Adiabatic turbocompound engine performance prediction". *SAE Transactions, 87 (1), 213-223.* (1978) (cit. on p. 126).

[287] R. Sekar, R. Kamo, and J. Wood. "Advanced adiabatic Diesel engine for passenger cars." *SAE Transactions, 93 (3), 250-258.* (1984) (cit. on p. 126).

[288] M. Ekström, A. Thibblin, A. Tjernberg, C. Blomqvistb, and S. Jonssona. "Evaluation of internal thermal barrier coatings for exhaust manifolds." *Surface and Coatings Technoly, 272, 198-212.* (2015) (cit. on p. 126).

[289] S. Rajadurai and S. Ananth. "Heat shield iInsulation for thermal challenges in automotive exhaust system". In: *SAE Technical Paper 2019-28-2539.* 2019 (cit. on p. 126).

[290] C. Viazzi, A. Deboni, J. Z. Ferreira, J. P. Bonino, and F. Ansart. "Synthesis of yttria stabilized zirconia by solgel route: influence of experimental parameters and large scale production." *Solid State Sciences, 8, 1023-1028.* (2006) (cit. on p. 134).

[291] M. A. Marr. "An investigation of metal and ceramic thermal barrier coatings in a spark-ignition engine". MA thesis. University of Toronto, 2009 (cit. on p. 134).

[292] S. Alaruri, L. Bianchini, and A. Brewington. "Effective spectral emissivity measurements of superalloys and YSZ thermal barrier coating at high temperatures using a 1.6 μm single wavelength pyrometer". *Optical and Lasers in Engineering, 30, 77-91* (1998) (cit. on p. 134).

Chapter 5

DPF active regeneration optimisation in altitude based on air management

Contents

5.1 Introduction **166**
5.2 Test campaign **167**
5.3 Analysis of the experimental and modelling results **169**
5.4 VGT position impact on the regeneration rate **180**
5.5 Summary and conclusions **186**
Bibliography **187**

5.1 Introduction

A previously introduced in Chapter 2, the increase of the PM emissions and the lower O_2 availability is harmful for the particulate filter actuation [174, 293] in altitude operation compared to sea-level case. Regarding the dynamics of active regenerations, an additional concern can appear associated with the DPF inlet temperature trends. This is because the active regeneration is only promoted when high temperatures levels are reached in the DPF inlet. In regular operations in altitude, this temperature is usually lower compared to sea-level operation, as it was previously seen in Chapter 4. In this case, the common adopted calibration consists of closing the VGT to compensate the reduction in ambient density with respect sea-level and thus recover the boost pressure [294].

Regarding the consequences of this procedure on the active regeneration in altitude, the higher turbine expansion in altitude results in a greater decrease on temperature across the turbine. Despite the effect of VGT closing on turbine inlet temperature, this actuation tends to decrease the aftertreatment inlet temperature. Nevertheless, the final response also depends on a complex interaction with the post-injection strategy. The objective is to increase the efficiency of the post-injection strategy, i.e. to make the post-injected fuel to be directly burned out in the oxidation catalyst and thus increase the DPF inlet temperature. The consequence is the increase on the soot depletion rate, which is, therefore, dependent on the post-injected fuel mass flow, the injection angle [183] and the air management.

Covering this issue, in this Chapter, the impact of serial calibrated active regeneration strategies on the regeneration dynamics of a Diesel PF is evaluated as a function of the driving altitude, which assessed at sea-level, 1300 m and 2500 m, and of the initial soot load. The experiments were carried out in the experimental set described in Section 3.2 and next reproduced computationally by the flow solver for wall-flow PFs presented in Section 3.3.2.2 [180]. The experimental results evidenced the reduction of the soot depletion rate as the altitude increased. In fact, the active regeneration strategy resulted inefficient, even reaching an early balance point with high soot mass remaining within the filter. The reasons for the deterioration of the regeneration dynamics are discussed disclosing thermal from O_2 diffusion and dwell time effects. From this analysis, assuming the serial post-injection calibration, the importance and potential of the boosting strategy in altitude is

next demonstrated. Besides the soot depletion rate being recovered to sea-level values, the engine efficiency and emissions during the regeneration are also improved.

The works, analysis and ideas described in this Chapter were the origins of publication number [5] from the publications list of the author of this doctoral thesis, which is shown at the beginning of the document. For the sake of readiness and to protect the thesis writing style the publication number [5] from author's list of publications have not been specifically cited each time that ideas, figures or discussions contained in it are addressed in this Chapter. This disclaimer corrects, compensates and justifies the fact that the work of the PhD candidate's doctoral thesis are the origin of the innovation component in the publications number [5] listed in the referred Section.

5.2 Test campaign

Active regeneration events were performed in the engine test bench varying the altitude and the initial DPF pressure drop to account for the case sensitive effect of different engine operating conditions and DPF boundaries. Sea-level, 1300 m and 2500 m were considered. The pressure drop thresholds to trigger the active regeneration and its corresponding soot load as a function of altitude are listed on Table 5.1. The trends in soot load showed a decrease with altitude for the same pressure drop, what was mainly governed by the exhaust density reduction according to the ambient one. Besides, the particular mass flows and temperatures across the DPF set the DPF pressure drop.

Table 5.1: DPF pressure drop and soot mass load at the beginning of the regeneration events.

Pressure drop [mbar]	Soot load [g/l]		
	Sea-level	1300 m	2500 m
80	3.75	3.65	3.32
120	7.23	7.05	6.63
175	10.03	9.71	9.06
230	13.12	12.82	12.03

The engine was run at 2000 rpm and iso-fuel (pedal at 37%) along every regeneration event. The injection profile and the in-cylinder pressure corresponding to the sea-level case with 175 mbar as DPF pressure drop are

depicted in Figure 5.1(a) for regular mode, i.e. prior to trigger the active regeneration strategy. The fuel mass per injection event is listed on Table 5.2. Two pilot injections close to the main one can be identified, mainly used to control emissions and noise, and a post-injection with the aim to reduce, specially, NO_x emissions [295]. The regeneration mode was activated applying the serial ECU calibration once the target DPF pressure drop was reached. The injection profile during the active regeneration events and the in-cylinder pressure corresponding to sea-level case are represented in Figure 5.1(b). The total injected fuel mass was increased during the active regenerations from 18.25 mg/cc to 26.32 mg/cc. Along this mode, the two pilot injections were also advanced to increase the premixed combustion phase whilst the main injection was delayed increasing its amount of fuel according to Table 5.2. Additionally, two post-injections were triggered. In addition to the fuel quantity increase in the post-injection, this was divided into two events to minimise oil dilution. The first post-injection was delayed with respect to the regular mode while the second one was placed at the very end of the expansion stroke aiming to prevent burning in the cylinder, thus promoting the oxidation of the HCs in the DOC with the subsequent DPF inlet temperature increase [183].

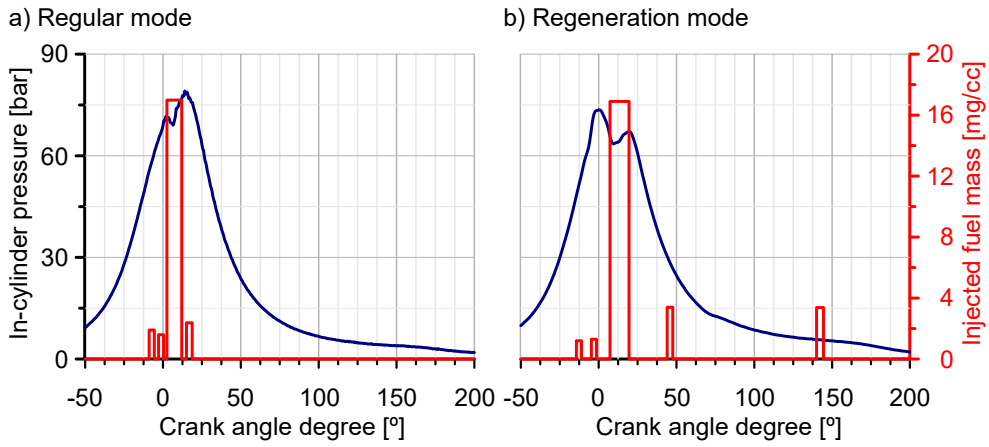

Figure 5.1: Fuel injection profile and in-cylinder pressure in (a) regular and (b) regeneration modes at 2000 rpm and pedal at 37 %.

Besides the change of the injection profile when triggering the regeneration, the LP-EGR rate and VGT position were also modified during this operating

mode. The impact of the actuation on these parameters is analysed in Section 5.3.

Table 5.2: Fuel injection profile in regular and regeneration modes at 2000 rpm and pedal 37%.

	Regular mode		Regeneration mode	
Injection	Angle [CA aTDC]	Mass [mg/cc]	Angle [CA aTDC]	Mass [mg/cc]
Pilot 1	-8.9	1.52	-14.3	1.2
Pilot 2	-2.9	1.27	-4.7	1.29
Main	2.5	13.57	7.3	17.03
Post 1	15.1	1.89	44	3.42
Post 2			140	3.38
Total		**18.25**		**26.32**

5.3 Analysis of the experimental and modelling results

Figure 5.2 shows in plots (a) and (b) the change in VGT position and LP-EGR rate from regular to regeneration mode cases applying serial ECU calibration. A variety function of altitudes and DPF pressure drops at the beginning of the active regeneration events are considered. Being 100% the fully closed position, the VGT position was gradually closed as the altitude increased, as observed in Figure 5.2(a).

During the active regeneration, the imposed fashion consisted of opening the VGT. The VGT position was opened from 74% to 49% at sea-level case, reducing the variation at 1300 m and finally keeping fully closed VGT at 2500 m. The differences in LP-EGR rate before and during regeneration were also reduced as a function of the altitude. In regular operation, the ECU decreased the LP-EGR rate as the altitude increased from 30% at sea-level to 12% at 2500 m. However, during active regeneration events, it was kept constant at 9%, regardless the DPF load and driving altitude. As shown in Figure 5.2(c), the air mass flow during regular operation increased with altitude as a consequence of the VGT and LP-EGR control.

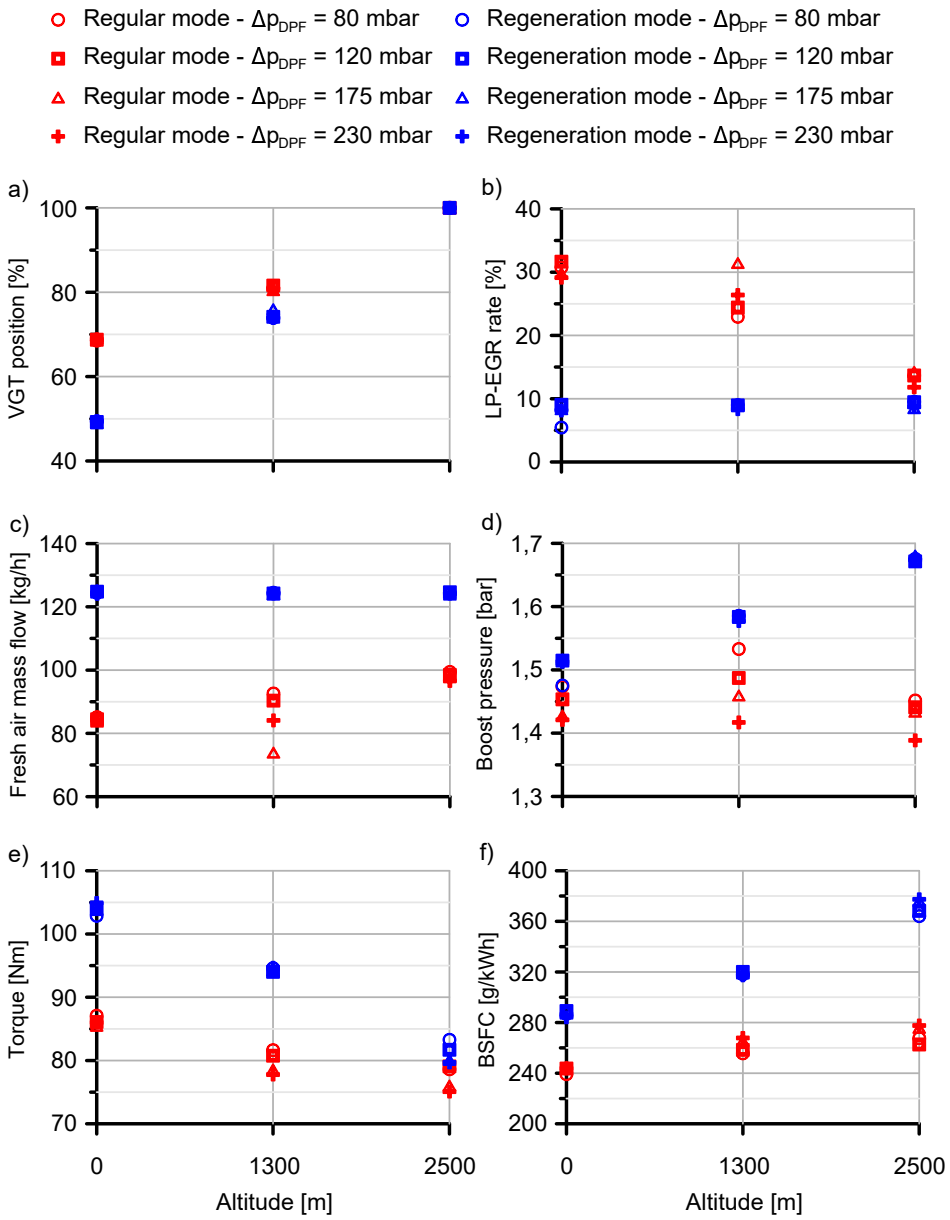

Figure 5.2: Actuation on VGT and LP-EGR due to active regeneration strategy and effects on engine performance, air mass flow and boost pressure as a function of altitude and initial DPF pressure drop.

The objective was to avoid the engine torque derating, as it was previously seen in Chapter 4. Figure 5.2(d) shows the boost pressure change with altitude. It was kept in a similar range for regular operation regardless the altitude, i.e. the ambient pressure decrease was compensated by the pressure ratio increase due to the closer VGT position. In fact, the boost pressure in regular mode showed higher sensitivity to the DPF pressure drop, whose increase penalised the boost pressure. However, the boost pressure was higher in regeneration mode as well as increasing with altitude due to the closer VGT and higher VGT inlet temperature, as shown in Figure 5.3(a). This strategy made the fresh air mass flow to remain constant with altitude in regeneration mode. Hence, the equivalence ratio remained also constant (iso-fuel tests) as well as the exhaust mass flow (also LP-EGR constant with altitude in regeneration mode). Consequently, the exhaust gas dwell time in the DPF during the regenerations was dependent on the exhaust gas density as a function of the altitude, as forward discussed.

Concerning torque and BSFC, their complementary variations with altitude were observed in Figures 5.2(e) and (f), respectively. As already observed in boost pressure, more sensitivity to DPF pressure drop was reflected on engine performance deterioration as altitude increased. The same trends in torque and BSFC were obtained during the active regeneration processes as in regular mode, but with further penalisation due to the constant air mass flow for all altitudes. In addition, although the torque increased during the regeneration mode with respect to regular operation because of the opener VGT and LP-EGR rate decrease, it did not compensated the fuel mass increase related to the active regeneration strategy and the BSFC was penalised, especially at the highest altitude.

Figure 5.3 shows additional exhaust flow properties. As suggested by the VGT closure with altitude, both VGT inlet temperature and pressure increased in regular and regeneration modes, as presented in Figure 5.3(a) and (b). Nevertheless, further sensitivity was observed in regeneration mode due to the injection setup. Higher temperature and pressure were found at the VGT inlet during regeneration mode that in regular one, with increasing differences as the altitude increased. As it has been discussed in Section 4.3.2, the very high VGT inlet pressure is negative for the BSFC due to the increased pumping work, despite of the boost pressure increase.

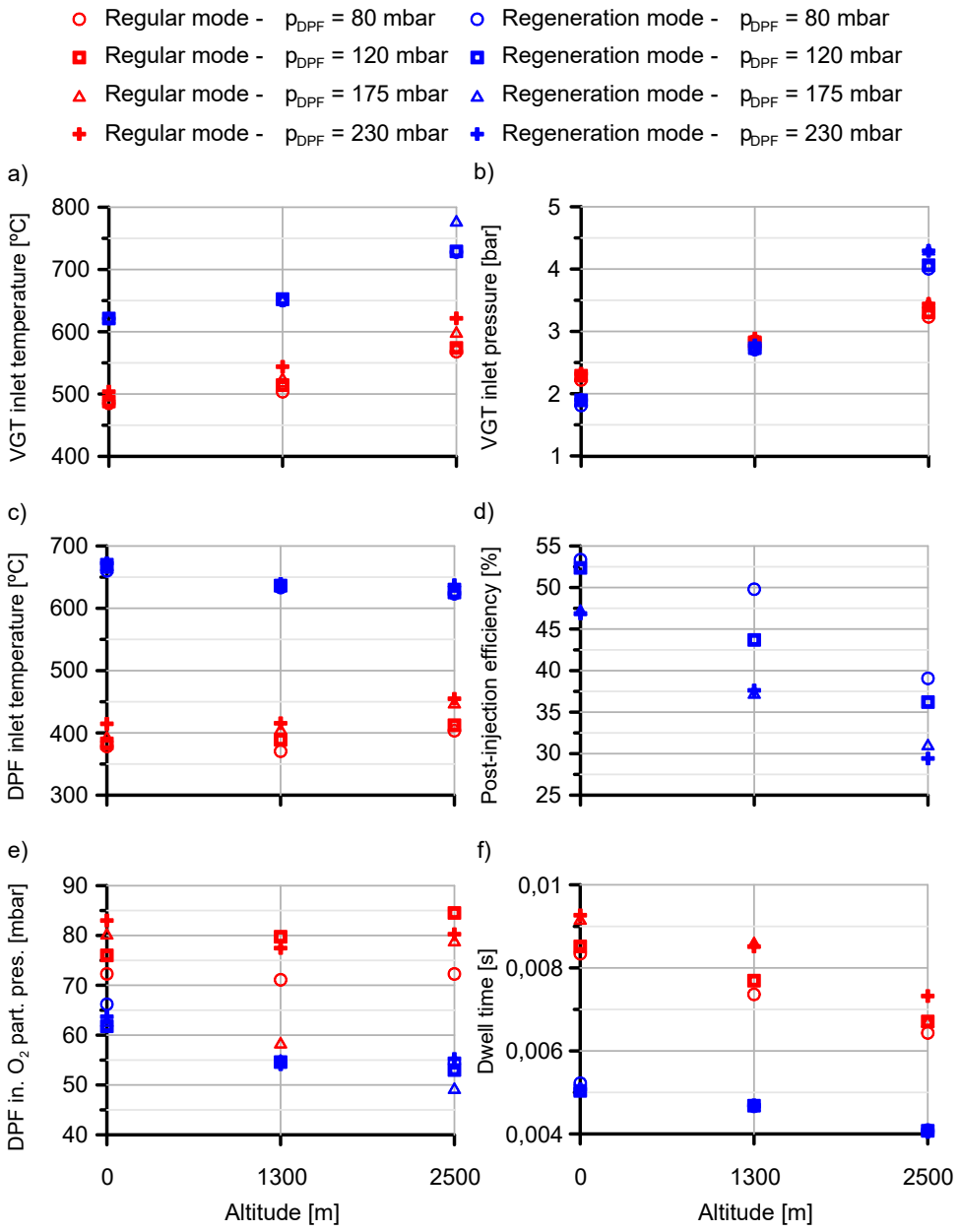

Figure 5.3: Exhaust flow properties at VGT and DPF inlet as a function of the engine operation mode, altitude and initial DPF pressure drop.

As regards to the DPF, the regeneration strategy produced a relevant increase of temperature with respect to the regular mode, but with decreasing benefit as the altitude increased, as represented in Figure 5.3(c). Despite the higher VGT inlet temperature with altitude, the higher VGT expansion ratio (higher VGT inlet pressure and lower DPF inlet pressure with altitude) along with low VGT efficiency due to the closed position produced a temperature drop that limited the DPF inlet temperature. The temperature gain due to the regeneration strategy activation changed from 275°C at sea level (675°C in DPF inlet temperature) to 175°C (625°C in DPF inlet temperature) at 2500 m. This trend indicates a deterioration of the efficiency of the post-injection strategy as the altitude increased.

The variation of this parameter, which is computed in temperature terms according to Eq. 5.1 [183], is shown in Figure 5.3(d).

$$E_{PI} = \frac{T_{DPF,in} - T_{DPF,in_{regular}}}{T_{DPF,in_{max}} - T_{DPF,in_{regular}}}, \tag{5.1}$$

$T_{DPF,in}$ represents the actual temperature at the DPF inlet during the regeneration, $T_{DPF,in_{regular}}$ is the DPF inlet temperature before the regeneration strategy is triggered and $T_{DPF,in_{max}}$ represents the maximum temperature that might be reached at the DPF inlet if all post-injected fuel was oxidised adiabatically within the DOC keeping constant the regular exhaust mass flow:

$$T_{DPF,in_{max}} = T_{DPF,in_{regular}} + \frac{\dot{m}_{f,PI} LHV}{\dot{m}_{exh_{regular}} c_p} \tag{5.2}$$

In addition to the lower DPF inlet temperature as altitude increased, the O_2 partial pressure at the DPF inlet and the dwell time also played a role in the effective regeneration rate. Figure 5.3(e) and (f) represent these variables respectively as a function of the altitude. The equivalence ratio reduction in regular operation as altitude increased allowed the O_2 partial pressure to be kept in similar levels at all altitudes, offsetting the ambient pressure decrease. However, the O_2 partial pressure was clearly reduced during the regeneration process, being this trend more important as the altitude increased due to the ambient pressure reduction while keeping constant the equivalence ratio. Likewise the DPF inlet temperature, this tendency contributed to the soot

oxidation rate decrease as the altitude increased. A similar conclusion is obtained from the analysis of the dwell time. On the one hand, it decreased at constant altitude during the regeneration mode because of the higher temperature and exhaust mass flow than in regular mode. On the other hand, the decrease of ambient pressure as the altitude increased did not compensate the slightly lower DPF inlet temperature and made the dwell time minimum at 2500 m lower during regeneration (Figure 5.3(f)).

According to these boundary conditions, the evolution of the DPF pressure drop along several regeneration cases is represented in Figure 5.4.

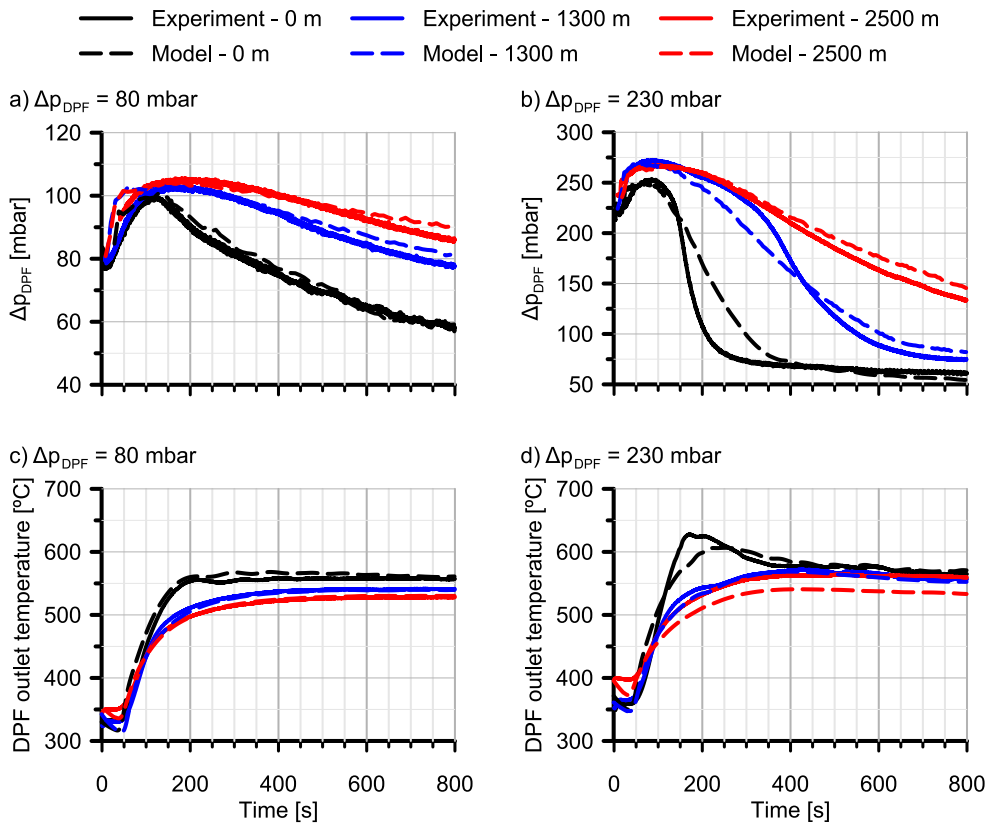

Figure 5.4: Experimental and modelled DPF pressure drop and outlet gas temperature as a function of altitude during active regeneration processes with initial DPF pressure drop of 80 and 230 mbar.

The extreme thresholds of DPF pressure drop to trigger the regeneration mode, i.e. 80 and 230 mbar, are shown at each column, comparing experimental and modelled DPF pressure drop and outlet temperature for the three studied altitudes. Regarding the model setup, Table 5.3 lists the pre-exponential factors and activation energies to calculate Arrhenius kinetic constants for soot oxidation. Those were calibrated from the complete set of experiments. Additionally, Table 5.3 provides the adsorption equilibrium constant parameters (ΔH_{S_n}), as explained in Section 3.3.2.2.

According to Figures 5.4(a) and (b), experimental and modelled results show very good agreement, especially for the lowest initial DPF pressure drop cases (80 mbar). Nonetheless, the trends at 230 mbar were also captured accurately despite predicting a lower pressure drop reduction rate at sea-level conditions. The good model ability to reproduce the soot oxidation was also evidenced in the prediction of the DPF outlet gas temperature, which is represented in Figure 5.4(c) and (d). Again, the main deviations appeared at 230 mbar case for sea-level conditions, where the temperature peak appearing during the maximum reactivity phase was smoothed by the lower predicted oxidation rate related to the model dependence on a lumped estimate of the wall temperature [180].

Table 5.3: Soot oxidation kinetic parameters in DPF model.

P_f [m · bar/s]	O_2	27
	NO_2	6
E_a [J/mol]	O_2	1.2×10^5
	NO_2	9.5×10^4
P_{S_n} [bar^{-1}]	O_2	1×10^{-4} [296]
	NO_2	5×10^{-5} [280]
ΔH_{S_n} [J/mol]	O_2	-7.7×10^4 [297]
	NO_2	-7.5×10^4 [298]
$S_{p,ext,pl}$ [m^{-1}]		6.72×10^7
$S_{p,ext,w}$ [m^{-1}]		3.67×10^6
$S_{p,int,pl}$ [m^{-1}]		1.897×10^8
$S_{p,int,w}$ [m^{-1}]		1.039×10^7

As regards the regeneration behaviour, the pressure drop reduction rate suffered a significant decrease as the altitude increased, as outlined from the analysis of the flow properties at the DPF inlet during the regeneration process. The pressure drop is directly related to the soot depletion rate, which is represented in Figure 5.5 along with its cumulative soot oxidised mass. The

low soot loading case (80 mbar in initial pressure drop) was the most affected one, since the soot depletion rate became extremely low. For this soot loading condition, the peak soot depletion rate reached 13.9 mg/s at sea-level operation whilst it was reduced to 6.9 mg/s at 1300 m and dropped till $\sim$ 4 mg/s at 2500 m, in both cases with a very flat soot depletion rate along time. Consequently, the low reactivity led to an earlier balance point as altitude increased.

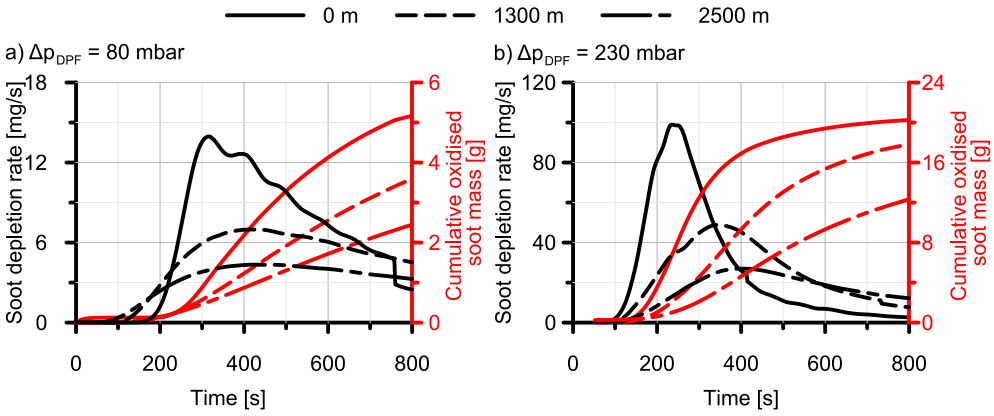

Figure 5.5: Soot depletion rate and cumulative oxidised soot mass as a function of altitude during active regeneration processes with initial DPF pressure drop of (a) 80 mbar and (b) 230 mbar.

By contrast, the higher soot depletion rate as the soot mass load increased, as observed from Figures 5.5(a) and (b) comparison, contributed to delay the balance point. In fact, the delay of the regeneration activation almost allowed the regeneration completeness at 1300 m, as observed in Figure 5.4(b). However, the performance was still very poor at 2500 m. Another interesting point is that the peaks of soot depletion rate for the maximum soot load (initial pressure drop of 230 mbar), i.e. 99.4 mg/s, 49.4 mg/s and 27.4 mg/s at sea-level, 1300 m and 2500 m, respectively, kept the same altitude-to-altitude ratio as for 80 mbar. This means that the maximum reactivity phases were kinetically controlled for all pressure drop thresholds and altitudes. The maximum depletion rate was not high enough, even in sea-level cases, to make the mass transfer phenomena limit the reaction rate. This fact also means that the reduction of the dwell time with the altitude increase, as previously shown in Figure 5.3(f), was not relevant on the regeneration response.

In this regard, the lack of mass transfer limitations can be also understood as constant O_2 surface coverage along the particulate layer during every

regeneration event. Nevertheless, the value of the O_2 surface coverage was specific for every test and dictated by the substrate temperature and O_2 partial pressure. Figure 5.6 shows the O_2 surface coverage as a function of these variables computed according to the Langmuir isotherm (Eq. 3.36).

The respective values for the regeneration processes corresponding to 80 mbar in initial DPF pressure drop are also depicted in Figure 5.6. Despite the lower O_2 inlet partial pressures in altitude (Figure 5.3(f)), the decrease of the substrate temperature, which was related to lower DPF inlet temperature (Figure 5.3(c)) and the subsequent lower soot oxidation rate, gave as a result higher O_2 surface coverage, which increased from 0.21 at sea level to 0.24-0.28 in altitude cases. Therefore, an enhancement of the oxidation rate was found from the O_2 point of view, but not enough to compensate the thermal conditions at the DPF inlet. This behaviour and the lack of influence of the mass transfer demonstrate that the thermal management was the only responsible for the regeneration process deterioration.

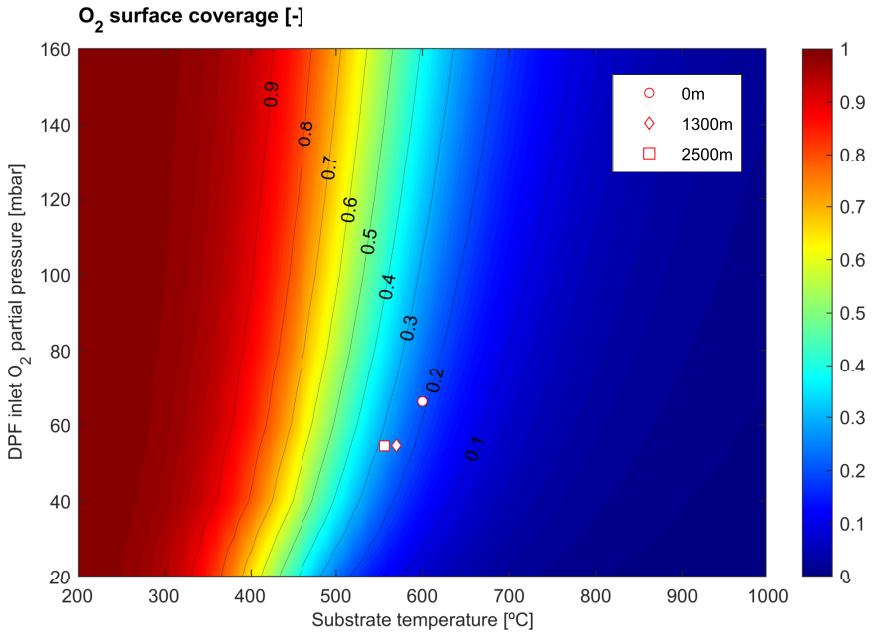

Figure 5.6: O_2 surface coverage as a function of the O_2 partial pressure and the substrate temperature.

In order to evaluate the coverage variation in the soot layer, Figure 5.7 shows the time variation of the O_2 surface coverage at the inlet and the outlet of the soot layer as a function of altitude during active regeneration processes with initial DPF pressure drop of (a) 80 mbar and (b) 230 mbar. In Figure 5.7(a), it can be seen that, the coverage barely varied from the inlet to the outlet in every altitude case. The small amount of accumulated soot in the particulate layer evidenced that the O_2 concentration remained almost constant along the particulate layer, even in the maximum reactivity time interval. At 230 mbar as initial pressure drop (Figure 5.7(b)), small differences in O_2 coverage can be noticed between inlet and outlet during the maximum reactivity phase. However, the differences were below 4.7% and greater as the altitude decreased because of the higher soot depletion rate. It can also be noted that the coverage is lower along the regenerations when the pressure drop threshold was set at 230 mbar than at 80 mbar due to the higher temperature reached in the DPF.

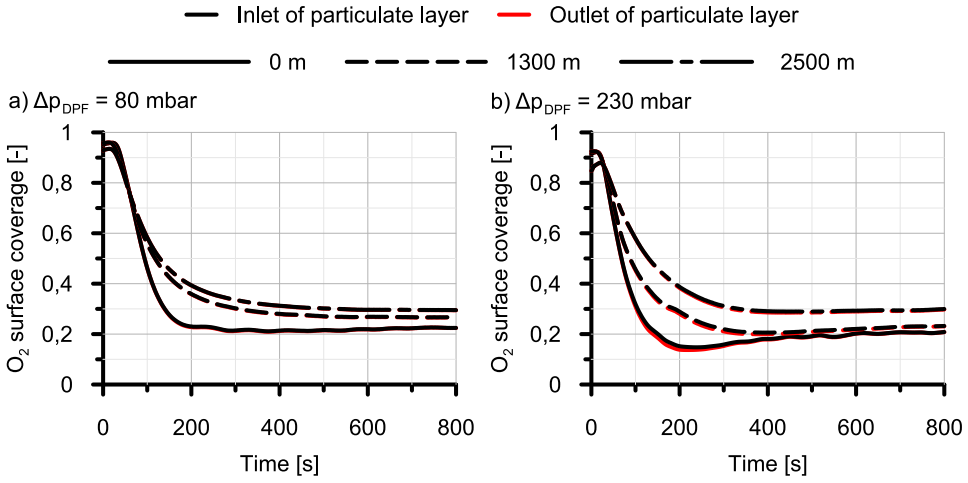

Figure 5.7: Evolution of O_2 surface coverage as a function of altitude during active regeneration processes with initial DPF pressure drop of (a) 80 mbar and (b) 230 mbar.

The deterioration of the regeneration process with altitude was also manifested in tailpipe CO and unburned HC emissions. As shown in Figure 5.8(a), the CO emissions during the regenerations remained unaltered with respect to regular mode at sea-level, but suffered a relevant increase at 1300 m ($\sim$ 3.5 times) and 2500 m ($\sim$ 4.5 times). Opposite to CO, a tailpipe

unburned HC emission increase took place at sea-level during the regeneration, reaching 8 times the regular mode emission, as observed in Figure 5.8(b). From this point on, the unburned HC emission showed a linear increase with altitude and reached up to 35 times the regular mode HC tailpipe emission at 2500 m. These trends also agree with the post-injection efficiency shown in Figure 5.3.

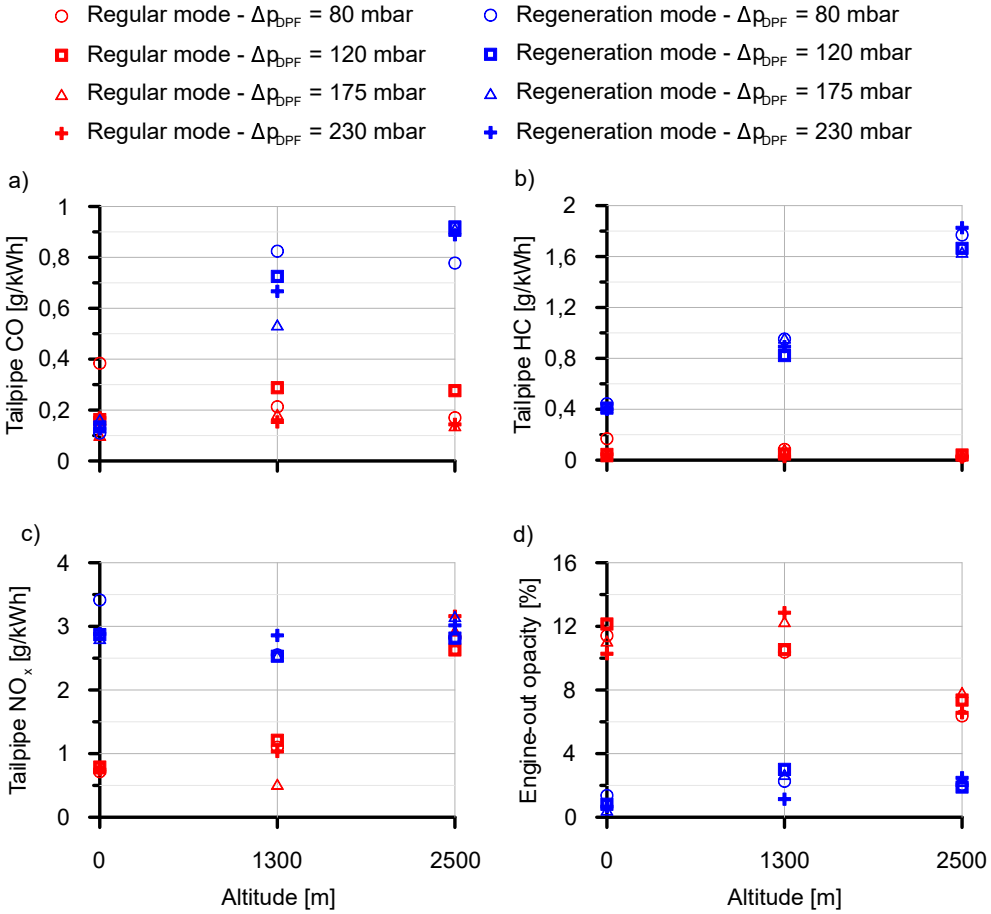

Figure 5.8: Tailpipe gaseous pollutant emissions and engine-out opacity as a function of the engine operation mode, altitude and initial DPF pressure drop.

As regards tailpipe NO_x emission, which is represented in Figure 5.8(c) the regeneration process played a role governing the air management strategy. Thus, the NO_x emissions increased during the regeneration processes at

sea-level and 1300 m due to the LP-EGR rate reduction (Figure 5.2(b)) with respect to regular mode. However, the LP-EGR rate was already very low in regular mode at 2500 m and just suffered a small drop during regeneration. Combined with the lower equivalence ratio at 2500 m resulted in constant NO_x emissions this altitude for all operation modes and threshold pressure drop for active regeneration. Finally, Figure 5.2(d) shows a decrease of the engine-out opacity during the regenerations, which was governed by the tendencies in LP-EGR rate and equivalence ratio. Despite the extremely low soot oxidation rates that were reached in altitude operation, the low opacity was even favouring the DPF balance point. This was delayed as the altitude increased by the displacement of the equilibrium towards soot oxidation due to the low filtration rate.

5.4 VGT position impact on the regeneration rate

Based on the analysis conducted over the Figures 5.2 and 5.3, the trend to close the VGT as the altitude increases in regular mode has been discussed to be negative for the engine operation at partial loads, which might be benefited by opener VGT with respect to sea-level in terms of BSFC and aftertreatment inlet temperature [294]. The actual calibration setting led to a poor soot oxidation performance at high altitude, even avoiding the regeneration completion. The need of VGT position optimisation to improve the thermal management of active filter regenerations is evidenced next.

Figure 5.9 shows the engine performance sensitivity to the VGT position operating in regeneration mode. The engine was run in this mode at each altitude under steady-state conditions with clean DPF. Next, the VGT position was swept in a row. The fuel post-injection strategy and LP-EGR valve position were kept the same as in the baseline tests, i.e. set by the serial ECU calibration. Figure 5.9(a) and (b) represent the torque and BSFC variation at 1300 m and 2500 m baseline and optimum (maximum torque) VGT positions are highlighted. At the view of the results, an optimum VGT position exists in terms of BSFC minimisation. The results also indicated that the higher the altitude the closer the VGT, as applied in serial calibration.

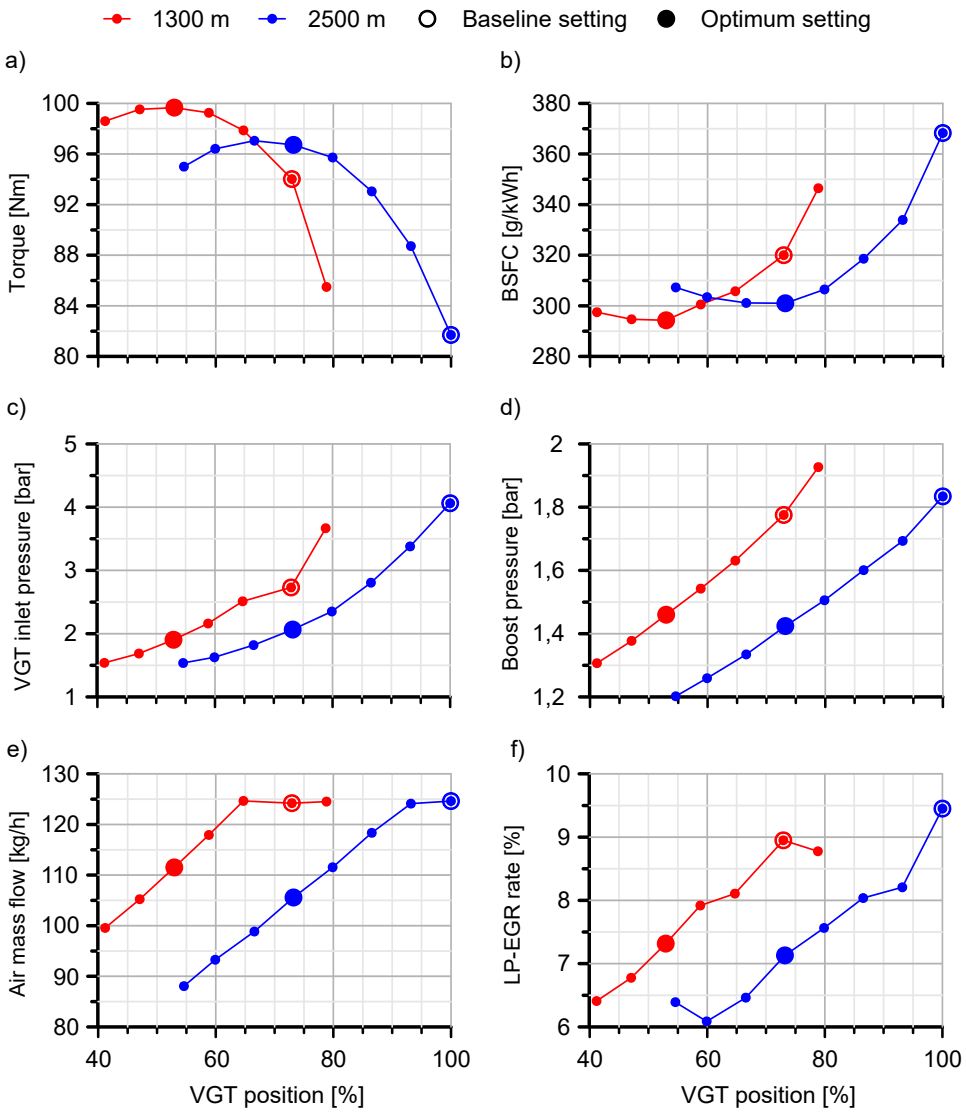

Figure 5.9: Engine performance sensitivity to VGT position at 1300 m and 2500 m operating in regeneration mode.

Nevertheless, the optimised setting pointed out that the VGT position should be placed at 53% instead of 73% at 1300 m and at 73% instead of 100% at 2500 m. These new settings provided an increase in torque that exceeded 6.5% at 1300 m and almost 19% at 2500 m in the baseline value.

This result was due to, mainly, the reduction of the pumping work as suggested by the huge reduction of the difference between the VGT inlet pressure and the boost pressure which are represented in Figures 5.9(c) and (d). Nevertheless, the boost pressure reduction at the optimum VGT position also produced the decrease of the air mass flow as well as the LP-EGR rate (Figure 5.9(e) and (f)). The impact on the emissions is analysed forwards.

Figure 5.10(a) shows how extreme closed VGT positions contributed to increase the VGT inlet temperature, related to the high exhaust manifold pressure. However, an intermediate opening minimized the VGT inlet temperature. From this point on, higher VGT opening led again to higher VGT inlet temperature because of the gradual higher equivalence ratio. In parallel, the DPF inlet temperature, which is represented in Figure 5.10(b), was also benefited by the VGT opening in the tested range due to an snowball effect bounded by the higher VGT inlet temperature and lower VGT expansion ratio. These conditions also contributed to improve the fuel post-injection efficiency, as plotted in Figure 5.10(c). It was increased around 20 percentage points with respect to the baseline VGT position for both altitudes. In fact, the fuel post-injection efficiency reached values above the corresponding to sea-level: 733.2°C and 718.3°C at 1300 m and 2500 m, respectively (Figure 5.10(b)) compared to 670°C at sea level case of Figure 5.3(c)).

Regarding other parameters influencing the soot oxidation rate, the DPF inlet O_2 partial pressure became lower by the VGT opening, as depicted in Figure 5.10(d) due to the increase of the equivalence ratio caused by the lower air mass flow. According to Figure 5.6, this trend deteriorated the O_2 surface coverage under the new DPF boundary conditions. Another reason for that was the higher DPF inlet temperature in the optimum conditions both at 1300 m and 2500 m. By contrast, the DPF dwell time, which is presented in Figure 5.10(e), showed little sensitivity to the VGT opening position, although with an increasing tendency at both altitudes compared to the baseline VGT position. Nevertheless, it remained below the corresponding counterpart at sea-level, which reached 0.0052 s (Figure 5.3(f)).

With the boundaries set by the VGT position providing the maximum torque at each altitude, in particular the increased temperature, the DPF regeneration process was improved as shown in Figure 5.11. The regeneration processes at sea-level are compared with those in altitude for the DPF pressure drop of 120 mbar. It was evidenced a great increase of the soot depletion rate at altitude (1300 m in the left column and 2500 m in the right one). As

observed in Figure 5.11(a) and (b), the proposed VGT position made the pressure drop profile converge to the trace corresponding to the baseline case at sea-level.

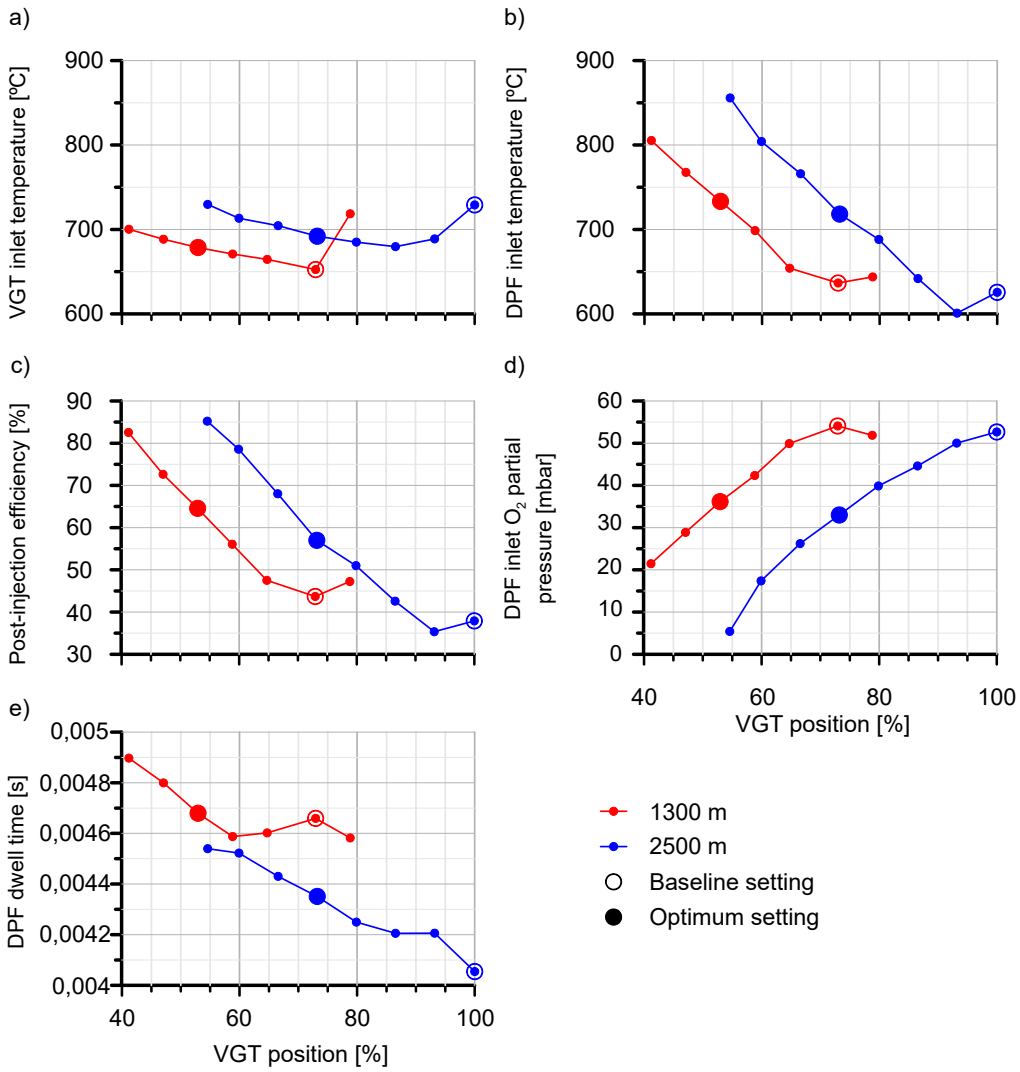

Figure 5.10: Sensitivity to VGT position of VGT and DPF inlet temperatures, fuel post-injection efficiency, DPF inlet O_2 partial pressure and DPF dwell time at 1300 m and 2500 m operating in regeneration mode.

The higher DPF inlet temperature required in altitude with respect to sea-level revealed itself to be the most important parameter. However the O_2 surface coverage still impacted on the results. Although this parameter was proved in Figure 5.6 to be unable to compensate a low DPF inlet temperature, its decrease, which was caused by the temperature increase along with O_2 partial pressure decrease, converged in a snowball effect towards the need of higher exhaust temperature than the sea-level case to obtain similar regeneration rates.

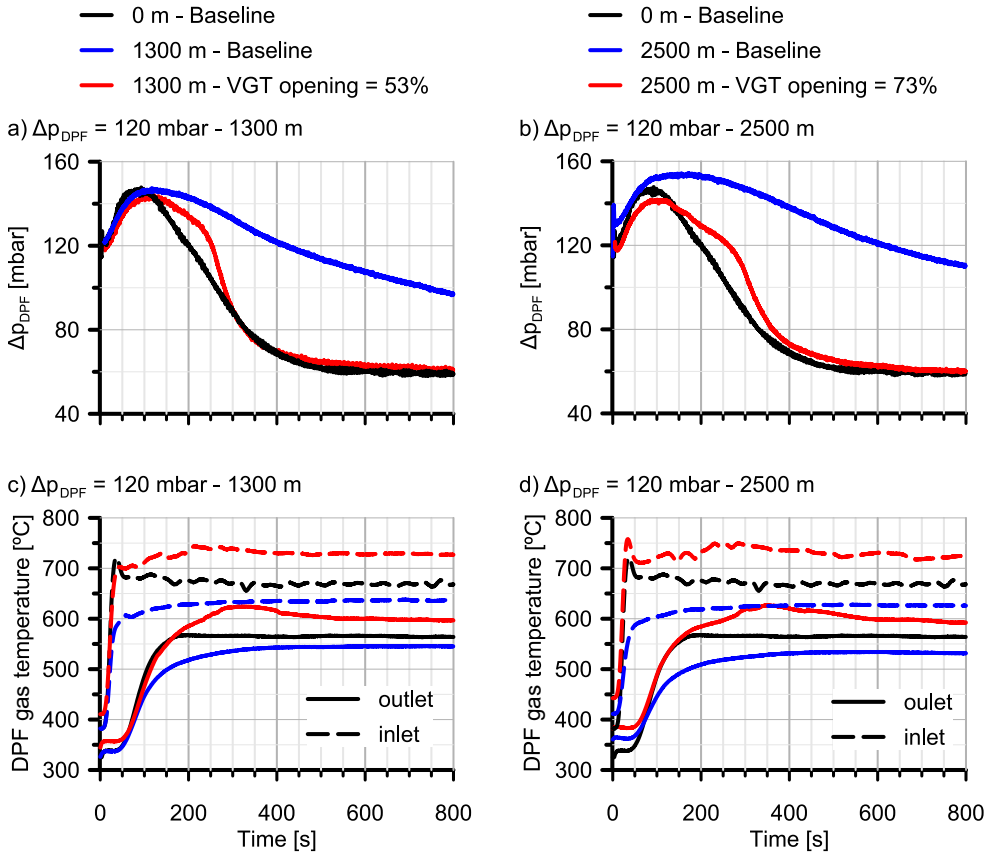

Figure 5.11: DPF pressure drop and outlet temperature at VGT optimised opening at altitude compared the altitude and sea-level baseline conditions.

Finally, the new air management settings proposed during the regeneration processes in altitude had also an effect on pollutant emissions. As summarised

in Figure 5.12 the decrease of the gaseous emissions, i.e. CO, unburned HC and NO_x, was favoured by the VGT opening at altitude operation. Nevertheless, although the tailpipe CO emission reached values in the same order of magnitude as the sea-level regeneration, the unburned HC and NO_x counterparts were still superior than the results for the serial calibration at sea-level (Figure 5.8). With respect to the engine-out opacity, the new VGT positions produced its increase from $\sim$ 2.5% to $\sim$ 7.5% for both altitudes. This was conditioned by the gradual increase of the equivalence ratio as the VGT was opened. Despite this tendency, its value was still kept below the baseline one at sea-level conditions ($\sim$ 11%).

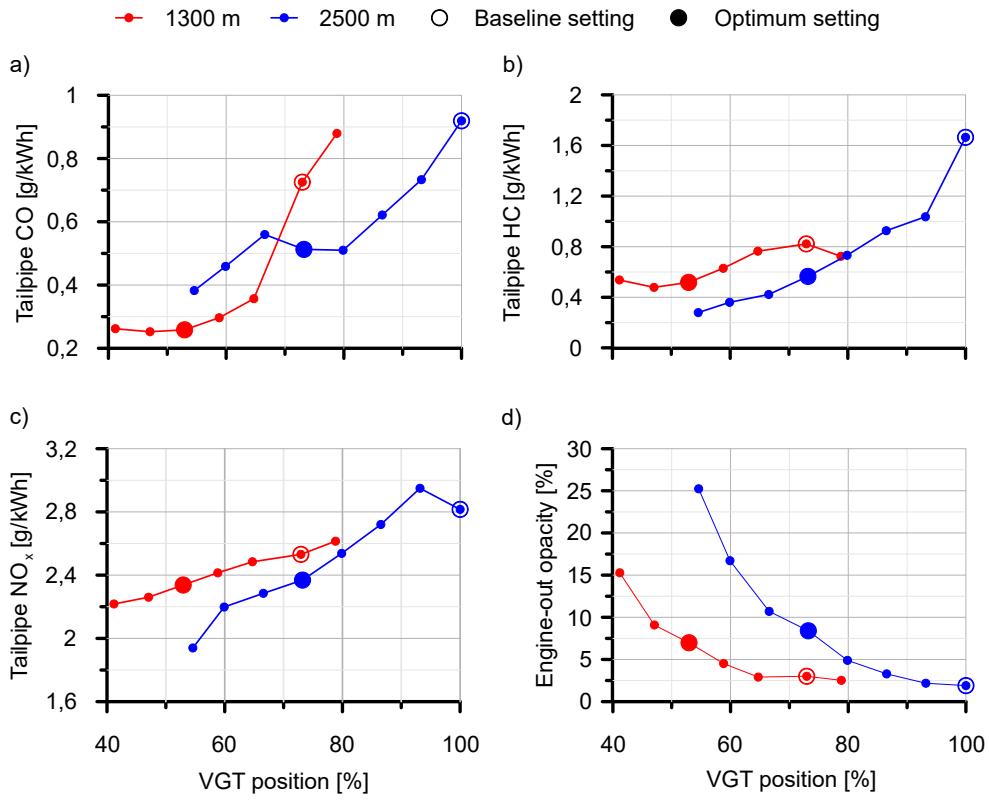

Figure 5.12: Tailpipe gaseous pollutant emissions and engine-out opacity as a function of the engine operation mode, altitude and initial DPF pressure drop.

5.5 Summary and conclusions

In this Chapter, the need to account for an specific VGT actuation during active regeneration processes of wall-flow monoliths when operating at high driving altitudes was shown. The experimental results obtained from serial calibration in the Euro 6d-Temp Diesel engine evidenced a dramatic deterioration of the soot depletion rate in the DPF. The balance point was even reached in some tested cases, especially as the threshold soot mass load to trigger the active regeneration was low and the altitude increased. The VGT actuation was observed to be the main difference in engine control as a function of the altitude, since the same fuel post-injection was applied by the serial ECU calibration. The analysis of the experimental response along with the modelling of the DPF revealed that to close the VGT as the altitude increases failed during active regenerations. The main consequence was the reduction of the fuel post-injection efficiency, manifested in the decrease of the DPF inlet temperature. The modelling results demonstrated that this parameter governed the oxidation rate, whilst minor effects caused by the O_2 mass transfer and adsorption were observed. In fact, the O_2 surface coverage was improved due to the lower temperature with respect to the sea-level case despite the lower O_2 partial pressure in altitude operation. However, it did not compensated the thermal management worsening in the exhaust line.

Against these baseline conditions, the optimisation of the VGT position was evidenced to be fundamental in the definition of the active regeneration strategy. Keeping constant the serial ECU calibration regarding the fuel post-injection and LP-EGR control, applying opener VGT positions than those in serial calibration provided an optimum engine torque. This condition defined the new VGT position used for the regeneration process assessment. At the same time, the higher VGT opening increased the exhaust temperature due to the combined effect of higher equivalence ratio and lower VGT expansion ratio. Consequently, the soot depletion rate suffered a great increase that made the DPF pressure drop profile equivalent to the one corresponding to baseline operation at sea-level. The tailpipe pollutant emissions were also kept in the same order of magnitude as those at sea-level, and clearly improved compared to altitude serial calibration cases. Nevertheless, altitude regenerations required higher DPF inlet temperature than sea-level cases because of the need to compensate the lower dwell time and the respective lower O_2 surface coverage found at higher temperatures and equivalence

ratios. Despite this constraint, the experimental results demonstrated that any penalty in active DPF regeneration dynamics can be avoided in high altitude driving conditions provided that the VGT control strategy is adapted, which is in turn in synergy with engine performance and emissions enhancement.

Bibliography

[5] P. Piqueras, R. Burke, E. J. Sanchis, and B. Diesel. "Fuel efficiency optimisation based on boosting control of the particulate filter active regeneration at high driving altitude". *Under review. Fuel* (2022) (cit. on pp. xii, 167).

[174] S. Soltani, R. Andersson, and B. Andersson. "The effect of exhaust gas composition on the kinetics of soot oxidation and diesel particulate filter regeneration". *Fuel, 220, 453-463* (2018) (cit. on pp. 33, 166).

[180] V. Macián, J. R. Serrano, P. Piqueras, and E. J. Sanchis. "Internal pore diffusion and adsorption impact on the soot oxidation in wall-flow particulate filters". *Energy, 179, 407-421* (2019) (cit. on pp. 33, 95, 96, 166, 175).

[183] J. R. Serrano, P. Piqueras, J. de la Morena, and E. J. Sanchis. "Late fuel post-injection influence on the dynamics and efficiency of wall-flow particulate filters regeneration". *Applied Sciences, 2019, 9 (24), 5384* (2019) (cit. on pp. 34, 40, 88, 166, 168, 173).

[280] A. Messerer, R. Niessner, and U. Pöschl. "Comprehensive kinetic characterization of the oxidation and gasification of model and real diesel soot by nitrogen oxides and oxygen under engine exhaust conditions: Measurement, Langmuir-Hinshelwood, and Arrhenius parameters". *Carbon, 44, 307-324* (2006) (cit. on pp. 96, 175).

[293] P. Piqueras, M. J. Ruiz, J. M. Herreros, and A. Tsolakis. "Sensitivity of pollutants abatement in oxidation catalysts to the use of alternative fuels". *Fuel, 297, 120686* (2021) (cit. on p. 166).

[294] A. T. Thompson. "The effect of altitude on turbocharger performance parameters for heavy duty Diesel engines: experiments and GT-Power modeling". PhD thesis. Colorado State University, 2014 (cit. on pp. 166, 180).

[295] Y. Wu, P. Wang, S. Farhan, j. Yi, and L. Lei. "Effect of post-injection on combustion and exhaust emissions in DI Diesel engine". *Fuel, 258, 116131* (2019) (cit. on p. 168).

[296] R. H. Essenhigh. "Rate equations for the carbon-oxygen reaction: an evaluation of the Langmuir adsorption isotherm at atmospheric pressure". *Energy Fuels, 5 (1), 41-46* (1991) (cit. on p. 175).

[297] K. J. Lee, I. H. Han, and K. H. Choi. "Oxygen chemisorption on microporous carbons: An analysis of experimental data". *Korean Journal of Chemical Engineering, 12, 228-235* (1995) (cit. on p. 175).

[298] M. Kalberer, M. Ammann, H. W. Gäggler, and U. Baltensperger. "Adsorption of NO_2 on carbon aerosol particles in the low ppb range". *Atmospheric Environment, 33 (17), 2815-2822* (1999) (cit. on p. 175).

Chapter 6

Engine and EATS synergy at low partial loads as a function of altitude

Contents

6.1 Introduction **190**
6.2 Test campaign **191**
6.3 Engine performance and exhaust temperature **193**
6.4 Pollutant emissions **201**
6.5 Summary and conclusions **207**
Bibliography **209**

6.1 Introduction

The final discussion addressed in this doctoral thesis is focused on the evaluation of the impact of engine calibration on its overall performance and emissions including the EATS operation, at different ambient temperatures and altitude conditions. This analysis was focused on partial loads with an experimental emphasis. In this framework and based on the conclusions obtained in Chapter 5, this Chapter is dedicated to the experimental evaluation of the effects of the boost pressure and low pressure exhaust gas recirculation settings when the engine runs low partial loads at high altitude, accounting for extreme warm and cold ambient temperature.

In this context, to further explore the boost pressure and EGR trade-off at partial loads, an experimental parametric study was conducted evaluating the sensibility of the engine response to these two variables. For the sake of understanding, an analysis of the parameters governing the engine response is also performed. The engine was tested under steady-state conditions in an engine test bench making use of the altitude simulator MEDAS. From the baseline engine serial calibration, the tests were performed varying the VGT and LP-EGR valve positions to sweep a representative range of boost pressure and EGR rate of three low load operating points of different engine speeds. The parametric study covered three ambient temperatures, from -10°C to 45°C including the standard temperature (25°C) and three altitudes, namely sea-level, 1300 m and 2500 m. The results established clear guidelines for an optimal calibration within the tested engine range with synergistic minimisation of specific fuel consumption and maximisation of the aftertreatment inlet temperature while balancing pollutant emissions.

The works, analysis and ideas described in this Chapter were the origins of publication number [4] from the publications list of the author of this doctoral thesis, which is shown at the beginning of the document. For the sake of readiness and to protect the thesis writing style the publication number [4] from author's list of publications have not been specifically cited each time that ideas, figures or discussions contained in it are addressed in this Chapter. This disclaimer corrects, compensates and justifies the fact that the work of the PhD candidate's doctoral thesis are the origin of the innovation component in the publications number [4] listed in the referred Section.

6.2 Test campaign

As advanced in Section 6.1, this Chapter is focused on studying the boost pressure and low pressure exhaust gas recirculation trade-off in low partial load engine operating conditions to put into proof the standard trends observed in the literature. Evaluating both sensitivities together makes it possible to find the optimum trade-off in terms of engine performance at different ambient conditions.

In this context, the purpose of this study is to identify the impact of the boosting pressure and EGR rate on the performance, emissions and exhaust thermal conditions of a Euro 6d-Temp turbocharged Diesel engine working at low partial load as a function of altitude and ambient temperature. For the sake of understanding, an analysis of the parameters governing the engine response is also performed. The engine was tested under steady-state conditions in the engine test bench described in Section 3.2.

Taking as baseline the engine serial calibration, experimental tests were conducted varying the VGT and LP-EGR valve positions, sweeping a representative ranges of boost pressure and EGR rate of three low partial load operating points of different engine speeds. This parametric study covered the ambient temperature of -10°C, 25°C and 45°C and three altitudes, namely sea-level, 1300 m and 2500 m. The test results allow defining and justifying clear guidelines for optimal engine calibration. Opposite to traditional strategies, a proper calibration of the boost pressure and LP-EGR enabled reductions in specific fuel consumption along with gas temperature increase at the exhaust aftertreatment system, as it will be seen next.

Table 6.1 enumerates the three tested engine operating points in this study, which ranged from 2 to 6 bar in BMEP. The engine speed selection covered 1250 to 3000 rpm. The points are designated by the engine speed and the BMEP in the serial calibration condition. Every operating point was evaluated at 9 different ambient boundaries. From the altitude point of view, sea-level, 1300 m, which is the maximum altitude in Euro 6d extended range, and 2500 m, which involves a global upper limit established in terms of maximum altitude for emission standards (for example, 2400 m in China 6b), were tested. In parallel, the ambient temperature was swept from very cold conditions (-10°C) to very hot ones (45°C) with an intermediate temperature represented by the standard ambient conditions (25°C).

Table 6.1: Definition of the tested operation conditions.

Operating point	Altitude [m]	Ambient temperature [°C]	WCAC outlet temperature [°C]
#A - 1250 rpm & 3 bar	0 / 1300 / 2500	-10	0
	0 / 1300 / 2500	25	28
	0 / 1300 / 2500	45	48
#B - 2000 rpm & 6 bar	0 / 1300 / 2500	-10	5
	0 / 1300 / 2500	25	29
	0 / 1300 / 2500	45	49
#C - 3000 rpm & 2 bar	0 / 1300 / 2500	-10	7
	0 / 1300 / 2500	25	35
	0 / 1300 / 2500	45	55

A parametric study was done for every operating point at every ambient condition sweeping boost pressure and EGR rate. The VGT rack was actuated to control the boost pressure. Concerning the EGR rate, only the LP-EGR was considered since the study was performed in steady-state conditions and the engine coolant temperature reached 60°C (threshold over which the HP-EGR is closed by the ECU). Therefore, the LP-EGR and the exhaust back-pressure valve positions were set to impose the target EGR rate. The study was carried out according to the following testing procedure:

1. The engine was set at every operating point condition referenced in Table 6.1 according to the serial calibration. The fuel mass flow obtained in this condition was kept constant for the entire parametric study.

2. From the baseline point, a boost pressure sweep was performed covering an amplitude of 200 mbar. As a general trend, the baseline VGT position tended to be very closed, so that the boost pressure was decreased in steps of $\sim$ 50 mbar. In the cases where the VGT reached fully opening condition without reaching a tested window of 200 mbar, additional VGT positions closer than the baseline one were tested to have comparable boost pressure windows and sensitivity to this variable in all the parametric studies.

3. For every boost pressure considered in the previous step, the LP-EGR rate was progressively decreased up to $\sim$ 15% in absolute value with respect to the baseline LP-EGR rate. To keep this range in the case of

reaching 0% of LP-EGR rate, the baseline LP-EGR rate was increased until achieving a range of at least 15% for the study.

As will next be presented in Section 6.3, this procedure enabled the creation of contour maps for each altitude and ambient temperature combination, which are depicted for each magnitude of interest as a function of the boost pressure and LP-EGR rate. In every contour plot, the tested operating conditions are marked by a black dot. The baseline operating point (serial calibration) is identified by a greater dot than its counterparts, in red or green colour depending on the background contour colour to be properly distinguished. For comparison proposals, some plots encompass more than one ambient condition contour map provided that there is not overlap between tested regions.

6.3 Engine performance and exhaust temperature

Figure 6.1 illustrates air mass flow, compressor pressure ratio and VGT position corresponding to the operating point #A of 1250 rpm & 3 bar at 25°C in ambient temperature as a function of the altitude, boost pressure and LP-EGR rate. Comparing the boost pressure and LP-EGR ranges corresponding to every altitude (columns in Figure 6.1), a decrease in LP-EGR rate window was noticed as altitude increased. In parallel, the boost pressure range also decreased. However, this response was expected from the ambient pressure decrease. The results point out that the tested regions at every altitude provided the same order of magnitude regarding air mass flow.

The engine actuated moving the serial calibrated point to lower LP-EGR rate progressively, but keeping the same air mass flow, i.e. the same air-to-fuel ratio, as the baseline case. However, as indicated by the coloured points in the contour plots, while the baseline LP-EGR rate was 39% at sea-level, it was decreased to 34% at 1300 m and dropped till 20% at 2500 m. The boost pressure also decreased from 1060 mbar at sea-level to 960 mbar at 1300 m and 860 mbar at 2500 m. Despite of the boost pressure decrease, the compressor pressure ratio of the baseline point was gradually increased as altitude did, closing the VGT to provide the same air mass flow as at sea-level. Therefore, the serial engine calibration maximized the LP-EGR rate to reduce the impact

on NO_x emissions. To do that, the pressure ratio was increased closing the VGT to keep the same equivalence ratio as at sea-level. This target of the calibration process found its limit in the specific fuel consumption penalty.

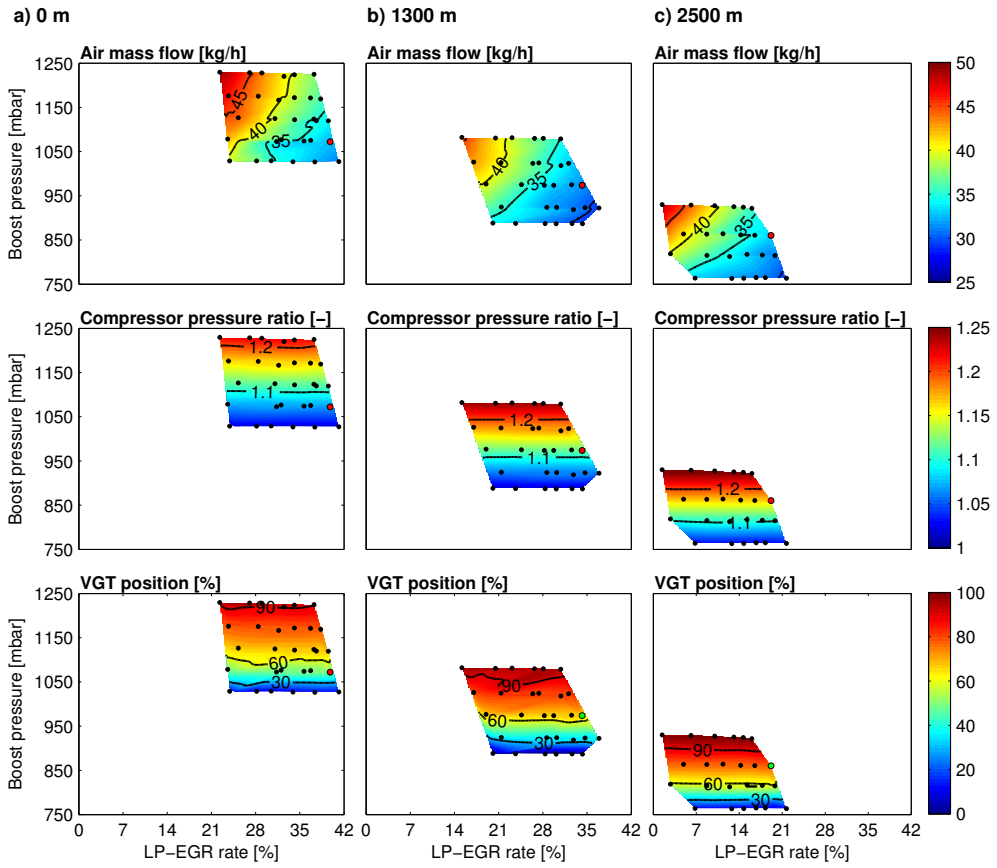

Figure 6.1: Air mass flow, compressor pressure ratio and VGT position corresponding to 1250 rpm & 3 bar BMEP at 25° C as a function of the altitude.

The increase of the compressor pressure ratio and the VGT closing involved a penalty in torque and BSFC, which are represented in Figure 6.2. The BSFC is normalized with respect to the BSFC obtained in the serial calibration condition at sea-level and 25°C. The BSFC deterioration was observed in the serial calibration points, particularly, and evidenced by the trends within the tested boost pressure and LP-EGR rate ranges at every altitude. Although the

serial calibration fell into the maximum torque and minimum BSFC regions at sea-level and 1300 m, these magnitudes might be optimised at 2500 m.

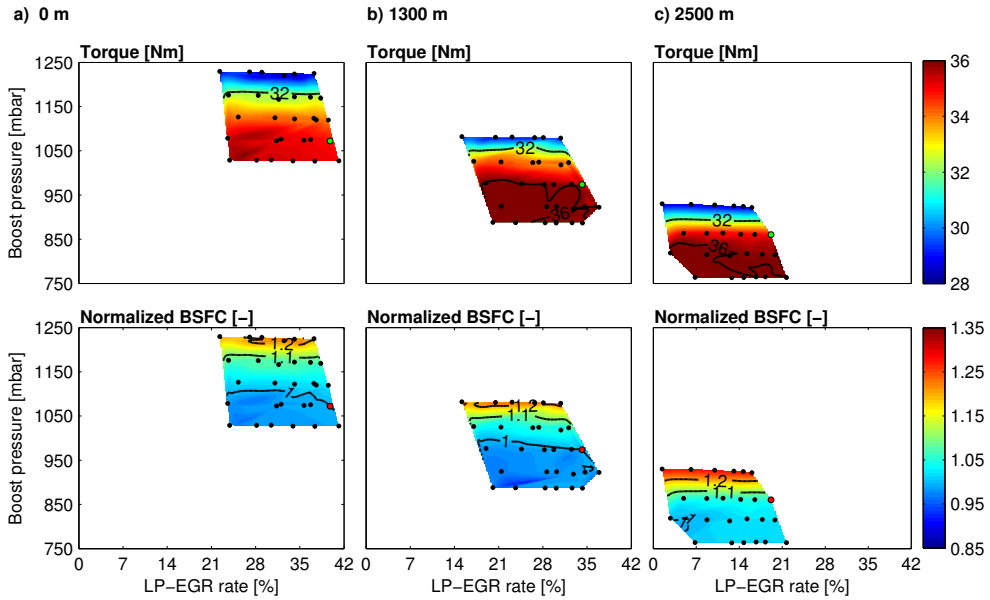

Figure 6.2: Engine torque and BSFC corresponding to 1250 rpm & 3 bar BMEP at 25° C as a function of the altitude.

The main output from Figure 6.2 was that the best strategy to minimize the fuel consumption in the low load operating point would consist of the VGT opening to reduce the boost pressure. This might be done regardless of the LP-EGR rate, so that to find the optimal balance between equivalence ratio and engine-out NO_x emission would be still possible.

Figure 6.3 depicts the VGT expansion ratio as well as inlet and outlet temperatures at every altitude for 1250 rpm & 3 bar. As in the previous variables, the LP-EGR rate played a negligible role being the boost pressure the governing parameter. The increase of the compressor pressure ratio required the VGT expansion increase induced by the VGT closing. Accordingly, the VGT expansion ratio behaved as the compressor pressure ratio, increasing as the altitude increased both within the tested range and, specifically, in the baseline operating point. Regarding temperature, the VGT

inlet temperature slightly increased from sea-level to 1300 m, with a more pronounced increase at 2500 m due to the the lower amount of exhaust mass flow.

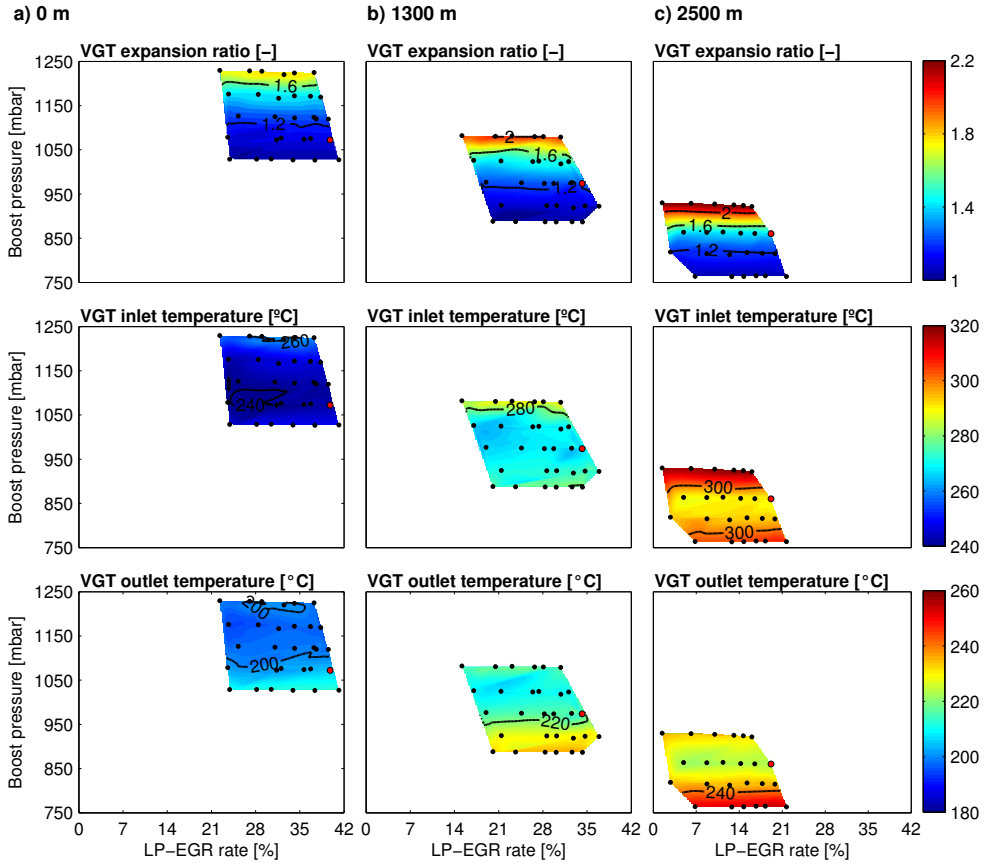

Figure 6.3: VGT expansion ratio, inlet temperature and outlet temperature corresponding to 1250 rpm & 3 bar BMEP at 25° C as a function of the altitude, boost pressure and LP-EGR rate.

These differences in temperature as a function of altitude were also present in the VGT outlet temperature, but with a different pattern. On the one hand, the maximum VGT inlet temperatures were obtained for the extreme VGT positions. The highest VGT inlet temperatures were caused by the high pressure in VGT fully closed condition and by the lower air mass flow (higher equivalence ratio) as the VGT was opened. However, the VGT outlet

temperature reached its maximum at the minimum boost pressure, i.e. open VGT. Despite the highest VGT inlet temperature being produced at maximum boost pressure, the resulting high expansion ratio gave as a result a low outlet temperature. By contrast, the fully VGT opening provided the expansion ratio convergence towards 1. Consequently, the temperature drop across the VGT was highly reduced and the VGT outlet temperature remained the highest regardless the altitude and LP-EGR rate.

The main trends observed at 1250 rpm & 3 bar were confirmed in additional operating points. Figure 6.4 represents the normalized BSFC and VGT outlet temperature corresponding to 2000 rpm & 6 bar and 3000 rpm & 2 bar at 25°C in ambient temperature, being each row an operating point. In these plots, the focus is directly put on the comparison between sea-level and 2500 m operation, whose contours are plotted together.

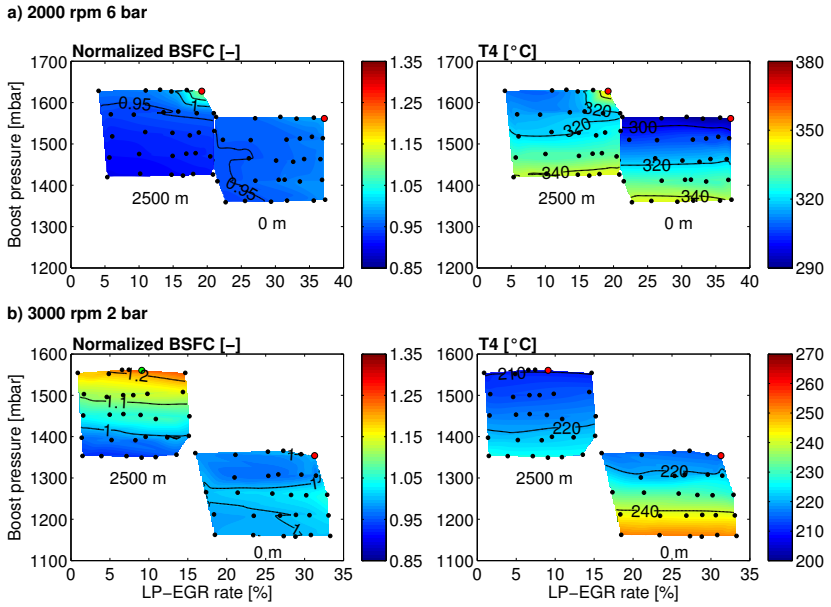

Figure 6.4: BSFC and VGT outlet temperature at 25° C in ambient temperature as a function of the altitude, boost pressure and LP-EGR rate.

A relevant difference is observed for these two operating points in baseline altitude operating points (coloured dots on contours) with respect to 1250 rpm & 3 bar. The serial calibrated boost pressure was increased from sea-level to

2500 m by closing further the VGT. As a result, the BSFC sharply increased with respect to sea-level case with a minor benefit in VGT outlet temperature. However, these settings can be optimised, both at sea-level and extreme altitude operation.

Again, operating at lower boost pressure by opening the VGT led to an increase in the VGT outlet temperature regardless the LP-EGR rate, because of the increase in VGT inlet temperature (higher equivalence ratio) and very low expansion ratio. This increase was around 40°C at sea-level for both 2000 rpm & 6 bar as 3000 rpm & 2 bar. At 2500 m in driving altitude, the benefit was lower. The VGT outlet temperature increased $\sim$ 20°C at 3000 rpm & 2 bar but at 2000 rpm & 6 bar it was kept as in the particular case of the serial calibration when reducing boost pressure keeping the maximum LP-EGR rate.

This was caused by a singularity of the serial calibration, which demanded a higher VGT closing leading to both high pumping losses (extremely high spot in BSFC) and VGT outlet temperature due to the poor VGT efficiency. This is noticed by the high dependence of both BSFC and VGT outlet temperature on the LP-EGR at the baseline boost pressure. In fact, the decrease of the LP-EGR rate at this pressure provided the same trends as observed in other operating conditions. Regarding BSFC, sea-level operation was almost unresponsive in both operating points. However, the benefits at 2500 m were evident, especially at 3000 rpm & 2 bar, due to the inherent poor efficiency and sensitivity to settings of the very low engine loads. In this point the BSFC was reduced around 25% as the boost pressure was reduced. The benefit also existed at 2000 rpm & 6 bar, reducing the BSFC above 15 % from the baseline settings.

Figure 6.5 represents the normalized BSFC and VGT outlet temperature for every engine operating point at sea-level and 2500 m corresponding to 45°C in ambient temperature. Complementary, Figure 6.6 provides the equivalent results for cold ambient conditions (-10°C). Those results support all the trends found at standard temperature: benefits from low boost pressure at low engine load operation in terms of simultaneous optimisation of BSFC and aftertreatment warm-up conditions. In addition, the determination of the optimal LP-EGR rate is independent of engine performance results and being only a determinant parameter for the air mass flow management.

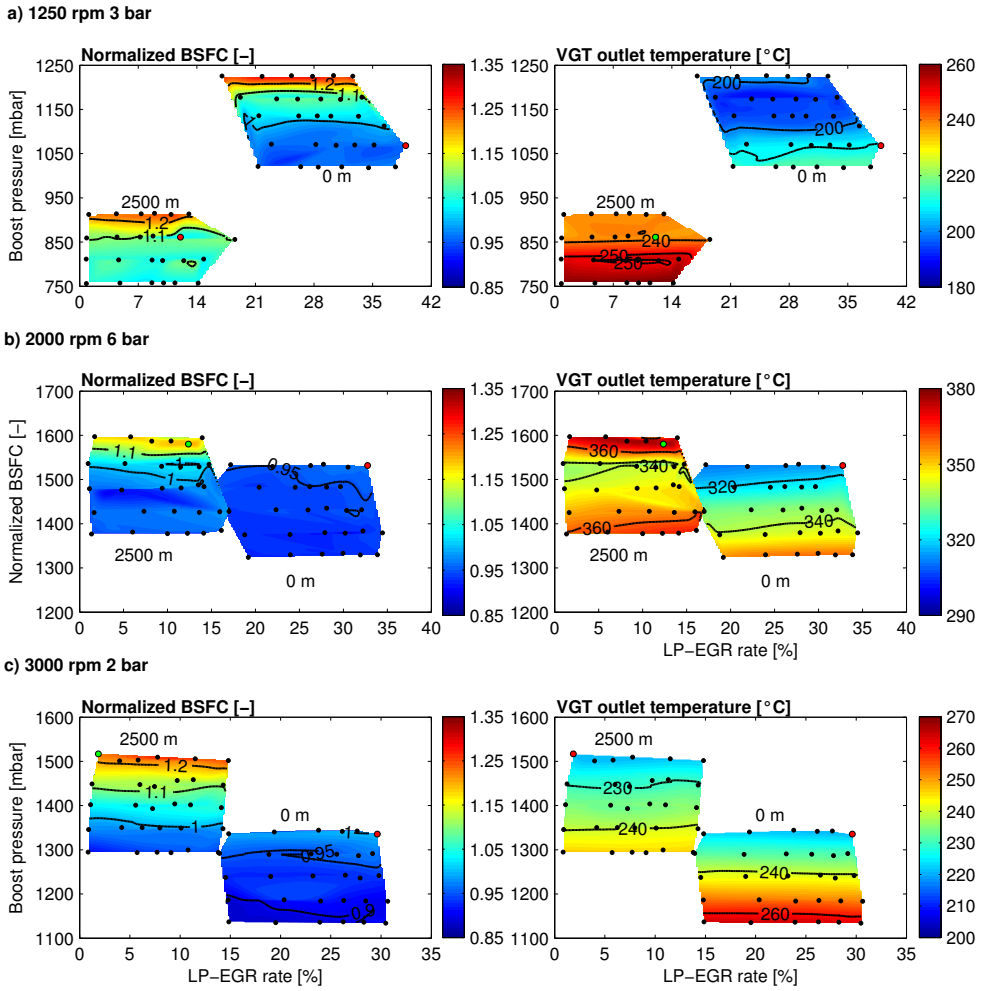

Figure 6.5: BSFC and VGT outlet temperature at 45° C in ambient temperature as a function of the altitude, boost pressure and LP-EGR rate.

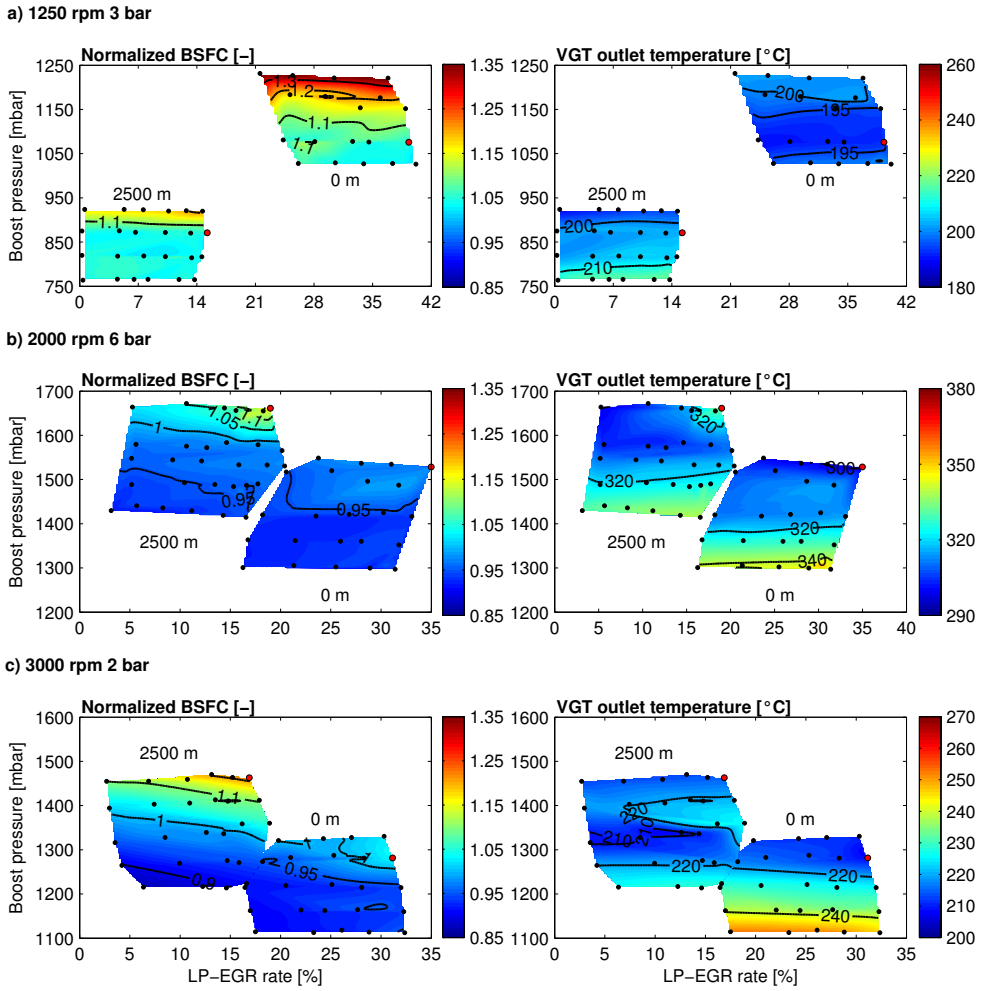

Figure 6.6: BSFC and VGT outlet temperature at -10° C in ambient temperature as a function of the altitude, boost pressure and LP-EGR rate.

6.4 Pollutant emissions

Figure 6.7 represents the engine-out NO_x emission and opacity corresponding to the three tested points as a function of the boost pressure and LP-EGR rate. In particular, the plots include the comparison between the results at sea-level and 25°C and those at 2500 m and -10°C, representing a standard versus extreme ambient conditions.

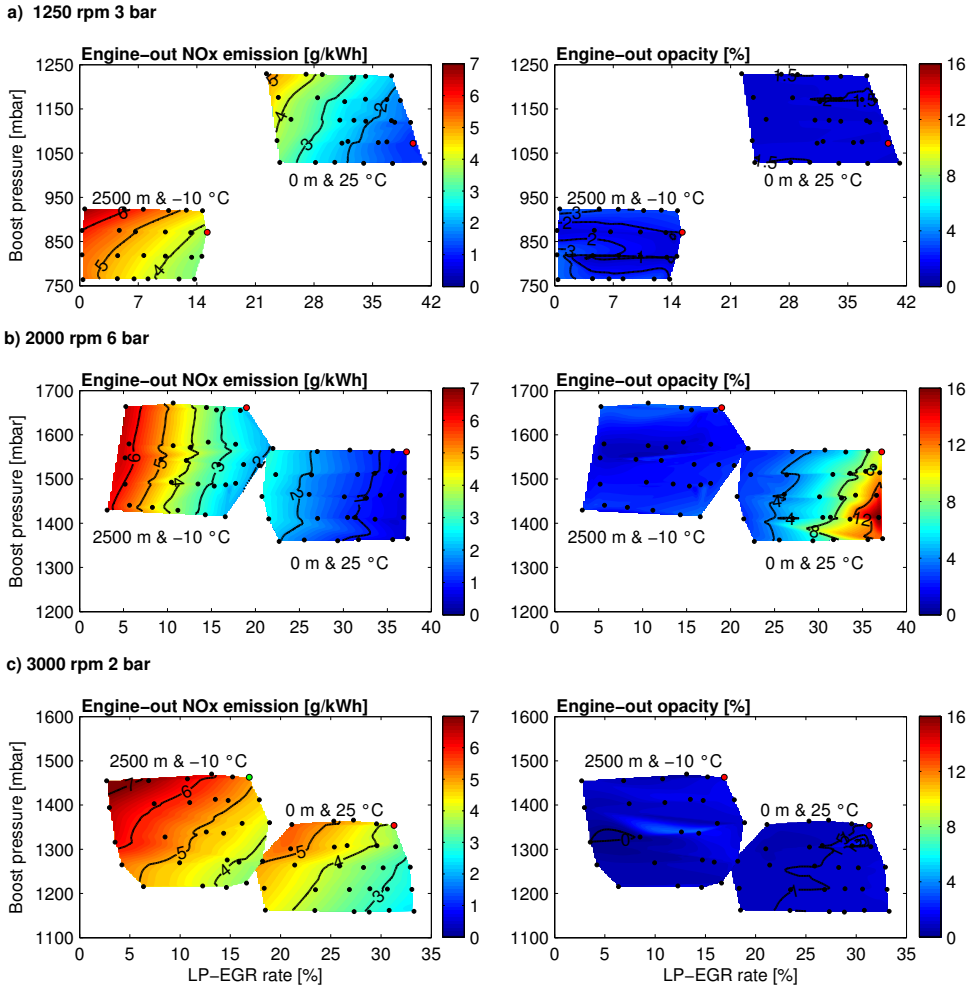

Figure 6.7: Engine-out NO_x emission and opacity as a function of the boost pressure and LP-EGR rate for sea-level at 25° C and 2500 m at -10° C.

As expected, the engine-out NO_x emission were mainly governed by the LP-EGR rate. Nonetheless, the boost pressure also had a relevant weight in very low load cases, as the 1250 rpm & 3 bar and 3000 rpm & 2 bar, and particularly at high boost pressure and low LP-EGR rates in tests at -10°C. This dependence disappeared progressively as the LP-EGR rate and engine load increased, as observed in Figure 6.7(b), corresponding to 2000 rpm & 6 bar.

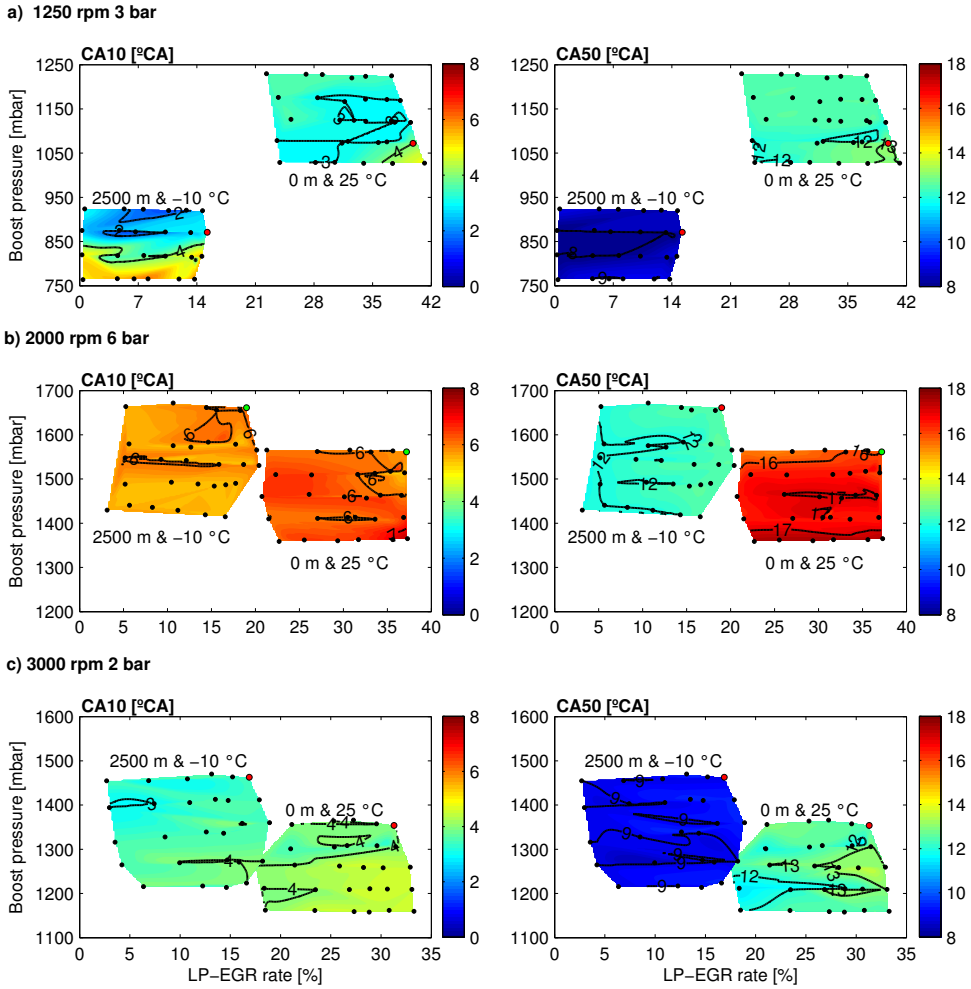

Figure 6.8: CA10 and CA50 as a function of the boost pressure and LP-EGR rate for sea-level at 25° C and 2500 m at -10° C.

In parallel, the sensitivity to the ambient temperature was also captured in every engine point, with lower NO_x emissions at -10°C despite the low LP-EGR rate, influenced by a lower equivalence ratio in those conditions. As a general trend, imposing low boost pressure resulted beneficial (or neutral) in this operating range to reduce the engine-out NO_x emission along with increasing LP-EGR rate, obtaining synergy with minimum BSFC and maximum aftertreatement inlet temperature regardless the ambient condition. Despite the lower air mass flow as the boost pressure was decreased, the low level of the equivalence ratio made its increase not responsible of any NO_x emission variation.

By contrast, the NO_x emission decreased at constant LP-EGR rate, as mainly observed in points 1250 rpm & 3 bar (Figure 6.7(a)) and 3000 rpm & 2 bar (Figure 6.7(c)), as the boost pressure did. This response was attributed to the in-cylinder temperature decay related to the combustion delay, which was in turn promoted by the ignition delay produced by the poorer mixing ratio as the boost pressure was decreased [299]. Figure 6.8 represents how the crank angle at 10% and 50 % of burned fuel mass (CA10 and CA50, respectively) were progressively increased as the boost decreased.

As regards soot emission, which is depicted in the right column of Figure 6.7, the opacity was kept very low in all cases ($< 3\%$), being comparable at both ambient conditions. The soot dependence on the LP-EGR rate was only noticed at 2000 rpm & 6 bar (Figure 6.7(b)) in sea-level case. This was the only point in which the soot emission showed some sensitivity to the LP-EGR rate. Nevertheless, the low opacity and its minor variation (from 10% to 15%) as the boost pressure was decreased even at maximum LP-EGR rate in this case, besides the results corresponding to other points, contribute to advocate for low boost pressure settings at low engine load conditions.

Figure 6.9 illustrates the engine-out CO emissions and their conversion efficiency as a function of the boost pressure and LP-EGR rate. An engine operating point is represented in every row comparing again sea-level and 25°C with 2500 m and -10°C as ambient boundaries, in the same manner as Figures 6.7 and 6.8. The engine-out CO emission was mainly dependent on LP-EGR rate at sea-level case, with an increase as the LP-EGR rate did in the three operating points, i.e. in trade-off with NO_x emission. In addition, a sensitivity to the boost pressure also appeared at high LP-EGR rate producing the maximum engine-out CO emission at minimum boost pressure.

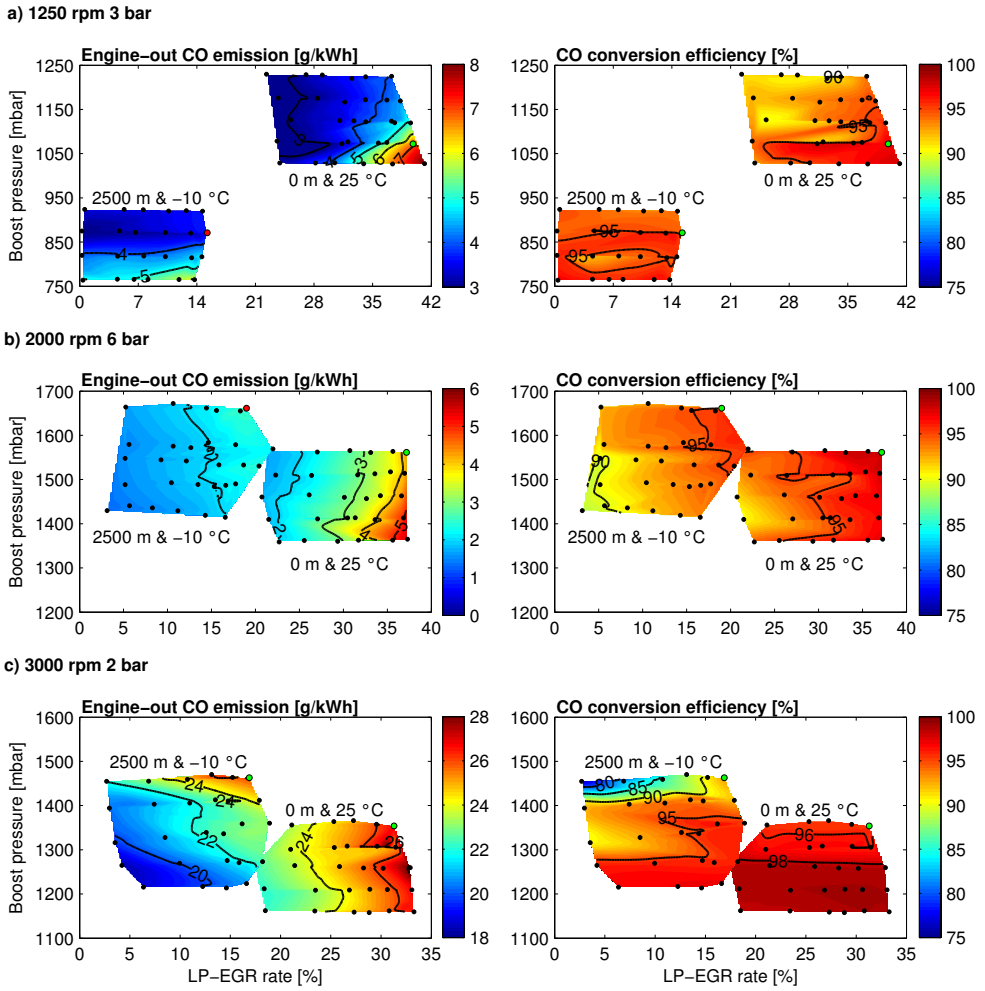

Figure 6.9: Engine-out CO emission and CO conversion efficiency as a function of the boost pressure and LP-EGR rate for sea-level at 25° C and 2500 m at -10° C: (a) 1250 rpm & 3 bar BMEP, (b) 2000 rpm & 6 bar BMEP and (c) 3000 rpm & 2 bar BMEP.

On the opposite, the main engine-out CO emission dependence moved to boost pressure at cold high altitude, along with a lower CO emission related to the lower LP-EGR rate in altitude operation. Nevertheless, the CO dependence on boost pressure in cold ambient resulted as a function of the

operating point, showing an increase with boost pressure in point 1250 rpm & 3 bar (Figure 6.9(a)), a decrease in point 3000 rpm & 2 bar (Figure 6.9(c)) and no sensitivity with the boost pressure in point 2500 rpm & 6 bar (Figure 6.9(b)).

According to these results, the general trend was a slight increase of the engine-out CO emissions in the region of interest, i.e. minimum boost pressure to increase the VGT outlet temperature combined with minimum BSFC and maximum LP-EGR rate to minimize NO_x emission, with respect to the baseline operating points.

The CO conversion efficiency is shown in the right column of Figure 6.9 for every operating point. The CO conversion efficiency yielded high values in agreement with VGT outlet temperatures above 190°C for all cases, as shown in Figure 6.6 even for to the most limiting ambient temperature (-10°C). It resulted on above 90% conversion efficiency with the only exception of cold altitude operation at 3000 rpm & 2 bar for high boost pressure and low LP-EGR rate settings.

In this last region, the CO conversion efficiency dropped to 80% evidencing sensitivity to the combination of the lowest VGT outlet temperature (Figure 6.6) and the maximum EATS mass flow (the lowest dwell time), which is represented in Figure 6.10. This last magnitude was governed by the highest air mass flow due to maximum boost pressure and minimum LP-EGR rate, which in turn led to maximum volumetric efficiency. Regarding the region of interest, the CO conversion efficiency showed its maximum, above 96%, in the three operating points for all ambient boundaries and compensated the slight increase in engine-out CO emission.

Similar results were obtained concerning HC abatement, as represented in Figure 6.11. The left column shows the engine-out HC emissions. These were kept very low with just certain trend to increase as the LP-EGR rate did as main rule. However, the lower HC reactivity in comparison to CO at medium-high temperature, where the HC adsorption on zeolites becomes negligible [3], gave as a result a more marked trend in HC conversion efficiency, which is depicted for every operating point in the right column of Figure 6.11.

As observed in row (a) of Figure 6.11, the HC conversion efficiency at 1250 rpm & 3 bar showed the major variability within the tested window at sea-level and 25°C in ambient temperature. For this case, the HC conversion efficiency is clearly governed by the boost pressure. Its decrease led to higher dwell time,

due to the exhaust mass flow decrease (Figure 6.10), and to higher temperature (VGT outlet temperature in Figure 6.3). Consequently, the HC conversion efficiency increased as the boost pressure was decreased. This was the case with the highest sensitivity due to the temperature range (190−210°C) around the light-off temperature [3].

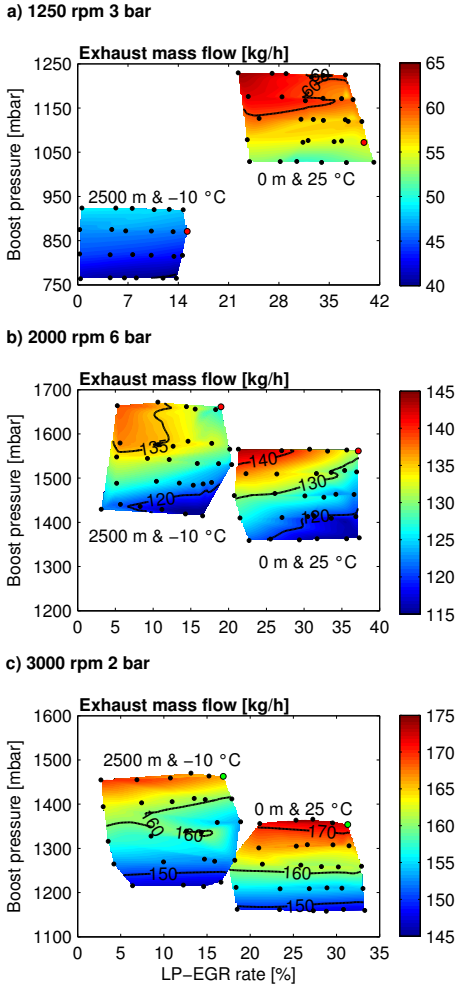

Figure 6.10: ATS mass flow as a function of the boost pressure and LP-EGR rate for sea-level at 25° C and 2500 m at -10° C: (a) 1250 rpm & 3 bar BMEP, (b) 2000 rpm & 6 bar BMEP and (c) 3000 rpm & 2 bar BMEP.

This behaviour was also found in cold altitude operation. In this case, the dwell time of the gas within the catalyst increased due to the lower boost pressure (lower exhaust mass flow) and the temperature moved to a higher range from 195 to $\sim$ 220°C (Figure 6.3). As a result, the HC conversion efficiency increased with respect to warm sea-level conditions. It varied from 65% at the highest boost pressure to 85% at the lowest one, corresponding to the maximum dwell time and VGT outlet temperature.

Similar results can be observed at 2000 rpm & 6 bar (Figure 6.11(b)) and 3000 rpm & 2 bar (Figure 6.11(c)), with clear trend to HC conversion efficiency increase as the boost pressure decreased, favoured by the temperature and dwell time, and regardless of the LP-EGR rate. As the CO case, despite the slight increase in engine-out HC emissions when applying this strategy, the conversion efficiency was also benefited, offsetting the drawbacks related to the optimal BSFC and NO_x emission calibration.

6.5 Summary and conclusions

In the present Chapter, the engine and aftertreatment performance were evaluated at different ambient pressure and temperature for low load operating conditions. The approach counted with an experimental study on the impact of extreme ambient boundaries defined by the driving altitude (sea-level to 2500 m) and ambient temperature (-10 to 45°C) on the performance and emissions of the Euro 6d-Temp engine which was used for all the experimental tests in this thesis.

The effect of the boost pressure and the LP-EGR rate were analysed putting focus on the fuel consumption and the exhaust temperature. The results highlighted that minimum specific fuel consumption could be obtained along with the highest VGT outlet temperature benefiting aftertreatment warm-up strategies. To reach them, the target boost pressure should be decreased towards maximum VGT opening without dependence on the LP-EGR rate, i.e. no limitations for NO_x emission control.

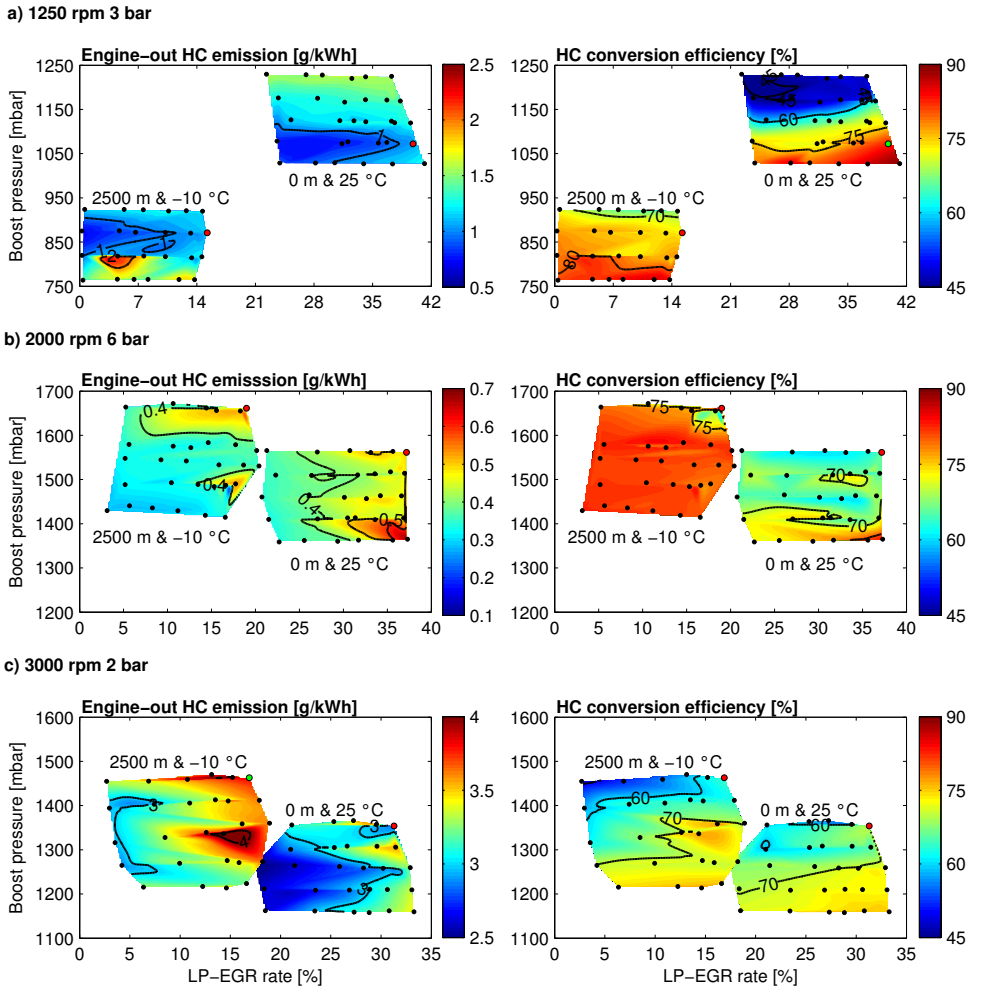

Figure 6.11: Engine-out HC emission and HC conversion efficiency as a function of the boost pressure and LP-EGR rate for sea-level at 25° C and 2500 m at -10° C: (a) 1250 rpm & 3 bar BMEP, (b) 2000 rpm & 6 bar BMEP and (c) 3000 rpm & 2 bar BMEP.

These trends were common in the three analysed points ranging from low to high speed and from 2 to 6 bar BMEP. Neither the variation of altitude nor ambient temperature did affect these calibration guidelines although more potential benefits on specific fuel consumption were found as the altitude increased. The reasons for the synergy between fuel consumption and exhaust

temperature after the VGT expansion was found in the combination of several processes. On the one hand, the VGT opening contributed to decrease the pumping losses. On the other hand, the low expansion ratio provided the maximum VGT outlet temperature taking advantage of the very high VGT inlet temperature resulting from the higher equivalence ratio with these boost settings.

The proposed guidelines for air management calibration were also supported by the trends in the pollutants emissions and the catalyst performance. The serial calibrated LP-EGR rate, which was the highest tested value for every altitude and ambient temperature, resulted compatible with low boost pressure setting. This combination led the engine-out NO_x emission to decrease with respect to the baseline one, being independent of the ambient boundary. Furthermore, an increase of the NO_x emission in altitude operation with respect to sea-level, which was caused by the LP-EGR rate decrease, was noticeable. This EGR reduction was required to provide the engine with similar fresh air mass flow as at sea-level operation.

The reduction of the NO_x emission did not show any relevant impact on the soot. It remained almost constant with respect to the serial engine calibration mostly due to the low equivalence ratio, despite of its increasing fashion with boost pressure reduction and LP-EGR rate increase. By contrast, the engine-out CO and HC emissions were slightly increased with these strategies, as a main trend, showing higher sensitivity to the equivalence ratio increase. Despite of this negative impact, the increase of CO and HC emission was restrained, keeping the emissions in the same order of magnitude as the baseline operating point at every altitude and ambient temperature. In fact, these slight increments were offset by the catalyst conversion efficiencies, which reached their maximum values at the lowest boost pressure and highest LP-EGR rates as a result of the higher exhaust temperature and catalyst.

Bibliography

[3] J. R. Serrano, P. Piqueras, E. J. Sanchis, and B. Diesel. “Analysis of the driving altitude and ambient temperature impact on the conversion efficiency of oxidation catalysts”. *Applied Sciences, 11, 1283* (2021) (cit. on pp. xii, 106, 107, 205, 206).

[4] V. Bermúdez, J. R. Serrano, P. Piqueras, and B. Diesel. "Fuel consumption and aftertreatment thermal management synergy in compression ignition engines at variable altitude and ambient temperature". *Internal Journal of Engine Research, Online First. https://doi.org/10.1177/14680874211035015* (2021) (cit. on pp. xii, 190).

[299] X. Wang, Y. Ge, and L. Yu. "Combustion and emission characteristics of a heavy-duty Diesel engine at idle at various altitudes". *SAE International Journal of Engines, 6 (2), 1145-1151* (2013) (cit. on p. 203).

Chapter 7

Concluding remarks

Contents

7.1 Introduction **212**
7.2 Main conclusions **213**
7.2.1 DOC response under extreme ambient conditions . 214
7.2.1.1 Role of flow properties on the EATS operation 214
7.2.1.2 DOC response to exhaust line thermal insulation 215
7.2.2 VGT actuation for DPF active regeneration under different altitudes 216
7.2.3 Engine calibration sensitivity 217
7.2.4 Final considerations 218
7.3 Future works **219**
7.3.1 Boundary conditions and experimental tests 219
7.3.2 Vehicle and EATS configurations 220
7.3.3 Active and passive strategies for the engine and EATS operation improvement 221
Bibliography **223**

7.1 Introduction

The conduction of this work was based on the ambient boundaries introduced in the newest emission legislations, forcing the homologation tests to be additionally carried out under a framework of a wide range of ambient temperatures and pressures. Those two variables affect the engine operation, finally impacting the EATS inlet gas flow conditions. Bibliographic evidences exposed in Chapter 2 included experimental end modelling analysis of this topic, leading to the interest for a deeper understanding, decomposing the phenomena happening in the engine and in the exhaust gases flow properties caused by extreme ambient conditions.

To do that, an experimental installation counting with a Diesel Euro 6d-Temp engine equipped with a DOC and a SCRf, which just covered the functionalities of a standard DPF, since the urea injection was inoperative, was implemented. For the emulation of the ambient conditions, the engine intake and exhaust were coupled to an altitude simulator to reproduce the desired engine inlet conditions of temperature and pressure. Additionally, the instrumental equipment made possible to capture the most relevant variables related to the engine and EATS performance for a proper analysis. The complete engine test bench description was approached in Chapter 3. In this Chapter, a description of the modelling tools, which were complementary employed in this work, was also conducted. They consisted of a 1D GT-Power engine model that counted with a user defined combustion sub-model and external turbocharger and aftertreatment sub-models implemented in VEMOD™.

The core engine model as well as the combustion and external turbocharger sub-models were firstly validated versus experimental full load tests and at low and partial engine range in Chapters 4 and 6. They provided an accurate prediction of the main combustion, boosting and combustion variables. The exhaust aftertreatment system sub-model that reproduced the DOC and DPF operation was also introduced in Chapter 3. An elevate accuracy was evidenced for the DOC and the DPF sub-models in terms of fluid-dynamic properties and pollutants abatement prediction.

In Chapter 4, it was discussed how the extreme altitude and temperature impact the DOC flow inlet conditions, influencing on the CO and HC conversion efficiency. This question was approached at low load engine operation points, when the DOC inlet temperature is around the light-off threshold, causing a higher environmental damage. The differences in the species conversion efficiency was decomposed, allowing the identification of how the emissions abatement physical processes are affected by the external ambient conditions. The role of the flow properties, including the dwell time and oxygen partial pressure on the DOC operation was analysed. Finally, passive strategies based on thermal insulation were computationally implemented to improve the EATS operation, and, in parallel, reduce the fuel consumption.

Chapter 5 was targeted to the analysis of the DPF active regeneration under several altitudes, evidencing the inlet temperature as the parameter dictating the regeneration reactivity but its high sensitivity to the driving altitude. The serial calibration for the active regeneration process was put into prove, also leading to the optimisation of VGT actuation during this event in altitude condition to be able to improve this EATS operation and reduce the fuel consumption penalty.

This thesis was concluded with the evaluation of the engine response when operating at regular mode of low partial loads under different ambient conditions of temperature and pressure. This study was addressed fully experimentally in Chapter 6, conducting the evaluation of the effect of the boosting and the LP-EGR rate strategies, based on bibliographic indications. An optimised calibration of the air management was finally proposed, agreeing between an optimised engine performance and pollutants conversion efficiency in the EATS.

7.2 Main conclusions

The current doctoral thesis was conducted according to the objectives outlined in Chapter 1. The first main objective focused on the evaluation of the extreme ambient conditions impact on the engine performance, tailpipe emissions and on the aftertreatment system's performance. This impact varies according to the imposed engine calibration. This way, the flow properties entering the EATS components suffer a previous influence and are consequently modified

according to the adopted calibration. This opened the way to the evaluation of the engine calibration role on the aftertreatment's response, combining with the application of possible active and passive solutions to improve the aftertreatment's operation, dealing with the drawbacks imposed by the extreme ambient conditions. Within this framework, a series of partial objectives were introduced, being accomplished over the main four Chapters of this doctoral thesis, 3 to 6. The main conclusions will be summarized in detail below, consolidating the ideas discussed in previous Chapters.

7.2.1 DOC response under extreme ambient conditions

The evaluation of the DOC response was carried out by performing experimental tests simulating warm sea-level (0 m and 20°C) and extreme operation in cold altitude (2500 m and -7°C). Departing from a cold and purged catalyst, the engine was run at operating points that were measured in steady-state, covering a common range of exhaust mass flows and catalyst inlet temperatures for both ambient conditions, so that the CO and HC light-off could be analysed. A deterioration of the CO and HC conversion efficiency at low temperature was observed at extreme conditions with different tendencies for each pollutant. Departing from the experimental results, the use of the model oriented the research towards the identification of the key flow parameters contributing to the variation of CO and HC conversion efficiency.

7.2.1.1 Role of flow properties on the EATS operation

The experimental results allowed to evidence the deterioration of the CO and HC conversion efficiency in the extreme ambient conditions, shifting the CO and HC light-off towards higher temperatures. The conversion efficiency sensitivity to the exhaust mass flow was also stated for both pollutants but with different trends. Through the modelling analysis, those different tendencies between the CO and HC conversion efficiencies were better identified, highlighting the role of the adsorption process in the HC conversion efficiency. Whereas a very marked decrease on CO conversion efficiency was stated at 2500 m and -7°C for low exhaust mass flow operation, this penalty progressively decreased by increasing the exhaust mass flow.

The DOC presented a higher damage for the HC abatement in extreme ambient conditions, for which temperatures higher than 150°C were needed to reach the light-off at low exhaust mass flow. At extreme ambient conditions, the HC adsorption on the transient cold start process impacted relevantly the oxidation conversion efficiency when higher exhaust temperatures were reached. The reason was the higher engine-out HC partial pressure emission present in cold altitude, which accelerated the adsorption rate. Consequently, the adsorption to desorption reaction rate was increased, despite the lower ambient pressure found in altitude. This process leaded to the increase on the HC surface coverage and further damage on the HC oxidation conversion efficiency due to the oxidation inhibition.

Further analysis of the modelling results and the literature review with respect to the DOC boundary conditions indicated the pollutants partial pressure and dwell time as determinants for the DOC response. The analysis of those factors evidenced, from one side, the inherent influence of the lower ambient pressure noted in altitude conditions. After the VGT expansion, the exhaust pressure is thus lower, and so the gas density, leading to a higher flow velocity, and, consequently, a lower dwell time in altitude operation. From the other side, the O_2 partial pressure was not always lower in altitude condition because its level depended on other engine parameters, like equivalence ratio, together with the EGR ratio, boost pressure or EATS inlet temperature.

In summary, increase on the engine speed, fuel mass flow and boost pressure can lead to the similar exhaust temperatures in cold altitude as in sea-level. It was stated, however, that the applied engine calibration, which consisted in closing the LP-EGR and the VGT was not enough to avoid the excessive CO and HC pollutants partial pressures and the oxidation inhibition at very low temperatures.

7.2.1.2 DOC response to exhaust line thermal insulation

Included in the discussion about the DOC performance at extreme ambient conditions, the application of exhaust line thermal insulation for the improvement of the pollutants conversion efficiency was performed in warm sea-level and cold altitude ambient conditions.

From a modelling perspective, exhaust ports and turbine thermal insulation strategies were applied in an Euro 4 engine. Both solutions demonstrated good results in terms of EATS inlet temperature enhancement and BSFC reduction. When those strategies were applied separately, it could be observed that, due to higher temperature at the turbine inlet or lower temperature drop across the VGT, it operated in opener positions. It represented a decrease in the VGT inlet pressure and thus lower pumping losses. Additionally, the combination of both solutions was evaluated, showing a synergistic result. When simulated on the studied Euro 6d-Temp Diesel engine model, for the same experimentally studied points, an increment on temperature of up to 50°C for warm sea-level and 60°C for cold altitude was observed at the turbine outlet. This increment represented an increase of around 40% in CO and HC conversion efficiency for any ambient conditions, demonstrating the potential of this strategy in extreme ambient conditions.

7.2.2 VGT actuation for DPF active regeneration under different altitudes

A complementary research was undertook in the next component following the exhaust line of a common Euro 6 Diesel engine, the DPF. The impact of the VGT position during active regeneration strategies on the regeneration dynamics of the wall-flow monoliths was evaluated as a function of the driving altitude, which comprised sea-level, 1300 m and 2500 m, and the initial soot load. Each condition was tested experimentally and further reproduced in the DPF computational model.

The serial ECU calibration imposed the same injection strategy in all cases, but the VGT position was closer with the increasing altitude. In the case of 2500 m, the VGT was even completely closed. With this engine calibration, it was observed an important reduction of the soot depletion rate as the altitude increased, together with a higher sensitivity to the DPF initial pressure drop. In parallel, the balance point between filtration and soot oxidation was reached at higher soot levels in the DPF as the altitude increased. This was attributed to the lower DPF inlet temperature, that damaged the fuel post-injection efficiency. In spite of the positive impact that lower temperature caused to the O_2 surface coverage, it did not compensate the drastic decrease on thermal levels in the DPF inlet. In fact, altitude regenerations required higher DPF inlet temperature than sea-level cases to compensate the lower

gas pressure conditions found in altitude. It was additionally seen that the higher temperature can compensate, in turn, the negative effect on the surface coverage caused by the lower O_2 partial pressure.

The potential of the boosting strategy adaptation for the active regeneration optimisation was next contrasted experimentally against the initial baseline results at sea-level. By applying opener VGT positions, the engine torque was improved at the same time as the soot depletion rate was increased. These results were obtained due to the higher equivalence ratio and lower VGT expansion ratio evidenced at opened VGT positions. In fact, the opener VGT provided the same depletion rate profile at 1300 m and 2500 m as at sea-level operation, highlighting the positive impact of the correct VGT position calibration during active regeneration events. The optimised engine calibration also contributed to the decrease of tailpipe gaseous pollutant emissions.

7.2.3 Engine calibration sensitivity

The importance of the engine boosting calibration for the aftertreatment system optimised performance was further evidenced. Other variables, as the LP-EGR rate also revealed an important impact on the EATS results. In this regard, the sensitivity of those two variables was analysed for the engine operation at partial loads, seeking to identify the engine behaviour in terms of performance and the EATS boundary conditions.

Experimental tests were performed at sea-level, 1300 m and 2500 m for the temperatures of -10°C, 25°C and 45°C. For every combination, the sensitivity of the VGT opening and the LP-EGR was evaluated. The results highlighted that, when working in partial loads, the target boost pressure should be decreased towards maximum VGT opening and high LP-EGR rate for an optimum NO_x emission control. While the VGT opening represented a decrease in pumping losses, the lower expansion ratio and the higher VGT inlet temperature resulting from the higher equivalence ratio with these boost settings contributed the increase the VGT outlet temperature in all ambient conditions.

In agreement with the literature review, in the tested engine, the serial calibration decreased the LP-EGR rate when operating in altitude to provide the engine with a similar fresh air mass flow as at sea-level operation. This

course of action contributed to the NO_x emissions increase. However, the strategy of opening the VGT presented a positive effect for NO_x emission. Its decrease was attributed to the in-cylinder temperature decay related to the combustion delay, which was, in turn, promoted by the ignition delay produced by the poorer mixing ratio. This strategy also presented no relevant impact for soot emission, which was kept in low levels. The CO and HC emissions were mainly increased through this strategy application, being however restrained by the higher EATS inlet temperature, which provided maximum DOC conversion efficiency of both pollutants in all studied cases. In summary, at low partial loads, working at an opener VGT position resulted positive for the engine operation, presenting no damage for the tailpipe emissions, and being therefore a plausible and consistent strategy to be applied for the engine operation.

7.2.4 Final considerations

To conclude the results brought by the investigations performed and presented in this thesis, some final considerations can be extracted. Regarding the extreme ambient conditions, special focus was given to low ambient temperatures and high altitude operation. It turns out that the low air pressure found in these conditions is precisely the key parameter impairing a good engine, DOC and DPF performance. By means of fundamental parameters recalibration, this drawback implied by the lower air pressure can be minimized. The studied approach consisted on the LP-EGR valve closure to allow more air mass flow in the cylinders, adding the positive effect of opening the VGT to decrease pumping losses. By this action, the engine performance in altitude can even equalize the one at sea-level at the expense of lower O_2 availability for the EATS operation.

Regarding the EATS operation in altitude, the low air pressure conditions the dwell time. This factor combined with the O_2, the pollutants partial pressure and EATS inlet temperature are determinant for the aftertreatment operation. Those three parameters are, however, a consequence of not only the low air pressure but also of the previous engine settings, as the equivalence ratio, LP-EGR rate and VGT opening. It was seen, for example, how the LP-EGR reduction is essential for the DOC and DPF regeneration operations in normal mode, supplying the adequate O_2 partial pressure. However, this reduction was not enough to avoid the delay on the CO and HC

pollutant's light-off temperature for the conversion in the DOC. Increases on the equivalence ratio are from one side positive, representing an increase on the exhaust temperature, but negative in terms of air mass flow rate availability.

Additionally, the VGT opening until matching an optimum value can contribute to a higher exhaust temperature due to the lower VGT expansion ratio and the equivalence ratio decrease, although offsetting the gain in O_2 partial pressure produced by the LP-EGR reduction. This is positive for the normal EATS operation as well as for the DPF in regeneration mode. By contrast, the VGT opening damages the HC and CO pollutants partial pressure, with secondary influence from the applied LP-EGR rate. This argument plays in favour of a LP-EGR increase as a way to minimize the NO_x emissions during normal engine operation. Nevertheless, during the DPF regeneration mode the VGT opening and LP-EGR reduction represents a positive engine control to avoid the engine torque derating. Additionally, this strategy maximizes the soot oxidation rate, limiting the time where a high NO_x emission is evidenced due to the reduced LP-EGR rate.

7.3 Future works

The conclusions reached from the studied cases led to the understanding of the engine and EATS behaviour in different ambient conditions. Furthermore, it made possible the access of optimised passive and active strategies to overcome the drawbacks caused by extreme ambient conditions. Departing from a solid basis established in this doctoral thesis, several topics which were treated in the present work are worth of further investigation. Some aspects that should be further considered are presented next.

7.3.1 Boundary conditions and experimental tests

- In the current thesis, the focus was put on the study of the engine and aftertreatment response in well controlled steady state conditions looking for an easier identification of the governing parameters explaining the change in EATS and engine response. To give continuity to this work, a first step could be to perform transient tests or duty cycles like the WLTC or RDE. Besides, the inclusion of altitude and temperature

variation over the tests to simulate the example of a current up- or downhill driving conditions is feasible through the altitude simulator MEDAS correct setup. It is also worth of investigation, since those are examples of validation tests imposed by the current regulations [26]. Similar conclusions should be obtained related to the DOC operation and during DPF active regenerations and their operation relationship with the flow properties, which are in turn marked by the engine calibration.

- Departing from the altitude and temperatures boundaries considered in the current regulation, which range from 0 to 1300 m and -7 to 35°C, respectively, a further considerable approach is the evaluation of extra variables that can be possibly covered in further norms [46]. One example is the evaluation of the ambient humidity for the engine response in terms of performance, emissions and EATS boundaries. Some studies have approached the effects of condensation [123] on the engine and the effect of water injection in the EATS [300]. This know-how at CMT-Motores Térmicos can be used as guidelines for the study of the humidity in the engine and EATS performance. Further studies can be based on these ideas to evaluate the sensibility of this variable on the engine and EATS calibration and control.

7.3.2 Vehicle and EATS configurations

- The DPF operation can be further studied, considering other important parameters involved in its operation. An example is the evaluation of extreme operating conditions impact on the particle size distribution and, in turn, on the filtration process concerning efficiency and pressure drop, to understand how the ambient conditions are related with the phenomena of nucleation and aggregation to complement the study of soot depletion.

- The current work was focused on a Diesel engine complying with a Euro 6d-Temp regulations, in which the studied aftertreatment systems were the DOC and the DPF. For future works, other current vehicle configurations should be evaluated, which can be approached by means of testing and modelling. Following this line, the NO_x abatement aftertreatment, with focus on the most extended SCR may be further considered. Those devices count with additional mechanisms based on

the principles to eliminate the nitrogen oxides emissions. In the SCR, a gaseous reductant, typically urea, is added to the flow stream or exhaust gas and adsorbed onto a catalyst to react with the nitrogen oxides forming N_2 and H_2O [84]. Those mechanisms must be individually considered, evaluating the kinetic of each additional reaction for the case of lower exhaust gas pressure and different ambient temperatures, so that the key flow properties can be identified. The effects on the ammonia slip as well as the performance of the ASC should also be considered.

- Regarding the models development, the studies performed in this thesis recalled the need to count with dynamic models suitable for catalyzed DPFs. The current model adopted in this thesis did not take into account the catalytic coating. The eventual implementation of the SCR system into the DPF would the demand the model to include the corresponding reaction mechanism.

- There is also an open field to study the comparable GDI Euro 6 engine at severe ambient condition. Current studies in which this topic was already approached, as McCaffery *et al.* [135] and Ko *et al.* [301], evaluated pollutant and particles emissions from GDI conducting RDE cycles at high-altitude. Following this basis, similar objectives could be applied for the researches on GDI systems, leading the focus to pollutant emissions formation and control with emphasis in understanding. In terms of EATS, it means to study the impact caused by different ambient temperature and pressure on the TWC and GPF boundary conditions and performance.

- The impact of the hybridization in the vehicles must be taken into account, specially due the more frequent and severe cold-starts performed in this kind of vehicle architectures due to the combination with the electric motor. To evidence how quickly the EATS can be preheated for their operation at extreme ambient conditions is eligible for further research.

7.3.3 Active and passive strategies for the engine and EATS operation improvement

- The work performed concerning the DPF regeneration could be further explored, increasing the parameters involved in the optimisation process.

Those may consist on the evaluation of the injection strategy and the EGR rate, for example.

- Regarding passive strategies, the continuity of the work developed in Chapter 4 could be an interesting approach to further improve the EATS and engine operation. For the analysed thermal insulation solutions, the still considerable gap between the adiabatic and the feasible results stated in Figure 4.34 leaves the way open for further optimisation, including the possibility of combination with other passive strategies. The implementation of other materials for the thermal insulation or combination between strategies involving different valve lift profiles of different exhaust line lengths to decrease the thermal loss, as in the work of Arnau *et al.* [218] or Serrano *et al.* [217], could be an initial further step about this topic.

- The further implementation and development of other passive solutions for EATS inlet temperature enhancement as introduced in the literature, as the TES and PCM methods for exhaust gas thermal energy storage has still a high potential to be covered. Those methods can represent a feasible solution to avoid the huge temperature drop in the exhaust line between driving cycles, specially under extremely cold environments. Departing from the conclusions obtained about the role of the flow properties on the EATS operation and the DOC response over the exhaust line thermal insulation, the TES and PCM method can be applied in combination with WLTC or RDE cycles, where engine shut-off periods are present, to evaluate the potential of the CO and HC emission reduction in extreme ambient conditions.

- Finally, the evaluation of the CO and HC conversion efficiencies response to the experimental or modelling application of e-catalysts over extended ranges of ambient pressures and temperatures is an interesting topic to be further evaluated. The sensitivity of the electrical resistance on the flow properties like dwell time and pollutants partial pressure can be considered by analysing similar catalyst characterization tests as the ones performed in the current theses with those devices. The results can give a good overview about the feasibility of electrical heated catalysts at extreme ambient conditions.

Bibliography

[26] *Commission Regulation (EU) 2017/1154 of 7 June 2017 amending Regulation (EU) 2017/1151 supplementing Regulation (EC) No 715/2007 of the European Parliament and of the Council on type-approval of motor vehicles with respect to emissions from light passenger and commercial vehicles (Euro 5 and Euro 6) and on access to vehicle repair and maintenance information, amending Directive 2007/46/EC of the European Parliament and of the Council, Commission Regulation (EC) No 692/2008 and Commission Regulation (EU) No 1230/2012 and repealing Regulation (EC) No 692/2008 and Directive 2007/46/EC of the European Parliament and of the Council as regards real-driving emissions from light passenger and commercial vehicles (Euro 6) (Text with EEA relevance).* 2017 (cit. on pp. 3, 4, 220).

[46] A. Joshi. "Review of vehicle engine efficiency and emissions." In: *SAE Technical Paper 2020-01-0352.* 2020 (cit. on pp. 16, 220).

[84] F. Gao, X. Tang, H. Yi, S. Zhao, C. Li, J. Li, Y. Shi, and X. Meng. "A review on selective catalytic reduction of NO_x by NH_3 over Mn-based catalysts at low temperatures: Catalysts, mechanisms, kinetics and DFT calculations". *Catalysts, 7, 199* (2017) (cit. on pp. 21, 221).

[123] J. Galindo, P. Piqueras, R. Navarro, D. Tarí, and C. M. Meano. "Validation and sensitivity analysis of an in-flow water condensation model for 3d-CFD simulations of humid air streams mixing". *International Journal of Thermal Sciences, 136, 410-419* (2019) (cit. on pp. 24, 220).

[135] C. McCaffery, H. Zhua, C. Li, T. D. Durbin, K. C. Johnson, H. Jung, R. Brezny, M. Geller, and G. Karavalakis. "On-road gaseous and particulate emissions from GDI vehicles with and without gasoline particulate filters (GPFs) using portable emissions measurement systems (PEMS)". *Science of the Total Environment. 710. 136366* (2020) (cit. on pp. 27, 221).

[217] J. R. Serrano, P. Piqueras, R. Navarro, J. Gómez, M. Michel, and B. Thomas. "Modelling analysis of aftertreatment inlet temperature dependence on exhaust valve and ports design parameters". In: *SAE Technical Paper 2016-01-0670.* 2016 (cit. on pp. 39, 74, 222).

[218] F. J. Arnau, J. Martín, B. Pla, and A. Auñón. "Diesel engine optimization and exhaust thermal management by means of variable valve train strategies". *Internal Journal of Engine Research, 22 (4), 1196-1213* (2021) (cit. on pp. 39, 222).

[300] V. Bermúdez, J. R. Serrano, P. Piqueras, and O. García-Afonso. "Pre-DPF water injection technique for pressure drop control in loaded wall-flow diesel particulate filters". *Applied Energy, 140, 234-245* (2015) (cit. on p. 220).

[301] J. Ko, K. Kim, W. Chung, C.-L. Myung, and S. Park. "Characteristics of on-road particle number (PN) emissions from a GDI vehicle depending on a catalytic stripper (CS) and a metal-foam gasoline particulate filter (GPF)". *Fuel, 238, 363-374* (2019) (cit. on p. 221).

Global bibliography

[1] J. M. Luján, J. R. Serrano, P. Piqueras, and B. Diesel. "Turbine and exhaust ports thermal insulation impact on the engine efficiency and aftertreatment inlet temperature." *Applied Energy, 240, 409-423* (2019) (cit. on pp. xii, 106, 107).

[2] J. R. Serrano, P. Piqueras, E. J. Sanchis, and B. Diesel. "A modelling tool for engine and exhaust aftertreatment performance analysis in altitude operation". *Results in Engineering, 4, 100054* (2019) (cit. on pp. xii, 66).

[3] J. R. Serrano, P. Piqueras, E. J. Sanchis, and B. Diesel. "Analysis of the driving altitude and ambient temperature impact on the conversion efficiency of oxidation catalysts". *Applied Sciences, 11, 1283* (2021) (cit. on pp. xii, 106, 107, 205, 206).

[4] V. Bermúdez, J. R. Serrano, P. Piqueras, and B. Diesel. "Fuel consumption and aftertreatment thermal management synergy in compression ignition engines at variable altitude and ambient temperature". *Internal Journal of Engine Research, Online First. https://doi.org/10.1177/14680874211035015* (2021) (cit. on pp. xii, 190).

[5] P. Piqueras, R. Burke, E. J. Sanchis, and B. Diesel. "Fuel efficiency optimisation based on boosting control of the particulate filter active regeneration at high driving altitude". *Under review. Fuel* (2022) (cit. on pp. xii, 167).

[6] N. Otto. "Improvement in gas-motor engines". Pat. US194047A. 1877 (cit. on p. 2).

[7] R. Diesel. "Internal combustion engine". Pat. US608845A. July 15, 1895 (cit. on p. 2).

[8] F. Sass. *Geschichte des deutschen Verbrennungsmotorenbaus von 1860 bis 1918*. German. Springer, 1962 (cit. on p. 2).

[9] O. von Fersen. *Ein Jahrhundert Automobiltechnik: Personenwagen*. German. Springer, 1986 (cit. on p. 2).

[10] BorgWarner. *Turbo Systems History. Available in: https://www.borgwarner.com/technologies/boosting-technologies. (accessed on 24 November 2021)* (cit. on p. 2).

[11] *Car Throttle. CRDI (common rail direct injection) and its history. Available in: https://www.carthrottle.com/post/y88zde8/. (accessed on 24 November 2021)* (cit. on p. 2).

[12] B. Stewart. *The 15 most important automotive tech milestones of the last 25 years. Available in: https://www.popularmechanics.com/cars/g2778/most-important-automotive-tech-milestones/. (accessed on 24 November 2021)*. Ed. by PopularMechanics. 2016 (cit. on p. 2).

[13] K. Wittek, F. Geiger, and M. G. Justino Vaz. "Characterization of the system behaviour of a variable compression ratio (VCR) connecting rod with eccentrically piston pin suspension and hydraulic moment support". *Energy Conversion and Management, 213, 112814* (2020) (cit. on p. 2).

[14] Z. Dimitrova, M. Tari, P. Lanusse, F. Aioun, and X. Moreau. "Development and control of a camless engine valvetrain". *IFAC-Papers OnLine, 52 (5), 399-404* (2019) (cit. on p. 2).

[15] EPAGOV. *History of reducing air pollution from transportation in the United States. Available in: https://www.epa.gov/transportation-air-pollution-and-climate-change/accomplishments-and-success-air-pollution-transportation. (accessed on 24 November 2021)*. 2021 (cit. on p. 2).

[16] *Earth Observatory NASA. Global warming. Available in: https://earthobservatory.nasa.gov/features/GlobalWarming/page2.php. (accessed on 24 November 2021)*. June 3, 2010 (cit. on p. 2).

[17] S. V. Venkataraman, S. Iniyan, and R. Goic. "A review of climate change, mitigation and adaptation". *Renewable and Sustainable Energy Reviews, 16 (1), 878-897* (2012) (cit. on p. 2).

[18] I. A. Reşitoğlu, K. Altinişik, and A. Keskin. "The pollutant emissions from Diesel-engine vehicles and exhaust aftertreatment systems". *Clean Technologies and Environmental Policy, 17, 15-27* (2015) (cit. on pp. 2, 17, 20).

[19] W. K. C. Morgan, R. B. Regerf, and D. M. Tucker. "Health effects of Diesel emissions". *The Annals of Occupational Hygiene, 41 (6), 643-658* (1997) (cit. on p. 2).

[20] J. N. S. Vianna, A. V. Reis, A. B. d. S. Oliveira, A. G. Fraga, and M. T. de Sousa. "Reduction of pollutants emissions on SI engines - accomplishments with efficiency increase". *Journal of the Brazilian Society of Mechanical Sciences and Engineering, 27, 3* (2005) (cit. on p. 3).

[21] N. Ladommatos, S. Abdelhalim, and H. Zhao. "The effects of exhaust gas recirculation on diesel combustion and emissions". *Internal Journal of Engine Research, 1, 107-126* (2000) (cit. on p. 3).

[22] TOTAL. *TOTAL explains how the Lean* NO_x *Trap (LNT) works, the alternative to the selective catalytic reduction (SCR). Available in: https://www.lubricants.total.com/news-press-releases/system. (accessed on 24 November 2021).* 2017 (cit. on p. 3).

[23] M. Soleimani, F. Campean, and D. Neagu. "Reliability challenges for automotice aftertreatment systems: A state-of-the-art perspective". *Procedia Manufacturing 16, 75-82* (2018) (cit. on pp. 3, 28).

[24] K. Kuklinska, L. Wolska, and J. Namiesnik. "Air quality policy in the U.S. and the EU - a review". *Atmospheric Pollution Research 6, 129-137* (2015) (cit. on p. 3).

[25] *Euro 1 emissions legislation. 91/441/EEC Council Directive 91/441/EEC of 26 June 1991 amending Directive 70/220/EEC on the approximation of the laws of the Member States relating to measures to be taken against air pollution by emissions from motor vehicles. Available in: eur-lex.europa.eu. (accessed on 24 November 2021).* 1991 (cit. on p. 3).

[26] *Commission Regulation (EU) 2017/1154 of 7 June 2017 amending Regulation (EU) 2017/1151 supplementing Regulation (EC) No 715/2007 of the European Parliament and of the Council on type-approval of motor vehicles with respect to emissions from light passenger and commercial vehicles (Euro 5 and Euro 6) and on*

access to vehicle repair and maintenance information, amending Directive 2007/46/EC of the European Parliament and of the Council, Commission Regulation (EC) No 692/2008 and Commission Regulation (EU) No 1230/2012 and repealing Regulation (EC) No 692/2008 and Directive 2007/46/EC of the European Parliament and of the Council as regards real-driving emissions from light passenger and commercial vehicles (Euro 6) (Text with EEA relevance). 2017 (cit. on pp. 3, 4, 220).

[27] *Commission Regulation (EU) 2017/1151 of 1 June 2017 supplementing Regulation (EC) No 715/2007 of the European Parliament and of the Council on type-approval of motor vehicles with respect to emissions from light passenger and commercial vehicles (Euro 5 and Euro 6) and on access to vehicle repair and maintenance information, amending Directive 2007/46/ EC of the European Parliament and of the Council, Commission Regulation (EC) No 692/2008 and Commission Regulation (EU) No 1230/2012 and repealing Commission Regulation (EC) No 692/2008 (Text with EEA relevance)*. 2017 (cit. on pp. 3, 16, 73).

[28] P. Arya, F. Millo, and F. Mallamo. "A fully automated smooth calibration generation methodology for optimization of latest generation of automotive Diesel engines". *Energy 178, 1, 334-343* (2019) (cit. on p. 4).

[29] J. Gómez. "Development of an altitude simulator and analysis of the performance and emissions of turbocharged Diesel engines at different altitudes". PhD thesis. UPV, 2018 (cit. on pp. 4, 72).

[30] *Green Car Congress. Available in: https://www.greencarcongress.com/2020/05/20200513-acea.html. (accessed on 24 November 2021)*. 2020 (cit. on p. 4).

[31] J. R. Serrano, R. Novella, and P. Piqueras. "Why the development of internal combustion engines is still necessary to fight against global climate change from the perspective of transportation". *Applied Sciences, 9 (21), 4597* (2019) (cit. on p. 4).

[32] *UNEP - World Conservation Monitoring Centre. The delineation of European mountain areas. Available in: https://ec.europa.eu/regional_policy/sources/docgener/studies/pdf/montagne/mount4.pdf (accessed on 24 November 2021)*. 2000 (cit. on pp. 4, 22).

[33] J. R. Serrano, P. Piqueras, A. Abbad, R. Tabet, S. Bender, and J. Gómez. "Impact on reduction of pollutant emissions from passenger cars when replacing Euro 4 with Euro 6d Diesel engines considering the altitude influence". *Energies, 12, 1278-1302* (2019) (cit. on pp. 4, 16, 26, 39).

[34] S. D'Ambrosio, A. Ferrari, E. Spessa, L. Magroa, and A. Vassallo. "Impact on performance, emissions and thermal behavior of a new integrated exhaust manifold cylinder head Euro 6 Diesel engine". In: *SAE Technical Paper 2013-24-0128.* 2013 (cit. on p. 4).

[35] H. Giraldo and J. I. Huertas. "Real emissions, driving patterns and fuel consumption of in-use diesel buses operating at high altitude". *Transportation Research Part D, 77, 21-36* (2019) (cit. on pp. 4, 26).

[36] J. M. Luján, H. Climent, S. Ruiz, and A. Moratal. "Influence of ambient temperature on Diesel engine raw pollutants and fuel consumption in different driving cycles". *Internal Journal of Engine Research, 20 (8-9), 877-888* (2019) (cit. on pp. 4, 23).

[37] Y. Wang, Y. Ge, J. Wang, X. Wang, H. Yin, L. Hao, and J. Tan. "Impact of altitude on the real driving emission (RDE) results calculated in accordance to moving averaging window (MAW) method". *Fuel, 277, 117929.* (2020) (cit. on pp. 4, 26).

[38] H. Zhou, H. Zhao, Q. Fenf, Z. Yin, J. Li, K. Qin, M. Li, and L. Cao. "Effects of environmental parameters on real-world NO_x emissions and fuel consumption for heavy-duty diesel trucks using an OBD approach". In: *SAE Technical Paper 2018-01-1817.* 2018 (cit. on pp. 4, 27).

[39] A. Ramos, R. García-Contreras, and O. Armas. "Performance, combustion timing and emissions from a light duty vehicle at different altitudes fueled with animal fat biodiesel, GTL and diesel fuels". *Applied Energy, 182, 507-517* (2016) (cit. on pp. 4, 26, 27, 120).

[40] L. Yu et al. "Experimental investigation of the impact of biodiesel on the combustion and emission characteristics of a heavy duty Diesel engine at various altitudes". *Fuel, 115, 220-226* (2014) (cit. on pp. 4, 26, 27).

[41] J. Gao, A. Tian G.and Sorniotti, A. E. Karci, and R. Di Palo. "Review of thermal management of catalytic converters to decrease engine emissions during cold start and warm up". *Applied Thermal Engineering, 147, 177-187* (2019) (cit. on pp. 4, 29).

[42] M. Lapuerta, O. Armas, J. R. Agudelo, and C. A. Sánchez. "Study of the altitude effect on internal combustion engine operation. Part 1: Performance". *Información Tecnológica, 17, 5* (2006) (cit. on p. 4).

[43] L. Shen and Y. Shen. "Combustion process of Diesel engines at regions with different altitude". In: *SAE Technical Paper 950857*. 1995 (cit. on pp. 4, 26).

[44] M. R. Hamedi, O. Doustdar, A. Tsolakis, and J. Hartland. "Thermal energy storage system for efficient diesel exhaust aftertreatment at low temperatures". *Applied Energy, 235, 874-887* (2019) (cit. on pp. 4, 37, 126).

[45] P. Piqueras, A. García, J. Monsalve-Serrano, and M. J. Ruiz. "Performance of a diesel oxidation catalyst under diesel-gasoline reactivity controlled compression ignition combustion conditions". *Energy Conversion and Management, 196, 18-31* (2019) (cit. on pp. 5, 30, 31, 89, 107, 122).

[46] A. Joshi. "Review of vehicle engine efficiency and emissions." In: *SAE Technical Paper 2020-01-0352*. 2020 (cit. on pp. 16, 220).

[47] *Council Directive 91/441/EEC of 26 June 1991 amending Directive 70/220/EEC on the approximation of the laws of the Member States relating to measures to be taken against air pollution by emissions from motor vehicles. Available in: eur-lex.europa.eu. (accessed on 24 November 2021)* (cit. on p. 16).

[48] A. Zardini and P. Bonnel. "Real driving emissions regulation: European methodology to fine tune the EU real driving emissions data evaluation method, EUR 30123 EN". *Publications Office of the European Union, Luxembourg, ISBN 978-92-76-17157-7* (2020) (cit. on p. 16).

[49] R. Suarez-Bertoa, M. Pechout, M. Vojtíšek, and C. Astorga. "Regulated and non-regulated emissions from Euro 6 diesel, gasoline and CNG vehicles under real-world driving conditions". *Atmosphere* (2020) (cit. on p. 16).

[50] *Delphi Technologies. Worldwide emissions standards: Passenger cars and light duty vehicles 2019-2020.* Delphi Technologies, 2019 (cit. on p. 16).

[51] *Delphi Technologies. Worldwide emissions standards: Passenger cars and light duty vehicles 2017-2018.* 2017 (cit. on p. 16).

[52] *China's stage 6 emission standard for new light-duty vehicles (final rule).* International Council on Clean Transportation (ICCT), 2012 (cit. on p. 16).

[53] *Flash Cleaner Machine. Available in: https://flashcleanermachine.com/italiano-euro-standard/?doing_wp_cron=1612006181. 2863910198211669921875. (accessed on 24 November 2021)* (cit. on p. 17).

[54] R. Prasad and V. R. Bella. "A review on diesel soot emission, its effect and control". *Bulletin of Chemical Reaction Engineering & Catalysis, 5 (2), 69-86* (2010) (cit. on p. 17).

[55] M. A. H. M. Nawi, M. H. M. Hanid, W. A. Mustafa, and R. I. R. Kasim M. S. Abdullah. "Pollutant emission in Diesel engine". In: *SympoSIMM 2019: Intelligent Manufacturing and Mechatronics, 288-298, Malaysia.* 2019 (cit. on p. 18).

[56] *EPA, Effects of Air Pollutants - Health Effects, Available in: http://www.epa.gov/apti/course422/ap7a.html. (accessed on 24 November 2021)* (cit. on p. 18).

[57] C. W. Wu, R. H. Chen, J. Y. Pu, and T. H. Lin. "The influence of air-fuel ratio on engine performance and pollutant emission of an SI engine using ethanol-gasoline-blended fuels". *Atmospheric Environment, 38, 7093-7100* (2004) (cit. on p. 18).

[58] M. R. Sumanlal, S. Nandakumar, and P. Mohanan. "The effect of air preheating on the performance and emission characteristics of a DI Diesel engine achieving HCCI mode of combustion". *International Journal of Theoretical and Applied Mechanics, 12 (3), 411-421* (2017) (cit. on p. 18).

[59] W. M. Pitts. "The global equivalence ratio concept and the formation mechanisms of carbon monoxide in enclosure fires". *Progress in Energy and Combustion Science, 21, 197-237* (1995) (cit. on p. 18).

[60] T. Alger, T. Chauvet, and Z. Dimitrova. "Synergies between high EGR operation and GDI systems". *SAE International Journal of Engines, 1 (1), 101-114* (2008) (cit. on p. 18).

[61] J. T. Kashdan, P. Anselmi, and B. Walter. "Advanced injection strategies for controlling low-temperature diesel combustion and emissions". *SAE International Journal of Engines, 2 (1), 1835-1856* (2009) (cit. on p. 19).

[62] K. N. Abdalla and E. A. Mustafa. "Effect of exhaust gas recirculation on CO emissions from a turbocharged Diesel engine". *UofKEJ, 4 (2), 43-48* (2014) (cit. on p. 19).

[63] Y. Hardalupas, C. Hong, C. Keramiotis, G. K. Ramaswamy, A. M. K. P. Soulopoulos N. Taylor, D. Touloupis, and M. A. Vourliotakis G. Founti. "Towards identifying flame patterns in multiple, late injection schemes on a single-cylinder optical Diesel engine". *Combustion Science and Technology, 188, 2217-2235* (2016) (cit. on p. 19).

[64] D. Demers and G. Walters. *Guide to exhaust emission control options.* Ed. by B. BAeSAME. 1999 (cit. on p. 19).

[65] R. K. Dadi, K. Daneshvar, D. Luss, V. Balakotaiah, C. M. Kalamaras, and W. Epling. "Comparison of light-off performance of Pt-Pd/γ-Al2O3 dual layer and dual brick diesel oxidation catalysts". *Chemical Engineering Journal, 335, 1004-1017* (2018) (cit. on p. 19).

[66] Y. Hiroyuki, K. Misawa, D. Suzuki, K. Tanaka, J. Matsumoto, M. Fujii, and K. Tanaka. "Detailed analysis of diesel vehicle exhaust emissions: nitrogen oxides, hydrocarbons and particulate size distributions". *Proceedings of the Combustion Institute, 33, 2895-2902* (2011) (cit. on p. 19).

[67] J. Bennett. "Sources of unburned hydrocarbons in a lean burn engine". PhD thesis. United Kingdom, 1992 (cit. on p. 19).

[68] B. Chehroudi. "Diesel engine emissions: Hydrocarbons (HC)". *ResearchGate* (2001) (cit. on p. 19).

[69] X. Miao, G. Zhang, Y. Ju, X. Wang, J. Hong, J. Zheng, X. Qiao, and Z. Huang. "Study on premixed combustion in a Diesel engine with ultra-multihole nozzle". *Journal of Combustion, 471648, 16 pages* (2011) (cit. on p. 19).

[70] M. Zheng, M. C. Mulenga, G. T. Reader, Wang, M. Ting, D. S., and J. Tjong. "Biodiesel engine performance and emissions in low temperature combustion." *Fuel, 87, 714-722* (2008) (cit. on p. 19).

[71] N. S. Ayoub and R. D. Reitz. "Multidimensional modeling of fuel composition effects on combustion and cold-starting in Diesel engines". In: *SAE Technical Paper 952425.* 1995 (cit. on p. 19).

[72] J. O'Connor, M. P. B. Musculus, and L. M. Pickett. "Effect of post injections on mixture preparation and unburned hydrocarbon emissions in a heavy-duty Diesel engine". *Combustion and Flame, 170, 111-123* (2016) (cit. on pp. 19, 40).

[73] K. Yamamoto, K. Takada, J. Kusaka, and Y. Kanno. "Influence of diesel post injection timing on HC emissions and catalytic oxidation performance". In: *SAE Technical Papers 2006-01-3442*. 2006 (cit. on p. 20).

[74] F. Payri, V. R. Bermúdez, B. Tormos, and W. G. Linares. "Hydrocarbon emissions speciation in diesel and biodiesel exhausts." *Atmospheric Environment, 43, 1273-1279* (2009) (cit. on pp. 20, 89, 110).

[75] Q. Xin. *Diesel engine system design, 503-525, Ed. 1.* Elsevier, 2013 (cit. on pp. 20, 41).

[76] K. Akihama, Y. Takatori, K. Inagaki, S. Sasaki, and A. M. Dean. "Mechanism of the smokeless rich diesel combustion by reducing temperature". *SAE Transactions, 110 (3), 648-662* (2001) (cit. on p. 20).

[77] S. E. Hosseini, M. Wahid, and A. Abuelnuor. "High temperature air combustion: Sustainable technology to low NO_x formation". *International Review of Mechanical Engineering, 6 (5), 947-953* (2012) (cit. on p. 20).

[78] T. Lee, J. Park, S. Kwon, J. Lee, and J. Kim. "Variability in operation-based NO_x emission factors with different test routes, and its effects on the real-driving emissions of light diesel vehicles." *Science of the Total Environment, 461-462, 377-385* (2013) (cit. on p. 20).

[79] X. Wang, D. Wasterdahl, H. Jingnan, Y. Wu, H. Yin, X. Pan, and K. M. Zhang. "On-road diesel vehicle emission factors for nitrogen oxides and black carbon in two Chinese cities". *Atmospheric Environment, 46, 45-55* (2012) (cit. on p. 20).

[80] V. Grewe, K. Dahlmann, S. Matthes, and W. Steinbrecht. "Attributing ozone to NO_x emissions: implications for climate mitigation measures". *Atmospheric Environment, 59, 102-107* (2012) (cit. on p. 20).

[81] P. E. Morrow. "Toxicological data on NO_x: An overview". *Journal of Toxicology and Environmental Health, 13, 205-227* (1984) (cit. on p. 20).

[82] P. Bedar and G. N. Kumar. "Exhaust gas recirculation (EGR) - Effective way to reduce NO_x emissions". *Journal of Mechanical Engineering and Biomechanics, 1 (2), 69-73* (2016) (cit. on p. 20).

[83] S. C. Ko, K. C. Oh, C. Seo, and C. B. Lee. "Characteristics on NO_x adsorption and intermediates of LNT catalyst". *International Journal of Automotive Technology, 15 (3), 347-352* (2014) (cit. on p. 21).

[84] F. Gao, X. Tang, H. Yi, S. Zhao, C. Li, J. Li, Y. Shi, and X. Meng. "A review on selective catalytic reduction of NO_x by NH_3 over Mn-based catalysts at low temperatures: Catalysts, mechanisms, kinetics and DFT calculations". *Catalysts, 7, 199* (2017) (cit. on pp. 21, 221).

[85] D. B. Kittelson, W. F. Watts, and J. P. Johnson. "On-road and laboratory evaluation of combustion aerosols - Part1: Summary of Diesel engine results". *Journal of Aerosol Science, 37 (8), 913-930* (2006) (cit. on p. 21).

[86] D. Agarwal and A. K. Agarwal. "Performance and emissions characteristics of Jatrophaoil (preheated and blends) in a direct injection compression ignition engine". *Applied Thermal Engineering, 27 (13), 2314-2323* (2007) (cit. on pp. 21, 38).

[87] J. Weidman and S. Marshall. *Soot Pollution 101. American Progress. Available in: https://americanprogress.org/article/soot-pollution-101/. (accessed on 24 November 2021).* 2012 (cit. on p. 21).

[88] C. A. Pope III and D. W. Dockery. "Acute health effects of PM10 pollution on symptomaticand asymptomatic children". *American Review of Respiratory Disease, 145 (5), 1123-1128* (1992) (cit. on p. 21).

[89] E. Boldo, S. Medina, A. Le Tertre, F. Hurley, H. Mücke, F. Ballester, and I. e. a. Aguilera. "Apheis: Health impact assessment of long-term exposure to PM2.5 in 23 European cities". *European Journal of Epidemiology, 21 (6), 449-458* (2006) (cit. on p. 21).

[90] H. Wiinikka, R. Gebart, C. Boman, D. Boström, and M. Öhman. "Influence of fuel ash composition on high temperature aerosol formation in fixed bed combustion of woody biomass pellets". *Fuel, 86 (1), 181-193* (2007) (cit. on p. 21).

[91] M. M. Maricq. "Chemical characterization of particulate emissions from Diesel engines: a review." *Journal of Aerosol Science, 38, 1079-1118* (2007) (cit. on p. 21).

[92] H. Bockhorn. *Soot Formation in Combustion, Ed. 1.* Springfield, 1994 (cit. on p. 21).

[93] B. Guan, R. Zhan, H. Lin, and Z. Huang. "Review of the state-of-the-art of exhaust particulate filter technology in internal combustion engines". *Journal of Environmental Management, 154 (1), 225-258* (2015) (cit. on pp. 21, 34, 38, 40).

[94] T. Kuki, Y. Miyairi, Y. Kasai, M. Miyazaki, and S. Miwa. "Study on reliability of wall-flow-type diesel particulate filter". In: *SAE Technical Paper 2004-01-0959.* 2004 (cit. on p. 21).

[95] R. Bosch. *Emissions-control technology for Diesel engines.* Robert Bosch GmbH, 2005 (cit. on p. 21).

[96] *ISO, Standard Atmosphere, ISO 2533:1975, International Standard Organization, 2533.* 1975 (cit. on p. 22).

[97] NORDREGIO. "Mountain areas in Europe: Analysis of mountain areas in EU member states, acceding and other European countries - Final report". *European Commission contract, 2002.CE.16.0.AT.136* (2002) (cit. on p. 22).

[98] J. M. Luján, H. Climent, L. M. García-Cuevas, and A. Moratal. "Pollutant emissions and diesel oxidation catalyst performance at low ambient temperatures in transient load conditions". *Applied Thermal Engineering, 129, 1527-1537* (2018) (cit. on pp. 22, 24, 31).

[99] A. Romagnoli, A. Manivannan, S. Rajoo, M. S. Chiong, A. Feneley, A. Pesiridis, and R. F. Martinez-Botas. "A review of heat transfer in turbochargers". *Renewable and Sustainable Energy Reviews, 79, 1442-1460* (2017) (cit. on p. 22).

[100] M. Hamdya, A. A. Akalany, K. Harbya, and N. Kora. "An overview on adsorption cooling systems powered by waste heat from internal combustion engine". *Renewable and Sustainable Energy Reviews, 51, 1223-1234* (2015) (cit. on p. 22).

[101] F. Westin, J. Rosenqvist, and H. E. Angström. "Heat losses from the turbine of a turbocharged SI-engine - Measurements and simulation". In: *SAE Technical Paper 2004-01-0996.* 2004 (cit. on p. 22).

[102] Y. Chang, B. Mendrea, J. Sterniak, and S. V. Bohac. "Effect of ambient temperature and humidity on combustion and emissions of a spark-assisted compression ignition engine". *Journal of Engineering for Gas Turbines and Power, 139 (5), 051501* (2017) (cit. on p. 23).

[103] J. V. Pastor, J. M. García-Oliver, J. M. Pastor, and J. G. Ramírez-Hernández. "Ignition and combustion development for high speed direct injection Diesel engines under low temperature cold start conditions". *Fuel, 90, 1556-1566* (2011) (cit. on p. 23).

[104] Q. Li, P. J. Shayler, M. McGhee, and A. La Rocca. "The initiation and development of combustion under cold idling conditions using a glow plug in Diesel engines". *Internal Journal of Engine Research, 18 (3), 240-255* (2017) (cit. on p. 23).

[105] K. Y. Cheng, P. J. Shayler, and M. Murphy. "The influence of blow-by on indicated work output from a Diesel engine under cold start conditions". *Proceedings of the Institution of Mechanical Engineers, Part D: Journal of Automobile Engineering, 218 (3), 333-340* (2004) (cit. on p. 23).

[106] R. Rahmani, H. Rahnejat, B. Fitzsimons, and D. Dowson. "The effect of cylinder liner operating temperature on frictional loss and engine emissions in piston ring conjunction". *Applied Energy, 191, 568-581* (2017) (cit. on p. 23).

[107] A. Maiboom, X. Tauzia, X. R. Shah, and J.-H. Hétet. "Experimental study of an LP EGR system on an automotive Diesel engine, compared to HP EGR with respect to PM and NO_x emissions and specific fuel consumption". In: *SAE Technical Paper 2009-24-0138*. 2009 (cit. on p. 23).

[108] J. M. Luján, C. Guardiola, B. Pla, and A. Reig. "Switching strategy between HP- and LP EGR systems for reducedfuel consumption and emissions". *Energy, 00, 1-20* (2015) (cit. on p. 23).

[109] M. Lapuerta, A. Ramos, D. Fernández-Rodríguez, and I. González-García. "High-pressure versus low-pressure exhaust gas recirculation in a Euro 6 Diesel engine with lean-NO_x trap: Effectiveness to reduce NO_x emissions". *Internal Journal of Engine Research, 20 (5), 155-163* (2018) (cit. on pp. 23, 24, 39).

[110] J. Galindo, R. Navarro, D. Tarí, and F. Moya. "Development of an experimental test bench and a psychrometric model for assessing condensation on a low-pressure exhaust gas recirculation cooler." *International Journal of Engine Research, 22 (5), 1540-1550* (2020) (cit. on pp. 23, 24).

[111] A. J. Torregrosa, A. Broatch, P. Olmeda, and C. Romero. "Assessment of the influence of different cooling system configurations on engine warm-up, emissions and fuel consumption". *International Journal of Automotive Technology, 9, 447-458* (2008) (cit. on p. 23).

[112] P. Bielaczyc, A. Szczotka, and J. Woodburn. "The effect of a low ambient temperature on the cold-start emissions and fuel consumption of passenger cars". *Proceedings of the Institution of Mechanical Engineers, Part D, 225, 1253-1264* (2011) (cit. on p. 23).

[113] M. Weilenmann, P. Soltic, C. Saxer, A.-M. Forss, and N. Heeb. "Regulated and nonregulated diesel and gasoline cold start emissions at different temperatures". *Atmospheric Environment, 39 (13), 2433-2441* (2005) (cit. on p. 23).

[114] M. V. Faria, R. A. Varella, G. O. Duarte, L. Farias T., and P. C. Baptista. "Engine cold start analysis using naturalistic driving data: City level impacts on local pollutants emissions and energy consumption." *Science of the Total Environment, 630, 544-559* (2018) (cit. on pp. 23, 25).

[115] M. Weilenmann, J.-Y. Favez, and R. Alvarez. "Cold-start emissions of modern passenger cars at different low ambient temperatures and their evolution over vehicle legislation categories". *Atmos Environ, 43, 2419-2429* (2009) (cit. on pp. 23, 24).

[116] J. Ko, D. Jin, W. Jang, C. L. Myung, S. Kwon, and S. Park. "Comparative investigation of NO_x emission characteristics from a Euro 6-compliant diesel passenger car over the NEDC and WLTC at various ambient temperatures". *Applied Energy, 187, 652-662* (2017) (cit. on pp. 23, 25).

[117] T. W. Chan, E. Meloche, J. Kubsh, R. Brezny, D. Rosenblatt, and G. Rideout. "Impact of ambient temperature on gaseous and particle emissions from a direct injection gasoline vehicle and its implications on particle filtration". In: *SAE Technical Paper 2013-01-0527*. 2013 (cit. on p. 23).

[118] C. H. Zhang, J. R. Pan, J. J. Tong, and J. Li. "Effects of intake temperature and excessive air coefficient on combustion characteristics and emissions of HCCI combustion". *Procedia Environmental Sciences, 11, 1119-1127* (2011) (cit. on p. 24).

[119] M. Torres García, F. José Jiménez-Espadafor Aguilar, and T. Sánchez Lencero. "Experimental study of the performances of a modified Diesel engine operating in homogeneous charge compression ignition (HCCI) combustion mode versus the original diesel combustion mode". *Energy, 34 (2), 159-171* (2009) (cit. on p. 24).

[120] W. A. Daniel. "Flame quenching at the walls on an internal combustion engine." *Proceedings of the Combustion Institute, 6, 886-902* (1957) (cit. on p. 24).

[121] A. Roberts, R. Brooks, and P. Shipway. "Internal combustion engine cold-start efficiency: A review of the problem, causes and potential solutions". *Energy Conversion and Management, 82, 327-350* (2014) (cit. on p. 24).

[122] J. Tian, H. Xu, R. A. Sakunthalai, D. Liu, C. Tan, and A. Ghafourian. "Low ambient temperature effects on a modern turbocharged Diesel engine running in a driving cycle". In: *SAE Technical Paper 2014-01-2713*. 2014 (cit. on pp. 24, 25).

[123] J. Galindo, P. Piqueras, R. Navarro, D. Tarí, and C. M. Meano. "Validation and sensitivity analysis of an in-flow water condensation model for 3d-CFD simulations of humid air streams mixing". *International Journal of Thermal Sciences, 136, 410-419* (2019) (cit. on pp. 24, 220).

[124] R. A. Sakunthalai, H. Xu, D. Liu, J. Tian, M. Wyszynski, and J. Piaszyk. "Impact of cold ambient conditions on cold start and idle emissions from Diesel engines". In: *SAE Technical Paper 2014-01-2715*. 2014 (cit. on pp. 24, 25).

[125] Z. Ning, C. S. Cheung, and S. X. Liu. "Experimental investigation of the effect of exhaust gas coolingon diesel particulate". *Journal of Aerosol Science, 35, 333-345* (2004) (cit. on p. 25).

[126] G. Olivares, C. Johansson, J. Ström, and H.-C. Hansson. "The role of ambient temperature for particle number concentrations in a street canyon". *Atmospheric Environment, 41 (10), 2145-2155* (2007) (cit. on p. 25).

[127] D. Ludykar, R. Westerholm, and J. Almén. "Cold start emissions at +22, -7 and -20°C ambient temperatures from a three-way catalyst (TWC) car: Regulated and unregulated exhaust components". *Science of The Total Environment, 235, (1-3), 65-69* (1999) (cit. on p. 25).

[128] V. Bermúdez, J. R. Serrano, P. Piqueras, J. Gómez, and S. Bender. "Analysis of the role of altitude on Diesel engine performance and emissions using an atmosphere simulator". *International Journal of Engine Research, 18, 105-117* (2017) (cit. on pp. 26, 27, 68, 120).

[129] Z. Kan, Z. Hu, D. Lou, P. Tan, Z. Cao, and Z. Yang. "Effects of altitude on combustion and ignition characteristics of speed-up period during cold start in a Diesel engine". *Energy, 150, 164-175* (2018) (cit. on p. 26).

[130] X. Wang, H. Yin, Y. Ge, L. Yu, Z. Xu, C. Yu, X. Shi, and H. Liu. "On-vehicle emission measurement of a light-duty diesel van at various speeds at high altitude". *Atmospheric Environment, 81 (2013) 263-269* (2013) (cit. on pp. 26, 27, 31).

[131] M. Szedlmayer and C. M. Kweon. "Effect of altitude conditions on combustion and performance of a multi-cylinder turbocharged direct injection Diesel engine". In: *SAE Technical Paper 2016-01-0742*. 2016 (cit. on pp. 26, 27).

[132] E. Zervas. "Impact of altitude on fuel consumption of a gasoline passenger car". *Fuel, 90, 2340-2342* (2011) (cit. on p. 26).

[133] C. P. Benjumea, J. Agudelo, and A. Agudelo. "Effect of altitude and palm oil biodiesel fuelling on the performance and combustion characteristics of a HSDI Diesel engine". *Fuel, 88, 725-731* (2009) (cit. on p. 27).

[134] C. A. Chaffin and T. L. Ullman. "Effects of increased altitude on heavy-duty Diesel engine emissions". In: *SAE Technical Paper 940669*. 1994 (cit. on p. 27).

[135] C. McCaffery, H. Zhua, C. Li, T. D. Durbin, K. C. Johnson, H. Jung, R. Brezny, M. Geller, and G. Karavalakis. "On-road gaseous and particulate emissions from GDI vehicles with and without gasoline particulate filters (GPFs) using portable emissions measurement systems (PEMS)". *Science of the Total Environment. 710. 136366* (2020) (cit. on pp. 27, 221).

[136] H. Wang et al. "The real driving emission characteristics of light duty diesel vehicle at various altitudes". *Atmospheric Environment, 191, 126-131* (2018) (cit. on p. 27).

[137] J. M. Luján, J. R. Serrano, P. Piqueras, and O. García-Afonso. "Experimental assessment of a pre-turbo aftertreatment configurations in a single stage turbocharged Diesel engine. Part 2: Transient operation". *Energy, 80, 614-27.* (2015) (cit. on pp. 28, 36, 126).

[138] C. K. Lambert. "Perspective on SCR NO_x control for diesel vehicles". *Reaction Chemistry and Engineering, 4 (6), 969-974* (2019) (cit. on p. 28).

[139] S. Shrestha, M. P. Harold, and K. Kamasamudram. "Experimental and modeling study of selective ammonia oxidation on multi-functional washcoated monolith catalysts". *Chemical Engineering Journal, 278, 24-35* (2015) (cit. on p. 28).

[140] T. C. Watling, M. R. Ravenscroft, and G. Avery. "Development, validation and application of a model for an SCR catalyst coated diesel particulate filter". *Catalysis Today, 188 (1), 32-41* (2012) (cit. on p. 29).

[141] A. P. E. York and A. Tsolakis. "Cleaner vehicle emissions". *Encyclopedia of Materials: Science and Technology, 2, 1-7* (2010) (cit. on p. 29).

[142] M. Fayad, A. Tsolakis, D. Fernández-Rodríuez, J. Herreros, F. Martos, and M. Lapuerta. "Manipulating modern Diesel engine particulate emission characteristics through butanol fuel blending and fuel injection strategies for efficient diesel oxidation catalysts". *Applied Energy, 190, 490-500* (2017) (cit. on p. 29).

[143] S. Ye, Y. H. Yap, S. T. Kolaczkowski, K. Robinson, and D. Lukyanov. "Catalyst 'light-off' experiments on a diesel oxidation catalyst connected to a Diesel engine- Methodology and techniques". *Chemical Engineering Research and Design, 90, 834-845* (2012) (cit. on pp. 29, 31).

[144] J. Cooper and J. Beecham. "A study of platinum group metals in three-way autocatalysts". *Platinum Metals Review, 57 (4), 281-288* (2013) (cit. on p. 29).

[145] P. Tayal. "Light off temperature based approach to determine diesel oxidation catalyst effectiveness level and the corresponding outlet NO and NO_2 characteristics". MA thesis. Purdue University, West Lafayette, United States, 2014 (cit. on p. 29).

[146] D. Kryl, P. Kočí, M. Kubíček, M. Marek, T. Maunula, and M. Härkönen. "Catalytic converters for automobile Diesel engines with adsorption of hydrocarbons on zeolites". *Industrial & Engineering Chemistry Research, 44 (25), 9524-9534* (2005) (cit. on p. 29).

[147] E. Zervas. "Parametric study of the main parameters influencing the catalytic efficiency of a diesel oxidation catalyst: parameters influencing the efficiency of a diesel catalyst". *International Journal of Automotive Technology, 9 (6), 641-647* (2008) (cit. on pp. 29, 31).

[148] K. Robinson, S. Ye, Y. Yap, and S. T. Kolaczkowski. "Application of a methodology to assess the performance of a full-scale diesel oxidation catalyst during cold and hot start NEDC drive cycles". *Chemical Engineering Research and Design, 91 (7), 1292-1306* (2013) (cit. on p. 29).

[149] A. A. Yusuf and F. L. Inambao. "Effect of cold start emissions from gasoline-fueled engines of light-duty vehicles at low and high ambient temperatures: Recent trends". *Case Studies in Thermal Engineering, 14, 100417* (2019) (cit. on pp. 30, 34).

[150] C. Guardiola, B. Pla, P. Bares, and J. Mora. "An on-board method to estimate the light-off temperature of diesel oxidation catalysts". *Intenational Journal of Engine Research, 21 (8), 1480-1492* (2018) (cit. on pp. 30, 107).

[151] S. R. Christensen, B. B. Hansen, K. H. Pedersen, J. R. Thøgersen, and A. D. Jensen. "Selective catalytic reduction of NO_x over V_2O_5-WO_3-TiO_2 SCR catalysts - A study at elevated pressure for maritime pre-turbine SCR configuration". *Emission Control Science and Technology, 5, 263-278* (2019) (cit. on p. 30).

[152] P. Y. Peng, M. P. Harold, and D. Luss. "Sustained concentration and temperature oscillations in a diesel oxidation catalyst". *Chemical Engineering Journal, 5, 263-278* (2019) (cit. on p. 30).

[153] D. Peitz, M. Elsener, and O. Kröcher. "Impact of catalyst geometry on diffusion and selective catalytic reduction kinetics under elevated pressures". *Chemie Ingenieur Technik, 90, 795-802* (2018) (cit. on p. 30).

[154] I. Langmuir. "The mechanism of the catalytic action of platinum in the reaction $2CO + O_2 = CO_2$ and $2H_2 + O_2 = 2H_2O$". *Transactions of the Faraday Society, 17, 607-654* (1922) (cit. on p. 30).

[155] C. Boerensen, D. Roemer, C. Nederlof, E. Smirnov, F. Linzen, F. Goebel, and B. Carberry. "Twin-LNT system for advanced diesel exhaust gas aftertreatment". *SAE International Journal of Fuels and Lubricants, 10, 619-633* (2017) (cit. on p. 30).

[156] F. Payri, F. J. Arnau, P. Piqueras, and M. J. Ruiz. "Lumped approach for flow-through and wall-flow monolithic modelling for real-time automotive applications". In: *SAE Technical Paper 2018-01-0954*. 2018 (cit. on pp. 31, 86, 92, 107).

[157] R. Hasegawa and H. Yanagihara. "HCCI combustion in DI Diesel engine". In: *SAE Technical Paper 2003-01-0745*. 2003 (cit. on p. 31).

[158] S. H. Oh and J. C. Cavendish. "Transients of monolithic catalytic converters. Response to step changes in feedstream temperature as related to controlling automobile emissions". *Industrial & Engineering Chemistry Product Research and Development, 21, 29-37* (1982) (cit. on p. 31).

[159] P. Piqueras, M. J. Ruiz, J. M. Herreros, and A. Tsolakis. "Influence of the cell geometry on the conversion efficiency of oxidation catalysts under real driving conditions". *Energy Conversion and Management, 233,113888* (2021) (cit. on p. 31).

[160] A. Russell and W. S. Epling. "Diesel oxidation catalysts". *Catalysis Reviews - Science and Engineering, 53 (4), 337-423* (2011) (cit. on pp. 31, 106).

[161] S. E. Voltz, C. R. Morgan, D. Liederman, and S. M. Jacob. "Kinetic study of carbon monoxide and propylene oxidation on platinum catalysts". *Industrial & Engineering Chemistry Product Research and Development, 12 (4), 294-301* (1973) (cit. on pp. 31, 90).

[162] O. Chiavola, G. Chiatti, and N. Sirhan. "Impact of particulate size during deep loading on DPF management". *Applied Sciences, 9, 3075* (2019) (cit. on p. 31).

[163] X. Hou, S. Du, Z. Liu, J. Guo, and Z. Li. "A transfer matrix approach for structural-acoustic correspondence analysis of diesel particulate filter". *Advances in Mechanical Engineering, 9 (9), 1-10* (2017) (cit. on p. 32).

[164] A. G. Konstandopoulos, M. Kostoglou, E. Skaperdas, E. Papaioannou, D. Zarvalis, and E. Kladopoulou. "Fundamental studies of diesel particulate filters: transient loading, regeneration, and aging". In: *SAE Technical Paper 2000-01-1016*. 2000 (cit. on p. 32).

[165] S. Choi, K.-C. Oh, and C.-B. Lee. "The effects of filter porosity and flow conditions on soot deposition/oxidation and pressure drop in particulate filters". *Energy, 77 (1), 327-337* (2014) (cit. on p. 32).

[166] A. J. Torregrosa, J. R. Serrano, F. J. Arnau, and P. Piqueras. "A fluid dynamic model for unsteady compressible flow in wall-flow diesel particulate filters". *Energy, 36 (1), 671-684* (2011) (cit. on pp. 32, 66).

[167] K. W. Lee and J. A. Gieseke. "Collection of aerosol particles by packed beds". *Envirnmental Science & Technology ,13 (4), 466-470* (1979) (cit. on pp. 32, 94, 95).

[168] B. van Setten, M. Makkee, and J. A. Moulijn. "Science and technology of catalytic diesel particulate filters". *Catalysis Reviews, 43 (4), 489-564* (2001) (cit. on p. 32).

[169] P. Tandon, A. Heibel, J. Whitmore, N. Kekre, and K. Chithapragada. "Measurement and prediction of filtration efficiency evolution of soot loaded diesel particulate filters". *Chemical Engineering Science, 65, 4751-4760* (2010) (cit. on p. 32).

[170] J. R. Serrano, H. Climent, P. Piqueras, and E. Angiolini. "Filtration modelling in wall-flow particulate filters of low soot penetration thickness". *Energy, 112, 883-898* (2016) (cit. on pp. 32, 93, 94).

[171] I. P. Kandylas and G. C. Koltsakis. "NO_2 - Assisted regeneration of diesel particulate filters: A modeling study". *Industrial & Engineering Chemistry Research, 41, 2115-2123* (2002) (cit. on pp. 33, 35).

[172] S. Quiles-Díaz, J. Giménez-Mañogil, and A. García-García. "Catalytic performance of CuO/Ce 0.8 Zr $0.2O_2$ loaded over SiC-DPF in NO_x-assisted combustion of diesel soot." *RSC Advances, 5 (22)* (2015) (cit. on p. 33).

[173] A. Abdalla, G. Wang, J. Zhang, and S.-J. Shuai. "Simulation of catalyzed diesel particulate filter for active regeneration process using secondary fuel injection". In: *International Powertrains, Fuels & Lubricants Meeting 10.4271/2017-01-2287*. 2017 (cit. on p. 33).

[174] S. Soltani, R. Andersson, and B. Andersson. "The effect of exhaust gas composition on the kinetics of soot oxidation and diesel particulate filter regeneration". *Fuel, 220, 453-463* (2018) (cit. on pp. 33, 166).

[175] S. Bai, G. Chen, Q. Sun, G. Wang, and G.-X. Li. "Influence of active control strategies on exhaust thermal management for diesel particular filter active regeneration". *Applied Thermal Engineering, 119, 297-303* (2017) (cit. on pp. 33, 41).

[176] M. Ahmadinejad, A. Tsolakis, J. M. Becker, C. F. Goersmann, A. D. Newman, and T. C. Watling. "Modelling of soot oxidation by NO_2 in a diesel particulate filter". *SAE International Journal of Fuels and Lubricants, 5, 359-369* (2012) (cit. on p. 33).

[177] T. C. Watling. "Understanding factors affecting the balance point (and rate of balance point approach) of a diesel particulate filter: an analytical expression for the balance point soot loading". *Emission Control Science and Technology, 6, 195-210* (2020) (cit. on p. 33).

[178] S. Bensaid, D. L. Marchisio, and D. Fino. "Numerical simulation of soot filtration and combustion within diesel particulate filters". *Chemical Engineering Science, 65, 357-363* (2010) (cit. on p. 33).

[179] B. R. Stanmore, J. F. Brilhac, and P. Gilot. "The oxidation of soot: A review of experiments, mechanisms and models". *Carbon, 39, 2247-2268* (2001) (cit. on p. 33).

[180] V. Macián, J. R. Serrano, P. Piqueras, and E. J. Sanchis. "Internal pore diffusion and adsorption impact on the soot oxidation in wall-flow particulate filters". *Energy, 179, 407-421* (2019) (cit. on pp. 33, 95, 96, 166, 175).

[181] E. Jiaqiang, M. Liu, Y. Deng, H. Zhu, and J. Gong. "Influence analysis of monolith structure on regeneration temperature in the process of microwave regeneration in the diesel particulate filter". *The Canadian Journal of Chemical Engineering, 94, 168-174* (2016) (cit. on p. 34).

[182] E. Jiaqiang, X. Zhao, L. Qiu, K. Wei, Z. Zhang, Y. Deng, D. Han, and G. Liu. "Experimental investigation on performance and economy characteristics of a Diesel engine with variable nozzle turbocharger and its application in urban bus". *Energy Conversion and Management, 1, 149-161* (2019) (cit. on p. 34).

[183] J. R. Serrano, P. Piqueras, J. de la Morena, and E. J. Sanchis. "Late fuel post-injection influence on the dynamics and efficiency of wall-flow particulate filters regeneration". *Applied Sciences, 2019, 9 (24), 5384* (2019) (cit. on pp. 34, 40, 88, 166, 168, 173).

[184] A. Suresh, A. Yezerets, N. Currier, and J. Clerc. "Diesel particulate filter system . Effect of critical variables on the regeneration strategy development and optimization". In: *SAE Technical Paper 2008-01-0329*. 2008 (cit. on p. 34).

[185] A. Kotrba, T. P. Gardner, L. Bai, and A. Yetkin. "Passive regeneration response characteristics of a DPF system". In: *SAE Technical Paper 2013-04-08*. 2013 (cit. on p. 35).

[186] A. P. E. York, M. Ahmadinejad, T. C. Watling, A. P. Walker, J. P. Cox, J. Gast, P. G. Blakeman, and R. Allansson. "Modeling of the catalyzed continuously regenerating diesel particulate filter (CCR-DPF) system: model development and passive regeneration studies". In: *SAE Technical Paper 2007-01-0043*. 2007 (cit. on p. 35).

[187] K. Ramanathan, D. H. West, and V. Balakotaiah. "Optimal design of catalytic converters for minimizing cold-start emissions". *Catalysis Today, 98, 357-373* (2004) (cit. on p. 35).

[188] A. Gurupatham and Y. He. "Architecture design and analysis of Diesel engine exhaust aftertreatment system and comparative study with close-coupled DOC-DPF system". In: *SAE Technical Paper 2008-01-1756*. 2008 (cit. on p. 35).

[189] L. Tingting. "Analysis on diesel aftertreatment system fault diagnosis for CRT ageing and failure". MA thesis. Beijing Jiaotong University, Beijing, China, 2012 (cit. on p. 35).

[190] A. Strzelec, R. Vander Wal, T. N. Thompson, and T. J. Toops. "NO_2 oxidation reactivity and burning mode of diesel particulates". *Topics in Catalysis, 59 (8), 686-694* (2016) (cit. on p. 35).

[191] A. Srinivasan and K. Price. "Consolidation of DOC and DPF functions into a single component". In: *SAE Technical Paper 2019-01-0583*. 2019 (cit. on p. 35).

[192] A. Punke, G. Grubert, Y. Li, J. Dettling, and T. Neubauer. "Catalyzed soot filters in close coupled position for passenger vehicles". In: *SAE Technical Paper 2006-01-1091*. 2006 (cit. on p. 36).

[193] V. Di Sarli, G. Landi, L. Lisi, A. Saliva, and A. Di Benedetto. "Catalytic diesel particulate filters with highly dispersed ceria: Effect of the soot-catalyst contact on the regeneration performance". *Applied Catalysis B: Environmental, 197, 116-124* (2016) (cit. on p. 36).

[194] N. He, Z. Jiang, and Z. Ning. "Comparison of catalytic conversion characteristics of different integrated aftertreatment systems in Diesel engine". *Journal of Physics: Conference Series, 1578, 012218* (2020) (cit. on p. 36).

[195] J. R. Serrano, P. Piqueras, J. De La Morena, and M. J. Ruiz. "Influence of pre-turbine small-sized oxidation catalyst on engine performance and emissions under driving conditions". *Applied Sciences, 10, 7714* (2020) (cit. on p. 36).

[196] C. Gökçöl and A. Uğurlu. "A review on thermal energy storage systems with phase change materials in vehicles". *Electronic Journal of Vocational Colleges, 2, 1-14* (2012) (cit. on p. 36).

[197] L. Xie, G. Jiang, and F. Qian. "Research on aftertreatment inlet outlet insulation for a non road middle range Diesel engine". *Catalysts, 10, 454* (2020) (cit. on p. 36).

[198] F. J. Arnau, J. Martín, P. Piqueras, and A. Auñón. "Effect of the exhaust thermal insulation on the engine efficiency and the exhaust temperature under transient conditions". *Internal Journal of Engine Research, Online First. https://doi.org/10.1177/1468087420961206* (2020) (cit. on p. 37).

[199] H. Zhang, J. Baeyens, G. Cáceres, J. Degrève, and Y. Lv. "Thermal energy storage: Recent developments and practical aspects". *Progress in Energy and Combustion Science, 53, 1-40* (2016) (cit. on p. 37).

[200] J. Jaguemont, N. Omar, P. Van den Bossche, and J. Mierlo. "Phase-change materials (PCM) for automotive applications: A review". *Applied Thermal Engineering, 132, 308-320* (2018) (cit. on p. 37).

[201] B. Zalba, J. M. Marín, L. F. Cabeza, and H. Mehling. "Review on thermal energy storage with phase change: materials, heat transfer analysis and applications". *Applied Thermal Engineering, 23 (3), 251-283* (2003) (cit. on p. 37).

[202] D. K. Johar, D. Sharma, S. L. Soni, P. K. Gupta, and R. Goyal. "Experimental investigation on latent heat thermal energy storage system for stationary C.I. engine exhaust". *Applied Thermal Engineering, 104, 64-73* (2016) (cit. on p. 37).

[203] S. D. Burch, T. F. Potter, and M. A. Keyser. "Reducing cold-start emissions by catalytic converter thermal management". *SAE Technical Paper 950409* (1995) (cit. on pp. 37, 126).

[204] E. Korin, R. Reshef, D. Tshernichovesky, and E. Sher. "Reducing cold-start emission from internal combustion engines by means of a catalytic converter embedded in a phase-change material". *Proceedings of the Institution of Mechanical Engineers, Part D: Journal of Automobile Engineering, 213 (6)* (1999) (cit. on p. 37).

[205] M. Nicholas, G. Tal, and T. Turrentine. "Advanced plug-in electric vehicle travel and charging behavior". *Advanced Clean Cars Symposium: The Road Ahead, California Environmental Protection Agency, Air Resources Board, Sacramento, CA, USA, 27-28 September* (2016) (cit. on p. 38).

[206] G. Blanchard, C. Colignon, C. Griard, C. Rigaudeau, O. Salvat, and T. Seguelong. "Passenger car series application of a new diesel particulate filter system using a new ceria-based fuel-borne catalyst: from the engine test bench to european vehicle certification". In: *SAE Technical Paper 2002-01-2781.* 2002 (cit. on p. 38).

[207] M. Piumetti, S. Bensaid, N. Russo, and D. Fino. "Nanostructured ceria-based catalystsfor soot combustion: investigations on the surface sensitivity". *Applied Catalysis B: Environmental, 165, 742-751* (2015) (cit. on p. 38).

[208] K. Krishna and M. Makkee. "Pt-Ce-soot generated from fuel-borne catalysts: soot oxidation mechanism". *Topics in Catalysis, 42 (1), 229-236* (2007) (cit. on p. 38).

[209] G. Blanchard, T. Seguelong, J. Michelin, S. Schuerholz, and F. Terres. "Ceria-based fuel-borne catalysts for series diesel particulate filter regeneration". In: *SAE Technical Paper 2003-01-0378.* 2003 (cit. on p. 38).

[210] M. Z. Zheng, G. T. Reader, D. Wang, J. Zuo, R. Kumar, M. C. Mulenga, U. Asad, and M. Ting D. S.-K. andWang. "A thermal response analysis on the transient performance of active diesel aftertreatment". In: *SAE Technical Paper 2005-01-3885*. 2005 (cit. on p. 38).

[211] S. Jindal. "Effect of injection timing on combustion and performance of a direct injection Diesel engine running on Jatropha methyl ester". *International Journal of Energy and Environment, 2 (1), 113-122* (2011) (cit. on p. 38).

[212] M. Zheng, G. T. Reader, and J. G. Hawley. "Diesel engine exhaust gas recirculation - A review on advanced and novel concepts". *Journal of Energy Conversion and Management, 45, 883-900* (2004) (cit. on p. 38).

[213] C. N. Pratheeba and P. Aghalayam. "Effect of exhaust gas recirculation in NO_x control for compression ignition and homogeneous charge compression ignition engines". *Energy Procedia, 66, 25-28* (2015) (cit. on p. 38).

[214] M. Yang, Y. Gu, K. Deng, Z. Yang, and Y. Zhang. "Analysis on altitude adaptability of turbocharging systems for a heavy-duty Diesel engine". *Applied Thermal Engineering, 128, 1196-1207* (2018) (cit. on p. 39).

[215] J. Wang, L. Shen, Y. Bi, and J. Lei. "Modeling and optimization of a light-duty Diesel engine at high altitude with a support vector machine and a genetic algorithm". *Fuel, 285, 119137* (2021) (cit. on p. 39).

[216] T. Lancefield, I. Methley, U. Räse, and T. Kuhn. "The application of variable event valve timing to a modern Diesel engine". In: *SAE Technical Paper 2000-01-1229*. 2000 (cit. on p. 39).

[217] J. R. Serrano, P. Piqueras, R. Navarro, J. Gómez, M. Michel, and B. Thomas. "Modelling analysis of aftertreatment inlet temperature dependence on exhaust valve and ports design parameters". In: *SAE Technical Paper 2016-01-0670*. 2016 (cit. on pp. 39, 74, 222).

[218] F. J. Arnau, J. Martín, B. Pla, and A. Auñón. "Diesel engine optimization and exhaust thermal management by means of variable valve train strategies". *Internal Journal of Engine Research, 22 (4), 1196-1213* (2021) (cit. on pp. 39, 222).

[219] J. R. Serrano, F. J. Arnau, J. Martín, and A. Auñón. "Development of a variable valve actuation control to improve diesel oxidation catalyst efficiency and emissions in a light duty Diesel engine". *Energies, 13, 4561* (2020) (cit. on p. 39).

[220] R. F. Horng and H. M. Chou. "Effect of input energy on the emission of a motorcycle engine with an electrically heated catalyst in cold-start conditions". *Applied Thermal Engineering, 24 (14), 2017-2028* (2004) (cit. on p. 39).

[221] S. R. Khan, M. Zeeshan, and S. Iqbal. "Thermal management of newly developed non-noble metal-based catalytic converter to reduce cold start emissions of small internal combustion engine". *Chemical Engineering Communications, 205 (5), 680-688* (2018) (cit. on p. 39).

[222] R. Szolak, B. Danckert, A. Susdorf, P. Beutel, K. Pautsch, C. Ewert, F. Rümmele, A. Kakadiya, and A. Schaadt. "CatVap®- a new heating measure for exhaust aftertreatment system". In: *Heavy-Duty-, On- und Off-Highway-Motoren, 37-52*. 2019 (cit. on p. 39).

[223] O. Holmer and Eriksson. "Modeling and analytical solutions for optimal heating of aftertreatment systems". *IFAC-PapersOnLine, 53 (5), 523-530* (2019) (cit. on p. 39).

[224] C. Beatrice, S. Di Iorio, C. Guido, and P. Napolitano. "Detailed characterization of particulate emissions of an automotive catalyzed DPF using actual regeneration strategies". *Experimental Thermal and Fluid Science, 39, 45-53* (2012) (cit. on p. 40).

[225] Y. Tanaka, T. Hihara, M. Nagata, N. Azuma, and A. Ueno. "Modeling of diesel oxidation catalyst". *Industrial and Engineering Chemistry Research, 44 (22), 8205-8212* (2005) (cit. on p. 40).

[226] M. Bouchez and J. B. Dementhon. "Strategies for the control of particulate trap regeneration". In: *SAE Technical Paper 2000-01-0472*. 2000 (cit. on p. 40).

[227] J. Parks, S. Huff, M. Kass, and J. Storey. "Characterization of in-cylinder techniques for thermal management of diesel aftertreatment". In: *SAE Technical Paper 2007-01-3997*. 2007 (cit. on p. 40).

[228] M. Jeftić, J. Tjong, G. Reader, M. Wang, and M. Zheng. "Combustion and exhaust gas speciation analysis of diesel and butanol post injection". In: *SAE Technical Paper 2015-01-0803*. 2015 (cit. on p. 40).

[229] J. O'Connor and M. P. B. Musculus. "Post injections for soot reduction in Diesel engines: A review of current understanding". *SAE International Journal of Engines, 6 (1), 400-421* (2013) (cit. on p. 40).

[230] M. Lapuerta, J. J. Hernández, and F. Oliva. "Strategies for active diesel particulate filter regeneration based on late injection and exhaust recirculation with different fuels". *International Journal of Automotive Technology, 15 (2), 209-221* (2012) (cit. on p. 40).

[231] J. Ko, C. Myung, and S. Park. "Impacts of ambient temperature, DPF regeneration, and traffic congestion on NO_x emissions from a Euro 6-compliant diesel vehicle equipped with an LNT under real-world driving conditions". *Atmospheric Environment, 200, 1-14* (2019) (cit. on p. 40).

[232] D. Liebig, R. Clark, J. Muth, and I. Drescher. "Benefits of GTL fuel in vehicles equipped with diesel particulate filters". In: *SAE Technical Paper 2009-01-1934*. 2009 (cit. on p. 40).

[233] H. Dwyer, A. Ayala, S. Zhang, J. Collins, T. Huai, J. Herner, and W. Chau. "Emissions from a diesel car during regeneration of an active diesel particulate filter". *Journal of Aerosol Science, 41 (6), 541-552* (2010) (cit. on p. 40).

[234] A. Mayer, T. Lutz, C. Lämmle, M. Wyser, and F. Legerer. "Engine intake throttling for active regeneration of diesel particle filters". In: *SAE Technical Paper 2003-01-0381*. 2003 (cit. on p. 40).

[235] L. Stenning. "Strategies for achieving pre DPF regeneration temperatures using in cylinder post injection on a common rail Diesel engine with EGR, DOC and intake throttle". In: *SAE Technical Paper Brasil 2010-36-0306*. 2010 (cit. on p. 40).

[236] V. Bermúdez, J. R. Serrano, P. Piqueras, and O. García-Afonso. "Influence of DPF soot loading on engine performance with a pre-turbo aftertreatment exhaust line". In: *SAE Technical Paper 2012-01-0362*. 2012 (cit. on p. 41).

[237] GAMMA Technologies, Available in: www.gtisoft.com. (accessed on 25 November 2021) (cit. on p. 66).

[238] J. Galindo, J. R. Serrano, P. Piqueras, and J. Gómez. "Description and performance analysis of a flow test rig to simulate altitude pressure variation for internal combustion engines testing". *SAE International Journal of Engines, 4 (7), 1686-1696* (2014) (cit. on p. 68).

[239] A. Broatch, V. Bermúdez, J. R. Serrano, R. Tabet, J. Gómez, and S. Bender. "Analysis of passenger car turbocharged Diesel engines performance when tested at altitude and of the altitude simulator device used". In: *Proceedings of the ASME 2018 Internal Combustion Engine Division Fall Technical Conference*. San Diego, CA, USA, 2018 (cit. on pp. 68, 72).

[240] J. M. Desantes, J. Galindo, F. Payri, P. Piqueras, and J. R. Serrano. *Device for atmosphere conditioning for testing combustion engines, and associated method and use*. Patent WO 2015/110683 A1. 2015 (cit. on p. 68).

[241] J. M. Desantes, J. Galindo, F. Payri, P. Piqueras, and J. R. Serrano. *Device for conditioning the atmosphere in test of alternative internal combustion engines, method and use of said device*. Patent WO 2016/116642 A1. 2016 (cit. on p. 68).

[242] V. Betageri and R. Mahesh. "Effects of the real driving conditions on the NO_x emission of a medium duty diesel commercial vehicle". In: *SAE Technical Paper 2017-26-0124*. 2017 (cit. on p. 72).

[243] A. Ashtari, E. Bibeau, and S. Shahidinejad. "Using large driving record samples and a stochastic approach for real-world driving cycle construction: Winnipeg driving cycle". *Transportation Science, 48, 170-183* (2014) (cit. on p. 72).

[244] AVL. *Intake air conditioning. Available in: https://www.avl.com/adas_simulation/-/asset_publisher/TzaHJXCoGgln/content/intake-air-conditioning. (accessed on 17 January 2022)*. 2021 (cit. on p. 72).

[245] R. García-Contreras, A. Gómez, P. Fernández-Yáñez, and O. Armas. "Estimation of thermal loads in a climatic chamber for vehicle testing". *Transportation Research Part D: Transport and Environment, 65, 761-771* (2018) (cit. on p. 72).

[246] D. G. Gardner, V. A. Zaccardi, P. A. Jalbert, and M. Denise Bryant. "Reducing the cost of aircraft engine emission measurements". *Proceedings of the International Instruments Symposium, 49, 57-66* (2003) (cit. on p. 72).

[247] G. Osculati et al. "Effects of hypobaric hypoxia exposure at high altitude on left ventricular twist in healthy subjects: Data from HIGHCARE study on Mount Everest". *European Heart Journal: Cardiovascular Imaging,17, 635-643* (2016) (cit. on p. 72).

[248] J. M. Desantes, A. J. Torregrosa, and P. Broatch A. Olmeda. "Experiments on the influence of intake conditions on local instantaneous heat flux in reciprocating internal combustion engines". *Energy, 36, 60-69* (2010) (cit. on p. 72).

[249] J. Galindo, J. R. Serrano, P. Piqueras, and O. García Afonso. "Heat transfer modelling in honeycomb wall-flow diesel particulate filters". *Energy, 43, 201-213* (2012) (cit. on pp. 72, 88).

[250] D. M. Human, T. L. Ullman, and T. M. Baines. "Simulation of high altitude effects on heavy-duty diesel emissions". In: *SAE Technical Paper 1990-04-01, 900883.* 1990 (cit. on p. 72).

[251] P. Roberts, A. Mason, A. Headley, L. Bates, S. Whelan, and K. Tabata. "RDE plus - A road to rig development methodology for whole vehicle RDE compliance: Road to engine perspective". In: *SAE Technical Papers 2021-01-1223.* 2021 (cit. on p. 72).

[252] D. Serio, A. Oliveira, and J. R. Sodré. "Effects of EGR rate on performance and emissions of a diesel power generator fueled by B7". *Journal of the Brazilian Society of Mechanical Sciences and Engineering, 39 (1-3)* (2017) (cit. on p. 76).

[253] OpenWAM webpage, CMT-Motores Tèrmicos, Universitat Politècnica de València, www.openwam.org. (Cit. on p. 77).

[254] J. Galindo, J. R. Serrano, F. J. Arnau, and P. Piqueras. "Description of a semi-independent time discretization methodology for a one-dimensional gas dynamics model". *Journal of Engineering for Gas Turbines and Power, 131 (3), 034504* (2009) (cit. on p. 77).

[255] J. B. Heywood. *Internal combustion engine fundamentals. pp. 506.* New York: McGraw-Hill, 1988 (cit. on p. 80).

[256] Gtisoft.com, (2015). Available in: *http://www.gtisoft.com/applications/a_Engine_Performance.php* (accessed on 20 Jun 2018) (cit. on p. 80).

[257] V. Venkateshmohan and M. Kumar. "Predictive diesel combustion using DI-Pulse in GT-Power". MA thesis. Chalmers University of Technology, 2015 (cit. on p. 80).

[258] J. R. Serrano, P. Olmeda, F. J. Arnau, A. Dombrovsky, and L. Smith. "Analysis and methodology to characterize heat transfer phenomena in automotive turbochargers". *Journal of Engineering for Gas Turbines and Power, 137 (2), 021901* (2015) (cit. on p. 82).

[259] J. R. Serrano, P. Olmeda, F. J. Arnau, and A. Dombrovsky. "Turbocharger heat transfer and mechanical losses influence in predicting engines performance by using one-dimensional simulation codes". *Energy, 86, 204-218* (2015) (cit. on p. 82).

[260] J. R. Serrano, P. Olmeda, A. Páez, and F. Vidal. "An Experimental Procedure to Determine Heat Transfer Properties of Turbochargers". *Measurement Science and Technology, 21 (3), 035109* (2010) (cit. on p. 82).

[261] R. D. Burke, P. Olmeda, F. J. Arnau, and M. Rayes-Belmonte. "Modelling of turbocharger heat transfer under stationary and transient conditions". In: *11th International Conference on Turbochargers and Turbocharging. London.* 2014 (cit. on p. 82).

[262] N. Baines, K. D. Wygant, and A. Dris. "The analysis of heat transfer in automotive turbochargers". *Journal of Engineering for Gas Turbines and Power, 132, 042301* (2010) (cit. on p. 82).

[263] M. Tu, R. Ratnakar, and V. Balakotaiah. "Reduced order models with local property dependent transfer coefficients for real time simulations of monolith reactors." *Chemical Engineering Journal, 383, 123074* (2020) (cit. on p. 89).

[264] R. D. Hawthorn. "Afterburner catalysts effects of heat and mass transfer between gas and catalyst surface." *American Institute of Chemical Engineers-Institution of Chemical Engineers, 70, 428-438* (1974) (cit. on p. 89).

[265] M. Masoudi. "Hydrodynamics of diesel particulate filters". In: *SAE Technical Paper 2002-01-1016.* 2002 (cit. on p. 91).

[266] A. G. Konstandopoulos and J. H. Johnson. "Wall-flow diesel particulate filters -Their pressure drop and collection efficiency". In: *SAE Technical Paper 890405.* 1989 (cit. on p. 91).

[267] E. J. Sanchis. "Modelado de la oxidación del hollín en filtros de partículas Diésel". PhD thesis. Universitat Politècnica de València, p. 36, 2019 (cit. on p. 92).

[268] A. G. Konstandopoulos. "Flow resistance descriptors for diesel particulate filters: Definitions, measurements and testing". In: *SAE Technical Paper 2003-01-0846*. 2003 (cit. on p. 92).

[269] A. Suresh, A. Khan, and J. H. Johnson. "An experimental and modeling study of cordierite traps - pressure drop and permeability of clean and particulate loaded traps". In: *SAE Technical Paper 2000-01-0476*. 2000 (cit. on p. 92).

[270] E. A. Kladopoulou, S. L. Yang, J. H. Johnson, G. G. Parker, and A. G. Konstandopoulos. "A study describing the performance of diesel particulate filters during loading and regeneration - A lumped parameter model for control applications". In: *SAE Technical Paper 2003-01-0842*. 2003 (cit. on p. 92).

[271] F. Payri, A. Broach, J. R. Serrano, and P. Piqueras. "Experimental-theoretical methodology for determination of inertial pressure drop distribution and pore structure properties in wall-flow diesel particulate filters". *Energy, 36, 6731-6744* (2011) (cit. on p. 92).

[272] J. R. Serrano, F. J. Arnau, P. Piqueras, and O. García Afonso. "Packed bed of spherical particles approach for pressure drop prediction in wall-flow (diesel particulate filters) DPF sunder soot loading conditions". *Energy, 58, 644-654* (2013) (cit. on p. 93).

[273] R. A. Yapaulo, E. Wirojsakunchai, T. Orita, D. E. Foster, M. Akard, L. R. Walker, and M. J. Lance. "Impact of filtration velocities and particulate matter characteristics on Diesel particulate filter wall loading". *International Journal of Engine Research, 10 (5), 287-304* (2009) (cit. on p. 93).

[274] C. Kamp, A. Sappok, and V. Wong. "Soot and ash deposition characteristics at the catalyst-substrate interface and intra-layer interactions in aged Diesel particulate filters illustrated using focused ion beam (FIB) milling". In: *SAE Technical Paper 2012-01-0836*. 2012 (cit. on p. 93).

[275] W. Feller. *An introduction to probability theory and its applications, Vol. 1, Ed. 3*. Wiley, 1968 (cit. on p. 95).

[276] B. Logan, D. G. Jewett, R. G. Arnold, E. J. Bouwer, and C. O'Melia. "Clarification of clean-bed filtration models". *Journal of Environmental Engineering, 121, 869-873* (1995) (cit. on p. 95).

[277] C. K. Dardiotis, O. A. Haralampous, and G. C. Koltsakis. "Catalytic oxidation in wall-flow reactors with zoned coating". *Chemical Engineering Science, 63 (4), 1142-1153* (2008) (cit. on p. 95).

[278] M. Jeguirim, V. Tschamber, J. F. Brilhac, and P. Ehrburger. "Oxidation mechanism of carbon black by NO_2: effect of water vapour". *Fuel, 84 (14), 1949-1956* (2005) (cit. on p. 96).

[279] M. M. Maricq and N. Xu. "The effective density and fractal dimension of soot particles from premixed flames and motor vehicle exhaust". *Journal of Aerosol Science, 35 (10), 1251-1274* (2004) (cit. on p. 96).

[280] A. Messerer, R. Niessner, and U. Pöschl. "Comprehensive kinetic characterization of the oxidation and gasification of model and real diesel soot by nitrogen oxides and oxygen under engine exhaust conditions: Measurement, Langmuir-Hinshelwood, and Arrhenius parameters". *Carbon, 44, 307-324* (2006) (cit. on pp. 96, 175).

[281] D. C. Quiros, S. Hu, S. Hu, E. S. Lee, S. Sardar, X. Wang, J. S. Olfert, H. S. Jung, Y. Zhu, and T. Huai. "Particle effective density and mass during steady-state operation of GDI, PFI, and diesel passenger cars." *Journal of Aerosol Science, 83, 39-54* (2015) (cit. on p. 108).

[282] C. Guardiola, B. Pla, P. Piqueras, J. Mora, and D. Lefebvre. "Model-based passive and active diagnostics strategies for diesel oxidation catalysts." *Applied Thermal Engineering, 110, 962-971* (2017) (cit. on p. 109).

[283] C. M. Allen, M. C. Joshi, D. B. Gosala, G. M. Shaver, L. Farrell, and J. McCarthy. "Experimental assessment of Diesel engine cylinder deactivation performance during low-load transient operations". *Internal Journal of Engine Research, 22 (2), 606-615* (2019) (cit. on p. 110).

[284] R. Suarez-Bertoa, V. Valverde, M. Clairotte, J. Pavlovic, B. Giechaskiel, V. Franco, Z. Kregar, and C. Astorga. "On-road emissions of passenger cars beyond the boundary conditions of the real-driving emissions test". *Environmental Resesearch, 176, 108572* (2019) (cit. on p. 110).

[285] I. Lefort and A. Herreros J. M. Tsolakis. "Reduction of low temperature engine pollutants by understanding the exhaust species interactions in a diesel oxidation catalyst." *Environment Science and Technology, 48, 2361-2367* (2014) (cit. on p. 115).

[286] R. Kamo and W. Bryzik. "Adiabatic turbocompound engine performance prediction". *SAE Transactions, 87 (1), 213-223.* (1978) (cit. on p. 126).

[287] R. Sekar, R. Kamo, and J. Wood. "Advanced adiabatic Diesel engine for passenger cars." *SAE Transactions, 93 (3), 250-258.* (1984) (cit. on p. 126).

[288] M. Ekström, A. Thibblin, A. Tjernberg, C. Blomqvistb, and S. Jonssona. "Evaluation of internal thermal barrier coatings for exhaust manifolds." *Surface and Coatings Technoly, 272, 198-212.* (2015) (cit. on p. 126).

[289] S. Rajadurai and S. Ananth. "Heat shield iInsulation for thermal challenges in automotive exhaust system". In: *SAE Technical Paper 2019-28-2539.* 2019 (cit. on p. 126).

[290] C. Viazzi, A. Deboni, J. Z. Ferreira, J. P. Bonino, and F. Ansart. "Synthesis of yttria stabilized zirconia by solgel route: influence of experimental parameters and large scale production." *Solid State Sciences, 8, 1023-1028.* (2006) (cit. on p. 134).

[291] M. A. Marr. "An investigation of metal and ceramic thermal barrier coatings in a spark-ignition engine". MA thesis. University of Toronto, 2009 (cit. on p. 134).

[292] S. Alaruri, L. Bianchini, and A. Brewington. "Effective spectral emissivity measurements of superalloys and YSZ thermal barrier coating at high temperatures using a 1.6 μm single wavelength pyrometer". *Optical and Lasers in Engineering, 30, 77-91* (1998) (cit. on p. 134).

[293] P. Piqueras, M. J. Ruiz, J. M. Herreros, and A. Tsolakis. "Sensitivity of pollutants abatement in oxidation catalysts to the use of alternative fuels". *Fuel, 297, 120686* (2021) (cit. on p. 166).

[294] A. T. Thompson. "The effect of altitude on turbocharger performance parameters for heavy duty Diesel engines: experiments and GT-Power modeling". PhD thesis. Colorado State University, 2014 (cit. on pp. 166, 180).

[295] Y. Wu, P. Wang, S. Farhan, j. Yi, and L. Lei. "Effect of post-injection on combustion and exhaust emissions in DI Diesel engine". *Fuel, 258, 116131* (2019) (cit. on p. 168).

[296] R. H. Essenhigh. "Rate equations for the carbon-oxygen reaction: an evaluation of the Langmuir adsorption isotherm at atmospheric pressure". *Energy Fuels, 5 (1), 41-46* (1991) (cit. on p. 175).

[297] K. J. Lee, I. H. Han, and K. H. Choi. "Oxygen chemisorption on microporous carbons: An analysis of experimental data". *Korean Journal of Chemical Engineering, 12, 228-235* (1995) (cit. on p. 175).

[298] M. Kalberer, M. Ammann, H. W. Gäggler, and U. Baltensperger. "Adsorption of NO_2 on carbon aerosol particles in the low ppb range". *Atmospheric Environment, 33 (17), 2815-2822* (1999) (cit. on p. 175).

[299] X. Wang, Y. Ge, and L. Yu. "Combustion and emission characteristics of a heavy-duty Diesel engine at idle at various altitudes". *SAE International Journal of Engines, 6 (2), 1145-1151* (2013) (cit. on p. 203).

[300] V. Bermúdez, J. R. Serrano, P. Piqueras, and O. García-Afonso. "Pre-DPF water injection technique for pressure drop control in loaded wall-flow diesel particulate filters". *Applied Energy, 140, 234-245* (2015) (cit. on p. 220).

[301] J. Ko, K. Kim, W. Chung, C.-L. Myung, and S. Park. "Characteristics of on-road particle number (PN) emissions from a GDI vehicle depending on a catalytic stripper (CS) and a metal-foam gasoline particulate filter (GPF)". *Fuel, 238, 363-374* (2019) (cit. on p. 221).

"Have the courage to follow your heart and intuition. They somehow already know what you truly want to become. Everything else is secondary."

Steve Jobs.